RHODES UNIVERSITY

Where leaders learn

New Geochemical Constraints on the Genesis of the Gamsberg Zinc Deposit, Namaqualand Metamorphic Province, South Africa

Thesis submitted in fulfilment of the requirements for Degree of Master of Science in the Department of Geology, Rhodes University.

Susan E Foulkes

g05f0753

March 2014

RHODES UNIVERSITY
DEPARTMENT OF GEOLOGY

New Geochemical Constraints on the Genesis of the Gamsberg Zinc Deposit, Namaqualand Metamorphic Province, South Africa

Thesis submitted in fulfilment of the requirements for Degree of Master of Science in the Department of Geology, Rhodes University.

Susan E Foulkes

g05f0753

March 2014

Supervisor: Dr Harilaos Tsikos

DECLARATION

I declare that this thesis is my own work, and any authors have been accordingly acknowledged. It is being submitted in fulfilment of the Degree of Master of Science at Rhodes University, Grahamstown, and has not been submitted before for the examination of any degree through any other university.

Miss Susan E Foulkes

Signed on the 05th day of March 2014 at Randburg.

ABSTRACT

The base metal massive sulfide deposits of the Aggeneys-Gamsberg (A-G) District are hosted within the Mesoproterozoic Bushmanland Group of the Namaqua-Natal Metamorphic Complex in the Northern Cape Province of South Africa. The district displays an apparent eastward trend in the economic concentration of base metals (+ barite) from relatively Cu-Pb-rich, Ba-poor mineralisation at Black Mountain to Zn- and Ba-rich ores at Gamsberg. Base metal sulfides at Gamsberg are restricted to the so called *Gams (Iron) Formation* which comprises a sulfidic mineralized unit ("B") enveloped within a sequence of meta-sedimentary units ("A" and "C"). The aim of the study was to shed further light on the genesis and chemical evolution of the sulfide mineralisation at Gamsberg in the context of the entire A-G District, by interrogating further the apparent district-wide trend in base metal distribution. The Gams Iron Formation was sampled and studied from one key drill core intersection ("G1") which intersects the largest part of it as described elsewhere; a small number of additional samples from a second drill core ("G2") complemented the main sample suite. Minerals that make up the silicate assemblages across the studied section include quartz, garnet, pyroxene, pyroxenoid, phyllosilicates, carbonates, amphiboles, oxides (chiefly magnetite) and graphite. In a stratigraphic context, the mineralogical variations conform directly to those documented in the relevant literature from the Gamsberg locality. These are coupled, where possible, with mineral-chemical profiles of selected silicate species which replicate those of bulk-rock compositions, particularly with respect to Mn, Fe and Ca in the upper C Unit of the studied section. These signals collectively track the characteristic transition from a terrigenous, siliciclastic sediment-dominated footwall to an exhalative sediment-dominated hanging wall to the sulfide mineralisation as also seen in similar deposits elsewhere, particularly with respect to the characteristic Mn-rich signature increasingly observed in the hanging wall C Unit.

The foregoing suggests that the examined section faithfully records the interpreted primary stratigraphy of the deposits, despite the complex structural and metamorphic overprint that characterises the region. This facilitates a stratigraphic analytical approach on the sulfidic Unit B, through a combination of mineral-chemical and stable isotope analyses. Dominant sulfides in Unit B are sphalerite and pyrite, with lesser pyrrhotite and minor galena.

Sphalerite shows high and generally invariant contents of Fe (mean 12.18wt%, as FeS) whereas Zn anti-correlates with Mn (mean 5.58wt%, as MnS). Isotopic analyses for S, Fe and Zn in hand-picked sphalerite and pyrite separates were used with a view to providing new evidence for chemical and isotopic variation within the sulfide ore-body in a vertical (*i.e.* stratigraphic) sense, discuss the implications thereof, and ultimately interpret the new data in light of similar existing data from the A-G District and elsewhere. The $\delta^{34}S$ data for pyrite (plus a single pyrrhotite grain) and sphalerite from both cores G1 and G2 show comparable compositional ranges between 22.9 and 30.4‰ and between 27 and 30.1‰ respectively. The $\delta^{56}Fe$ data for pyrite show a range between -1.85 and 0.19‰, whereas seven sphalerite separates have a very narrow range of $\delta^{66}Zn$ from 0.06 to 0.20‰. The atypically high sulfur isotope data reported in this study are interpreted to reflect sedimentary deposition of primary sulfide ore at Gamsberg from an isotopically highly evolved seawater sulfate source through large-scale Rayleigh fractionation processes. Thermogenic sulfate reduction is proposed to have been the main reductive mechanism from seawater sulfate to sulfide, given the absence of very low $\delta^{34}S$ data for sulfides anywhere in the A-G District. By contrast, the $\delta^{66}Zn$ values for sphalerite are for all intents and purposes invariant and very close to 0‰, and therefore suggest little Zn isotope fractionation from an original exhalative fluid source. On this evidence alone, Zn isotopes therefore appear to hold little promise as a proxy of the chemical and isotopic evolution of SEDEX deposits in space and time, although this can only be verified through further application in the broader A-G District and similar deposits elsewhere. The apparent decoupling of Zn and S isotopes in the Gamsberg sulfide deposit, however, points towards diverse sources of these two components, *i.e.* ascending metalliferous brines *versus* seawater respectively. Finally, pyrite $\delta^{56}Fe$ data do show a stratigraphic trend of generally declining values up-section, which are interpreted to reflect the influence of broadly coeval precipitation of isotopically heavy Fe-oxides on a broader-scale – now preserved as abundant magnetite through metamorphism. Further work on the iron isotope composition of silicate-and oxide-hosted Fe on a local-to-district scale will assist in testing this interpretation.

ACKNOWLEDGEMENTS

Firstly, I am indebted to my parents, David and Margaret Foulkes, who provided me the opportunity to study. When my father suggested geology as a subject for first year my immediate response was “Why would I want to study rocks?” After attending the geology introductory lecture in first year I have found a passion for geology; the way ‘just a rock’ can tell an enormous story. They too were there with words or encouragement and brutal honesty when it was necessary and without their understanding and support none of this would have been possible.

This project became available to me through Prof John Moore and Dr Hari Tsikos. They had a very close working and personal relationship that brewed and stoked the flames of this project; the introduction of isotopes to me was challenging but also rewarding when I became more in tune with them. Thank you John! Despite not knowing me you allowed me this chance. And thank you Hari, you have been an amazing supervisor; we’ve each had our ups and downs through the years but in the end I am happy that I did this masters project with you. Thank you goes to Mr Potgieter of Black Mountain for the sample material.

Bursary sponsorship came to me through MINTEK. Hari came to the rescue and encouraged me to apply for it. They provided me with the opportunity to study for 2 years and afford to do expensive and interesting lab work. MQA provided me with a second bursary for 2012 for which to complete my thesis and engage in some undergraduate teaching.

Analytical work could not have been possible without the patience and help of:

- John Hepple, Thulani Royi and Andile Pikoli, Rhodes University, for sample preparation
- Prof. Goonie Marsh, for XRF analyses
- Mr Archie Adlington-Corfield, for your patience with me when operating (or breaking!) the MINTEK microprobe
- Dr Gabi Costin, Rhodes University, for helping me with my initial EDS-SEM analyses and further help with microprobe analyses at Rhodes University
- Joel JXA 8230 Superprobe, instrument sponsored by NRF/NEP grant 40113 (UID 74464) is kindly acknowledged

- Dr Adrian Boyce, Glasgow University and Dr Jamie Wilkinson, Imperial College London for running the S and Fe and Zn isotopes, respectively

Over eight years you see a lot of friends come and go, however, they have made a lasting impression on me, especially the three 'families' that I lived with in digs: LaShandre Coetzee, James Teng and Neo Khanyile, as well as Lindi Fryer, Ania Barma, Ode Oosthuysen and Kay Santho. Thank you for not only putting up with me over the years but also keeping me (in)sane!

My department family: Brenton Fairey, Bantu Ntsaluba, Jamie Lodge, Jarred Land, Mark Raines, Geoff Howarth, Adrian Williams, Jason Moodley and Ashley Goddard but especially John Hepple. Thank you for all the wonderful memories. The Geology Department became a second home to me. Thank you also goes to Steffen and Jane Buttner, Emese Bordy, Goonie Marsh and Steve and Rosie Prevec.

Finally I dedicate this project to Profs John Moore and Hugh Eales who are no longer with us today. They always had fascinating stories to tell and advice to give. RIP.

List of mineral abbreviations used in the thesis (Whitney and Evans, 2010).

Mineral	Abbreviation	Mineral	Abbreviation
Feldspar	Fsp	Garnet	Grt
Pyroxenoid	Pxm	Clinopyroxene	Cpx
Biotite	Bt	Muscovite	Ms
Chlorite	Chl	Amphibole	Amp
Magnetite	Mag	Rutile	Rt
Quartz	Qz	Garnet	Grt
Pyrophanite	Pph	Pyroxene	Px
Sillimanite	Sil	Hedenbergite	Hd
Diopside	Di	Johannsenite	Jhn
Orthoclase	Or	Albite	Ab
Anorthite	An	Sphalerite	Sp
Pyrrhotite	Po	Pyrite	Py
Galena	Gn	Graphite	Gr

TABLE OF CONTENTS

LIST OF FIGURES

LIST OF TABLES

1. INTRODUCTION

a. Preamble

Base-metal sulfide deposits form a wide range of deposit types and yield a large variety of metal sulfides generally dominated by copper, zinc and lead. They represent key economic resources of base metals on a global scale (Emsbo, 2009). Sedimentary rocks host a significant proportion of the global inventory of massive sulfide deposits that have developed through either syngenetic or epigenetic hydrothermal processes of ore formation (Leach *et al.,* 2005).

Epigenetic deposits (such as those of the *Mississippi Valley-type*, or *MVT*) fall beyond the scope of the present thesis and will not be discussed further. In some instances, the syngenetic *versus* epigenetic character of certain deposits is unclear or debatable, such as with the carbonate-hosted *Irish-type* deposits (Pohl, 2011). Typically syngenetic deposit types form in a variety of environments and related range of rock types (sedimentary and/or igneous), and themselves form a series of subtypes that are traditionally classified under two major end-member classes: *volcanogenic massive sulfide* (VMS) and *sedimentary exhalative* (SEDEX). Volcanogenic massive sulfide deposits are also beyond the scope of this thesis and will not be discussed further.

Sedimentary exhalative deposits represent prime sources of Pb and Zn sulfide ore globally. They typically form in extensional submarine settings where contemporaneous volcanism is either absent or, if present, is thought to be genetically unrelated to ore-formation. The deposits are massive to semi-massive and stratiform, with a generally high-aspect ratio (Goodfellow and Lydon, 2008). Variants of the SEDEX class include those of McArthur- and Selwyn-type deposits (Cooke *et al.,* 2000). As will be discussed in more detail in the introductory chapters, the Broken Hill-type (BHT) of deposits, named after the homonymous deposit in Australia (Spry *et al.,* 2009) is also variously defined as a SEDEX sub-type. This definition however, remains problematic due to the strong metamorphic and deformational overprint that characterises these deposits on a global scale.

b. SEDEX Deposits: General

The acronym SEDEX, a contraction of the term 'sedimentary exhalative', was first proposed by Carne and Cathro (1982). It referred to: "bedded or laminated, tabular sulfide-rich bodies in carbonaceous shales or other, fine-grained clastic rocks of Proterozoic to upper Palaeozoic age... volcanic rocks associated with the ore-bodies are generally absent, although tuffaceous rocks may be spatially associated with the ore-hosting sedimentary package" (Sangster and Hillary, 1998; Large *et al.,* 2002; Holland, 2005; Emsbo, 2009). Many authors now contend that this definition is ambiguous and may include some deposit types of a hybrid origin in terms of the timing of ore formation (*e.g.* Irish-type). The definition of SEDEX deposits has therefore more recently been restricted to sulfide deposits formed in a sedimentary basin by the submarine venting of hydrothermal fluids, whose principal ore minerals are sphalerite and galena (Goodfellow *et al.,* 1993; Lydon, 1995; Sangster and Hillary, 1998; Holland, 2005; Goodfellow and Lydon, 2008).

The dominant ore constituents of SEDEX deposits are thought to have formed on or below the seafloor from warm (~100° to 200°C), saline (10 to 30 wt% dissolved solids) basinal brines, that have ascended along basin-controlling syn-sedimentary faults (Emsbo, 2009). The metals were transported as dissolved solids in the form of chloride complexes and precipitated when these fluids mixed and reacted with H_2S within the sedimentary basin. Hydrogen sulfide would have been produced either by bacterial or thermochemical sulfate reduction (BSR or TSR). The mineral deposits may also have formed by sulfide replacement and infill of particular sedimentary facies below the basin floor (Large *et al.,* 2002), in which case the syngenetic *versus* epigenetic character of the ores becomes obscured.

Gangue mineralogy includes carbonates, barite and quartz, typically accompanied by interbedded iron sulfides. The majority of the ore is in the form of a stratiform sulfide body with a high aspect ratio (Goodfellow and Lydon, 2008), that exhibits a tabular shape with internal layering. A significant feature of some SEDEX deposits is the so-called *feeder pipe*, which is the zone of reaction between up-flowing hydrothermal fluids and footwall sediments (Sangster, 2002). The existence, or lack, of a feeder pipe and alteration zone

under the vent complex of a deposit, leads to further classification of SEDEX deposits into vent-proximal and vent-distal, respectively.

Sangster (2002), based on earlier work by Sato (1972), further illustrates the formation of vent-proximal and vent-distal deposits (Figure 1). Here, the density of the venting hydrothermal fluid compared to that of the surrounding basin water is a key parameter controlling whether a deposit forms proximally or distally to the vent. Sangster (2002) argues that an exhaling fluid that is denser than the surrounding seawater (which has a lower temperature and salinity; above iso-density line AB) will form "bottom-hugging" brines. These would be more likely to move down-slope away from a vent zone and thus accumulate in a distal fashion to a vent. Distal precipitation of zinc and lead sulfides would consequently produce a laminated deposit with no apparent spatial link to a feeder zone or vent complex (Figure 2a; Large *et al.,* 2002).

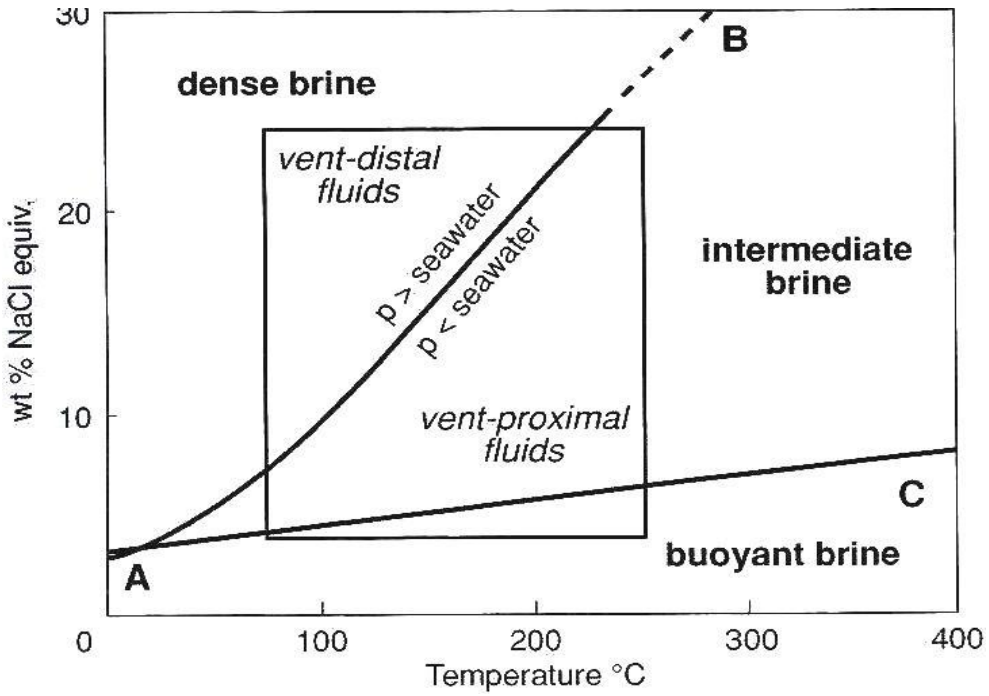

Figure 1. Fluid inclusion temperature and salinity measurements for fluids venting into seawater (Sangster, 2002). AB and AC represent iso-density lines.

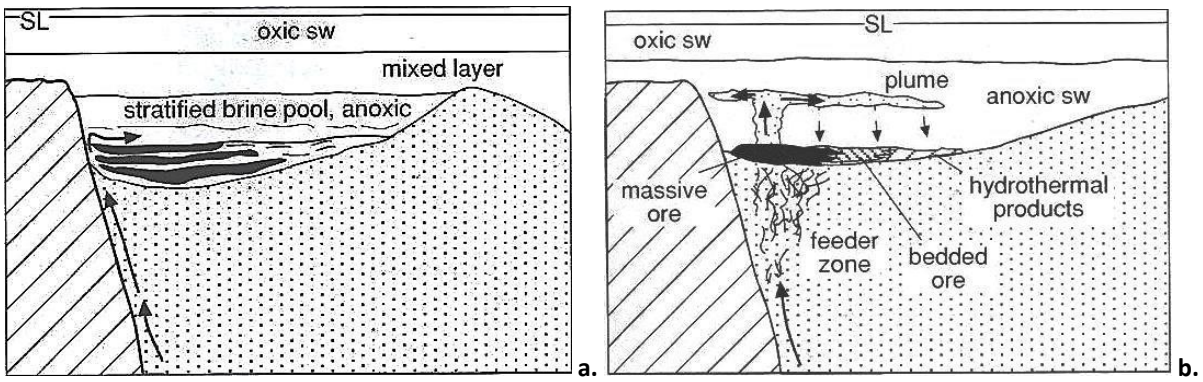

Figure 2. Setting and formation of (a) a vent-distal deposit; (b) a vent-proximal deposit (both from Large *et al.,* 2002). SL = sea level.

On the other hand, fluids with lower density than the seawater into which they vent (below iso-density line AC, Figure 1) would form buoyant plumes with the tendency to mix more rapidly with the seawater upon cooling, thus leading to vent-proximal deposits adjacent to the vent (Figure 2b). A third case also exists whereby fluids that are denser than surrounding seawater will form vent-proximal deposits if they are discharged into pre-existing depressions (Sangster, 2002). Fluids with an intermediate density are more likely to form buoyant plumes that mix with the surrounding water (between iso density lines AB and AC), thus increasing their density, becoming bottom-hugging brines that move away from a vent zone.

Cooke *et al.,* (2000) considered the redox potential of the ore fluid in controlling whether a vent-proximal or vent-distal deposit forms. Reduced ore fluids will precipitate metals below the seafloor, forming a vent complex, due to cooling, increase in pH or mixing. Oxidized ore fluids are less likely to form in this zone as sulfide precipitation is not promoted by cooling, mixing or pH changes, but rather by *reduction* of dissolved sulfate (Large *et al.,* 2002). Accordingly, the *McArthur*- and *Selwyn*-type deposits have been defined: the former type represents those deposits that have formed from low-temperature, oxidized, acidic to near-neutral brines that evolved from sedimentary basins dominated by carbonates, evaporites and hematitic sandstones and shales. Selwyn-type constitutes those deposits that formed from higher temperature, acidic and reduced brines that evolved in reduced siliciclastic and shale basins (Cooke *et al.,* 2000; Large *et al.,* 2002).

c. BHT versus SEDEX deposits

Broken Hill-type deposits are arguably one of the most important types of stratiform sediment-hosted Zn-Pb deposits. They are metamorphosed, strata-bound deposits, akin to SEDEX deposits but with their own distinct characteristics. The Broken Hill deposit in Australia is used as a type example for three reasons (Parr and Plimer, 1993):

- It exhibits most of the features associated with this type of mineralisation;
- More than 100 years of mining, exploration and documentation make it one of the most extensively studied deposits in the world; and,
- It is approximately an order of magnitude larger than most other BHT deposits, and thus a large number of geological and geochemical variations are preserved and may even be magnified within this deposit.

The classification of BHT deposits is contentious as reflected through a number of published studies. Some authors classify BHT deposits as a sub-type of the SEDEX type (*e.g.* Large *et al.,* 2002; Leach *et al.,* 2005; Goodfellow and Lydon, 2008), while others regard them as an independent class altogether (*e.g.* Parr and Plimer, 1993; Large *et al.,* 1996; Walters, 1996; Spry *et al.,* 2000; McClung, 2006). This contentious classification is due to the high-grade of metamorphism, metasomatism and deformation that the host terranes have undergone. Consequently, published genetic models range from syngenetic exhalative or sub-sea-floor replacement, distal skarn, metamorphogenic, or hybrid combinations (Leach *et al.,* 2005).

Apart from the type locality in Australia, the other most important districts considered to be representative of the BHT class of deposits are all Proterozoic in age and include the *Aggeneys District* in the *Namaqua-Natal Metamorphic Complex* of South Africa (Gamsberg, Black Mountain, Broken Hill, Big Syncline); the *Zinkgruvan Terrane* in the southern Bergslagen Province, Sweden; and the *Soldiers Cap Terrane* of the Mt Isa Eastern Succession, Australia, including Cannington (Walters, 1996). In terms of grade and tonnage, the Broken Hill deposit of Australia and the Gamsberg deposit in South Africa are classified as supergiant Zn-Pb deposits, whereas a further four are classified as giant deposits (Cannington, Australia; Broken Hill and Big Syncline, South Africa; and Dariba-Rajpura, India;

see also Figure 3 from Large *et al.,* 2002). It should be noted here though, that the classification of the South African deposits in the A-G District remains conjectural, with some authors (*e.g.* Spry *et al.,* 2000) arguing that only the Black Mountain and Broken Hill deposits in the area should be considered to be more typical of the BHT class, whilst the Gamsberg deposit is more akin to a metamorphosed SEDEX deposit with BHT affinities.

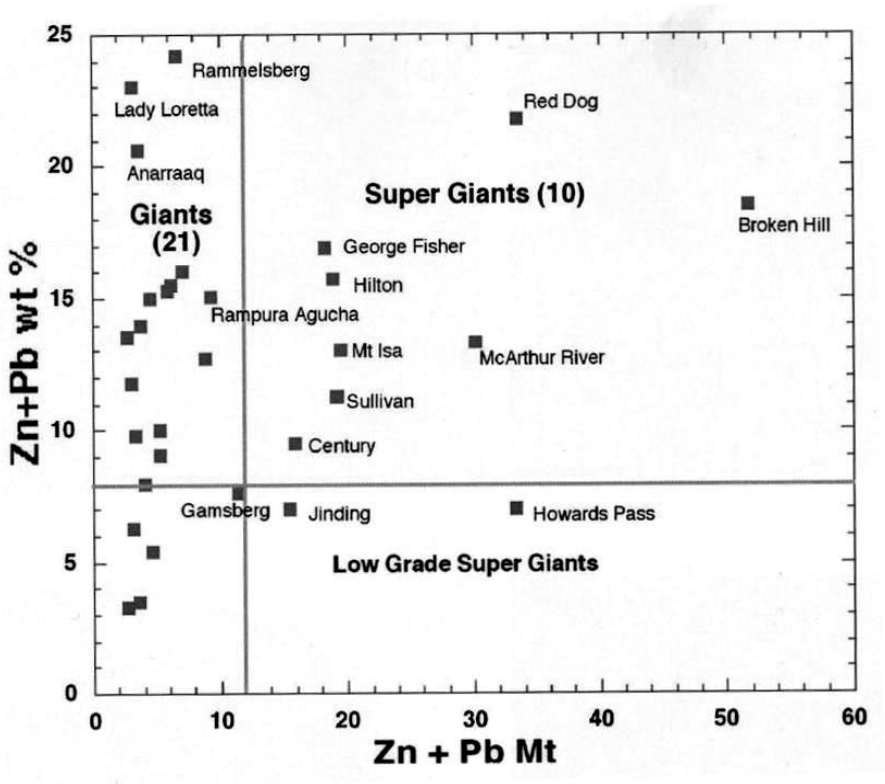

Figure 3. Classification of sediment-hosted Pb-Zn deposits according to metal concentration and ore-grade (after Large *et al.,* 2002).

When the BHT class of deposits is considered as an *independent* class in its own right, the following set of criteria needs to be met (Walters, 1996):

- Amphibolite-granulite facies metamorphism of Proterozoic clastic meta-sedimentary host sequences;
- Spatial association with possible metavolcanic units;

- Laterally-extensive marker units (iron-formations and gahnite-rich quartzites);
- Little or no association with organic (graphite)-rich stratigraphy;
- Stacked, structurally-overprinted lenses;
- Large-scale strata-bound alteration halos (high K/Na and Fe-(Mn) in garnet);
- Lack of associated feeder zone;
- Association with Fe-Mn-Ca-F-rich skarn-like gangue assemblages;
- Extreme zonation between Pb-Ag versus Zn-dominant ore-lenses;
- General lack of pyrite; and,
- A distinctive elemental association, including Sb, Cu, As, Bi and Au.

If BHT deposits are considered to be a sub-type of SEDEX deposits, then differences between SEDEX and BHT deposits are essentially attributed to metamorphism. Some authors believe the differences to be also, in part, due to geochemical variations in the ore-forming environment (Figure 4a and b; Large *et al.,* 1996). For example, Large and Davidson (1991) state that SEDEX deposits form from high salinity, reduced ore fluids during exhalation into a reduced (anoxic) sedimentary package, while BHT deposits form from a similar type of reduced ore fluid moving into an oxidized (oxic) sedimentary basin. These differences lead to SEDEX deposits being metal- and sulfur-rich, hosted in a very reduced package of sediments and surrounded by a weak manganese halo; BHT deposits would then be metal-rich, sulfur-poor deposits hosted in oxidized facies sediments and surrounded by a very intense manganese halo (Large *et al.,* 1996). In both cases, temperature decrease of the discharging fluid is an obvious key factor in ore genesis; moreover, in SEDEX deposits sulfate reduction takes place while in BHT deposits oxidation and a pH increase occurs which leads to the peripheral development of iron oxide exhalative facies. These processes are thought to have led to the BHT deposits displaying enrichments in Ca, Fe, Mn, P, F, Si and REE, whereas SEDEX deposits record a Mg, Ca, Fe, Mn, Ba, Tl association (Large *et al.,* 2002).

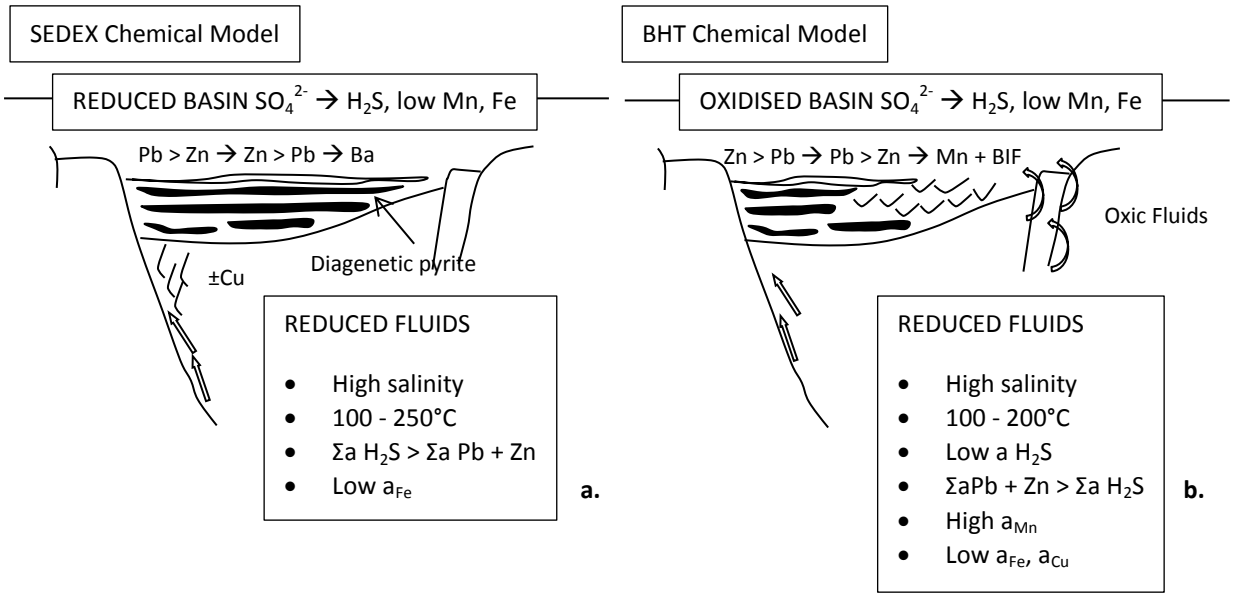

Figure 4. Chemical models for (a) SEDEX genesis; and (b) BHT genesis. Redrawn from Large *et al.,* 1996.

Other differences may include the greater Mn enrichment in BHT than in SEDEX deposits, the relatively higher Pb/Zn ratio and Ag content in BHT deposits, and the associated magnetite-rich facies in BHT deposits which are virtually unknown in SEDEX deposits (Large *et al.,* 2002).

d. Modern Analogues for SEDEX Mineralisation

Modern analogues of base metal sulfide mineralisation have been described from the Salton Sea, Gulf of Mexico and the Red Sea (Robb, 2005) as well as Lake Kivu and Lake Malawi of the East African Rift; the California Borderlands of the San Andreas transform zone; and the Lake Baikal Rift (Goodfellow *et al.,* 1993). The Red Sea is considered by many to be the foremost modern analogue of these deposit types (Goodfellow *et al.,* 1993). Here, an intracontinental rift is developing between Egypt, Sudan and Eritrea on the African continent to the west and Saudi Arabia and Yemen on the Asian continent to the east. The Red Sea deposit contains base metal-rich muds deposited from high salinity, high temperature fluids in seafloor depressions. Similarly, the Salton Sea, situated in the San Andreas Fault system along the western coast of USA, is characterized by circulation of

hydrothermal fluids at depths of 1 to 3 km. These are relatively hot (350°C) and dense, containing considerable dissolved salts (Robb, 2006). Base metal transport and deposition is attained in a syngenetic fashion when the hot ascending fluid encounters colder seawater within the basin.

2. GEOLOGICAL BACKGROUND

a. Regional Setting

The massive sulfide deposits of the A-G District are hosted within the *Bushmanland Group* of the *Namaqua-Natal Metamorphic Complex* (NNMC; Stowe *et al.,* 1984; Hartnady *et al.,* 1985; Thomas *et al.,* 1994; Cornell *et al.,* 2006). The NNMC extends along the southern margin of the Kaapvaal craton from southern Namibia to the Kwa Zulu Natal coastline of South Africa (Figure 5). Regional-scale structural discontinuities permit the subdivision of the western belt of the NNMC into a number of domains of distinct tectonometamorphic history. These, from west to east, include the *Richtersveld Subprovince*, *Bushmanland Terrane*, *Kakamas Terrane*, *Areachap Terrane* and the *Kaaien Terrane*. The A-G District deposits are hosted by multiply-deformed and metamorphosed amphibolite-facies metasedimentary rocks within the Bushmanland Terrane. The Bushmanland Terrane is composed of quartzite, metapelitic to metapsammitic schist and amphibolite that overlies a suite of quartz-feldspar gneiss (Stalder and Rozendaal, 2005b).

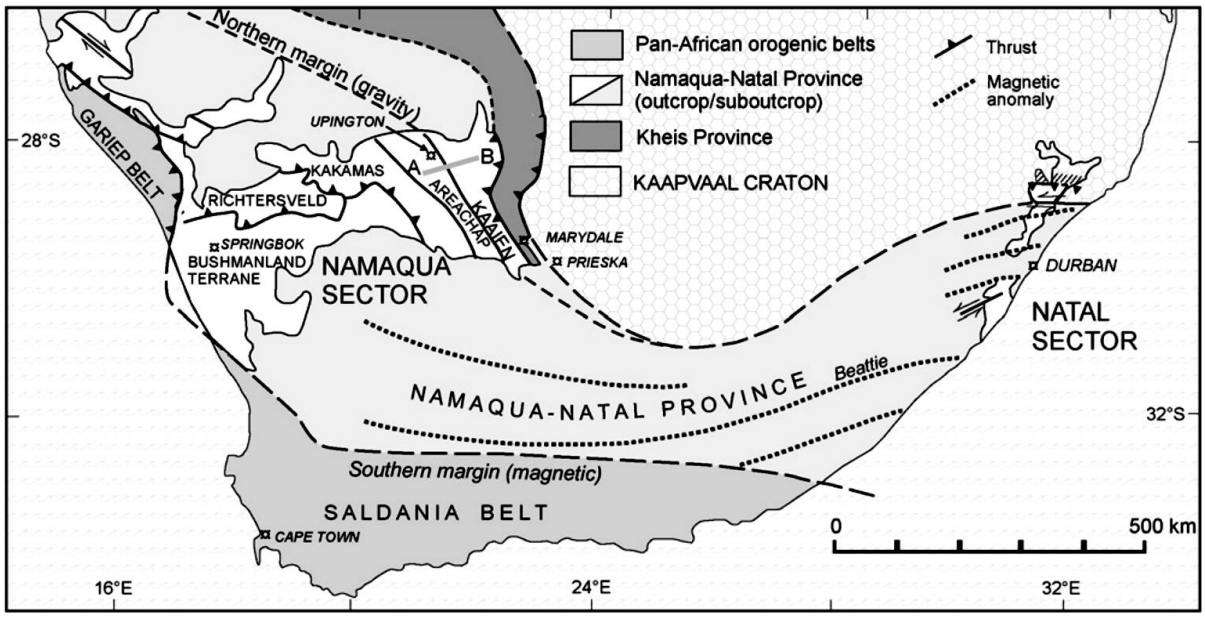

Figure 5. Geological setting of the Namaqua-Natal Metamorphic Complex (Cornell *et al.,* 2006).

Moore *et al.,* (1990) considered the following factors in re-constructing the development of the western belt of the NMC:

- A heterogeneous 2000Ma basement comprising three components – a central calc-alkaline igneous suite of coeval metavolcanic and intrusive rocks (*Richtersveld Subprovince*); a northern metasedimentary component (*Grunau Sequence* of the *Gordonia Subprovince*); and a southern component dominated by orthogneisses (*Bushmanland Terrane*);

- A 1650Ma supracrustal succession that overlaps Richtersveld and Bushmanland basement, and comprises a basal intrusive-to-extrusive leucogneiss and an upper schist/quartzite succession;

- An early tectono-magmatic event of uncertain age and duration, involving low-angle thrust faulting, isoclinal folding and syntectonic emplacement of tabular granitic bodies; and,

- Subsequent tectonic reactivation involving shearing, open folding and syntectonic-to-post-tectonic granite intrusion, resulting in a major thermal peak at 1100Ma. This caused large-scale isotopic resetting and high-T metamorphism. Deformation and metamorphism of the ore deposits of the region occurred during this latter set of events.

The absolute age envelope for the deposition of the Bushmanland Group rocks remains unresolved. Bailie *et al.,* (2007) present a ~2.05Ga age for the basement rocks to the Bushmanland Group (*Achab Gneiss*) and place the deposition of the Bushmanland Group itself at ~2.0 to ~1.8Ga. Overlying amphibolites of the *Koeris Formation* have, in turn, been dated at 1.65 ± 0.09 Ga by Reid *et al.,* (1987). Cornell *et al.,* (2009) argue that the Bushmanland Group formed before or around 1.6Ga as part of a suite of clastic and chemical sediments deposited on the 2.0Ga Achab Gneiss. The Bushmanland Group rocks then underwent a series of deformation and metamorphism events and were later intruded by the *Aroams Gneiss* of the *Little Namaqualand Suite* between 1.21 and 1.13Ga. Further deformation and metamorphism during the Namaquan event occurred between 1.15 and

1.05Ga. The ages of the base metal deposits of the A-G District and their host sequence, are thus described as generally Mesoproterozoic in age.

The Gamsberg deposit is the eastern-most of the four deposits in the region; the other three being Swartberg (*Afrikaans for "Black Mountain"*), Broken Hill and Big Syncline (Figure 6). These deposits show an apparent eastward trend in the economic concentration of base metals from relatively Cu-Pb-rich at Black Mountain and Broken Hill to Zn-rich at Big Syncline and Gamsberg (Thomas *et al.,* 1994). Barite is common albeit quantitatively variable in all deposits, with a clear peak at Gamsberg. The base metals at Gamsberg are hosted within the Gams Iron Formation, the equivalent of which is the Aggeneys Ore Formation in the more westward deposits. Minor barite is intermixed with the base metals at Black Mountain and Broken Hill but is more voluminous but spatially separated from the sulfide mineralisation at Gamsberg.

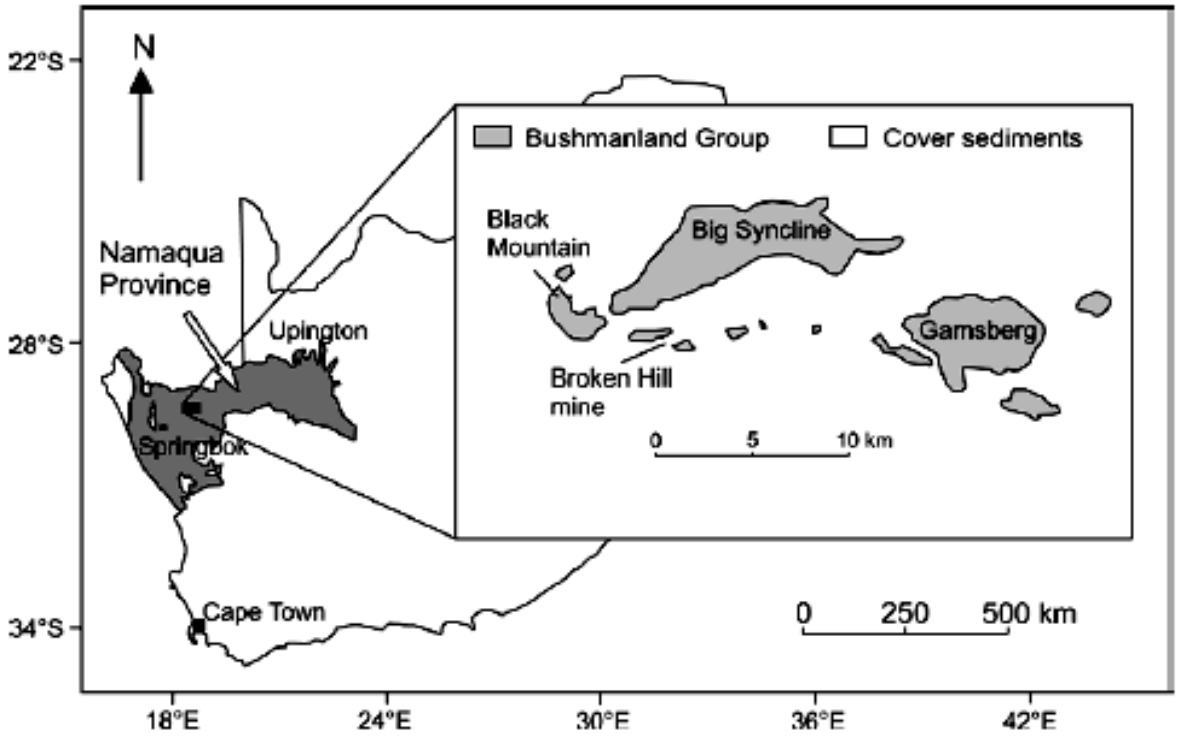

Figure 6. Location map of the Aggeneys-Gamsberg District in the Northern Cape Province of South Africa. Note that Black Mountain denotes "Swartberg" (Stalder and Rozendaal, 2004).

The ore-bearing and enveloping units of the A-G District were exposed to the above-mentioned amphibolite facies metamorphism during the Namaquan and Kibaran metamorphic events between 1.3 and 1.0Ga (Robb *et al.,* 1999; Stalder and Rozendaal, 2005a); P-T estimates range from 630° to 670°C and 3 to 4.5kbar, respectively (Parr and Plimer, 1993; Stalder and Rozendaal., 2005a). Joubert (1971) identified the deformational events in the area and termed them F_1 to F_4. Moore (1976) and Ryan *et al.,* (1986) identified the periods of metamorphism as M_1 to M_4, with M_1 and M_2 corresponding to *prograde* metamorphism while M_3 and M_4 correspond to *retrograde* metamorphism. The main episode of metamorphism is recorded by E-W-trending recumbent isoclinal folds (F_2) and prominently developed subhorizontal foliation (S_2; Stalder and Rozendaal, 2004). Evidence of F_1 has mostly been obliterated in the area due to the high grades of metamorphism.

b. History of the Aggeneys-Gamsberg Mining District

The A-G District had received little attention up until 1952, when R.G. Niemöller began a systematic mineral evaluation of the area (McClung, 2006). This led to the discovery of most of the massive sillimanite bodies in the area, the massive barite of Gamsberg and other smaller mineral occurrences such as manganiferous iron ore (Rozendaal, 1986; Stalder, 2003). In 1968, copper-zinc sulfide mineralisation was discovered at the Prieska area to the SE of the A-G District. This triggered intense exploration activities in the entire north-western region of the then Cape Province (Rozendaal, 1986).

In 1970, O'okiep Copper Company Ltd. undertook the initial sponsorship of a regional mapping project, conducted by the Precambrian Research Unit of the University of Cape Town that eventually covered the Aggeneys-Pofadder geographical area (Rozendaal, 1986). In the course of this mapping (during the early '70s), Joubert, (1974) recognized the stratigraphic similarity between Gamsberg and the Aggeneys area where exploration of a stratabound sulfide deposit was in progress (Rozendaal, 1986). The company *Phelps Dodge* acquired prospecting options over the farms *Aggeneys* and *Zuurwater* in May 1971 (Stalder, 2003). In June 1971, the first diamond drill hole on Black Mountain was collared, and shortly thereafter, intersected payable Pb-Cu-rich sulfide mineralization (Ryan *et al.,* 1986; Stalder,

2003; McClung, 2006). Following this discovery, geologists of Phelps Dodge were quick to take note of similar gossan occurrences on *Noeniepoort se Kop* (widely known as "Broken Hill") and *Aggeneysberg* ("Big Syncline"), while the Gamsberg deposit was discovered by geologists of the O'okiep Copper Company (McClung, 2006). As a result of all these discoveries, exploration interest rapidly shifted towards the A-G District (Stalder, 2003).

The O'okiep Copper Company and Newmont South Africa Ltd. performed an extensive magnetic survey over the Gamsberg area and disclosed a prominent magnetic anomaly (Stalder, 2003). Over a period of 6 days in March 1972, the entire Gamsberg was mapped and detailed ground magnetic surveys were completed (Stalder, 2003) by personnel of the O'okiep Copper Company and Newmont South Africa Ltd. (Rozendaal, 1986). Surface drilling was commenced at Gamsberg on 13th June 1972. Massive sulfides were struck by the second diamond drill hole which made an intersection during July 1972 (Rozendaal, 1986).

In 1977, Phelps Dodge entered into a joint venture with *Gold Fields of South Africa Ltd*. that resulted in the formation of the *Black Mountain Mineral Development Co*. (Pty.) Ltd. (BMMD) (McClung, 2006). By the end of 1978, a total of 42 130m of surface diamond drilling and 16 317m of percussion drilling, as well as 22 026m of underground diamond drilling had established a reserve at Gamsberg of 150Mt averaging 7.10% Zn and 0.55% Pb (Rozendaal, 1986). The Broken Hill mine was subsequently opened in 1979 and mining continued unhampered until 1998 when the mining giant *AngloAmerican* purchased BMMD (McClung, 2006). It was at this time that the mine geologists discovered the Broken Hill Deeps deposit, a down-dip extension of the Broken Hill ore body (McClung, 2006).

Since that time, mining in the A-G District by *AngloAmerican Base Metals* has continued with development of the Black Mountain, Broken Hill Deeps and Gamsberg deposits (McClung, 2006). As a result, total resources at Gamsberg alone were revised to approximately 160Mt at 7.40% Zn and 0.55% Pb (Stalder, 2003; Stalder and Rozendaal, 2004). McClung (2009) and McClung and Viljoen (2010a; 2010b; 2011) report total resources at Gamsberg to be 265Mt at 6.1% Zn and 0.3% Pb. The entire A-G District reportedly has an estimated combined grade and tonnage of 439Mt at 3.60% Zn, 1.43% Pb, 0.21% Cu and 21 g/t Ag, as well as an estimated 6Mt of barite from the Gamsberg deposit (McClung *et al.,*

2007). In 2010, and following the commencement of this research project, *AngloAmerican* Base Metals sold its portfolio of zinc assets to *Vedanta Resources* (Anglo American Plc., 2010). According to Vedanta Resource Plc., (2012), the Gamsberg Project's open pit mine hosts a defined ore resource of 186Mt and >250Mt of potential ore resources.

c. Lithostratigraphy of the Mineralised Sequence at Gamsberg

Ryan (1986) and Rozendaal (1986) mapped and described in considerable detail the generalized stratigraphic succession at the A-G District, and the interpreted lithostratigraphic framework remains largely unchallenged to date (Moore *et al.,* 1990; Stalder, 2003; McClung *et al.,* 2007). The regional sequence consists broadly of a basal gneiss overlain by a thick succession of pelitic schists, in which occur up to three discrete stratiform massive sulfide ore bodies. Overlying the ore-bearing sequence and constituting what is interpreted to be the top of the stratigraphic succession in the area, is a variable package of conglomerate, amphibolite and leucocratic to grey gneiss (Ryan, 1986). With specific reference to the Gamsberg locality, Rozendaal (1986) provides a comprehensive lithostratigraphic description of the Bushmanland Group with emphasis on the ore-bearing Gams Iron Formation (Table 1), hereafter referred to as GIF. From base to top, the lithological succession comprises a pink granite-gneiss (*Haramoep Gneiss*), followed by a quartz-biotite-muscovite-sillimanite schist interbedded with quartzite bands and lenticular massive sillimanite bodies (*Namies Schist*). Above the Namies Schist and directly beneath the GIF lies the Pella Quartzite, a series of dark recrystallized quartzite, with conglomerate and quartz-biotite-muscovite-sillimanite schist bands and massive recrystallized milky quartzite. The GIF itself is subdivided into a series of three units namely "A", "B" and "C", of which Unit B is the mineralized horizon (Table 1). Capping the GIF is the Nousees Mafic Gneiss, composed of amphibolite, quartz-feldspar-amphibole gneiss/fels and quartz-muscovite schist. These are interbedded with quartzite bands and conglomerate lenses as well as feldspathic schist ± biotite.

Table 1. Lithostratigraphic subdivision of the Bushmanland Group at Gamsberg considering the Overturned Limb and the North Body (after Rozendaal, 1986; Stalder and Rozendaal, 2004).

Formation	Lithology				
Nousees Mafic Gneiss	Amphibolite, quartz-feldspar-amphibole gneiss/fels, pyroxene-plagioclase-quartz(±amphibole) fels. Quartz-muscovite schist, interbedded quartzite bands and conglomerate lenses, feldspathic schists ± biotite				
				Overturned Limb	**North Body**
Gams Iron Formation	**C Unit**	Garnet-pyroxenoid rhythmite, pyroxenoid-amphibole-garnet-clinopyroxene rock, quartz-garnet-amphibole-magnetite rock and magnetite-hematite quartzite with interbedded barite.	**C2**	Garnet-pyroxenoid ± carbonate ± quartz rocks with Fe oxides.	Garnet-pyroxenoid rhythmite with Fe oxides.
			C1	Iron formations hosting locally major apatite.	Variety of carbonate-, garnet-, amphibole- and magnetite-bearing rocks.
	B Unit	Sulfide-bearing zone, mineralized quartz-sericite-sillimanite schist, mineralized quartz-grunerite-garnet rock.	**B2**		Mineralized quartz-garnet-amphibole rocks.
			AMU	Pyritic metapelitic schist.	Marker horizon of sedimentary apatite nodules.
			B1		Mineralised metapelitic schist.
	A Unit	Quartz-garnet-feldspar-clinopyroxene rock, carbonate-quartz-garnet-clinopyroxene marble, garnet-pyroxene-amphibole rock.	**A4**	Garnet-quartz rocks with variable Fe rocks.	Quartz-garnet rocks.
			A3	-	Ca-Mn carbonates with variable clinopyroxene and amphibole.
			A2	-	Garnet-pyroxene-amphibole rock.
Pella Quartzite	Dark, recrystallized quartzite, with conglomerate and quartz-biotite-muscovite-sillimanite schist bands. Quartz-biotite-muscovite-sillimanite schist, quartz-muscovite schist, interbedded quartzite bands. Massive recrystallized milky quartzite.				
Namies Schist	Quartz-biotite-muscovite-sillimanite schist, interbedded quartzite bands and lenticular massive sillimanite bodies.				
Haramoep Gneiss	Pink granite-gneiss.				

Stalder and Rozendaal (2004) provide detailed descriptions of the lithostratigraphic sub-divisions of the A, B and C Units of the GIF (Table 1). The oldest A Unit is composed of a

basal garnet-pyroxene-amphibole-magnetite rock (A2 sub-unit), followed upwards by impure marbles (A3 sub-unit) as well as fine-grained, moderately banded, quartz-garnet-feldspar-clinopyroxene rocks (A4 sub-unit). The ore-bearing B Unit can locally be subdivided into a basal, metapelite-hosted member (B1 sub-unit), which is generally less well mineralised than the upper high-grade calc-silicate-hosted member (B2 sub-unit). The boundary between the two sub-units is defined by an apatite nodule-rich layer termed by Stalder and Rozendaal (2004) as the "Apatite Marker Unit" (AMU) and interpreted by the same authors as a primary phosphatic deposit associated with an anoxic setting of primary sulfide precipitation. Support for the latter interpretation is lent by the abundant graphite in the B Unit which is interpreted by Rozendaal (1986) to represent the metamorphosed organic-component of the original host sediments. Finally, the upper C Unit of the GIF is composed primarily of an Fe-Mn-rich assemblage, dominated by magnetite+amphibole+carbonate(+garnet) in the lower C1 sub-unit, becoming more pyroxenoid/garnet-dominated in the uppermost sub-unit C2.

3. MATERIALS, AIMS AND LAYOUT

As indicated in the foregoing chapter, a variety of geological attributes of the A-G District in the Northern Cape Province of South Africa have been studied extensively in the past, ranging from regional and local stratigraphy, structural and metamorphic evolution, as well as petrography and geochemistry of the massive sulfide deposits and their host rocks (*e.g.* Rozendaal, 1982, 1986; McClung, 2009; McClung and Viljoen, 2010a, 2010b, 2011; McClung *et al.,* 2007, 2010; Stalder, 2003; Stalder and Rozendaal, 2004, 2005a, 2005b). The latter include petrographic, structural as well as isotopic studies on the base metal sulfides themselves, as well as on temporally associated barite mineralization (Von Gehlen, 1987; McClung *et al.,* 2007; McClung *et al.,* 2010). This body of published or otherwise publically available work (in the form of MSc and PhD theses), constitutes an important benchmark for further and more focused research on the ore deposits of the A-G District.

The principal aim of this thesis is to help unravel the depositional history of Zn-dominated massive sulfide mineralization at Gamsberg by interrogating further the postulated genetic link between the latter and other sulfide deposits in the A-G District (*i.e.* Black Mountain, Broken Hill and Big Syncline). This will be achieved using a combination of basic petrography, mineral chemistry and, more importantly, conventional and novel stable isotope geochemistry of the massive sulfide ore.

a. Sample Locality and Selection

The drill core material selected for this study *(# GPFD 006*) was accessed, logged and sampled by the author and her project supervisors in July 2009, following consultation with the resident geologists of *AngloAmerican* Base Metals at the A-G District, led by Mr J.E. Potgieter. The drill core (hereafter referred to as “G1”: Gamsberg 1), was selected from the northern part of the Gamsberg area (broadly referred to as “North Body” on Figure 7); here, the target sequence of the GIF is generally characterised by minimal stratigraphic and structural complexity, and therefore lends itself for studies designed to detect, assess and interpret mineral-chemical and/or stable isotope signals in a *stratigraphic* context.

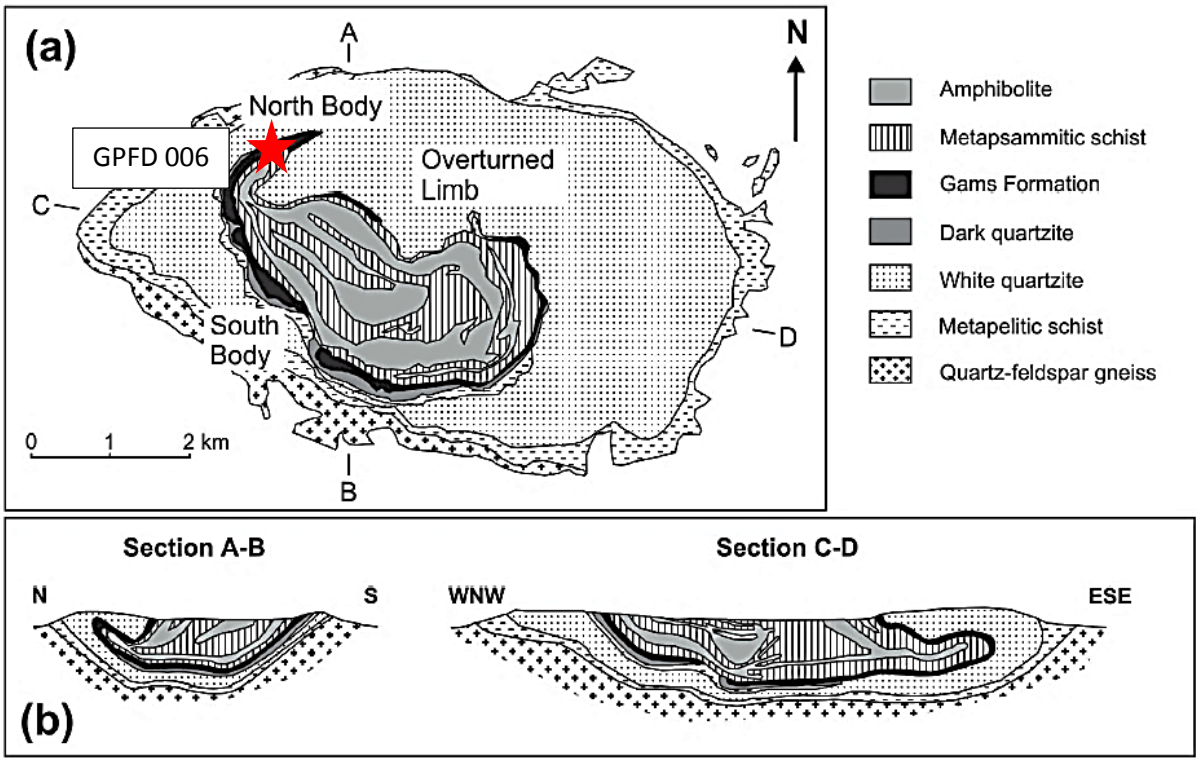

Figure 7. Geological map of the Gamsberg Deposit highlighting the so-called Overturned Limb, the North and South Bodies as well as two cross-sections through the deposit, one from north to south (A-B), the second from west to east (C-D; Stalder and Rozendaal, 2004). Locality of drill core G1 is indicated.

The coordinates of G1, in the *LO19* and *WGS34* coordinate system, as provided by the company are as follows:

	WG 19 X	WG 19 Y	UTM 34 X	UTM 34 Y	Z
GPFD006	-4194.55	-3235384.38	301428.4271	6764180.885	1108.15

Sampling of drill core G1 was aided by existing core-log information, kindly made available to the author by the mining company. Approximately 3-5 cm-long quartered-core samples were taken every 2 m, from 160 m depth below surface (DBS) to 234 m DBS. Sample names were assigned according to the depth at which each sample was collected. The sampled intersection and resultant total suite of 38 samples capture the largest part of the GIF in the North Body (Figure 7and Figure 8): on macroscopic evidence alone, samples 234 to 220 represent the upper part of Unit A and specifically that of sub-unit A4 (Table 1); samples

216-182 straddle the entire sulfide-mineralised Unit B; and samples 180-160 capture Unit C, and specifically the entire sub-unit C1 and the lower part of sub-unit C2. With specific reference to the mineralised B Unit, sampling was biased towards the collection of visually semi-massive to massive sulfide material in order to facilitate subsequent manual separation of individual sulfide phases for isotopic analysis. Therefore, the selected samples from this unit are not truly representative of the bulk average composition of Unit B and, unlike with samples from the A and C Units, were not treated via bulk-geochemical techniques in this study.

A small number of additional drill core samples from the North Body at Gamsberg were also kindly provided to the author for comparative purposes by Prof. Abraham Rozendaal of the University of Stellenbosch, South Africa. These intersect the B and C Units but do not represent one continuous length of core. These samples will hereafter be referred to and discussed briefly under the label “G2” (“Gamsberg 2”).

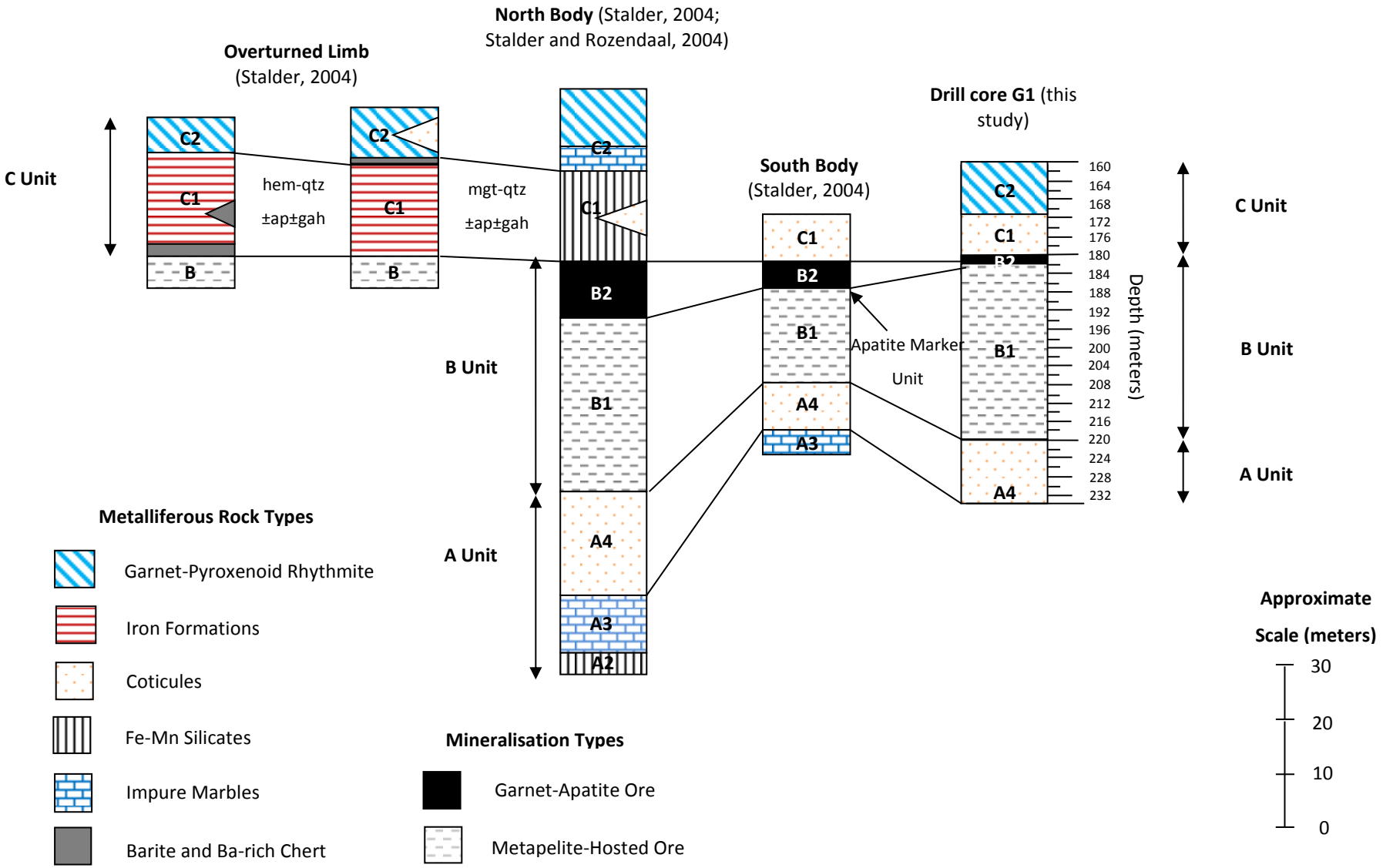

Figure 8. Simplified log and sample locations of drill core G1, against the interpreted stratigraphy at Gamsberg from the Overturned Limb, the North and South Bodies (after Stalder, 2004; Stalder and Rozendaal, 2004).

b. Objectives and Approach

One key attribute of the Gamsberg deposit in the broader geographical and metallogenic context of the A-G District, is its apparent end-member character with respect to its base metal endowment: the deposits at Aggeneys (Black Mountain, Broken Hill) are known to be dominantly Pb(+Cu)-rich with minor barite, the Gamsberg deposit (as well as the mineralisation at Big Syncline) is dominated by Zn in the form of manganiferous sphalerite, as well as associated massive barite mineralisation. This has variously led to the suggestion that these deposits represent a broad continuum of SEDEX-"style" metallogenesis in the A-G District, with the Gamsberg deposit representing the most distal member thereof in a spatial and/or temporal sense. Specific genetic models that employ the above proposal, however, lack consensus and range between purely syngenetic formation (Stalder, 2003; Stalder and Rozendaal, 2004) to a combination of syngenetic and epigenetic (McClung *et al.,* 2007).

This study is essentially an attempt to interrogate and further constrain the genesis of the Gamsberg Deposit in a district-wide context. For that reason, the question of whether or not the Gamsberg deposit (or some/all of the base-metal deposits in the A-G District for that matter) is a typical metamorphosed SEDEX-type or a BHT deposit, becomes essentially a semantic one for the purposes of this study. Instead, the key focus here is to attest whether or not a common ore-forming mechanism can indeed account for the genesis of the Gamsberg deposit as an end-member candidate across the entire A-G District, both spatially and temporally. In addition can this body of work provide new geochemical – including conventional as well as novel stable isotope – evidence that constrains the specifics of such a mechanism? In terms of the structure of this thesis, the above objective is achieved through:

- The establishment of a chemical-stratigraphic framework (on bulk-rock and mineral-specific level where possible) for the examined drill core intersection carried out both on the silicate host Units A and C (chapter 4), as well as on the mineralised Unit B itself (early part of Chapter 5), and through comparison with existing literature information. The above provide insights into the interpreted syngenetic character of the mineralised sequence at Gamsberg

(GIF) and its chemical evolution through time, as well as a benchmark for the interpretation of the stable isotope data that follow.

- The acquisition and evaluation of conventional (S) as well as novel (Zn, Fe) stable isotope data from individual mineral phases (sphalerite, pyrite/pyrrhotite) in the mineralised B Unit across stratigraphy, in order to critically compare and assess these with available data from the relevant literature, and to identify any vertical trends that can be of value to elucidating further the primary ore-forming environment (largest part of Chapter 5). To this end, this study constitutes (to the knowledge of the author) the first attempt whereby mineral-specific Zn and Fe stable isotope geochemistry has been coupled with sulfur isotopes as a potential tool in understanding metallogenic processes in the A-G District and in SEDEX/BHT deposits in general. And finally;
- Interpretation and synthesis of all new results with existing relevant literature and in light of previously-proposed genetic models, with a view to making informed suggestions, where possible, with regard to the genesis and evolution of the Gamsberg massive sulfide orebody, and in the context of other similar deposits in the A-G District (Chapters 5 and 6).

4. PETROGRAPHY, MINERAL CHEMISTY AND GEOCHEMISTRY OF THE A AND C UNITS

a. Macroscopic Observations

Samples representing the A Unit of drill core G1 are generally grey in hand-specimen, fine-grained and with conspicuous mm- to cm-scale banding at variable angles of apparent dip (0-60°). The prominence of banding decreases gradually with increasing stratigraphic height. Samples from the ore-bearing B Unit represent mostly semi-massive to massive, fine- to coarse-grained crystalline sulfide ore dominated by variable pyrite and sphalerite (Figure 9a). Minor galena is macroscopically seen mainly in samples from the middle part of the B Unit, whereas pyrrhotite is much less common, occurring mostly with pyrite across the section. Banding in individual samples is observed only in the lower portion of the B Unit, as the contact with the underlying A Unit is gradually approached. Samples from the C Unit are much coarser-grained than those from the stratigraphically lower A Unit, darker in colour, with very prominent yellowish to light pink mm-scale banding (Figure 9b). Magnetite is macroscopically visible across the entire C Unit in the form of mm-scale laminations and exhibits an apparent modal increase up-section. Minor disseminated sulfides in Unit A (mainly pyrite and lesser sphalerite) are macroscopically visible right up to sample 172.

a. **b.**

Figure 9. (a) Coarse-grained sulfides (galena and pyrite) visible in sample 202, B-Unit, drill core G1; (b) Rhythmic banding manifested by alternating, honey-yellow, garnet-rich bands with pinkish quartz-pyroxene-pyroxenoid-rich ones (sample 166, C Unit).

b. Laboratory Methodology

A number of previous studies have dealt with the mineralogy and mineral chemistry of the silicate-facies assemblages from the A and C Units of the GIF (Rozendaal, 1986; Stalder, 2003; Stalder and Rozendaal, 2004, 2005a; McClung, 2006), not only from the Gamsberg locality but from the entire A-G District. Rozendaal (1986) describes the silicate-rich facies of the GIF at Gamsberg as a succession of metamorphosed silicate ore-bearing rocks. These rocks contain a mineral suite dependent on substitutions between Fe, Mn, Ca and Mg, that resulted from polyphase deformation and medium- to high-grade metamorphism. The aim of this chapter is therefore not to reproduce a very detailed petrographic account for the A and C Units at Gamsberg, but rather to provide a stratigraphic mineralogical and, where possible, mineral-chemical record of the examined intersection, which will serve as a benchmark for geochemical (including isotopic) applications presented in subsequent chapters.

Petrographic work was carried out using the standard transmitted light microscope, in conjunction with SEM-EDS analyses, in the Geology and Life Sciences Departments, respectively, Rhodes University. Data and images were processed using the Leica application and Oxford Instruments' INCA Energy 350 © EDS software. Electron probe micro-analyses were performed on polished thin sections and briquettes. Initial microprobe analyses were carried out at the Mineralogy Division of MINTEK in Randburg, Johannesburg, under the supervision of Mr A. Adlington-Corfield using a Cameca SX50 Superprobe and the accompanying *SamX* processing software. Additional microprobe analyses were performed at Rhodes University, Grahamstown, under the supervision of Dr G. Costin using a JEOL JXA-8230 Superprobe.

Details of the standards and operating conditions are provided in Table 2 whilst all raw, single point microprobe data are presented in the Appendix. Total Fe values were recalculated to FeO and Fe_2O_3 components according to the method of Droop (1987), in order to permit distinction of end-member compositions on relevant classification plots, with the aid of Deer *et al.,* (1992) as well as Anthony *et al.,* (1990).

Table 2. Microprobe operating conditions and standards used during operation of the Cameca SX50 at Mintek as well as the JOEL JXA-8320 at Rhodes University. Multiple standards were used for measurements of single elements at Rhodes University.

	Mintek, Cameca SX50			Rhodes University, JOEL JXA- 8320		
Excitation Conditions	**20kV, 30nA**			**15 kV, 20 nA**		
Spot Size	**10 µm**			**<1µm**		
Standard	**Crystal**	**Mineral**	**ADL* (wt%)**	**Crystal**	**Mineral**	**ADL* (wt%)**
Mn	LIF	Rhodonite	0.033	LIF	Rhodonite	0.0068
Si	TAP	Si_{23} (Quartz)	0.047	TAP	Olivine Quartz	0.00063
Al	TAP	Corundum	0.013	TAP	Orthoclase Almandine	0.00036
Ca	PET	Wollastonite	0.016	PET	Diopside Cr-diopside	0.00025
Fe	LIF	Hematite	0.034	LIF	Fayalite Almandine	0.0218
Mg	TAP	Periclase	0.016	TAP	Diopside Olivine Periclase	0.00036
K	PET	Orthoclase	0.014	PET	Orthoclase	0.00021
Na	TAP	Jadeite	0.025	TAP	Albite Plagioclase (An60)	0.00026
P	PET	Apatite	0.026	PET	Apatite	
Ti	PET	Rutile	0.017	PET	Sphene Rutile	0.0004
Ba	LIF	Barite	0.084	PET	Barite	
S	PET	Barite	0.044	PET	Barite	
Zn	LIF	Zn_{metal}	0.064	LIF	Sphalerite Willemite	
Pb	PET	Galena	0.064	LIF	Galena	
Ag	PET	Ag_{metal}	0.068	PET	Ag_{metal}	
Cu	LIF	CuS	0.056	PET	Chalcopyrite	
As	TAP	Arsenopyrite	0.061	TAP	Arsenopyrite	
V	PET	VO_2	0.015	PET	V_{metal}	

*Average detection limit

The mineralogy of the A and C Units as captured and sampled in drill core G1 compares well with previous petrographic descriptions available in the literature (*e.g.* Stalder and Rozendaal, 2004). Minerals that make up the studied assemblages include quartz, garnet, pyroxene, pyroxenoids, phyllosilicates, carbonates, amphiboles, oxides (mainly magnetite) and graphite.

Sillimanite characterizes only the additional few samples from drill coreG2, but was not observed in the G1 section. Stalder and Rozendaal (2004) also noted the presence of olivine at the base of the A and C Units, which was also not observed in the studied sample suites.

All photographic images were captured in plane-polarised light, unless otherwise stated. The depth profiles constructed for selected mineral species depict average concentrations for the contained elemental oxides at any given depth (sample number), derived in most instances by at least four spot analyses. However in a few instances this was limited to a minimum of two analyses due to the lack of suitable grains for analysis. This problem was especially prevalent with regard to samples from the A Unit, hence no stratigraphic mineral-chemical data from the latter were possible to be obtained and displayed at sufficient resolution.

c. Mineralogy and Textures: Sample Suite G1, A Unit

The lower unit in drill core G1 is composed predominantly of **quartz**, which makes up the bulk of the rock groundmass. It occurs in the form of fine- to medium-grained granoblastic aggregates that commonly display triple junctions and undulose extinction. Quartz also dominates the inclusion populations within other silicate minerals such as garnet and pyroxene. **Calcite** and **K-feldspar** accompany quartz throughout the section in the form of fine-grained subhedral disseminations (Figure 10a). **Phyllosilicate** minerals, namely biotite, muscovite and chlorite, are also abundant species here; **biotite** exhibits a medium-grained habit (0.05 to 1.5mm) of lath-shaped, mottled grains, whose orientation imparts a crude foliation in the quartz-dominated matrix (Figure 10b). **Muscovite** occurs as colourless to pale green, fine- to medium-grained laths and flakes, occasionally with a finer-grained sericitic halo of likely retrograde origin (Figure 10c). Green to brown pleochroic **chlorite** with anomalous blue birefringence occurs mainly as a retrograde phase with magnetite after other silicate minerals (Figure 10d).

Garnet is the next most dominant silicate species, primarily in the lower half of the studied section (from sample 234 to sample 224), where its distribution macroscopically defines a crudely banded texture with magnetite-rich and garnet-free quartz/carbonate bands. Under the microscope, garnet grains are medium- to coarse-grained (<0.1 to >2mm), and exhibit subhedral to anhedral habit with characteristically "ragged" grain boundaries and common sieve textures. Garnet grains contain numerous poikiloblastic inclusions of mostly quartz (Figure 10e, Figure 10f). Individual grains of pale green, pleochroic **pyroxene** and rose-pink to cream **pyroxenoids** are also observed, albeit in very small modal amounts and fine-grained habit (Figure 10f and Figure 11a).

Magnetite (Figure 11a, b and c) occurs throughout the section as fine-grained, subhedral to anhedral, medium- to coarse-grained overgrowths, along with minor **sulfides** (<5% modal, mainly pyrite, less sphalerite and very occasional galena). Magnetite-rich layers define part of the banding as observed mainly in the lower part of the section. **Amphiboles** are present in small modal concentrations, readily identifiable by their well-developed 60°/120° cleavage in suitable sections (Figure 11b). Amphiboles here, as well as in the C Unit, are mostly fine-grained with irregular, anhedral grain boundaries.

Finally, accessory phases identified as individual grains and/or inclusions in other minerals are subhedral, medium-grained **apatite**; anhedral pleochroic **titanite** up to 1.2mm in size (Figure 11d); fine-grained **rutile** (Figure 11e) and **zircon**; flaky particles of **graphite**; as well as a single occurrence of **pyrophanite** (Figure 11f).

d. Mineralogy and Textures: Sample Suite G1, C Unit

The main mineralogical difference that distinguishes the C Unit from the A Unit is the abundance of **garnet**, along with increased modal abundances of **pyroxene**, **pyroxenoid** and **magnetite**; these all relative to quartz and phyllosilicate minerals. Similar to the A Unit, amphiboles are relatively minor phases in terms of modal abundance, as are feldspars and

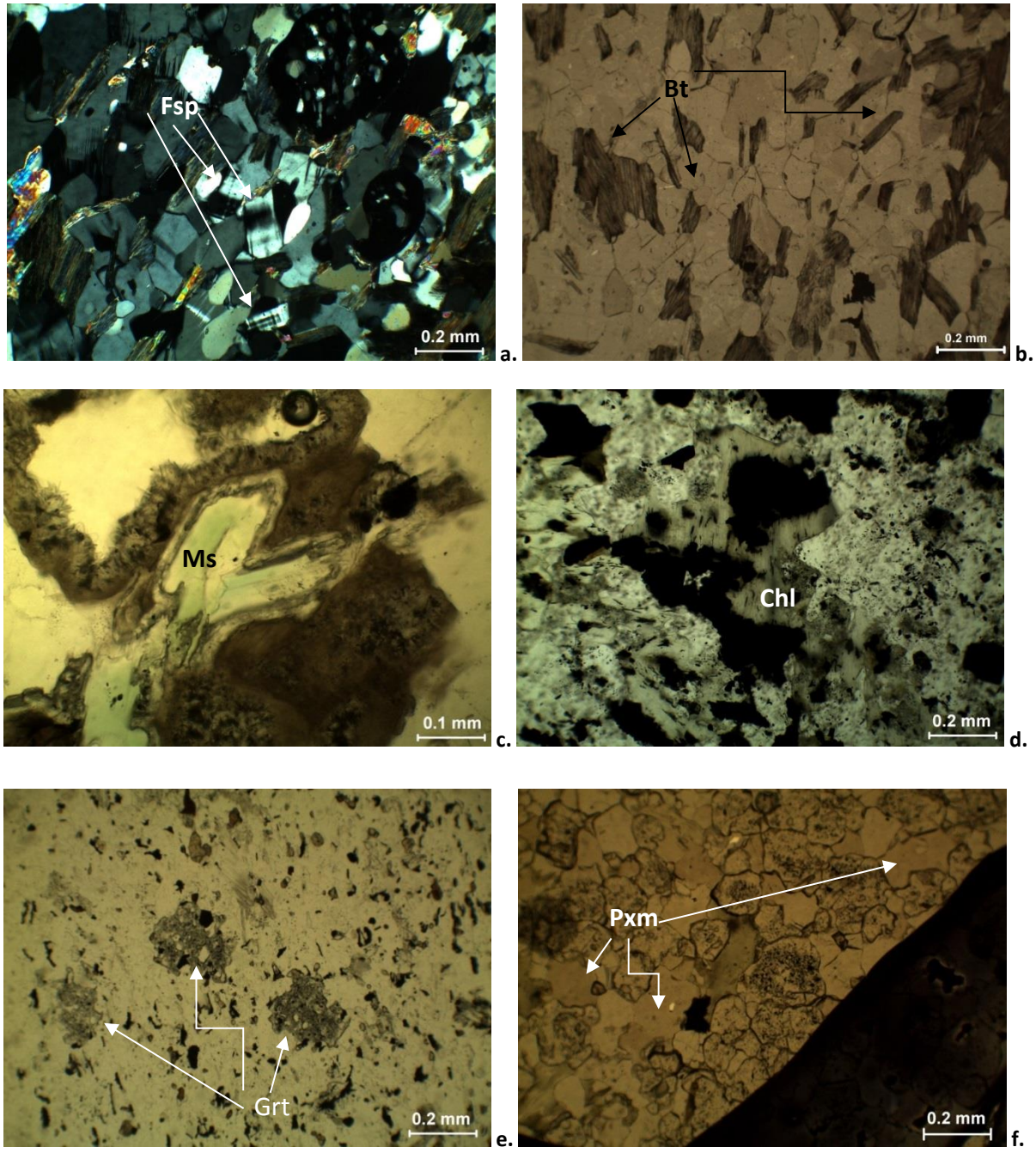

Figure 10. Transmitted light optical images of non-sulfide minerals from the A Unit**:** (a) cross polarised optical image of feldspar grains in a matrix of quartz, biotite, pyroxene and garnet, sample 234; (b) biotite laths in granoblastic quartz, sample 234; (c) sericite corona surrounding muscovite, sample 224; (d) green/brown pleochroic chlorite in a quartz-magnetite matrix, sample 220; (e) poikiloblastic garnet in a quartz-dominated matrix, sample 224; and (f) pale pink/cream, anhedral pyroxenoid in a quartz-garnet matrix, sample 232.

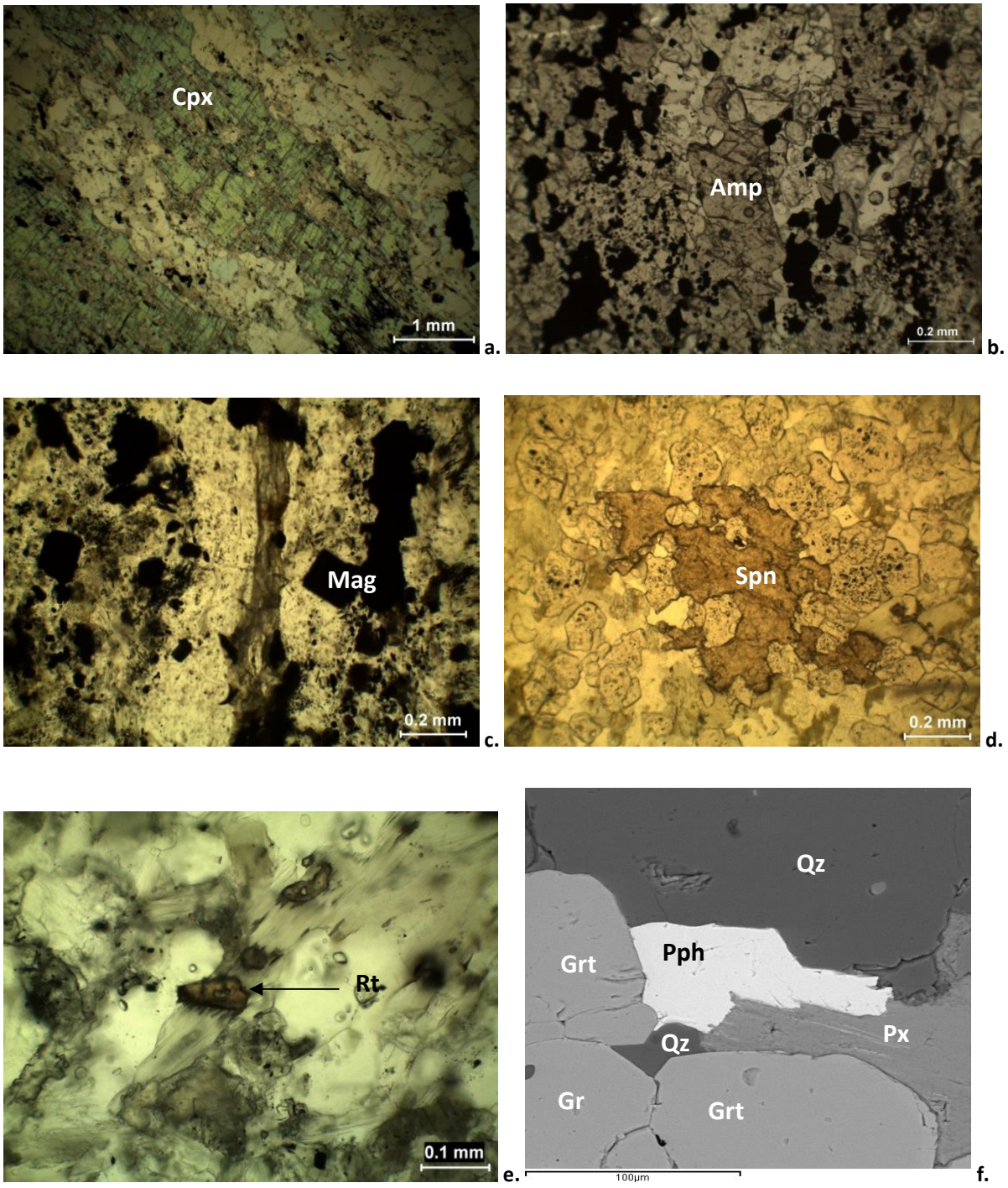

Figure 11. Transmitted light optical images of non-sulfide minerals from the A Unit: (a) green pyroxene, sample 218; (b) subhedral amphibole in a quartz matrix surrounded by pyroxene and magnetite, sample 226; (c) subhedral to anhedral magnetite in a matrix of quartz, pyroxene and muscovite, sample 220; (d) titanite in a matrix of garnet, quartz, biotite and chlorite, sample 232;(e) rutile crystals in a matrix of quartz, muscovite and chlorite, sample 228; and (f) back-scattered electron image of pyrophanite in a matrix of garnet, pyroxene and quartz, sample 232, scale is 100µm.

accessory minerals. Therefore, the account that follows concentrates chiefly on the above three dominant silicate species of the C Unit.

Authors such as Spry (1990) refer to garnet-rich rocks as *coticules* – that is, rocks that consist mostly of quartz and Mn-rich garnet with lesser quantities of other silicate minerals. These rocks are commonly associated with metamorphosed massive sulfide deposits of sedimentary exhalative affinity, notably those of the Broken Hill-type, including Gamsberg (Spry, 1990; Stalder and Rozendaal, 2005a; Heimann *et al.,* 2009). **Garnet** is a ubiquitous mineral in the C Unit, visible macroscopically through the development of rhythmic yellowish bands (Figure 12a and b) alternating with light pink-cream ones. These also contain relatively increased concentrations of pyroxene and pyroxenoids. Microscopically, individual garnet grains are dominantly honey-yellow to light brown, medium- to course-grained poikiloblasts (<0.1 to >2mm), and often define massive granoblastic-polygonal aggregates. Inclusions in garnets of the C Unit include pyroxene, magnetite as well as quartz (Figure 12a and b).

Pyroxenes and **pyroxenoids** occur along with variable modal proportions of garnet, quartz and magnetite, to form the rhythmic banding seen macroscopically. Pyroxenoids are predominantly developed as discrete, high relief, medium-sized (up to 2mm), and weakly pleochroic pinkish grains that often exhibit up to two perfect cleavages under the microscope (Figure 12c and d). The habit of pyroxenoids is dominantly subhedral to euhedral, tabular to prismatic. Inclusions of other minerals (*e.g.* quartz, magnetite and accessories) are common in pyroxenoid grains and occasionally result in a poikiloblastic texture. Pyroxenes are also medium-grained, pleochroic, creamish to light-brown in colour with well-developed grain boundaries (Figure 12e and f). Similar to pyroxenoids, pyroxenes also contain inclusions of other silicate minerals, notably garnet, as well as of magnetite.

Finally, a further unique feature recorded in the upper-most two samples (160 and 162) of Unit C is the occurrence of medium-sized grains of the mixed Fe/Mn oxide mineral **jacobsite; this species** was determined through SEM-EDS analysis and occurs as an additional oxide phase in association with magnetite.

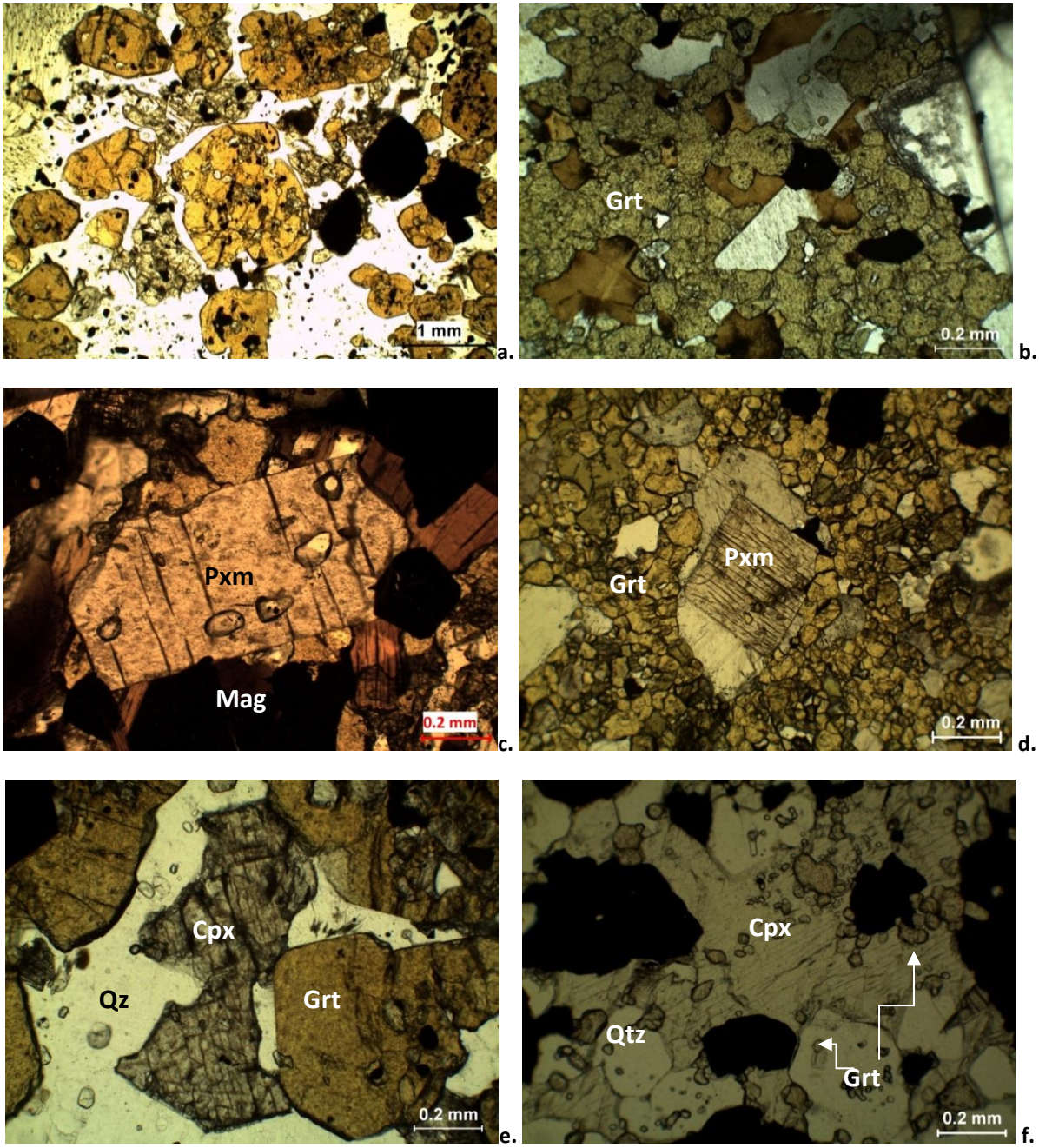

Figure 12. Transmitted light optical images of non-sulfides minerals in the C Unit, (a) honey-yellow, poikiloblastic, subhedral garnet with inclusions of pyroxene, quartz and magnetite, associated with pyroxene, pyroxenoid, quartz and partly overgrown by magnetite, sample 160; (b) granoblastic aggregates of garnet showing triple junctions, associated with pyroxenoid, magnetite and altered biotite, sample 166; (c) rose-pink pyroxenoid, exhibiting one good cleavage and small pyroxene inclusions, sample 162, (d) euhedral pyroxenoid embedded in a matrix dominated by granoblastic garnet and lesser quartz and carbonate, sample 166; (e) brownish pyroxene surrounded by andraditic garnet grains in a matrix of quartz and accessory zircon, sample 160; and (f) pyroxene with small garnet inclusions and magnetite overgrowths in a quartz matrix, sample 178

e. Mineralogy and Textures: Sample Suite G2, C Unit

The silicate mineralogy of G2 compares closely with that of G1. The most notable difference is the occasional presence of **sillimanite**, which occurs in the form of individual, colourless subhedral prismatic grains and as creamish, pale-pink needles inundated with inclusions (Figure 13a). Furthermore, one sample contains the Al-spinel **hercynite** in the form of sub-rounded, medium-sized green crystals embedded in a matrix of magnetite and pyroxene (Figure 13b).

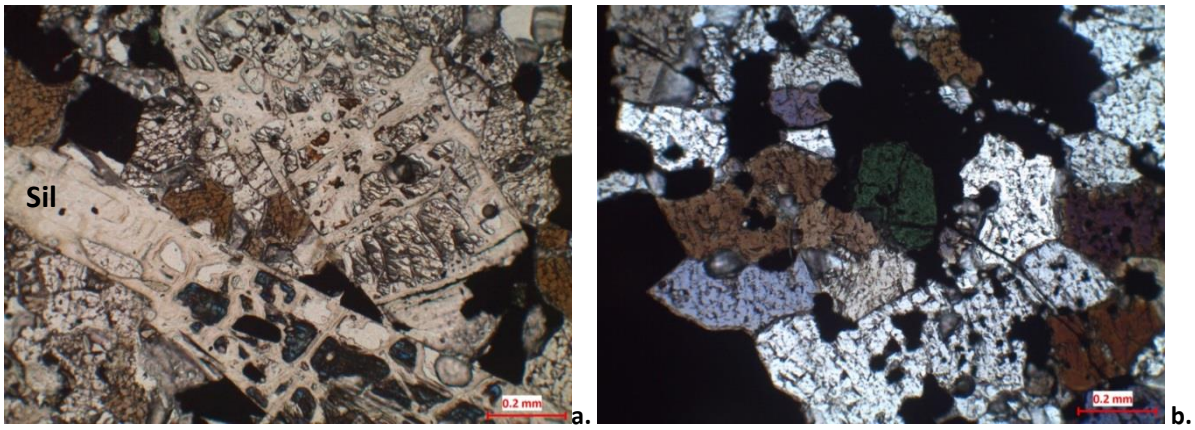

Figure 13. Transmitted light optical image of non-sulfide minerals in sample suite G2: (a) cream / pale pink needles of sillimanite, rich in inclusions of quartz and pyroxene; and (b) cross polarised light optical image of emerald-green hercynite enclosed in an assemblage of magnetite and pyroxene grains

f. Mineral Chemistry of Selected Mineral Species

i. Garnets

With regard to garnet chemical compositions (Appendix), the A Unit is dominated by spessartine-grossularite compositions, whereas Unit C is dominated by spessartine-almandine compositions. The upper part of Unit C, however (samples 166-160), records a relative increase in the modal component of andradite at the expense of almandine. This essentially marks the transition between sub-units C1 and C2 as described elsewhere (Rozendaal, 1986; Stalder and Rozendaal, 2004; see also Table 1). In absolute mineral-chemical terms, average garnet from

the A Unit has higher total Fe-oxide and MnO and lower Al_2O_3 and CaO values that those registered in the C Unit. The MgO content is very low (generally <1 wt%) throughout the A and C Units, in agreement with Stalder (2003).

The lack of suitable quality and quantity of garnet data from Unit A precluded their use in stratigraphic considerations, hence the latter will focus entirely on garnet analyses from the C Unit. Table 3 lists such average chemical analyses and standard deviation values from 52 garnet grains from the C Unit.

Table 3. Average mineral-chemical analytical data and corresponding standard deviation values (1σ) for garnet grains from drill core G1 in the C Unit of the GIF.

	Sample Number / Depth (m)											
	160 (n = 13)		**168 (n = 7)**		**172 (n = 9)**		**176 (n = 4)**		**178 (n = 13)**		**180 (n = 6)**	
	Ave	**StdDev**	**Ave**	**StdDev**	**Ave**	**StdDev**	**Ave**	**StdDev**	**Ave**	**StdDev**	**Ave**	**StdDev**
SiO_2	36.05	0.51	36.38	0.26	36.47	0.12	37.02	0.11	36.25	0.26	36.36	0.05
TiO_2	0.18	0.04	-	-	-	-	-	-	0.01	0.01	0.05	0.02
Al_2O_3	13.55	0.70	18.19	0.18	19.32	0.22	20.36	0.40	18.44	0.74	18.37	0.61
FeO	4.57	3.69	4.40	5.76	16.53	5.07	11.35	0.59	11.45	1.37	5.75	0.24
Fe_2O_3*	7.37	4.35	13.46	5.99	16.11	1.65	0.00	0.00	0.00	0.00	0.00	0.00
MnO	33.59	1.04	21.61	0.41	9.40	3.12	26.43	0.36	27.55	1.25	36.36	0.22
MgO	0.58	0.05	0.54	0.01	2.15	0.46	1.07	0.06	0.99	0.05	1.24	0.13
CaO	4.26	0.32	5.85	0.36	0.51	0.14	3.79	0.41	4.66	0.39	1.48	0.27
Na_2O	-	-	-	-	0.01	0.01	-	-	0.01	0.01	-	-
P_2O_5	0.01	0.01	-	-	-	-	-	-	-	-	-	-
K_2O	-	-	0.02	0.01	0.02	0.01	-	-	0.01	0.02	0.02	0.01
Total	100.16	0.36	100.45	0.32	100.52	0.29	100.02	0.25	99.36	0.47	99.64	0.20

n = number of samples; * = calculated; - = not detected

Averaged compositional profiles for major element oxides in garnet across the C Unit are illustrated in Figure 14. The average MgO concentration does not exceed the value of 1.3 wt%, with the single exception of sample 172 where a value of just over 2 wt% is recorded. From a quantitative point of view, the concentrations of Fe_{Total} and MnO show an apparent antithetic behaviour, at least over the lower part of the profile (sub-unit C1). Fe_{Total} increases from ~6 wt% at the transition with the mineralized B Unit to ~32 wt% at sample 172; thereon, the concentration of Fe_{Total} fluctuates over a narrow range and declines mainly at the top of the intersection (from sample 166 upwards) to a value of ~12 wt% at the top of the C Unit (sub-unit C2). The concentration of MnO mirrors that for Fe_{Total}: a progressive decline is seen in the lower half of the section from 26.36 wt% at the base to the value of 8.61 wt% in sample 172. Thereafter, MnO values remain effectively invariant up to sample 164, where the onset of increasing MnO occurs up to a value of 33.50 wt% at the stratigraphic top, reflecting a corresponding increase in modal spessartine.

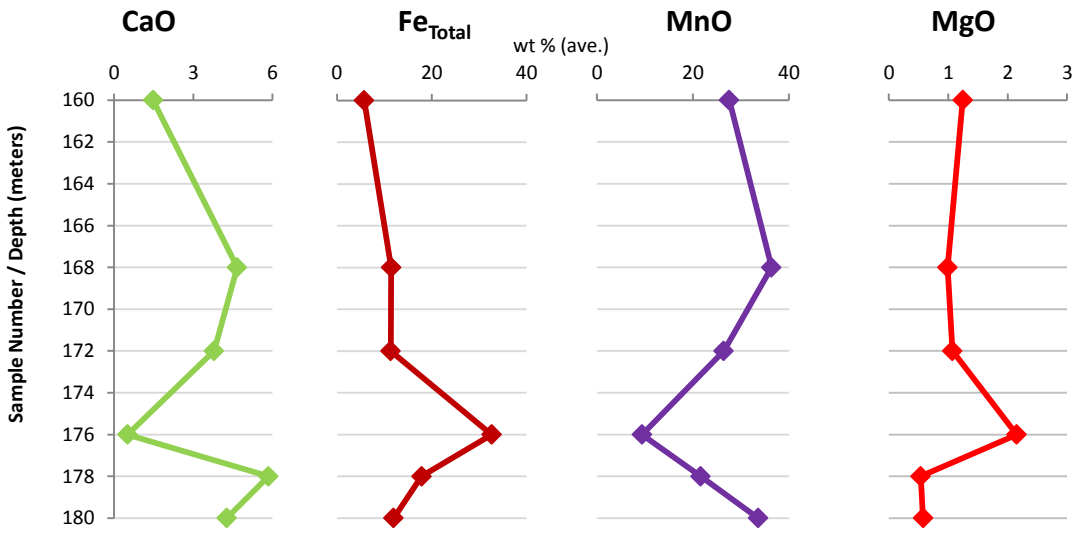

Figure 14. Mineral-chemical depth profiles for averaged garnet compositions across the C Unit of drill core G1.

Finally, the behaviour of CaO in the upper part of the C Unit reflects the change in the mineralogy of Ca-bearing garnet across the section: the lower half is characterized by very low average CaO contents hosted mostly in the grossularite component. However, the general increase in modal andradite in the upper part of the section results not only in an attendant sharp increase in average CaO up to 18.47 wt% at a depth of 164m, but also a broadly comparable stratigraphic profile with that of Fe_{Total}. From 164m to the topmost part of the sample section, the concentration of CaO decreases down to 4.26wt%, in unison with a relative decline in modal andradite towards the stratigraphic top.

ii. Pyroxenes and Pyroxenoids

Averaged elemental oxide concentrations for pyroxene grains from a total of 52 micro-analyses obtained from the C Unit, are listed in Table 4.

Table 4. Average mineral-chemical analytical data and corresponding standard deviation values (1σ) for pyroxene grains from drill core G1 in the C Unit of the GIF.

	Sample Number / Depth (m)											
	164 (n = 6)		**168 (n = 2)**		**170 (n = 32)**		**172 (n = 6)**		**174 (n = 4)**		**176 (n = 2)**	
	Ave	**StdDev**			**Ave**	**StdDev**	**Ave**	**StdDev**	**Ave**	**StdDev**		
SiO_2	52.47	0.36	50.28	0.18	47.64	1.14	48.58	0.38	48.81	0.31	50.68	0.11
TiO_2	0.02	0.00	0.00	0.00	0.00	0.00	0.00	0.01	0.03	0.01	0.00	0.00
Al_2O_3	0.30	0.06	0.15	0.00	0.07	0.06	0.35	0.02	0.19	0.03	0.13	0.02
FeO	7.12	0.21	8.71	0.29	24.48	2.80	34.71	1.07	31.20	1.10	18.00	0.27
MnO	9.12	0.36	9.80	0.31	16.79	4.44	4.14	0.33	11.09	0.40	15.95	0.27
MgO	10.14	0.41	9.26	0.60	4.19	1.05	11.27	0.57	6.86	0.43	12.89	0.17
CaO	18.84	0.18	20.29	0.14	5.93	5.18	0.03	0.03	0.43	0.02	1.09	0.02
Na_2O	1.32	0.13	0.29	0.12	0.04	0.03	0.03	0.01	0.02	0.01	0.02	0.01
P_2O_5	0.01	0.00	0.00	0.00	0.00	0.00	0.00	0.00	0.01	0.01	0.00	0.00
K_2O	0.00	0.00	0.04	0.01	0.02	0.01	0.02	0.01	0.00	0.00	0.00	0.00
Total	99.34	0.37	98. 82	0.16	99.16	0.49	99.15	0.67	98.64	0.13	98.76	0.03

n = number of samples

The chemical composition of pyroxene here reveals two end-member compositional “clusters”, namely a Ca-poor group dominated by ferrosilite in the lower part of the section (12 analyses, samples 176-172); and a Ca-rich group in the upper part of the section (samples 170-164) which is also represented by the majority of micro-analyses available (n=40). These two pyroxene groups would respectively correspond to subzones C1 and C2. The Ca-rich group, when plotted on a ternary diagram for end-member Ca-pyroxenes (Figure 15) reveals compositional variability from diopside-poor to more diopside-rich assemblages stratigraphically upwards.

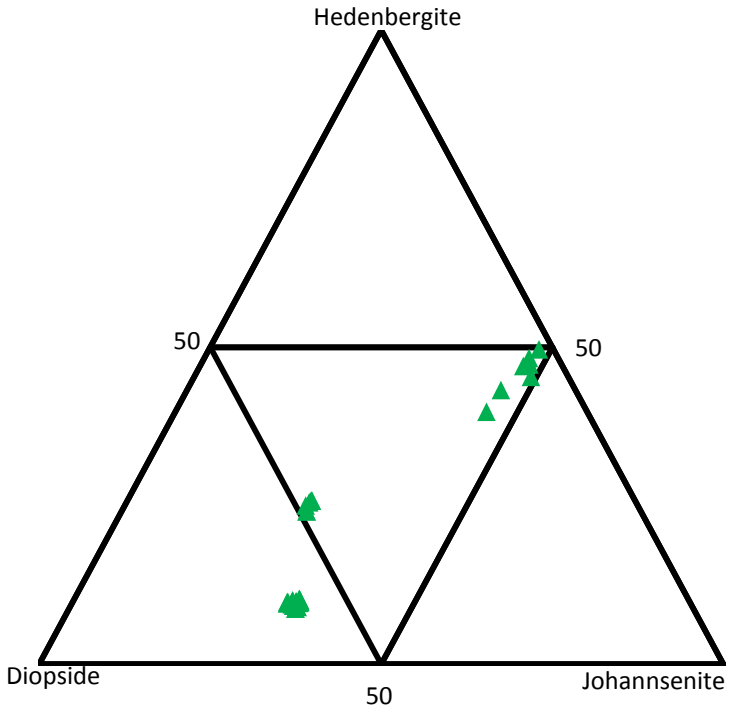

Figure 15. Hedenbergite-Diopside-Johannsenite ternary plot for Ca-clinopyroxene grains in the upper part of the C Unit (sub-unit C2) of drill core G1.

Depth profiles for averaged pyroxene compositions across Unit C from adjacent to the contact with the sulfidic B Unit (sample 176) up to sample 164 are shown in Figure 16. Arguably the most striking signature observed on the profiles is the stratigraphic distinction between the

lower, Ca-poor pyroxene group and the upper, Ca-rich one. The profiles indicate a broadly antithetic relationship between FeO and MnO in the Ca-poor portion of the profile, followed by an antithetic relationship between CaO and FeO in the upper, Ca-rich portion with respect to pyroxenes. MnO displays a largely sympathetic relationship with CaO in the latter, whilst MgO appears, for all intents and purposes, invariant across the entire C Unit.

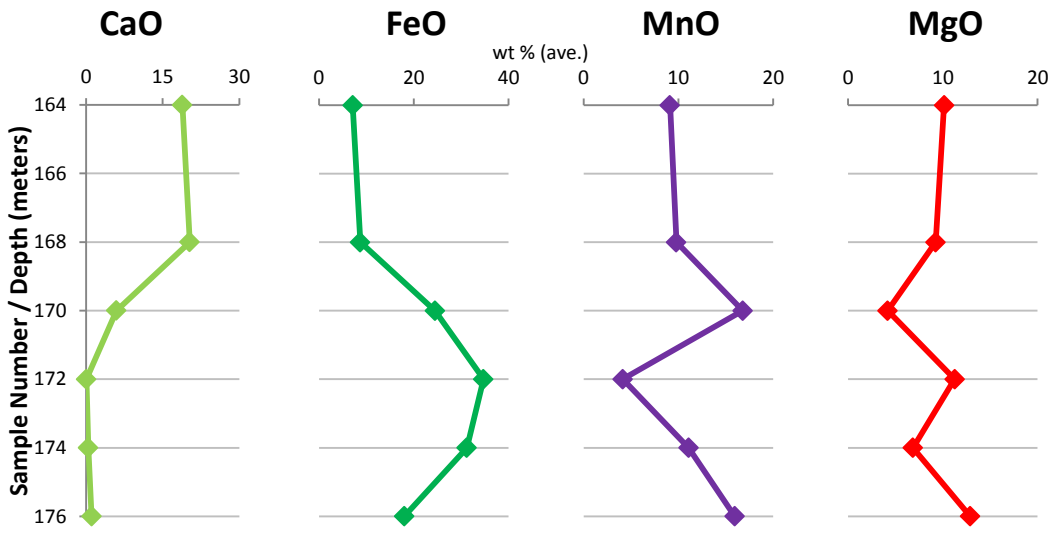

Figure 16. Mineral-chemical depth profiles for averaged pyroxene compositions across the C Unit of drill core G1.

With regard to pyroxenoids, averaged elemental oxide concentrations are listed in Table 5. The lack of sufficiently well-resolved mineral-chemical data did not permit the construction of stratigraphic profiles for neither the C, nor the A Unit. Nonetheless, with regard to pyroxenoid compositions in the upper portion of the C Unit, these contain more manganese in their structure than those seen stratigraphically lower, with MnO values up to 41.27wt%; accordingly, these pyroxenoid grains are readily classified as reflecting the Mn end-member rhodonite.

Table 5. Average mineral-chemical analytical data and corresponding standard deviation values (1σ) for pyroxenoid grains from drill core G1 in the C Unit of the GIF.

	Sample Number / Depth (m)							
	160 (n = 2)		164 (n = 8)		166 (n = 2)		168 (n = 17)	
			Ave	StdDev			Ave	StdDev
SiO_2	48.22	47.80	48.18	0.28	46.39	47.20	46.65	0.46
TiO_2	0.00	0.00	0.00	0.00	0.00	0.00	0.00	0.00
Al_2O_3	0.01	0.01	0.04	0.06	0.03	0.01	0.09	0.31
FeO	3.16	5.14	3.59	1.02	5.17	5.11	5.50	0.57
MnO	41.79	40.87	38.62	1.09	39.33	41.93	39.12	1.22
MgO	2.22	4.50	1.99	0.45	2.04	4.29	1.99	0.39
CaO	4.62	2.23	7.08	0.70	6.89	2.31	6.54	0.19
Na_2O	0.00	0.00	0.03	0.04	0.02	0.03	0.09	0.07
P_2O_5	0.00	0.00	0.00	0.01	0.00	0.00	0.00	0.00
K_2O	0.01	0.04	0.00	0.01	0.02	0.03	0.03	0.01
Total	100.03	100.58	99.55	0.23	99.89	100.91	100.00	0.58

n = number of samples

iii. Amphiboles

Averaged elemental oxide concentrations and standard deviation values for amphibole micro-analyses of selected samples from Unit C, are presented in Table 6 and graphically illustrated in Figure 17. In general, amphibole compositions here are dominated by variable relative abundances in Fe-Mg-Mn-Ca oxides, in comparison with the compositions of other silicate species discussed earlier (*i.e.* garnets and pyroxenes). The mean oxide abundances of magnesium is at 15.29wt%; calcium at 4.57wt%; iron (as FeO) at 11.76wt%; and MnO at 11.82wt%.

Table 6. Average mineral-chemical analytical data and corresponding standard deviation values (1σ) for amphibole grains from drill core G1 in the C Unit of the GIF (*H_2O is assumed; all iron calculated as Fe^{2+}).

	Sample Number / Depth (m)					
	162 (n = 10)		168 (n = 2)		178 (n = 10)	
	Mean	StdDev			Mean	StdDev
SiO_2	52.26	2.02	54.19	51.73	52.98	0.67
TiO_2	0.01	0.01	-	-	-	-
Al_2O_3	0.20	0.10	0.16	0.05	0.12	0.06
FeO	12.35	3.71	8.87	13.28	14.05	0.72
MnO	14.91	9.56	6.83	17.25	13.72	2.47
MgO	14.81	4.87	15.79	13.41	15.27	1.59
CaO	2.09	1.43	10.53	0.33	1.11	0.55
Na_2O	0.04	0.02	0.12	0.02	0.03	0.02
K_2O	0.02	0.01	0.02	0.02	0.02	0.01
Total	96.70	0.46	96.50	96.08	97.30	0.56

n = number of samples; - = not detected

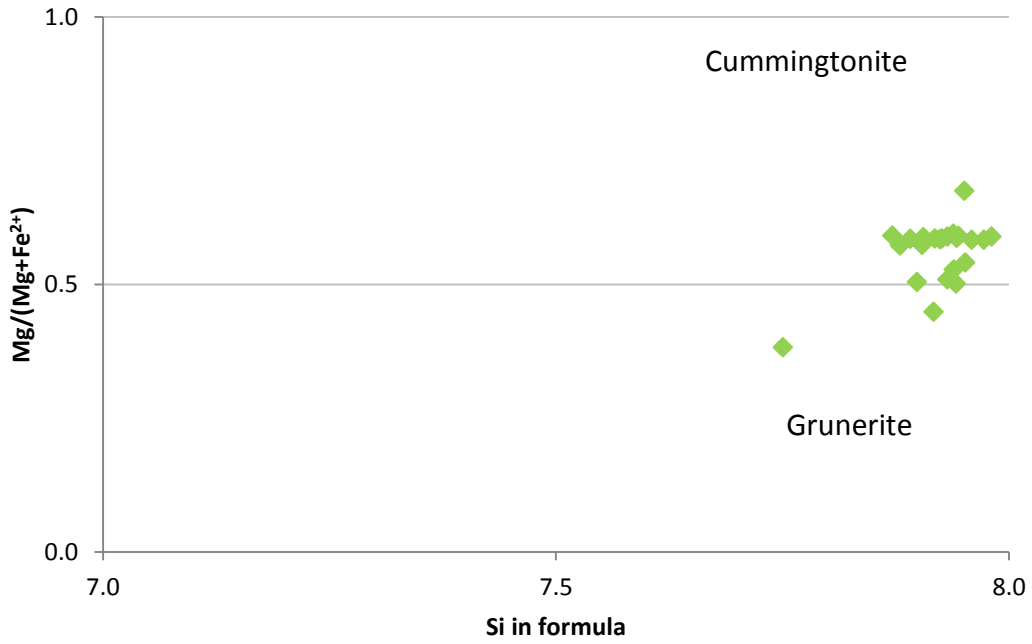

Figure 17. Amphibole classification diagram for Mg-Fe-Mn-Li amphiboles in the C Unit of drill core G1 in the GIF, calculated according to the parameters of Leake *et al.* (1997): (Ca + Na) < 1.00; (Mg, Fe^{2+}, Mn, Li) ≥ 1.00; and Li < 1.00.

iv. Carbonates

Table 7 reports compositional data for calcite grains from both the A and C Units of drill core G1. Notable here is the relatively increased abundance of MnO in calcites of the C Unit relative to those from the A Unit, with respective mean values at 5.36 wt% and 3.12 wt% (note however, the appreciable standard deviation values in both instances). Irrespective of those variations, the average MnO calcite across both Units A and C of drill core G1 permits the classification as *manganoan*.

Table 7. Compositional mean and standard deviation (1σ) values for calcite grains in the A and C Units of drill core G1 of the GIF.

	A Unit n = 14		**C Unit n = 26**	
	Mean	**StdDev**	**Mean**	**StdDev**
SiO_2	0.12	0.12	0.25	0.96
FeO*	0.48	0.34	0.36	0.18
MnO	3.12	1.65	7.45	2.71
MgO	0.16	0.12	0.27	0.27
CaO	55.77	3.79	50.34	2.37
P_2O_5	0.01	0.01	0.01	0.01
Total	59.70	2.31	58.71	4.19

n = number of samples; * = calculated; - = not detected

g. Bulk geochemical considerations

A total of 16 samples from the A and C Units of drill core G1 (eight from each unit) were subjected to bulk-rock geochemical analyses for their major and minor element oxide compositions. Analyses were carried out via the X-ray fluorescence (XRF) technique at Rhodes University on a Phillips PW1410 instrument available in-house. Measurements were obtained on fusion discs made from original rock powders by the author. Preparation was based on the protocol of Norrish and Hutton (1969), following ashing procedures in a blast furnace at 1000^{o}C for a minimum of 6 hours to determine the *loss on ignition* (LOI). Reduction of analytical data

and relevant correction procedures were carried out using a variety of international standards as well as custom-made in-house standards and blanks, especially with respect to Mn and Fe.

Although trace element analyses were beyond the scope of this study, pressed powder pellets were also made in accordance with the method of Norrish and Hutton (1969) for the determination of whole-rock abundances of Na, Zn, Pb and Cu. Whereas Na is routinely measured on pressed pellets via the XRF technique, the concentrations of especially Zn and Pb were evidently too high for the standards available in-house for samples adjacent to the contact with the B unit (reflecting their appreciable modal concentrations of sphalerite and much less so of galena), thus rendering the XRF technique unsuitable for these elements in this instance. For that reason, powders of the same samples were analysed for Zn and Pb at the Analytical Services Division (ASD) at Mintek, Randburg, using the ICP-OES for the determination of their absolute abundances. The resultant data were converted to sulfides and added to the XRF analyses, and all data are provided in Table 8. The main added objective of the acquisition of bulk geochemical data in this study was to draw comparisons with data from similar deposits elsewhere, assess and interrogate them against mineral chemical data presented earlier and *vice versa*, and draw some first conclusions with regard to the origin of the mineralised GIF at Gamsberg.

i. Results

Table 8 presents all bulk geochemical results. The dominant oxide in the A Unit is SiO_2 (from 52.88 to 67.13 wt%), reflecting the prevalence of quartz as the main silicate phase, followed by bulk Al_2O_3 which ranges between 8.98 and 24.64 wt%. K_2O varies from as low as 0.01 to as high as 5.52 wt%, reflecting a correspondingly variable combined potassium phyllosilicate±feldspar component across the A Unit. Bulk Fe (as FeO) and Mn (as MnO) values range from 5.01 to 15.17 wt% and 0.65 to 8.11 wt% respectively, whilst CaO varies from 0.28 to 7.59 wt%, with the highest values recorded in the lower part of the A Unit, similarly to MnO. MgO values exhibit a

narrow compositional range that does not drop below 0.5wt% nor does it exceed the maximum of 3wt%, in either the A Unit nor in the C Unit.

By comparison with the A Unit, Unit C displays significantly lower bulk SiO_2 (although sample 172 is exceptionally siliceous); the same applies also to the range of bulk Al_2O_3 values, the latter not exceeding 6.6wt% (sample 160). Bulk FeO and MnO are most certainly the dominant oxide species here, with the former ranging between 15 and 43 wt% whilst the latter is as high as 27.24wt% in the upper part of the C Unit (sample 162). Bulk CaO fluctuates widely, from as low as 0.06 (sample 172) to as high as 18.56wt% (sample 166).

The behaviour of major element oxides across the A and C Units of drill core G1 is shown graphically in the profiles of Figure 18. In general, the profiles of the A Unit show relatively narrow stratigraphic variations for practically all elemental oxides, in marked contrast to Unit C where fluctuations in practically all elemental oxides is noteworthy, except for the profiles for combined bulk values of Al_2O_3 + TiO_2. MnO and CaO display a generally good sympathetic behaviour across the entire section. In absolute terms, the higher absolute abundance of FeO, MnO and CaO and lower SiO_2 + Al_2O_3 in the C Unit relative to the A Unit, is perhaps the most notable feature of the respective profiles. Further evaluation and discussion of these and other geochemical relationships will follow in subsequent sections of this chapter.

Table 8. Bulk, major element oxide (via XRF), and Zn and Pb sulfide (via ICP-OES) concentrations of samples from the A and C Units of drill core G1 of the GIF. All Fe reported as FeO; bd = below detection.

	Concentration (wt%)														
Sample	**SiO_2**	**MgO**	**Al_2O_3**	**TiO_2**	**CaO**	**MnO**	**FeO**	**Na_2O**	**K_2O**	**P_2O_5**	**LOI**	**H_2O^-**	**ZnS**	**PbS**	**Total**
SF 160	38.95	0.91	6.61	0.44	2.68	16.96	23.17	0.07	0.71	0.31	8.67	0.25	0.27	bd	100.01
SF 162	36.86	1.99	4.40	0.38	7.10	27.24	17.93	0.11	1.08	0.48	1.66	0.28	0.63	bd	100.14
SF 164	33.70	2.63	4.22	0.27	9.31	12.77	29.32	0.27	2.77	0.52	3.93	0.26	0.58	bd	100.56
SF 166	31.08	1.22	2.28	0.20	18.56	15.49	26.84	0.14	0.15	0.46	2.64	0.28	0.43	bd	99.76
SF 168	28.29	1.37	2.11	0.15	11.84	16.65	34.82	0.08	0.00	0.69	4.80	0.16	0.70	bd	101.66
SF 172	75.58	0.56	1.96	0.09	0.06	1.23	15.71	0.33	0.05	0.03	1.54	0.28	1.66	0.36	99.44
SF 174	49.22	1.11	3.68	0.23	0.86	4.74	35.08	0.08	bd	0.36	3.59	0.14	0.45	0.08	99.61
SF 176	33.65	2.34	2.24	0.16	1.55	6.29	42.28	1.02	0.01	0.70	4.14	0.28	5.19	0.60	100.44
SF 218	52.88	2.10	24.64	0.82	1.52	0.65	5.01	0.09	4.98	0.25	3.49	0.56	0.40	1.00	98.40
SF 220	64.13	2.49	10.21	0.59	0.28	1.34	15.17	0.15	1.88	0.16	1.71	0.28	1.09	0.65	100.13
SF 222	66.61	1.56	9.74	0.61	1.11	1.82	8.41	0.07	2.47	0.16	5.96	0.29	0.40	0.08	99.29
SF 224	63.22	1.44	10.22	0.67	2.61	2.12	12.29	0.04	2.62	0.19	1.42	0.28	0.25	bd	97.37
SF 226	67.13	0.99	9.49	0.59	1.97	1.54	7.38	0.05	5.52	0.29	4.15	0.26	0.14	bd	99.51
SF 230	55.23	2.54	8.98	0.56	7.28	8.11	11.34	0.00	0.01	0.31	3.58	0.31	0.09	bd	98.34
SF 232	54.40	2.38	12.11	0.76	7.59	6.44	12.03	0.02	0.71	0.42	1.22	0.28	0.18	0.65	99.18
SF 234	58.54	2.73	13.49	0.78	5.41	2.27	10.07	0.01	1.27	0.23	3.86	0.28	0.11	bd	99.04

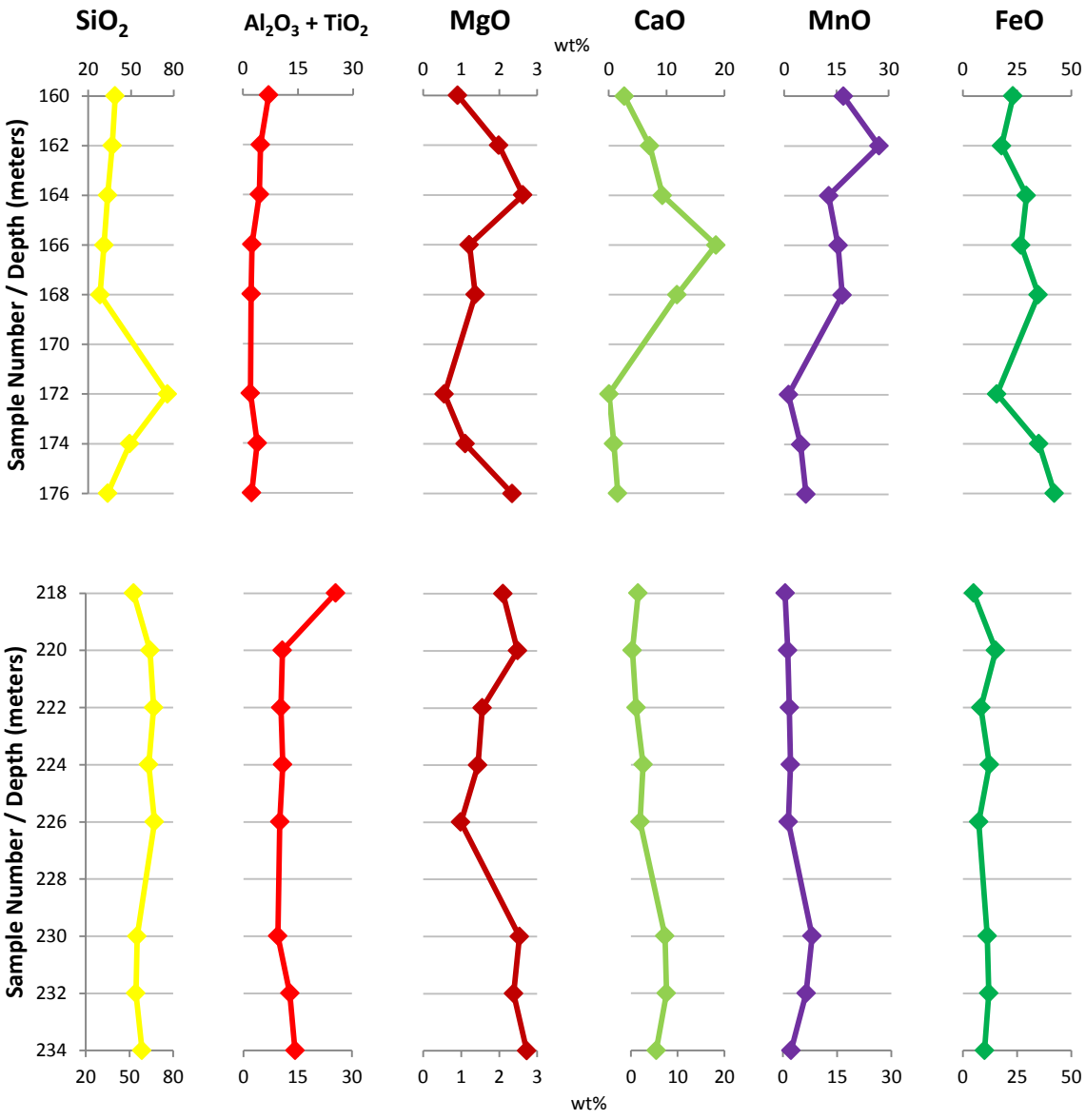

Figure 18. Depth profiles for major element oxide concentrations (in wt%) for Si, Al+Ti, Mg, Mn, Ca and Fe (as Fe^{2+}) *versus* depth for samples in the A and C Units of drill core G1 of the GIF.

ii. Mineralogical Controls on Bulk Geochemistry

The dearth of sufficiently well-resolved stratigraphic mineral-chemical data for the A Unit does not allow for considerations to be made in terms of vertical variations in the mineralogy of Unit A and their possible effects in bulk geochemistry. By contrast, data from the C Unit are

sufficiently well-resolved from a stratigraphic viewpoint, and therefore do permit some additional insights on comparison to bulk geochemical data. These are graphically illustrated in the collation of bulk, garnet- and pyroxene-specific compositional profiles of Figure 19.

With respect to CaO, it appears that a key control in the bulk variation across stratigraphy, and particularly the increase followed by a decline in the upper part of Unit C, is exerted by the sharp increase in Ca-pyroxene up-section, probably coupled by that of carbonate, and not so much by the relative abundance of Ca-garnet (*i.e.* andradite). Concerning FeO, it appears that the broad decline in bulk FeO up-section is reflected in the mineral-specific compositions of both average garnet and pyroxene. The same may also be said for bulk and at least garnet-hosted MnO, although these relationships may be obscured at least in part by other manganiferous phases such as calcite and locally jacobsite as well.

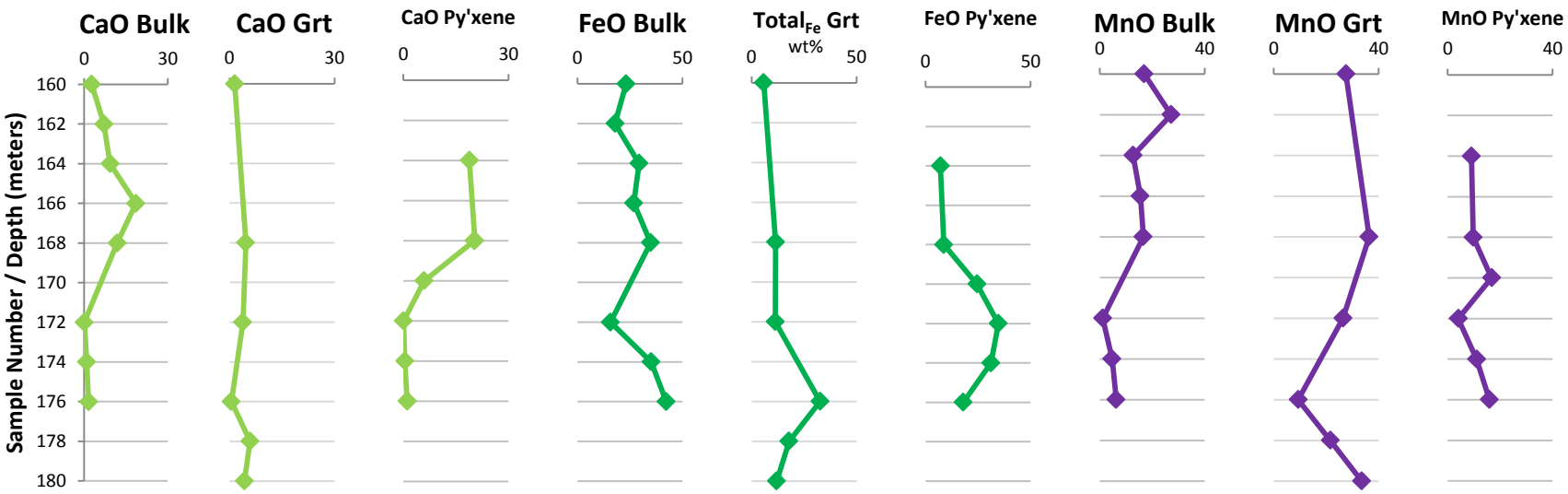

Figure 19. Summary of compositional depth profiles for MnO, CaO and total Fe (as FeO) for bulk rock, average garnet and average pyroxene, across the C Unit of drill core G1 of the GIF. Grt = garnet; Py'xene = pyroxene.

iii. Comparisons with Literature – Genetic Considerations

Spry *et al.,* (2000) as well as Heimann *et al.,* (2009) (based on previous work of Böstrom, 1973), propose a variety of geochemical applications and corresponding plots, aimed at constraining the origin and provenance of metamorphosed sediment-hosted massive sulfide deposits and associated host-rocks such as those from the classic locality of Broken Hill, Australia. The fundamental premise for the use of such diagrams is that the host rocks to sediment-hosted massive sulfide deposits will be expected to be dominated by two end-member primary components; namely an *allochtonous terrigenous* component reflected in the alumina-silicate siliciclastic fraction of the rocks and an *autochtonous hydrothermal-exhalative* component, which will be characterised by increased input to the sediment of base metal oxides of primarily Fe and Mn through submarine hydrothermal venting.

In principle, the contribution of Fe and Mn in (meta-)sedimentary rocks hosting SEDEX sulfide mineralisation, would vary through time and space in response to one or more pulse(s) of hydrothermal exhalation of metalliferous brines that punctuate background terrigenous clastic sedimentation. Amongst the plots used by Spry *et al.,* (2000) and Heimann *et al.,* (2009) and employed here, are the Al_2O_3-TiO_2 binary plot (Figure 20) as well as the binary plot of the bulk ratio of Al/(Al + Fe + Mn), against the log ratio of Fe/Ti (Figure 21).

Figure 20 illustrates a good linear relationship between Al_2O_3 and TiO_2 for the bulk dataset of this study, along with those from other similar deposits from the literature, including coticules (Spry, 1990; Stalder and Rozendaal, 2004, 2005; Heimann *et al.,* 2009). The strong positive correlation recorded for the new dataset presented in this thesis, and its striking similarity to previous data from Gamsberg in terms of the apparent slope and intercept of the data regressions, strongly argues for a common and essentially homogeneous terrigenous provenance for Al and Ti in both Units A and C of this study. Therefore, the relatively higher abundance of Al and Ti in Unit A relative to Unit C simply reflects the higher, albeit variable from one sample to the next, terrigenous detrital component in the former.

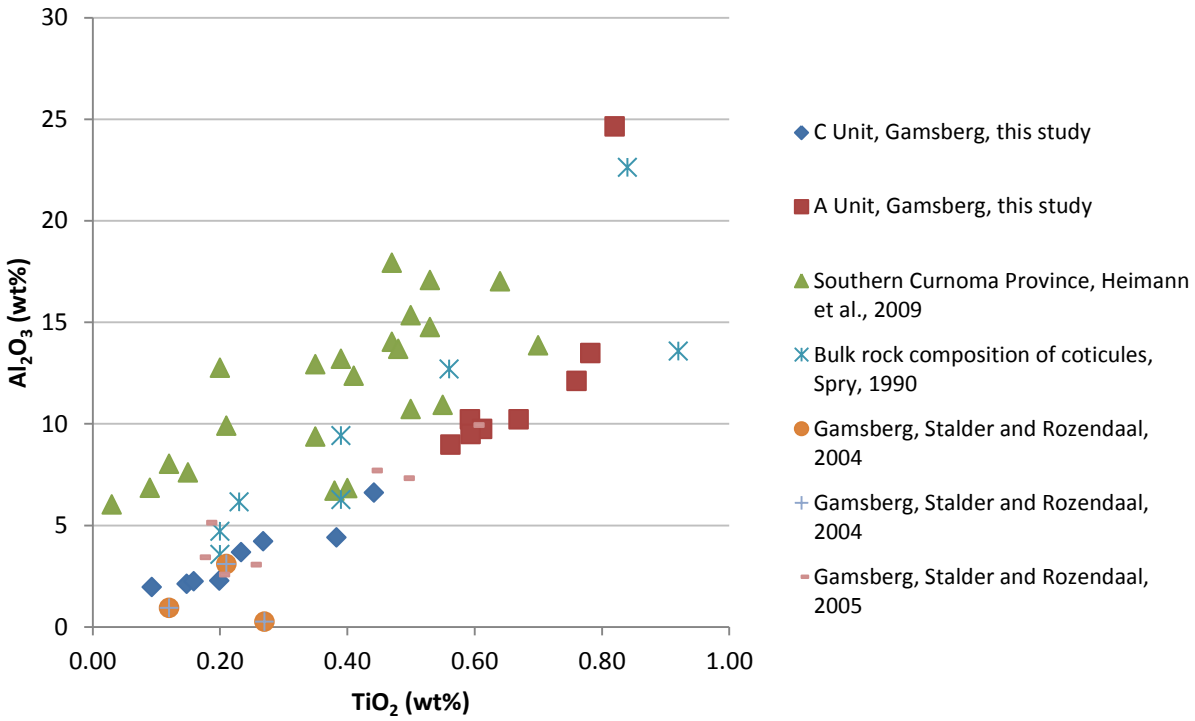

Figure 20. TiO_2 *versus* Al_2O_3 geochemical plot for the A and C Units of drill core G1 of the GIF. For comparison, data have also been plotted from deposits in Australia (Southern Curnamona Province and Broken Hill; Heimann *et al.,* 2009, and Spry, 1990) as well as from Gamsberg (Stalder and Rozendaal, 2004; 2005).

The relationship of Figure 20 forms a sound basis for the introduction of further geochemical parameters that can permit inference of the relative contribution of a hydrothermal component to the rocks comprising Units A and C. The application of the normal bulk ratio of Al/(Al + Fe + Mn), against the log ratio of Fe/Ti as illustrated in Figure 21 provides clues as to the relative interplay between hydrothermal and terrigenous-detrital components at Gamsberg. The distribution of all data points from this study, coupled with that of additional data from Gamsberg by Stalder and Rozendaal (2004; 2005) coincides very well with the mixing trajectory that links purely detrital/pelagic sediment from the Pacific Ocean, with end-member hydrothermal-exhalative sedimentary material from the East Pacific Rise (EPR). The diagram clearly illustrates that the C Unit examined in this study plots predominantly in the part of the trajectory adjacent to the EPR compositional point and for all intents and purposes can be referred to as a hydrothermal exhalite in origin. Unit A, whilst also containing a substantial hydrothermal component, has a much more dilute

hydrothermal signature as it is dominated by substantially more detrital material than in Unit C. In the context of the primary environment of deposition of these rocks, the foregoing relationships are collectively interpreted as reflecting a key syngenetic transition from a terrigenous-dominated (Unit A) to a hydrothermal-dominated (Unit C) style of deposition, punctuated by the main phase of massive sulfides in between (Unit B).

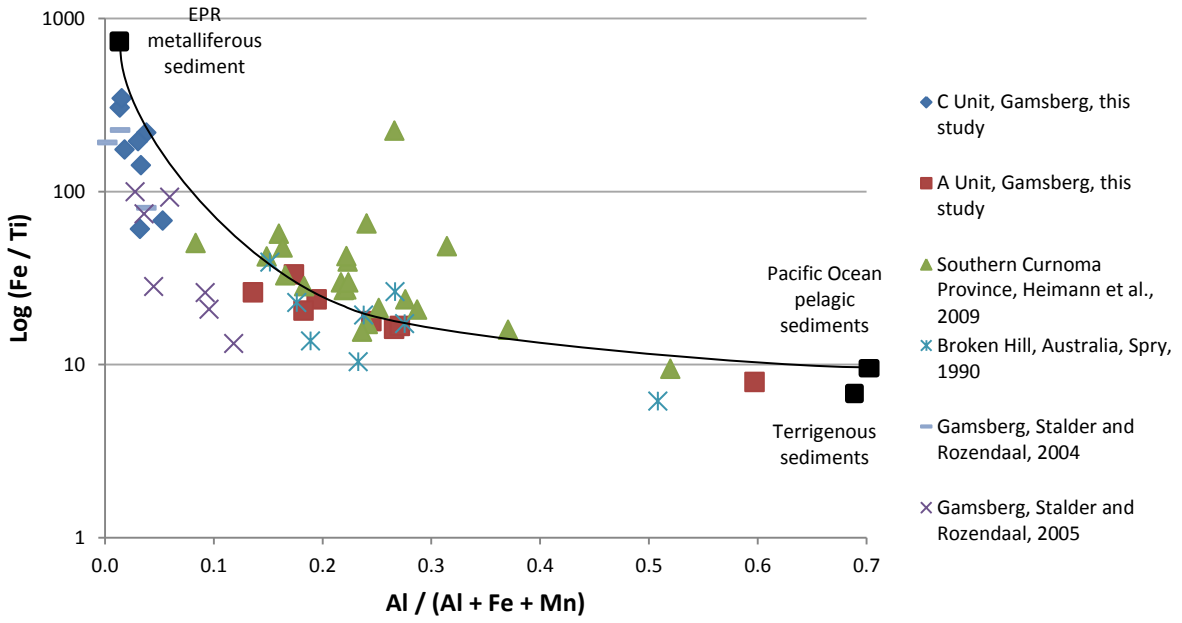

Figure 21. Al/(Al + Fe + Mn) *versus* Fe/Ti diagram showing bulk compositions of samples from the A and C Units of drill core G1 from the GIF. These are compared with additional data obtained from Heimann *et al.* (2009; and references therein) and Spry (1990), as in those of Figure 20. The black curve represents a mixing trajectory defined between the average end-member compositions of metalliferous sediment of the East Pacific Rise and pelagic/terrigenous sediments from the Pacific Ocean. Modified after Böstrom *et al.,* (1973).

h. Summary

The key results as presented in the foregoing sections of this chapter are summarized below:

- The A and C Units enveloping the Zn-rich sulfide mineralization in drill core G1 at Gamsberg, represent metamorphic silicate-facies assemblages dominated mostly by a mixed detrital/hydrothermal character in the footwall A Unit, and by a predominantly

hydrothermal-exhalative signature in the hanging wall C Unit. This is in broad accordance with previous descriptions of the same rocks in adjacent localities at Gamsberg by Rozendaal (1986), amongst others. The mineralogical and geochemical similarities between the Gamsberg deposit as examined here and the classic Broken Hill deposit of Australia, are also further reinforced.

- Geochemical profiles at bulk-rock and mineral-specific level, particularly of Unit C, reveal insightful stratigraphic relationships between the elemental oxides of Mn, Ca and Fe. A broadly sympathetic relationship between bulk CaO and bulk MnO is registered essentially across both units, whereas both profiles for Unit C are broadly replicated in the respective stratigraphic mineral-chemical records for pyroxene and garnet.
- Especially with regard to the uppermost, manganiferous portion of Unit C (sub-unit C2), it appears that the generation of complex Mn-containing metamorphic mineral assemblages faithfully retains the Mn-rich hydrothermal signature of the primary sediment at bulk as well as single-species level. Considering that the same part of the sequence is essentially devoid of co-existing metal sulfide, it is contended that any evidence (macroscopic, petrographic, geochemical or otherwise) that would point to high Mn content in similar rocks elsewhere, can potentially provide a reliable measure of the degree of hydrothermal input to the primary sediments and, by extension, the likelihood that they may be associated with economic, sediment-hosted base-metal massive sulfide mineralisation in geographic proximity.

5. MINERALOGY AND STABLE ISOTOPE GEOCHEMISTRY OF THE SULFIDIC B UNIT

The mineralized B Unit of the GIF at Gamsberg as captured in drill core G1 constitutes the focus of this chapter. The chapter is subdivided into two main parts: the first and shorter part is a presentation of the main petrographic and mineral chemical signatures of the sulfide ore, with emphasis on sphalerite as the key mineral species of economic value. Descriptions are based on standard ore microscopy performed on polished sections, coupled with electron microprobe analyses of sphalerite across the sampled section. The latter pertain mainly to the mineralized B Unit, but include limited data from the lower part of the C Unit as well. A small number of additional mineral-chemical and isotope data have also been obtained on ore separates from drill core G2, and are assessed in combination with the main sample suite of drill core G1.

The second – and longer – part of the chapter deals with the application of both traditional (*i.e.* S) as well as novel (*i.e.* Zn, Fe) stable isotope ratios obtained from hand-picked mineral separates (mainly sphalerite and pyrite) from across the B Unit. The primary aim is to detect any stratigraphic variations, where possible, in any of those parameters, assess the data in light of similar relevant information from the literature, and ultimately attempt to interpret these in the context of the primary environment of formation of the sulfide mineralization at Gamsberg. It should be emphasized here that, to the knowledge of the author, no *metal* isotope determinations have ever been carried out on the ores of the entire A-G District.

a. General Observations

The bulk ore mineralogy in the B Unit of drill core G1 conforms closely with previous reports in the literature on massive sulfide mineralization elsewhere at Gamsberg (*e.g.* Rozendaal, 1986; McClung, 2009; Stalder and Rozendaal, 2005a). The dominant ore constituent is sphalerite, accompanied with large modal amounts of pyrite right across the B Unit. These two minerals are followed by subordinate galena and lesser pyrrhotite in terms of modal abundance. Much smaller amounts of chalcopyrite and very minor arsenopyrite are also

observed. Graphite constitutes a common accessory opaque species throughout the largest part of the B Unit in section G1. Gangue mineralogy is in broad agreement with literature information (*e.g.* Rozendaal, 1986; Stalder, 2003) and includes primarily quartz, magnetite and phyllosilicates over the larger part of the B Unit, but becomes more calc-silicate-rich at the very top of the examined section and close to the transition with the C Unit.

i. Sphalerite Petrography and Mineral Chemistry

Sphalerite is essentially the only economically-important sulfide phase in the mineralized B Unit of drill core G1. This mineral occurs in modal amounts up to 5% in the lowermost sample of the overlying C Unit as well, implying an essentially gradual transition between Units B and C. The basal A Unit is much more impoverished in sphalerite and sulfides in general, with modal abundances in individual samples never exceeding 1% in total. Individual sphalerite grains range in shape and size from near-euhedral to anhedral, and from very fine- to medium-grained (0.01 to >2 mm). Microscopically, sphalerite from the B Unit appears dark brownish to grey in colour in plain polarised light, and exhibits pervasive deep-red internal reflections under cross-polarised light. A similar optical effect is observed on sphalerite-bearing polished thin sections from the C Unit under plain-polarised transmitted light (Figure 22a). The only exception to the above is the light-green to yellow, anhedral, medium- to coarse-grained sphalerite grains that are specifically seen at the transition between the B and C Units (sample 180); similar variations across this transition have also been reported by Stalder (2003).

In terms of textures under the microscope, sphalerite exhibits a variety of forms. These range from disseminated anhedral grains to porous, granoblastic aggregates with grain boundaries noticeable in part from the concentration of chalcopyrite exsolution. Symplectic textures of sphalerite with pyrite and less so pyrrhotite are also commonly noted. These are generally thought to represent mineral intergrowths resulting from metamorphic reactions that are said to have run to completion (Winter, 2001; see Figure 22b). Finally, replacement textures of sphalerite by silicate minerals are observed especially at the intersection of the B and C Units (Figure 23, Table 9);

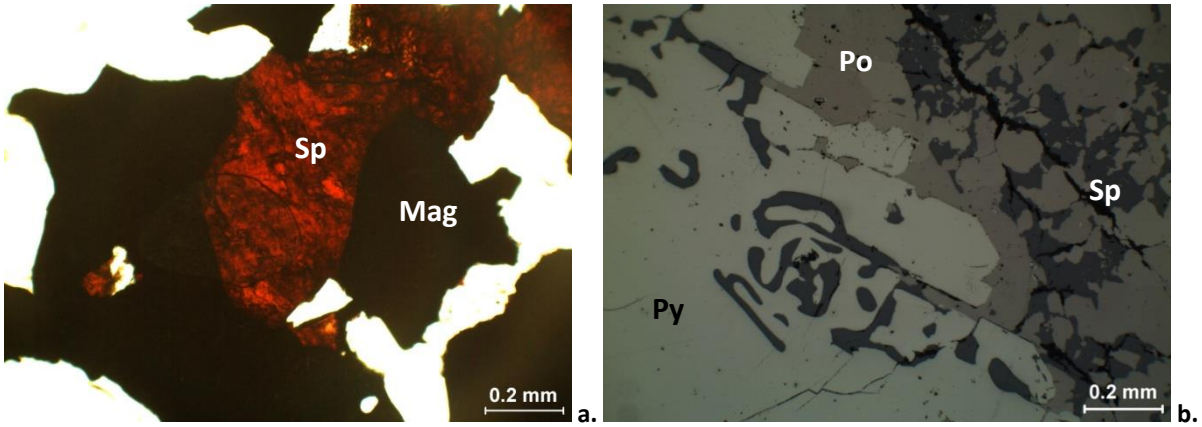

Figure 22. Reflected light optical images of: (a) red sphalerite in contact with magnetite, as seen under plane polarised transmitted light on polished thin section, sample 178; and (b) symplectic sphalerite intergrowth with pyrite and pyrrhotite, sample 188.

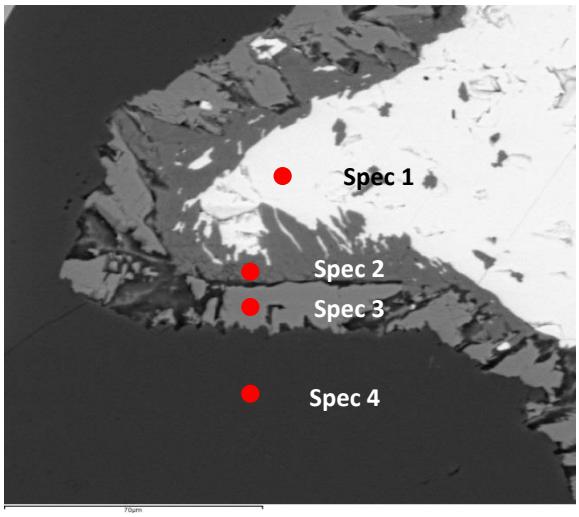

Figure 23. . Back-scattered electron image of a sphalerite grain (Spectrum 1) surrounded by a corona of pyroxene (spectrum 2) and pyroxenoid (Spectrum 3) in a quartz matrix (Spectrum 4), sample 180. Scale is 70µm.

Table 9. Semi-quantitative, normalized compositional values obtained from EDS-SEM spectra for the four analysed spots shown as red dots on Figure 23.

	Spec 1	Spec 2	Spec 3	Spec 4
Si	0.00	43.67	37.72	100.00
Mn	0.77	8.18	46.17	0.00
Fe	5.72	28.63	7.39	0.00
Mg	0.00	6.00	1.02	0.00
Ca	0.00	13.51	7.71	0.00
Zn	60.19	0.00	0.00	0.00
S	33.31	0.00	0.00	0.00
Total	**99.99**	**99.99**	**100.01**	**100.00**

Here, the use of SEM-EDS imaging and qualitative chemical analysis has permitted the identification of two successive replacement rims at the expense of sphalerite, suggesting an accompanying net loss in sulfur: the inner rim corresponds to a Fe-Ca-Mn-Mg-pyroxene composition, followed by an outer rim composed of Mn-rich pyroxenoid, all set in a matrix of quartz.

The sphalerite ore at Gamsberg is known to contain significant levels of substitution of Zn by Fe and Mn. This results in a relatively inferior ore quality when compared to other sphalerite-rich ores from the A-G District (Rozendaal, 1986; Stalder, 2003; McClung and Viljoen, 2010b; McClung and Viljoen, 2011). Moles (1983) notes colour variations in sphalerite in the Foss stratiform Ba-Zn-Pb deposit, Scotland, and attributes these to variations in the minor element contents; this equates to the now widely known variations of sphalerite as Fe-poor *versus* Fe-rich, with respectively contrasting optical properties. In the case of sphalerites from the B and C Units in drill core G1, and a few from the B Unit of drill core G2, microprobe analyses of sphalerite grains (Table 10) reveal significant substitutions of Zn by both Fe (up to 19wt% as FeS) and Mn (up to 11wt% as MnS).

Table 10. Mean and standard deviation (1σ) values for end-member sulfide components in sphalerite in drill cores G1 and G2 of the GIF.

	B Unit, Drill core G1**, n = 26**					**B Unit,** Drill core G2, **n = 8**					**C Unit,** Drill core G1**, n = 5**				
	Zn	**Fe**	**Mn**	**S**	**Total**	**Zn**	**Fe**	**Mn**	**S**	**Total**	**Zn**	**Fe**	**Mn**	**S**	**Total**
Mean	52.90	8.50	4.30	33.94	99.64	53.98	9.04	3.51	33.55	100.08	55.97	8.57	1.50	34.41	100.44
StdDev	4.98	2.60	2.23	0.36	0.51	5.73	2.72	2.80	0.26	0.37	1.11	0.80	0.39	0.57	0.46
	ZnS	**FeS**	**MnS**		**Total**	**ZnS**	**FeS**	**MnS**		**Total**	**ZnS**	**FeS**	**MnS**		**Total**
Mean	78.84	13.38	6.81		99.02	80.44	14.24	5.55		100.23	83.41	13.49	2.37		99.26
StdDev	7.42	4.09	3.52		0.40	8.54	4.28	4.44		0.47	1.66	1.26	0.62		0.31

n = number of analyses

Figure 24 displays stratigraphic profiles of mean sphalerite analyses. These profiles represent the majority of samples collected across the B Unit, as well as three samples from the lowermost portion of the overlying C Unit. The data are expressed as averaged end-member modal proportions of ZnS, FeS and MnS components in the analysed sphalerites, based on at least 4 spot analyses for each sample.

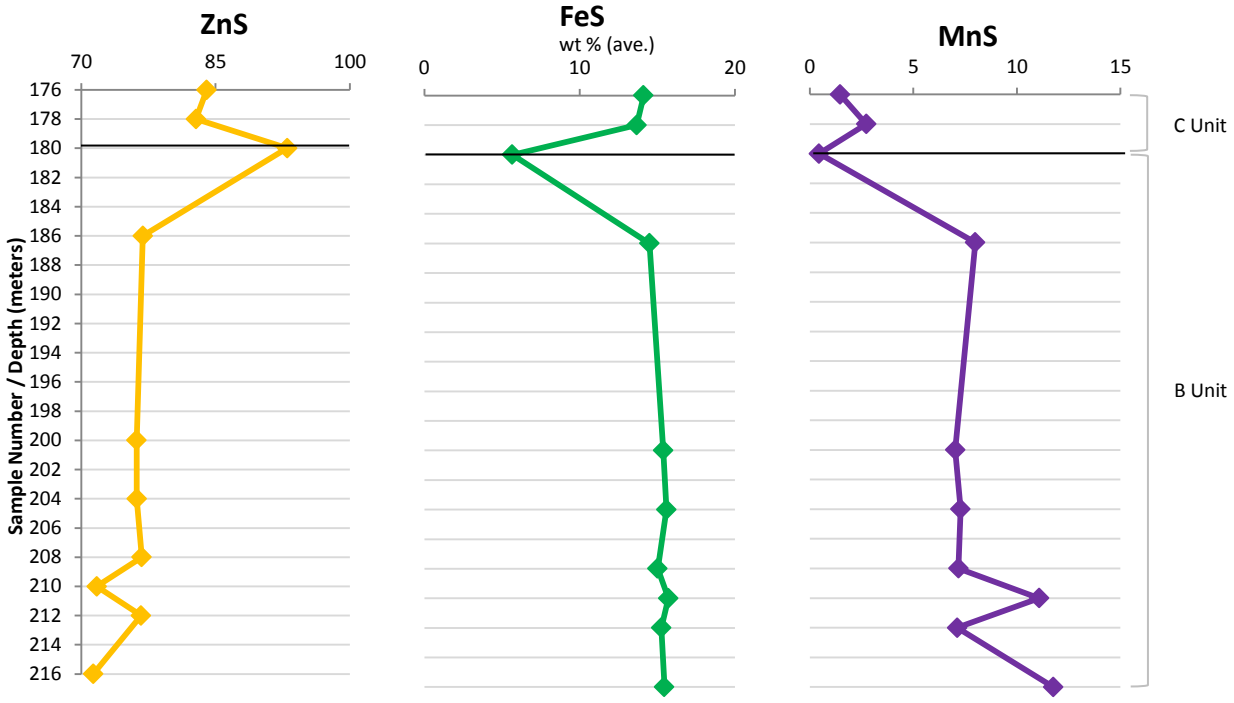

Figure 24. Stratigraphic variation in the averaged ZnS, FeS and MnS modal components within sphalerite grains in the B and lowermost C Units of the GIF, drill core G1.

The profiles of Figure 24 display relatively moderate variations in the concentrations of the three end-member sulfide components. The profile for modal FeS shows negligible stratigraphic variation across the entire profile at values around 13-14 wt%, with the single exception of sample 180. The profiles for ZnS and MnS, on the other hand, display somewhat more substantial fluctuations, particularly with regard to the uppermost part of the examined profile, *i.e.* the transition from Unit B to Unit C. These profiles are essentially antithetic in nature; that is, fluctuations in the modal abundance of ZnS in the structure of sphalerite appear to be controlled almost exclusively by corresponding fluctuations in the modal MnS component. The highest ZnS values are seen essentially at and above of the boundary between Unit B and Unit C, where both the optical properties of sphalerite (as mentioned earlier) and the gangue assemblage also differ from those over the largest part of Unit B. The reason for the relatively more Mn poor sphalerite across the said transition, may be sought in the gangue mineralogy of the ore, and specifically in the increased abundance of Mn-rich minerals such as pyroxenoid associated with the sphalerite (see also

Figure 23 and Table 9 earlier), which may control the preferentially partitioning of manganese in the silicate fraction relative to the sulfide fraction of the rock, whether *via* primary depositional processes and/or ones related to metamorphic overprint.

ii. Other Opaque Minerals

Pyrite (Figure 25a) is the most common sulfide phase in the B Unit and also occurs in the transition with the A Unit and through the entire C Unit. It occurs in a range of grain sizes and habits, from fine- to coarse-grained (0.01 to >2mm) and from sub-rounded to euhedral, respectively. **Pyrrhotite** (Figure 25a, b) occurs in close association with pyrite in the B Unit and occasionally in the C Unit as well. It occurs as individual dispersed grains (fine- to coarse-grained, subhedral to anhedral in habit), as granoblastic aggregates, and as complex intergrowths with pyrite. Grain boundary relationships between pyrite and pyrrhotite are variable and complex, reflecting the strong metamorphic and deformational processes that the ores have evidently experienced. Amongst the textures observed are recrystallised, annealed pyrite crystal aggregates, *en echelon* micro-lenses of pyrite filling apparent tension fractures in pyrrhotite; and deformation twinning along pyrrhotite grain boundaries.

Galena occurs in highly variable and generally very small modal amounts in association with sphalerite and iron sulfides. Medium-grained clusters of galena aggregates are readily visible with the naked eye. Under the microscope, galena displays its typical optical properties of high reflectance, very low polishing hardness, subhedral to sometimes euhedral habit, and very well developed double cleavage as manifested by triangular polishing pits (Figure 25c).

Chalcopyrite and arsenopyrite occur very rarely throughout the entire core section. **Chalcopyrite** occurs most commonly as exsolution “blebs” in sphalerite (Figure 25d), often concentrated along grain boundaries, but also as very fine- to fine-grained (0.01 to 0.1 mm) subhedral to anhedral grains included in other sulfides. **Arsenopyrite** was observed in only two samples in the form of fine-grained, subhedral to euhedral crystals in association with pyrite. Finally, **graphite** occurs widely across the B Unit as an accessory, non-sulfidic opaque

phase. It is present in the form of small (0.04 to 1 mm), subhedral flakes which may be strongly deformed (Figure 25e).

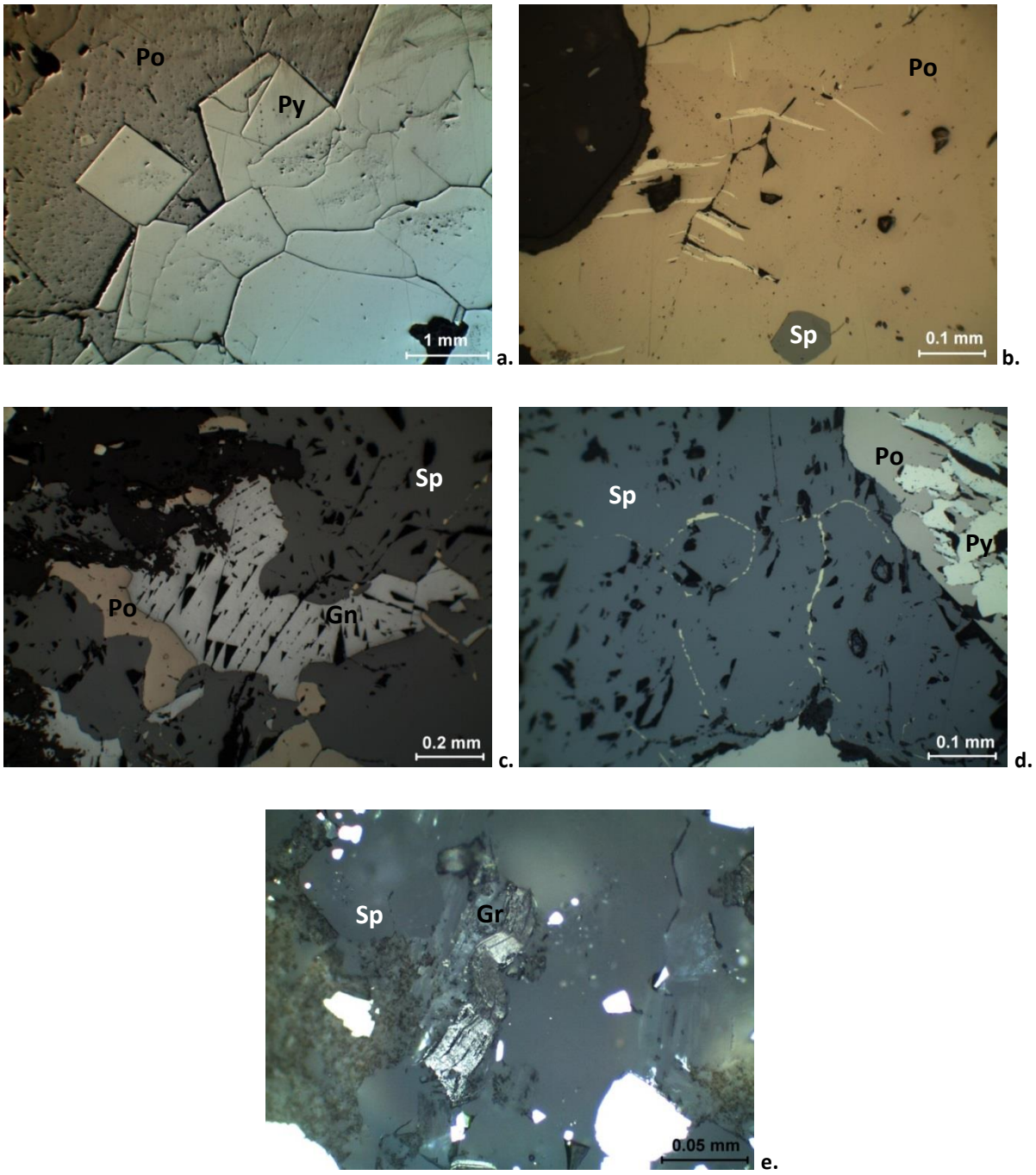

Figure 25. Reflected light optical images of: (a) annealed, subhedral to euhedral pyrite aggregate in a pyrrhotite matrix, sample 206; (b) *en echelon*, pyrite-filled tension gashes in pyrrhotite, sample 188; (c) anhedral galena displaying well developed polishing cleavages and surrounded by sphalerite and pyrrhotite, sample 202; (d) chalcopyrite exsolution along sphalerite grain boundaries, sample 202; and (e) bent/folded graphite in a sphalerite matrix, sample 216.

b. Stable Isotope Applications: Introduction and Methodology

A large number of published studies are available in the literature that document the use of sulfur isotopes of sulfides and sulfates from across the rock record as a whole, with emphasis both on ore genesis and palaeoenvironmental reconstructions. A good deal of the relevant literature has a direct focus on sulfide and barite pairs from SEDEX/BHT and VMS deposits, including the South African case studies from the A-G District (*e.g.* Von Gehlen, 1983; Strauss, 1993, 1997; Bailie *et al.,* 2010; McClung *et al.,* 2010). However, application of the so-called "non-traditional" stable isotopes (*e.g.* Fe, Zn and Cu, among others) has only recently begun to constitute a much more widely-used geochemical tool. Due to the revolutionary developments in mass spectrometry over the last few years, stable isotope abundances of heavier elements are now accessible and investigation of transition metal isotopes has become a new and fast developing research area (Zhu *et al.,* 2002). Fractionation of these metals has been attributed to processes such as fluid-solid reactions, redox reactions, inter-mineral equilibrium fractionation and the involvement of microorganisms (Markl *et al.,* 2006). However, unlike sulfur, the fractionation of metals such as Fe and Zn only takes place at low to moderate temperatures and decreases with increasing temperature; although fractionations of up to ~10‰ have been noted experimentally at temperatures up to 250°C (Markl *et al.,* 2006). Examples of studies with emphasis on Fe isotopes in hydrothermal ore deposits include those by Anbar (2004), Markl *et al.,* (2006) and Gagnevin *et al.,* (2012), whereas in a South African context, Fe isotopes have also recently found application in the study of manganiferous BIF from the Palaeoproterozoic Hotazel Formation (Tsikos *et al.,* 2010). Zinc isotope analyses have specifically been applied on sphalerite grains from the Red Dog District deposit of Alaska (Kelley *et al.,* 2009) as well as the Irish-type deposits (Wilkinson *et al.,* 2005).

In this study, a combination of S, Fe and Zn isotope analyses was applied on hand-picked mineral separates of sphalerite and pyrite (and one pyrrhotite) from the Gamsberg massive sulfide ore-body as available in drill core G1. This is the first instance where a combination of traditional and novel stable isotopes has been carried out in ores of the A-G District. A few such analyses were also carried out on additional sulfide separates from drill core G2 for comparative purposes.

Due to the intrinsic textural difficulties in picking pure sphalerite grains from each and every sample of the B Unit available to the author, combined with the prohibiting cost of the analyses themselves, only a relatively small and stratigraphically representative dataset was produced. Guided by ore petrography of corresponding polished sections, samples were fragmented into mm-scale particles from which mineral separates for both sphalerite and pyrite were hand-picked under the binocular microscope. With regard to sphalerite, special care was taken to pick as clean monominerallic grains as possible; to this end, in a few instances two adjacent samples were combined in order to provide sufficient volume of hand-picked material for analyses. In those cases, the ensuing sample label became a combination of the two samples originally blended (*e.g.* sample "SF205" represents a mix of fragmented material from samples "SF206" and "SF204"). Hand-picking of pyrite was a somewhat easier exercise, as the mineral occasionally forms much coarser grains than those of sphalerite.

i. Analytical Protocols

Analyses for S isotopes were carried out at the laboratory of stable isotope geochemistry of the Scottish Universities Environmental Research Centre (*SUERC*) in East Kilbride, Scotland, under the supervision of Dr. A.E. Boyce. Around 5 to 10mg aliquots of the powdered mineral separates were utilised for isotopic analysis. Minor contamination by non S-bearing phases was tolerated, and has no isotopic effect on the final data. Sulfides were analysed by standard techniques (Robinson and Kusakabe, 1975) in which SO_2 gas was liberated by combusting the sulfides with excess Cu_2O at 1065°C, *in vacuo*. Liberated gases were analysed on a VG Isotech SIRA II mass spectrometer, and standard corrections applied to raw $\delta^{66}SO_2$ values to produce true $\delta^{34}S$. The standards employed were the international standards NBS-123 and IAEA-S-3, and the SUERC standard CP-1. These gave $\delta^{34}S$ values of +17.1‰, -31.5‰ and -4.6‰ respectively, with 1σ reproducibility around ±0.2‰. Data are reported in $\delta^{34}S$ notation as per mil (‰) variations from the Vienna Cañon Diablo Troilite (V-CDT) standard.

Analyses for Zn and Fe isotopes were performed on powdered aliquots of the same hand-picked separates of sphalerite and pyrite, (as well as a single pyrrhotite), at the department of Earth Science and Engineering, Imperial College, London, under the supervision of Prof. J.J. Wilkinson. The analytical protocol of the iron isotope method used is comprehensively described in Chapman *et al.,* (2006), whereas for zinc isotopes, the double-spike method as presented in Arnold *et al.,* (2010) was employed.

The preparation of samples for Zn analyses was carried out in the clean room facility of the Imperial College, London. The digestion of the sulfides took place by the addition of HNO_3 and HCl at 120°C on a hotplate for 48 hours (Arnold *et al.,* 2010). The digested samples were then evaporated and dissolved in HCl and H_2O_2. These solutions were then redried and redissolved in HCl containing H_2O_2 to produce the aliquot for analysis. Removed zinc (by anion exchange chromatography) was evaporated and redissolved in HNO_3 and spiked with NIST-SRM 976 Cu for use as an independent mass discrimination monitor (Wilkinson *et al.,* 2005).

Isotopic measurements were performed with a GVi IsoProbe MC-ICP-MS instrument connected to a desolvating sample introduction system that was operated with a T1-H type nebulizer with an Aridus membrane. The Zn isotope data collected represents raw Zn isotope compositions and thus these were corrected to calculate true mass-bias-corrected values.

The Fe isotope protocol followed that of Zhu *et al.,* (2002). Specifically, samples were initially chemically purified by ion exchange chromatographic separation followed by complete digestion. The samples were treated with H_2O_2 and dissolved in HCl. For Fe separation, the samples were loaded and washed with 6M HCl to remove ions other than Fe and Zn, and then 2M HCl was used to strip Fe. Samples and standards were introduced into the mass spectrometer in dilute HCl solutions through a modified desolvating nebuliser.

ii. Sulfur Isotopes

The element sulfur is an important constituent in the exogenic cycle of the Earth: the evolution of the Earth's surface chemistry, the atmosphere and the oceans has resulted, in part, from changes in its sulfur cycle. The sulfur cycle (Figure 26) is dependent on the precipitation of evaporites from seawater (Strauss, 1997) as well as on the biological or abiotic fractionation between oxidized and reduced sulfur (Machel *et al.,* 1995). The isotope record of marine sedimentary sulfate through time has been successfully used to determine global variations of the composition of seawater sulfate (Strauss, 1997), through the construction of secular $\delta^{34}S$ curves (Figure 27). These are compiled primarily from the $\delta^{34}S$ record of evaporites which evolved in semi-closed or closed basins from oceanic water.

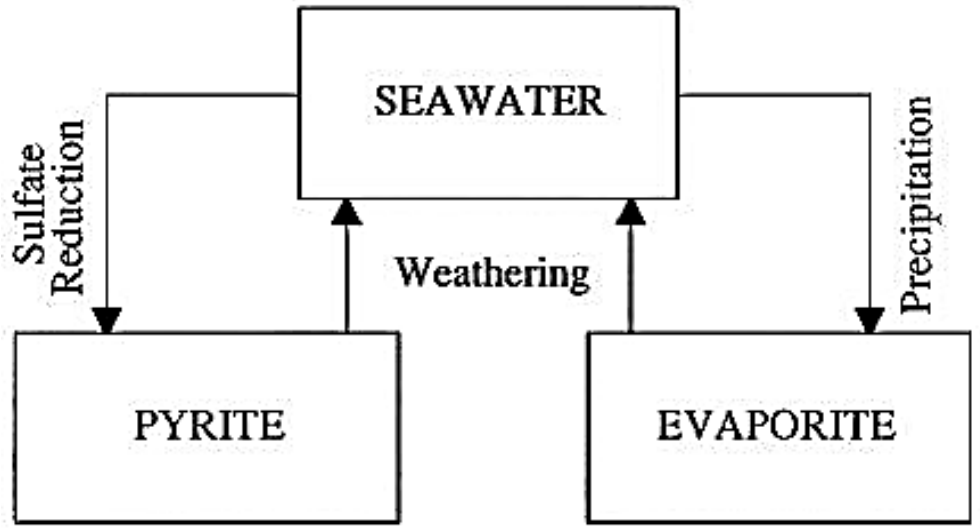

Figure 26. Main reservoirs of the sedimentary sulfur cycle (from Strauss, 1997).

As expected, only a limited number of Precambrian sulfate occurrences have been preserved (Strauss, 1993). The few available occurrences of evaporites from the Archean and Paleoproterozoic result in a very fragmentary record for that period, which is followed by a more continuous and thus better-resolved one from sedimentary sulfates of Meso- and Neoproterozoic age (Strauss, 1993). On the basis of such secular variations, the model for

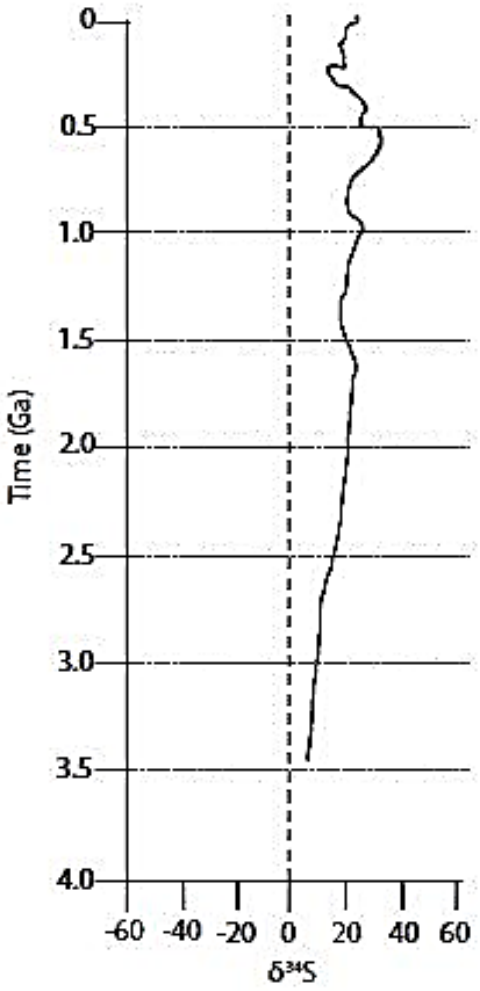

Figure 27. Secular variation curve of the isotopic composition of seawater sulfate through time (modified after Holland, 2006).

the evolution of sulfur incorporates three broad stages (Strauss 1997; Seal II, 2006; Farquhar *et al.,* 2010): (1) an Archean to early Proterozoic stage, where ancient seawater sulfate had a mean $\delta^{34}S$ value of ca. 4‰; (2) from ~2.4Ga to Permian and Triassic times, where the value of $\delta^{34}S$ ranged from a high of 33‰ to a low of about 10‰; and (3) to post-Triassic values, which despite sharp short-term fluctuations, $\delta^{34}S$ ranges about the average value of modern seawater sulfate of 21‰.

The sulfur isotope fractionation that accompanies the transformation from an oxidized to a reduced sulfur species is sensitive, dependent on temperature and pH, and occurs in both

biotic and abiotic environments. Two key processes are known to be responsible for such fractionation: **bacterial sulfate reduction** (**BSR**) and **thermochemical sulfate reduction** (**TSR**). Bacterial sulfate reduction takes place by the action of sulfate-reducing bacteria typically in shallow, low-temperature diagenetic environments (often close to the sediment-seawater interface), as well as in the water column of euxinic basins; TSR takes place abiotically in relatively higher-temperature environments.

According to Seal II (2006), sulfate-reducing bacteria are known to be active at temperatures between 0 and 110°C and pH values between 5 and 9.5. Machel *et al.,* (1995) and Machel (2001) report that the typical temperature range for BSR is from 0°C to 60/80°C. At temperatures above 60-80°C, most sulfate-reducing bacteria will cease to metabolize; however, some hyperthermophilic sulfate-reducing bacteria can live at temperatures as high as about 110°C (Machel, 2001). Thermochemical sulfate reduction has only more recently been recognized, and is said to take place at temperatures between 80 - 100°C and 150 - 200° (Machel *et al.,* 1995; Machel, 2001). Anderson and Thom (2008), however, place the upper temperature limit of TSR as high as 350°C. Thermochemical sulfate reduction is known to be thermodynamically possible at temperatures as low as 25°C, however, reaction rates are so sluggish as to be geologically insignificant (Machel, 2001).

The redox transformation of dissolved sulfate by both BSR and TSR are described by Seal II (2006) and Anderson and Thom (2008) and encapsulated by the following two reactions:

$$2CH_2O + SO_4^{2-} \rightarrow H_2S + 2HCO_3^- \quad (1)$$

$$SO_4^{2-} + CH_4 \rightarrow H_2S + CO_3^{2-} + H_2O \quad (2)$$

In both reactions, H_2S is the common end-product. Under open system conditions accompanied by sulfate replenishment, the reduction of sulfate through both pathways produces ^{34}S-depleted H_2S. Under closed-system conditions, the concentration of reactant sulfate decreases progressively and the isotopic compositions of both the reactant and product change predictably with time by Rayleigh fractionation processes (Strauss, 1997). In closed system conditions, early-formed H_2S will thus be expected to have a relatively low $\delta^{34}S$ isotope value, while the residual reservoir will be progressively enriched in isotopically

heavy sulfur; towards the end of the fractionation process, the H_2S produced will have an isotopic value that will approach that of the initial composition of the reservoir H_2S. If either of the reactions (1) and (2) take place in an environment where there are sufficient dissolved metals available, the H_2S produced reacts with the metals and readily forms metal sulfides (*e.g.* FeS, ZnS, etc.) through cooling, dilution or acid neutralization (Seal II, 2006). Precipitation of these metal sulfides is accompanied by relatively small isotopic fractionation from the source H_2S at any given time, and therefore will broadly record its isotopic signature in a conservative fashion.

The onset of BSR is nearly instantaneous and rates are extremely high in most geologic settings. However, this rate may be limited by a lack of and/or slow supply of reactive organic matter or sulfate (Machel, 2001). The rate of TSR is dependent on the initial total sulfur concentration, metal complexes, and the catalytic action of metals such that $Ni^{2+} > Co^{2+} > Mn^{2+} > Cu^{2+} > Fe^{2+} > Ca^{2+} = Mg^{2+}$, as well as the 'wettability' of sulfur (*i.e.* the amount of S that is dissolved in solution), amongst others (Machel, 2001). According to Machel *et al.,* (1995), the process of BSR may produce sulfur-isotope fractionations from -15 to as high as -65‰, while TSR is expected to produce the highest fractionation of up to -20‰ at 100°C, declining to around -15‰ at 150°C and -10‰ at 200°C: metal sulfides will thus be from 15 to 65‰ lighter than parent sulfate through BSR, and up to 20‰ lighter than parent sulfate by TSR depending on temperature.

Table 11 presents a compilation of ranges of $\delta^{34}S$ data for a wide range of geological reservoirs, where processes such as either bacterial and/or thermochemical sulfate reduction have taken, or are presently taking place.

Table 11. $\delta^{34}S$ values from various natural reservoirs of sulfides and sulfates.

	$\delta^{34}S$ value (‰)	Source
Modern seawater sulfate	+21.0 ± 0.2	Seal II, (2006)
Modern sedimentary sulfide	-50 to +20	Seal II, (2006)
Bulk MOR basalts	+0.3 ± 0.5	Seal II, (2006)
Sphalerite, galena and pyrite (Red Dog)	-45.8 to +12.3	Seal II, (2006), Kelley et al., (2004)
Modern MOR	0 to +6	Seal II, (2006)
Pyrite, pyrrhotite, sphalerite and galena (Sullivan)	-11 to 6‰	Seal II, (2006)
Pyrite, sphalerite and galena (Balmat-Edwards)	+11.5 to +17.5	Seal II, (2006)
CD-Pb-Zn (Phanerozoic) Sulfide	+12.2 ± 10.7	Farquhar *et al., (*2010)
CD-Pb-Zn (Phanerozoic) Sulfate	+25.1 ± 7.2	Farquhar *et al., (*2010)
CD-Pb-Zn (Proterozoic) Sulfide	+7.9 ± 9.9	Farquhar *et al., (*2010)
CD-Pb-Zn (Phanerozoic) Sulfate	+23.6 ± 10.4	Farquhar *et al., (*2010)
Barite (SEDEX)	+19 to +64	Johnson *et al., (*2009)
Seafloor hydrothermal deposits in non-sedimented MOR's	~0	Rouxel *et al., (*2004)
Sphalerite (Navan)	-13.2 to +14.6	Gagnevin *et al., (*2012)

iii. Iron Isotopes

Iron is the 4th most abundant element in the Earth's crust. During the Archean and Paleo-Proterozoic, large amounts of Fe were present in dissolved form as Fe^{2+} in the relatively oxygen-poor oceans of the time (Anbar, 2004; Beard and Johnson, 2004). As modern oceans (and the atmosphere) are oxygen-rich and constantly ventilated, the residence time and dissolved concentrations of iron within them are consequently much lower.

Iron occurs in two redox states: as reduced Fe^{2+} in oxygen-deficient environments or as oxidized Fe^{3+} in oxygenated environments. However, only the reduced, divalent form is soluble in aqueous solutions, unless the pH is low (Beard and Johnson, 2004). Ferrous iron plays a very important role in the anaerobic metabolism of bacterial micro-organisms (anaerobic iron oxidizers) that utilize it in respiration processes with solid ferric-hydroxide

being the key end-product. Chemoautotrophic bacteria also use iron (oxy-)hydroxides, whether biologically or abiotically produced, as electron acceptors for the re-mineralisation of organic matter during early diagenesis. This process is known as **dissimilatory iron reduction** (DIR) (Johnson *et al.,* 2008).

The metabolic activities of both iron-oxidising and iron-reducing bacteria involve a significant degree of iron isotope fractionation, of up to ~2‰ between the source ferrous/ferric species and resultant ferric/ferrous iron, in marked contrast to non-redox fractionation processes (Butler *et al.,* 2005). In biological systems, the reaction products produced by Fe^{3+} reduction are thus isotopically lighter than the reactants in terms of Fe isotopes, whereas ferric precipitates from the oxidation Fe^{2+} will be isotopically heavier than the source iron; the foregoing apply also during abiotic redox transformations (Johnson *et al.,* 2008).

Much of the research work concerning the isotopic fractionation of iron has taken place in controlled laboratory environments through experiments. However, a good deal of work on geological materials from a variety of ages and settings has paralleled the experimental work, and the relevant literature is steadily increasing. For example, Anbar (2004) reports that aqueous Fe^{2+} produced by the dissimilatory Fe-reducing bacteria *S. alga* was fractionated by ca. -1.3‰ from a ferrihydrite substrate in terms of $\delta^{56}Fe$. Anbar (2004) also reports that variations of similar magnitude are recorded in a handful of analyses of marine ferromanganese nodules and Precambrian BIF, with an overall $\delta^{56}Fe$ range from -1.6 to +0.9 ‰. Hydrothermal sulfides from the Lucky Strike vent site show a range of $\delta^{56}Fe$ from -2.1 to -1.1 ‰ for pyrite and marcasite samples, while pyrite from hydrothermally altered ocean crust from the Pacific Ocean showed a much narrower and less fractionated range of $\delta^{56}Fe$ values between -0.25 and -0.01 ‰.

Archer and Vance (2012) present coupled S and Fe isotopic data for sedimentary pyrite from the 2.7Ga Belingwe sedimentary basin in Zimbabwe, and they estimate that the isotopic composition of the source hydrothermal Fe^{2+}_{aq} falls within a range of $\delta^{56}Fe$ values between -0.3 and -0.7 ‰, whereas $\delta^{56}Fe$ of up to -1.6‰ in pyrite is interpreted to have formed from

coupled bacterial Fe^{2+} and S reduction. This may have taken place either below the sediment-seawater interface or in stratified euxinic bottom waters.

The Fe isotope variation in pyrite is sensitive and dependent on the concentration of dissolved Fe^{2+} in a basin (Rouxel *et al.,* 2005). Pyrite formation in sedimentary systems takes place in two steps according to Butler *et al.,* (2005), where FeS acts as an intermediate phase:

$$FeS_{(S)} \rightarrow FeS_{(aq)} \quad (3)$$

$$FeS_{(aq)} + H_2S = FeS_2 + H_2 \quad (4)$$

Rouxel *et al.,* (2005) analysed the Fe isotope composition of sulfides in black shales as well as of BIF, the former ranging in age from Precambrian to Late Cretaceous, and noted a general pattern of Fe isotopes that suggests that Earth history may be divided into three major stages (Figure 28): 2.8 to 2.3 Ga, 2.3 to 1.7 Ga and 1.7 Ga to modern times. According to Rouxel *et al.,* (2005), stage I is characterized by highly variable and negative $\delta^{56}Fe$ values for black shale pyrite; stage II is characterised by the disappearance of negative $\delta^{56}Fe$ values and the emergence of positive $\delta^{56}Fe$ values up to 1.2‰; and the third stage occurs after the disappearance of BIFs at ca. 1.8Ga, whence the deep ocean became either progressively oxic or euxinic. Iron at stage III would have been derived from hydrothermal venting but produced only few possibilities for iron isotope fractionation (Rouxel *et al.,* 2005). The massive deposition of BIF during stage I, presumably in the form of primary ferric precursor species produced oxidatively, has been used as a plausible driver for the general depletion of the global ocean in the heavy isotopes of iron during that period, which is quantitatively recorded in the sulfide fraction of largely coeval black shale deposits.

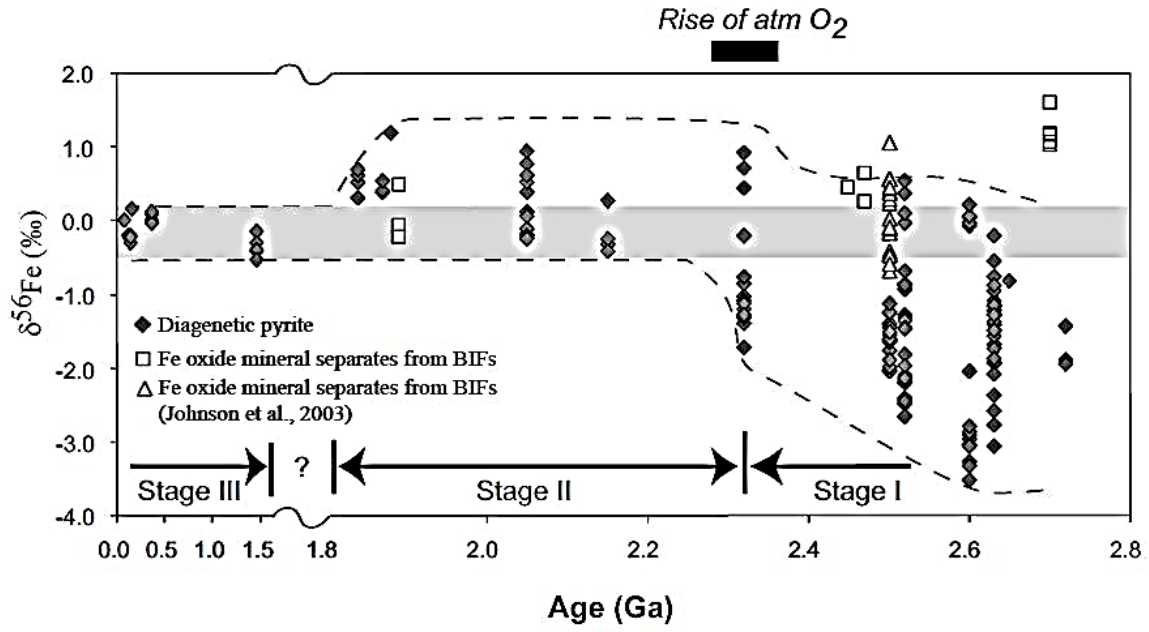

Figure 28. Plot of δ^{56}Fe versus sample age for Fe-sulfides from black shales and Fe-oxides from BIF. Fe ocean cycle is divided into three stages: I) 2.8 to 2.3 Ga; II) 2.3 to 1.8 Ga; and III) 1.7Ga to recent. Grey area corresponds to δ^{56}Fe of Fe derived from igneous rocks (at 0.1‰) and hydrothermal sources (ca. 0.5‰). Dashed lines represent contour maximum and minimum Fe isotope compositions of sedimentary sulfides used to define stages I to III. See text for discussion (after Rouxel *et al.,* 2005).

iv. Zinc Isotopes

The application of zinc isotopes is becoming an increasingly attractive geochemical tool for deciphering the history of Zn-rich sulfidic ore deposits, such as those in the Irish Midlands ore field (Wilkinson *et al.,* 2005). Zinc isotope analyses have hitherto been obtained from rocks, marine sediments, biological materials, seawater and ore deposits, and have revealed a wide range in δ^{66}Zn values, particularly in sulfide minerals which include both the heaviest and lightest Zn isotope samples reported to date (δ^{66}Zn = −0.43‰ and δ^{66}Zn = +1.33‰ respectively; Mason *et al.,* 2005; Wilkinson *et al.,* 2005). Zinc isotope fractionation mechanisms contrast with those for Fe (oxidation/reduction) as Zn occurs in only one oxidation state (Zn^{2+}) and consequently displays only small fractionations (<0.5‰ in most cases; Gagnevin *et al.,* 2012) which takes place usually under high pH conditions (Fujii *et al.,* 2011).

Zinc isotope studies carried out in the Alexandrinka volcanic-hosted massive sulfide ore deposit in Urals, Russia (Mason *et al.,* 2005) and the Irish Midlands ore field (Wilkinson *et al.,* 2005) link Zn isotope fractionations to hydrothermal processes. The Alexandrinka ore deposit was formed as a seafloor hydrothermal system similar to modern systems studied. Samples from the Alexandrinka deposit were analysed from the hydrothermal-metasomatic stockwork believed to be the feeder zone to the hydrothermal deposit, as well as from a seafloor chimney and some clastic sediments. δ^{66}Zn values from the deposit ranged from −0.43‰ to +0.23‰. Crucially, a systematic increase in δ^{66}Zn values recorded from the chimney core to the chimney rim has been attributed to either temperature dependence in the fractionation factor for Zn-sulfide precipitation or Rayleigh distillation as fluids diffuse through the chimney wall. In the Irish Midlands ore field, Zn isotopes show a general trend of lighter Zn isotopes precipitated in the deep feeder veins and heavier Zn isotopes near the top of the hydrothermal system. Based on these data, Wilkinson *et al.,* (2005) were the first to suggest that the precipitation of isotopically light Zn into Zn sulfides could influence the δ^{66}Zn of hydrothermal fluids. John *et al.,* (2008), report δ^{66}Zn analyses of hydrothermal fluids sampled from modern active submarine hydrothermal systems (TAG, EPR, Guyamas Basin) and report a range of fluid δ^{66}Zn values from 0 to 1.04‰. They conclude that the main cause for that variation relates to temperature changes, with cooling and attendant Zn precipitation as low-δ^{66}Zn sulfide resulting in the largest fractionation in the parent fluid itself.

Finally, Kelley *et al.,* (2009) report Zn isotope results from sphalerite in the Red Dog SEDEX deposit of Alaska. Their results show a range of δ^{66}Zn values from zero to 0.60 per mil, whereby the lowest values are observed in proximal vein breccia deposits, whereas stratigraphically overlying shale-hosted massive sulfide deposits show a systematic trend of increasing δ^{66}Zn values from south to north. They also show that the δ^{66}Zn values are inversely correlated with sphalerite Fe/Mn ratio and also tend to be higher in low Cu sphalerite, consistent with precipitation of lower δ^{66}Zn sphalerite closer to the principal hydrothermal fluid conduits. Kelley *et al.,* (2009) conclude that the most likely control on Zn isotopic variation is Rayleigh fractionation during sulfide precipitation, with lighter zinc isotopes preferentially incorporated in the earliest sphalerite to precipitate from ore fluids

at deeper levels (vein breccias) and close to the principal fluid conduits in the orebodies, followed by precipitation of sulfides with higher δ^{66}Zn values in shallower and/or more distal parts of the hydrothermal fluid-flow path.

c. Stable Isotope Results

All stable isotope analyses obtained for this study have been compiled and are presented in Table 12. The table contains all δ^{34}S analyses performed on sphalerite, pyrite and a single pyrrhotite (sample 182) separates, as well as δ^{66}Zn and δ^{56}Fe analyses for sphalerite and pyrite/pyrrhotite respectively. The δ^{66}Zn and δ^{56}Fe data are reported against the conventional *Lyon* and *IRMM-14* international standards, respectively, and are accompanied by 2σ standard deviations where possible. Data are mainly from the sulfidic B Unit of drill core G1, but are supplemented by four pyrite analyses from drill core G2. It should be stressed that every attempt was made to produce sphalerite and pyrite data from single sample separates; in some cases this was possible, in others it was not. In some instances, as pointed out earlier in this chapter, adjacent sample pairs had to be combined in order to permit the manual separation of sufficient amount of pure mineral separates for analysis. Nevertheless, the final dataset does allow for the assessment and interpretation of the ensuing data in a stratigraphic context, albeit on a relatively low sample resolution.

All δ^{34}S results are shown graphically on the histogram of Figure 29. The δ^{34}S data for pyrite/pyrrhotite and sphalerite from drill core G1 show very similar ranges between 27 and 30.4‰ and between 27 and 30.1‰ respectively. The three samples of pyrite analysed from drill core G2 exhibit a much more variable range from 22.9 to 28.3 ‰. The δ^{56}Fe data for pyrite show an appreciable range of values which are negative except for one sample from drill core G2. The observed range is between -1.85 and -0.55 ‰ (mean -0.91‰) for samples from drill core G1, whilst the four samples from drill core G2 record somewhat higher values (up to 0.19‰). The seven sphalerite samples from drill core G1 display a very narrow range of δ^{66}Zn values which is only marginally above the value of 0‰, namely from a minimum of 0.06 to a maximum of 0.20 ‰ (at a mean of 0.13‰). All iron and zinc isotope data are also shown graphically in the histograms of Figure 30.

Table 12. Compilation of stable isotope ratio data for $\delta^{34}S$, $\delta^{56}Fe$ and $\delta^{66}Zn$ analyses on pyrite (plus one pyrrhotite) and sphalerite separates from drill core G1, including a selection of four samples from drill coreG2. py = pyrite, sph = sphalerite, n = number of samples, * = pyrrhotite, ** = combined material from 196 and 198 m, 200 and 202 m, 204 and 206 m and 208 and 210 m, respectively.

	G1				G2	
n	9	8	7	8	3	4
Sample Number	**$\delta^{34}S_{V\text{-}CDT}$ (‰) (py)**	**$\delta^{34}S_{V\text{-}CDT}$ (‰) (sph)**	**$\delta^{66}Zn_{LYON}$ (‰) (sph)**	**$\delta^{56}Fe_{IRMM\text{-}14}$ (‰) (py)**	**$\delta^{34}S_{V\text{-}CDT}$ (‰) (py)**	**$\delta^{56}Fe_{IRMM\text{-}14}$ (‰) (py)**
SF-182	28.7*	29.2	0.11±0.02	-1.85±0.14		
SF-188	30.4	29.7	0.07±0.03	-1.02±0.09		
SF-192	27.8			-1.14±0.13		
SF-194	29.7	29.6	0.10±0.02	-0.96±0.09		
SF-197**	30.1	29.1	0.06±0.07	-0.77±0.15		
SF-200		30.1	0.20±0.07	-		
SF-201**	29.5			-0.57±0.13		
SF-204	29.4			-0.55±0.04		
SF-205**		28.0				
SF-206	28.1			-0.70±0.05		
SF-208		27.0	0.14±0.01			
SF 209**	27.0			-0.60±0.08		
SF-210		27.3	0.20±0.06			
G4-1500					24.5	-0.44±0.06
G58-1300					22.9	-0.44±0.06
G58-1455					28.3	-0.56±0.07
G2						0.19±0.07

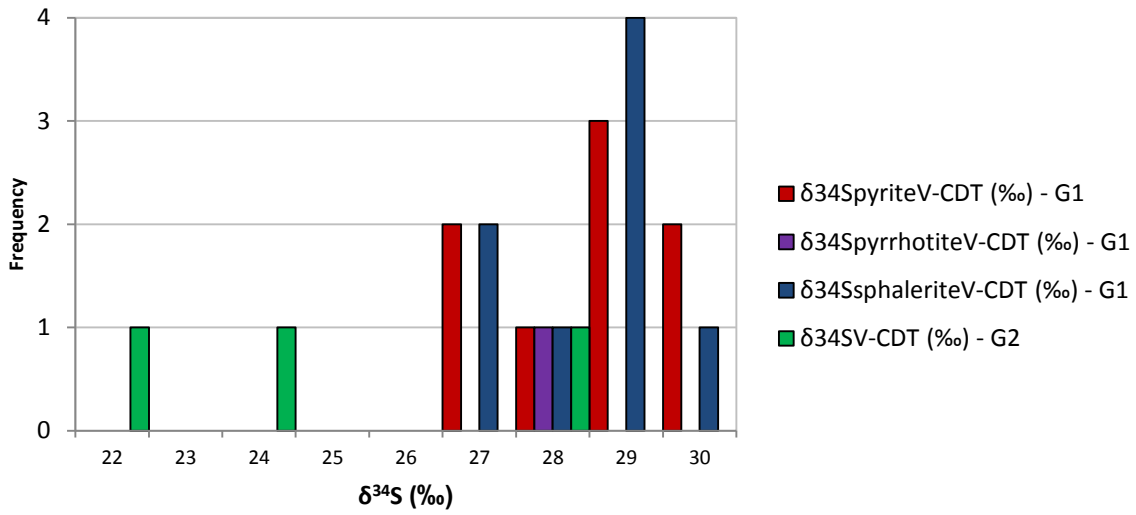

Figure 29. Frequency histogram of $\delta^{34}S_{Pyrite}$ and $\delta^{34}S_{Sphalerite}$ for samples from drill cores G1 and G2.

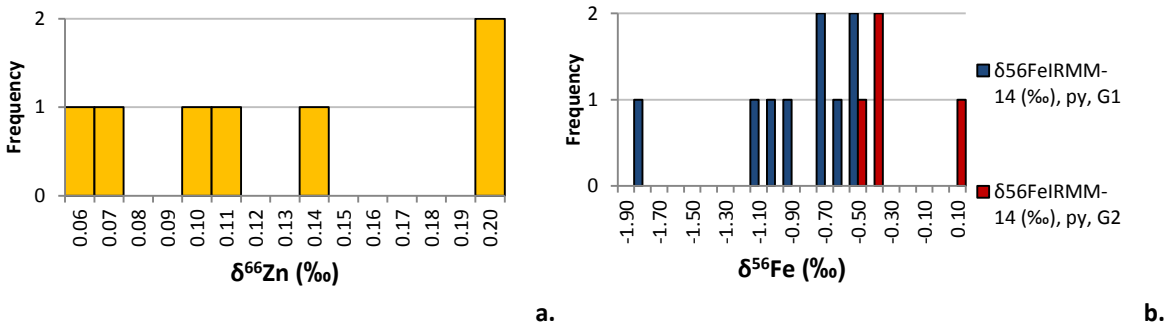

Figure 30. Frequency histogram of (a) $\delta^{66}Zn_{Sphalerite}$ for samples from drill core G1 and (b) $\delta^{56}Fe_{Pyrite}$ from drill cores G1 and G2.

Further insights into the behaviour of the isotopes of S, Fe and Zn across stratigraphy, can also be obtained through plotting the isotope data on depth profiles shown on Figure 31.

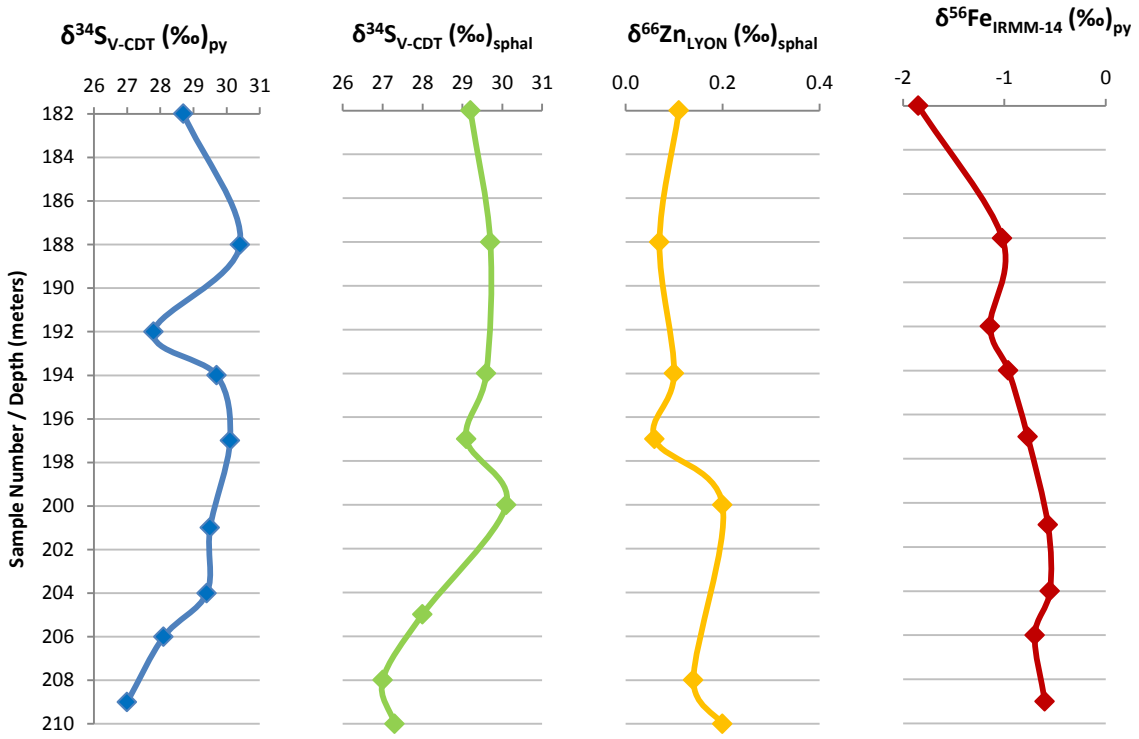

Figure 31. Depth profiles of $\delta^{34}S_{Pyrite}$, $\delta^{34}S_{Sphalerite}$, $\delta^{66}Zn_{Sphalerite}$, $\delta^{34}S_{Sphalerite}$, and $\delta^{56}Fe_{Pyrite}$ across the B Unit of the GIF, drill core G1.

The isotopic depth profiles of Figure 31 permit the following additional observations:

- The $\delta^{34}S$ data for both sphalerite and pyrite/pyrrhotite show a general increase towards higher values up-section; this is specifically manifested by a steep rise in $\delta^{34}S$ for both profiles in the lower half of the section to a value of *ca.* 30‰ (up to a stratigraphic depth of ca. 197m and 200m, respectively). This is followed by essentially no variation thereafter for sphalerite but some fluctuation for pyrite/pyrrhotite, between 27.80 and 30.40 ‰.
- The $\delta^{66}Zn$ data are much more challenging to interpret stratigraphically, as the absolute values obtained are guarded by significant 2σ errors in most instances. Notwithstanding, one can *cautiously* argue for a single-step decrease in $\delta^{66}Zn$ halfway up-section by about 0.14‰ on average. This appears to broadly conform, in a stratigraphic sense, with the behaviour of the sulfur isotopes for both sphalerite and pyrite/pyrrhotite as mentioned earlier.

- The δ^{57}Fe profile for pyrite (including the stratigraphically uppermost pyrrhotite sample) shows arguably the most interesting vertical profile: here, the obtained δ^{57}Fe data show an overall shift of over 1.25‰ from base to top, on a vertical trend of broadly *declining* values from the lowermost to the uppermost data points.

d. Controls of Stable Isotope Variations in the Gamsberg Orebody

In this section, evaluation and interpretation will be attempted of the stable isotope data for sphalerite and pyrite from the massive sulfide mineralisation at Gamsberg. This will be done in light of similar information from the published literature for other SEDEX and BHT deposits, with the inclusion and discussion of data from the A-G District where applicable.

e. Sulfur Isotopes from other SEDEX Deposits Worldwide

A large and diverse volume of δ^{34}S data from a number of classic SEDEX massive sulfide deposits of Australia and Canada, including the Broken Hill deposit, are available in the literature; only a selection of these are shown in Figure 32 (see caption for specific data sources). In some instances, the δ^{34}S data ranges shown represent individual mineral species (*e.g.* sphalerite and pyrrhotite: Spry, 1987; sphalerite and pyrite: Dixon and Davidson, 1996); in others, data represent undifferentiated "sulfides" (*e.g.* Parr and Plimmer, 1993). In general, the data shown for the Australian deposits as well as for their Canadian counterparts, register an overall range of values between –8 and 23 ‰, with the Sullivan deposit recording the lowest δ^{34}S values and the Howards Pass the highest.

Spry (1987) reports sulfur isotope compositions between -1.2 and 6.7 ‰ for pyrrhotite and between -0.6 and 6.7 ‰ for sphalerite from the lode horizons of the Broken Hill deposit of Australia. At the time those data were reported, it was noted that they were the highest δ^{34}S values for that deposit, and that they show an increase – albeit a weak one – from the footwall to the hanging wall of the deposit. A similar conclusion is presented in the review paper by Leach *et al.,* (2005) who emphasize the increase in δ^{34}S values in the later stages of

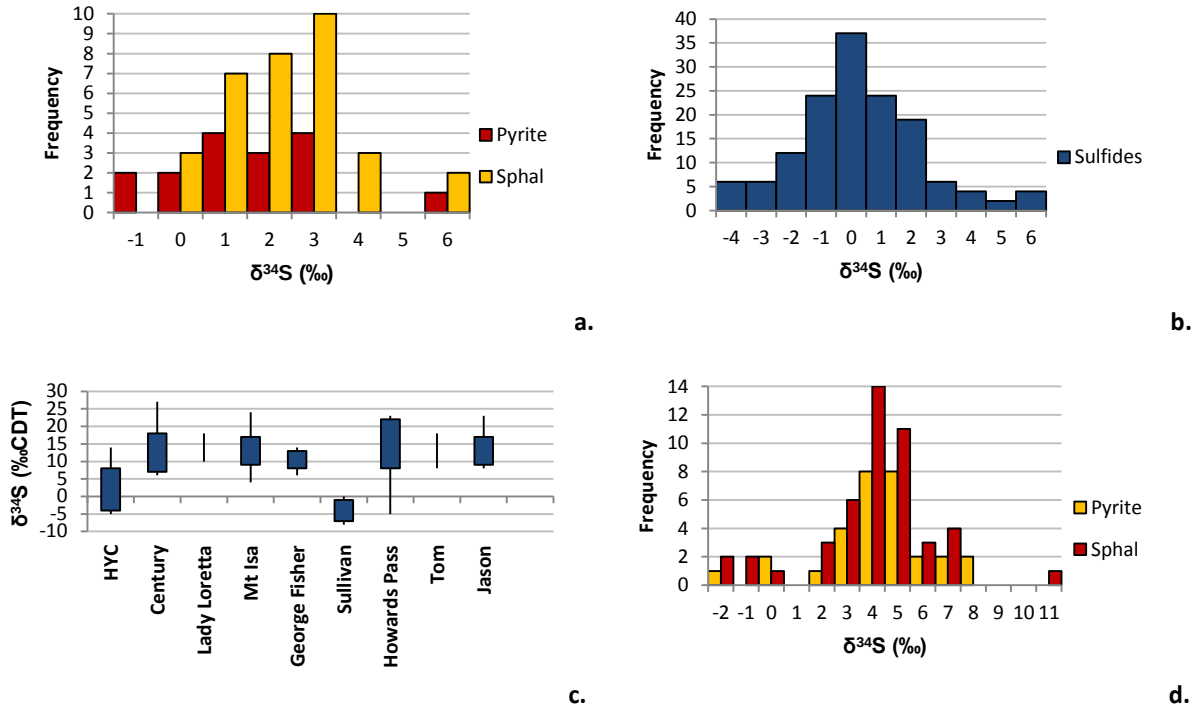

Figure 32. (a) Frequency histogram of $\delta^{34}S$ data for pyrite and sphalerite from Broken Hill, Australia (after Spry, 1987); (b) Frequency histogram of $\delta^{34}S$ data for undifferentiated sulfides from Broken Hill, Australia, (after Parr and Plimer, 1993); (c) Distribution of sulfur isotope compositions for sphalerite from SEDEX deposits from North Australia and Canada (after Leach *et al.,* 2005); and (d) $\delta^{34}S$ frequency histogram of Main Lode sphalerite and pyrite, Dugald River, Australia (after Dixon and Davidson, 1996).

ore paragenesis. According to Goodfellow and Jonasson (1984) and Goodfellow *et al.,* (1993), such enrichment in isotopically heavy sulfur is attributed to the removal of formed sulfides from the water column by sedimentation in a closed or semi-closed system, or a slow replenishment in sulfate in the ambient waters. This allows the latter to become progressively depleted in isotopically light sulfur

A number of explanations have been put forward as to the source of reduced sulfur for the Broken Hill deposit. Spry (1987) suggests that seawater sulfate was reduced by inorganic processes and mixed with some magmatic H_2S, or that sulfate from contemporaneous seawater, pore-water or pre-existing sulfate minerals was reduced biologically at low temperatures. In a similar fashion, Parr and Plimer (1993) also suggest that the range of $\delta^{34}S$ data for the Broken Hill deposit reflect a mixed source of reduced sulfur that involves a

hydrothermal/magmatic source and a seawater source through biogenic or thermogenic sulfate reduction.

In their review paper on sediment-hosted Pb-Zn deposits, Leach *et al.,* (2005) provide insights into the mechanisms for deriving reduced sulfur for the genesis and time-evolution of such deposits. They state that sulfate reduction would have progressed from BSR (producing relatively low values) to TSR (producing relatively high values) through time and with increasing temperature. They also propose that the reduction of sulfate is likely to have occurred in an isotopically closed system that became progressively enriched in heavy sulfur over the life the mineralisation.

The close similarity in the $\delta^{34}S$ ranges for the Broken Hill and Dugald River deposits (Figure 32a, b and d) warrants a closer look at the interpretation of the sulfur isotope data of the latter (Dixon and Davidson, 1996). The Dugald River deposit exhibits interesting variations in both base-metal zonation and $\delta^{34}S$ along strike as well as down-dip; the latter ranges from -1 to as high as 8 ‰. Dixon and Davidson (1996) discount a number of possible causes for the isotopic variations observed, such as fluid temperature variations, BSR, digestion of pre-existing *in-situ* biogenic sulfide, and H_2S derived from thermal cracking of organic matter. They instead propose that TSR is the only plausible mechanism that would have produced the observed $\delta^{34}S$ signatures and their distribution in space. In support of their contention, Dixon and Davidson (1996) present $\delta^{13}C$ data from ore-related carbonate, mass-balance considerations, and the relatively high temperatures of ore formation which would preclude any biogenic activity such as BSR.

f. Sulfur Isotopes in the Aggeneys-Gamsberg District

Recent work by Stalder (2003), Stalder and Rozendaal (2005) and McClung *et al.,* (2007) has placed emphasis on the primary source of sulfur for metal sulfides and barite in the A-G District. This has been suggested to be ultimately ambient seawater present in the basin at the time of ore formation. In the A-G District, a general increase is recorded towards more positive $\delta^{34}S$ values from the westernmost mineralization at Black Mountain to the

easternmost at Gamsberg. This is interpreted to reflect a proximal *versus* distal relationship in the context of the primary ore-forming environment; the Black Mountain deposit would represent mineralization proximal to the locus of submarine hydrothermal discharge, whilst Gamsberg would have been a more distal equivalent (McClung *et al.,* 2007). It is worth noting that the regional trend in the $\delta^{34}S$ variation of sulfides is broadly paralleled by the $\delta^{34}S$ variation in barite (Figure 33), a feature which intuitively suggests that sulfur in both sulfides and sulfates must have been derived from a common seawater source.

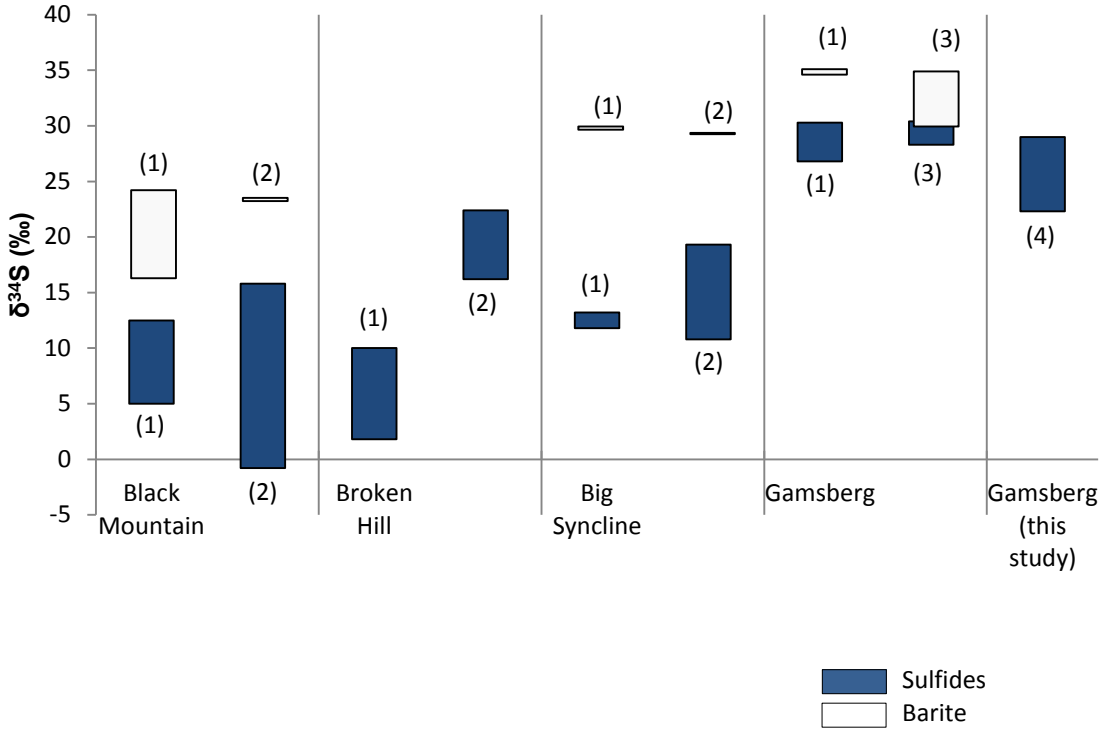

Figure 33. Compilation of $\delta^{34}S$ values (‰) for sulfides and barite from samples from Black Mountain, Broken Hill, Big Syncline and Gamsberg. Sources: (1) von Gehlen, (1983); (2) McClung *et al. (*2010); McClung *et al. (*2007); and (4) this study.

In light of the foregoing, the sulfur isotope data for sphalerite and pyrite of this study can provide valuable insights when interpreted either in a stratigraphic sense or in a regional context. The stratigraphic pattern of $\delta^{34}S$ for both pyrite(+pyrrhotite) and sphalerite are remarkably similar in terms of absolute values and vertical variation, and are interpreted

here to reflect a common sulfur source and co-genetic history for both sulfides. In terms of $\delta^{34}S$ values alone, however, the minimum values registered in the G1 drill core intersection for either sulfide are still amongst the highest recorded in metal sulfides of the A–G district (Figure 33), and for SEDEX/BHT deposits in general (Figure 32). At the same time, the *lowest* sulfur isotope value registered in sulfides from Black Mountain deposit is only barely below the value of 0‰ (Figure 33). Assuming a seawater-sulfate isotope value for the Mesoproterozoic around 15-20 ‰ (Holland *et al.,* 2006; see also Figure 27), and given the range of sulfide $\delta^{34}S$ values at the A-G District between ~0 and ~31 ‰ (*i.e*. a maximum of ±15‰ or so about the paleo-seawater value), it is considered unlikely that the source of sulfide-sulfur in the district would have been derived via BSR, as the latter is commonly expected to result in large fractionation effects that typically produce much lower $\delta^{34}S$ signatures in precipitated metal sulfides.

It is therefore suggested that the primary fractionation mechanism with regard to Gamsberg and the broader A-G District, would have been TSR of seawater sulfate over a range of possible temperatures, and against an essentially closed and isotopically evolving reservoir of aqueous sulfate with time, resulting in a basin-wide Rayleigh fractionation effect. This interpretation conforms to that of Dixon and Davidson (1996) for the Dugald River ore-body and lends support to the prevailing notion that the Gamsberg deposit is indeed a distal end-member in the A-G District. The barite $\delta^{34}S$ data of Figure 33 would be expected to closely track the isotopic evolution of the dissolved sulfate pool (as little sulfur isotope fractionation is expected via the precipitation of sulfate minerals), with highest and therefore most evolved signature recorded in the barite deposit at Gamsberg which is also known to postdate the sulfide mineralisation there (McClung *et al.,* 2007).

On the other hand, the isotopic signal of sulfides at Gamsberg and elsewhere in the district would be expected to have been more variable at least on local scales, with temperature most likely being an additional factor affecting isotopic fractionation. To this end, McClung *et al.,* (2007) have used oxygen isotope compositions of barites across the district to place temperature constraints from the proximal Black Mountain deposit at >250°C to that of the Gamsberg deposit at >120°C. Corresponding temperature variations during sulfide

precipitation may therefore have been – at least partly – responsible for the vertical variation in $\delta^{34}S$ values such as observed at Gamsberg alone, and/or the lateral variation as observed on a district-wide scale.

g. Interpretation of Zinc Isotopes

Assessment of the zinc isotope data of sphalerite from the Gamsberg orebody as presented earlier in this chapter, hinges to a large degree on interpretation of similar results from Zn-rich massive sulfide deposits elsewhere, as the application of Zn isotopes on sediment-hosted sulfide deposits is still in its infancy. For that reason, emphasis is placed here on two publications, namely the paper by Kelley *et al.,* (2009) on the Red Dog Deposit, Northern Alaska, and the paper by Mason *et al.,* (2005) on the Alexandrinka VHMS deposit of Russia. In both papers, sphalerite $\delta^{66}Zn$ data exhibit apparent variations in space on a variety of scales, which are interpreted as a result of Zn isotope evolution of the hydrothermal systems in space and time. The work of Mason *et al.,* (2005) focused on zinc and copper isotopic variability in the Alexandrinka VHMS ore deposit of Russia. One of the key findings of this study concerns Zn isotope variability observed from the core to the rim of a hydrothermal chimney, whereby the $\delta^{66}Zn$ of sphalerite shows a systematic increase away from the core from -0.03 to +0.18 ‰ as illustrated in Figure 34.

In their study of the Red Dog deposit of Alaska, Kelley *et al.,* (2009) found that $\delta^{66}Zn$ values range between 0.04 and 0.60 ‰ with an apparent increase in $\delta^{66}Zn$ from the south of the deposit to the north (Figure 35a). They also noted that sulfur isotope compositions compared to zinc showed an apparent decoupling. The source of zinc was interpreted to be homogenous and the decoupling of S and Zn was explained in either of two ways: (1) multiple fluids tapped multiple sources, the sources being distinct in $\delta^{34}S$ but indistinguishable in $\delta^{66}Zn$, with co-transport of sulfur and zinc; or (2) mixing between homogeneous metal- and sulfur-bearing fluids occurred at the depositional site. The trend from isotopically lighter sphalerite in deeper/proximal parts of the hydrothermal system at Red Dog to isotopically heavier sphalerite in the upper/distal parts of the system has been attributed to Rayleigh distillation processes during precipitation (Kelley *et al.,* 2009).

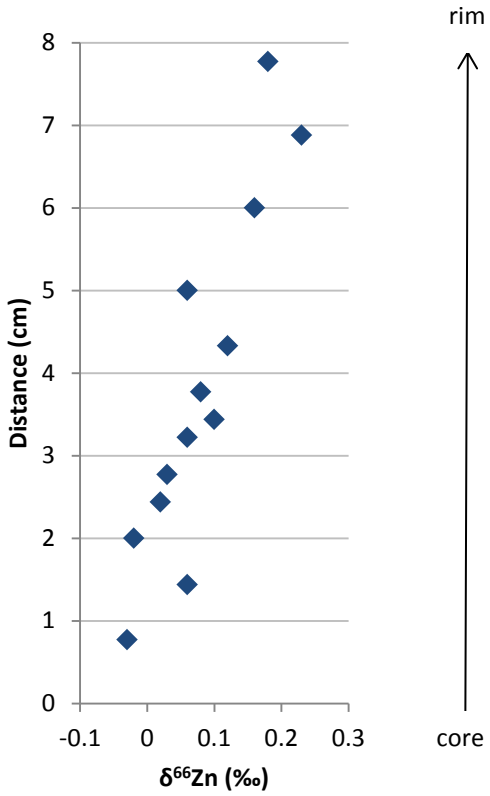

Figure 34. Variation in $\delta^{66}Zn$ from core to periphery though a hydrothermal chimney in the Alexandrinka VHMS ore deposit, Urals, Russia (Mason *et al.,* 2005).

It was suggested that the first (early) sphalerite to precipitate in the deeper/hotter parts of the hydrothermal system were enriched in light Zn isotopes by kinetic fractionation, and consequently the fluids evolved towards heavier isotopic compositions via a Rayleigh distillation effect as they migrated outwards (Kelley *et al.,* 2009). A similar explanation has also been reached by Wilkinson *et al.,* (2005) for the Irish Midlands (Figure 35b), as well as Mason *et al.,* (2005) for the Alexandrinka Deposit.

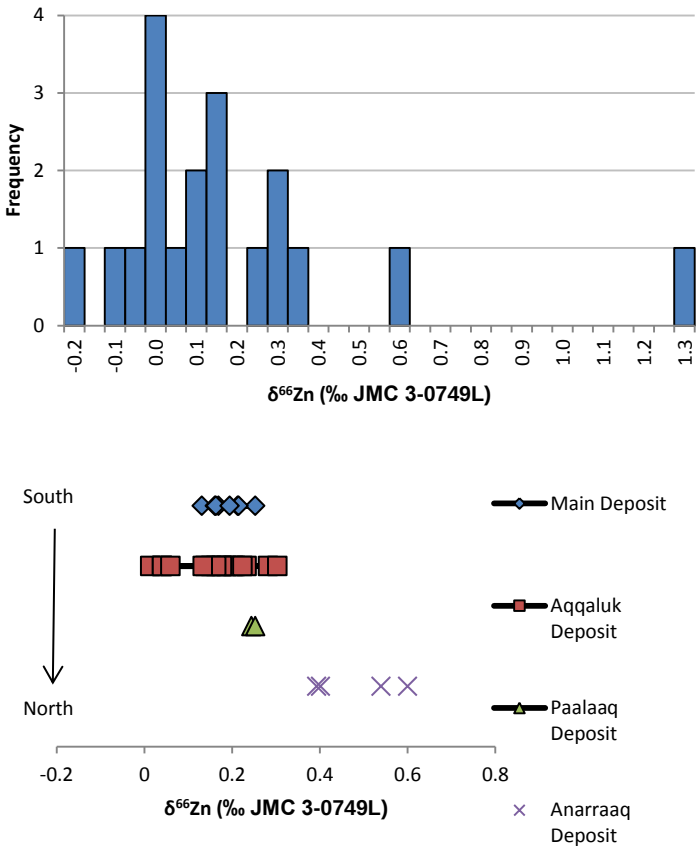

Figure 35. Range of δ^{66}Zn sphalerite values from (a) The Red Dog District, Northern Alaska (Kelley *et al.,* 2009) and (b) The Irish Midlands (Wilkinson *et al.,* 2005).

The Zn isotope results of this study appear to be rather inconclusive in a stratigraphic and regional sense. The main aim of the zinc isotope analyses was to test whether a stratigraphic pattern of change in δ^{66}Zn up-section is recorded, and whether it could be interpreted in similar ways to the case studies of Red Dog and Alexandrinka. The very marginally positive δ^{66}Zn values obtained and the statistically insignificant variation thereof across the sampled section would imply minor effects of Rayleigh distillation processes either in a stratigraphic sense (*i.e.* on a local scale) or in a district-wide sense (*i.e.* as part of a larger scale hydrothermal system across the entire A-G District). The potential significance of the Zn isotope data will be briefly discussed further in the last chapter of this thesis in conjunction with the other isotopic data.

h. Interpretation of Iron Isotopes

The average crustal reservoir of Fe has a δ^{56}Fe value near zero (Johnson *et al.,* 2008). As indicated earlier, the largest fractionation effects in the isotopes of iron (up to ~3‰) are known to be controlled by redox transformations (biological or inorganic), especially at low temperatures. With regard to the alteration of oceanic crust by hydrothermal fluids, this is known to cause the preferential leaching of isotopically light Fe^{2+} from basaltic source rocks; this consequently shifts the isotopic composition of altered basalt towards higher δ^{56}Fe values (Möller, 2012). Therefore, the high-temperature end-member fluids within these vent systems display values that are depleted in isotopically heavy Fe relative to the basalts themselves. Subsequent precipitation of iron sulfides from hydrothermal fluids tend to kinetically fractionate the isotopes of iron, causing iron mono- and di-sulfides to be even further depleted in heavy Fe isotopes (Möller, 2012). Continued sulfide precipitation and migration of residual dissolved Fe in buoyant plumes away from hydrothermal vents, would thus result in a general increase in the Fe isotope values of hydrothermal fluids with distance from the vent.

On the basis of the foregoing, and irrespective of the stratigraphic variation recorded, the overall negative δ^{56}Fe values of pyrite(+pyrrhotite) seen in the mineralised B Unit of drill core G1 would be at apparent odds with precipitation of primary sulfide in a vent-distal fashion, and thus would not support a distal character for the Gamsberg orebody in the A-G District. However, the cycle of Fe in this instance is expected to have been much more complex, as the metal is present is significant amounts across the entire GIF and in variable mineralogical forms, ranging from oxide (*i.e.* magnetite) to a variety of Fe-silicate species (*e.g.* Fe-rich garnet). The apparent stratigraphic decrease in δ^{56}Fe values up-section may therefore reflect kinetic fractionation effects linked to primary precipitation of Fe under variable redox conditions across time.

One way in which the iron isotope signal of the Fe sulfides at Gamsberg may have progressively lowered, could have been in response to broadly simultaneous sequestration of iron in the ferric form elsewhere in the basin (subsequently transformed to magnetite through metamorphic reactions involving partial iron reduction). Ferric iron precipitation in

a basin-wide scale would have resulted in preferential deposition of isotopically heavy iron into primary Fe-(oxy)hydroxides, resulting in progressive depletion of the source aqueous reservoir in isotopically heavy iron, so long as deposition took place in an essentially closed system. In other words, the Gamsberg Fe-sulfide may be recording a progressively isotopically depleted aqueous iron pool through time. The above interpretation can only be tested, however, through rigorous iron isotope analyses of the silicate and oxide fractions of Fe-rich minerals in the GIF, accompanied by considerations on isotopic mass balance.

i. Summary

- Sulfur, iron and zinc stable isotope analyses were carried out on sulfide separates (sphalerite, pyrite and pyrrhotite) from the ore-bearing B Unit of the GIF at Gamsberg. The $\delta^{34}S$ data from drill core G1 show a range from 27.0 to 30.4 ‰ for pyrite and 27.0 to 30.1 ‰ for sphalerite. $\delta^{66}Zn$ data for sphalerite range marginally above the value of 0‰, specifically from 0.06 to 0.20 ‰, whereas $\delta^{56}Fe$ data for pyrite (including a single pyrrhotite) separates, define a range of values from -1.85 to -0.55 ‰. Supplementary sulfur and iron isotope data for four samples from drill core G2 show relatively lower $\delta^{34}S$ (22.9 to 28.3 ‰) and higher $\delta^{56}Fe$ values (-0.56 to +0.19 ‰) than those of drill core G1.
- The sulfur isotope data are interpreted to reflect primary deposition of sulfide ore (and by extension barite) at Gamsberg from an isotopically evolved seawater sulfate source. The unusually high $\delta^{34}S$ values for the sulfides suggests that the reductive mechanism for sulfide generation from seawater sulfate would have been TSR rather than BSR, in close accordance with similar suggestions by Davidson and Dixon (1996) for the Dugald River deposit of Australia.
- The very narrowly-ranging and marginally positive $\delta^{66}Zn$ values of sphalerite across the B Unit at Gamsberg provide no clear constraints on the mechanism of Zn sulfide precipitation. The data record no statistically measurable fractionation of Zn isotopes relative to standard, either stratigraphically (*i.e.* locally) or in a proximal *versus* distal context in the A-G District, thus putting into question their use in this regard in other

similar deposits elsewhere. This, however, has to be further tested through further Zn isotope analyses of sphalerite from at least other deposits in the A-G District.

- Iron isotope analyses of pyrite show a stratigraphic trend of progressively decreasing $\delta^{56}Fe$ values up-section; this is interpreted to reflect the influence of broadly coeval precipitation of Fe-oxides regionally – now preserved as abundant magnetite through metamorphism – which would have acted as a sink for isotopically heavy Fe. A signal of progressive enrichment of the ambient aqueous Fe pool in isotopically light iron thus appears to be faithfully transferred (at least in part) into the iron isotope record of the precipitated Fe-sulfides.

6. SYNTHESIS AND CONCLUSIONS

The focus of the present study has been to provide new insights, where possible, into the genesis of the Gamsberg massive sulfide mineralization in the context of the entire A-G District. The Gamsberg deposit is located in the Namaqualand Metamorphic Complex of South Africa and is associated with 3 other massive sulfide deposits of metamorphosed SEDEX/BHT affinity: these are known as *Black Mountain* (*Swartberg*), *Broken Hill* and *Big Syncline*. A single drill core (G1) capturing approximately 40m apparent thickness of massive sphalerite-rich ore was targeted, along with the overlying and underlying silicate-rich units that envelope it. The specific drill core was chosen as it appears to capture the stratigraphic succession of the mineralization with no obvious deformational disturbance of the interpreted stratigraphy. This was confirmed through the petrographic and mineralogical examination of the chosen intersection, and by comparison with literature information from the Gamsberg area.

Basic petrographic studies of the sulfide ore and host-rocks was coupled with detailed microprobe analyses of individual mineral species as well as with bulk-rock analyses of the silicate host-rocks, in an attempt to create a rigorous chemo-stratigraphic framework for the examined section and reveal any stratigraphic trends of potential value in the context of the primary ore-forming environment. Mineral-specific stable isotope analyses performed on samples collected across the whole stratigraphy of the mineralised B Unit were then applied, in order to shed further light into the genesis of the ore-body in a local and possibly regional context as well. These ranged from standard, mineral-specific sulfur isotope analyses, to corresponding Zn and Fe isotope determinations which have never been applied in the region. In the sections that follow, an attempt is made to integrate the results presented in this thesis in light of previously-proposed metallogenic models for the Gamsberg orebody and the polymetallic A-G District as a whole, followed by suggested new directions for future work in the A-G region.

a. Genetic Considerations

A number of physico-chemical parameters are known to be important for the solubility of metals in hydrothermal fluids. These include *salinity*, *temperature*, *redox state*, *chloride:sulfide* ratio and *pH* (Stalder, 2003). Metal solubility can be considered in terms of the electron donor-acceptor theory of *hard* (class 'a') and *soft* (class 'b') *Lewis acids* and *bases* (Table 13). 'Hard' donors and acceptors are characterised by high charge and/or small ionic radius and will form more electrostatic bonds than 'soft' donors and acceptors. 'Soft' donors and acceptors have a large number of *d* electrons in their outer shells and easily form covalent bonds (Seward and Barnes, 1997). As such, 'hard' metals form the most stable complexes with 'hard' ligands and 'soft' metals form the most stable complexes with 'soft' ligands. This classification, however, is still highly dependent on the physico-chemical properties of any given transporting fluid, particularly temperature.

Table 13. Classification of some metals and ligands (*i.e.* electron acceptors and donors) in terms of their class 'a' (hard) and class 'b' (soft) behaviour (from Seaward and Barnes, 1997).

Class 'a' Metals	**Borderline**	**Class 'b' Metals**
H^+, Li^+, Na^+, K^+, Be^{3+}, Ca^{2+}, Mg^{2+}, Sr^{2+}, Al^{3+}, Fe^{3+}, Cr^{3+}, La^{3+}	Divalent transition metals including Zn^{2+}, Pb^{2+} and Bi^{3+}	Cu^+, Ag^+, Au^+, Au^{3+}, Hg^{2+}, Cd^{2+}, Sn^{2+}, Tl^+, Tl^{3+}
Class 'a' Ligands	**Borderline**	**Class 'b' Ligands**
F^-, OH^-, NH_3, NO^{3-}, HCO_3^-, CO_3^{2-}, HSO_4^-, SO_4^{2-}, $H_3SiO_4^-$, HPO_4^{2-}, PO_4^{3-}, CH_3COO^-	Cl^-, Br^-	I^-, HS^-, $S_2O_3^{2-}$, SCN^-, CN^-

There is broad agreement in the geological literature that chloride complexes are amongst the most common carriers of base metals (*e.g.* Zn, Pb, Cu and Fe) in natural hydrothermal fluids. Figure 36 presents the variation in the equilibrium formation constant for simple chloride complexes with temperature (Seward and Barnes, 1997). The equilibrium formation constant represents the stability of the metal complex: as temperature increases, the stability of the metal complex increases. Concerning Zn and Pb, which are the key metal commodities in sediment-hosted massive sulfide deposits, the stability of $PbCl^+$ increases by about 2.5 orders of magnitude as temperature rises from 25° to 300°C (Seward and Barnes,

1997). The stability of $ZnCl^+$ under the same temperature range increases by six orders of magnitude so that $ZnCl^+$ is more stable at higher temperatures (up to 400°C) than $PbCl^+$. The stability of $FeCl^{2+}$ increases up to a temperature of 150°C after which it becomes unstable; however the stability of $FeCl^+$ increases up to a temperature of 310°C (Figure 36).

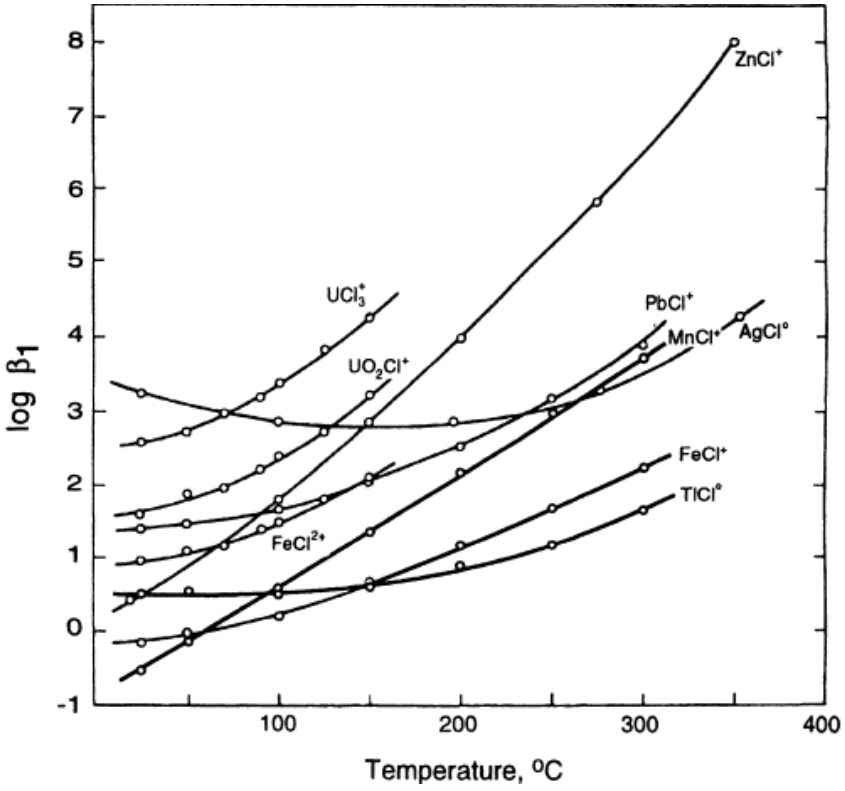

Figure 36. Variation of the equilibrium formation constant, β_1, with temperature for simple chloride complexes at the saturated vapour pressure (from Seward and Barnes, 1997).

Oxygen fugacity (fO_2) as a key-factor for the optimum transport of Pb and Zn chloride complexes in hydrothermal solutions capable of producing an economic ore-body can be discussed with reference to the equations 5 and 6 (Cook *et al.,* 2000):

$$MeS_{solid} + 2H^+ + 4Cl^- \rightarrow MeCl_4^{2-} + H_2S \quad (5)$$

$$MeS_{solid} + 4H_2O + 4Cl^- \rightarrow MeCl_4^{2-} + SO_4^{2-} + 4H_2 \quad (6)$$

Where Me = Pb, Zn

According to equation (5), low fO_2, reduced brines with low pH, high salinity as well as low activity of H_2S, will favour the increased solubility of Pb and Zn. This can be further augmented by increasing temperature associated with, for example, high heat flow in active rift zones or intrusive activity into the rift sequence. Factors that will promote metal precipitation here include an increase in pH and/or the activity of H_2S, or a decrease in salinity through, for example, dilution by lower-salinity fluids (*e.g.* meteoric water; Figure 37a, b, line A-C). However, the solubility of Zn and Pb in oxidised brines is independent of pH (Figure 37a, b, line B-C; Stalder, 2003). Therefore, according to equation (6), the main causes of Zn and Pb precipitation in the form of sphalerite and galena are addition of H_2S and/or a decrease in the salinity at the site of deposition.

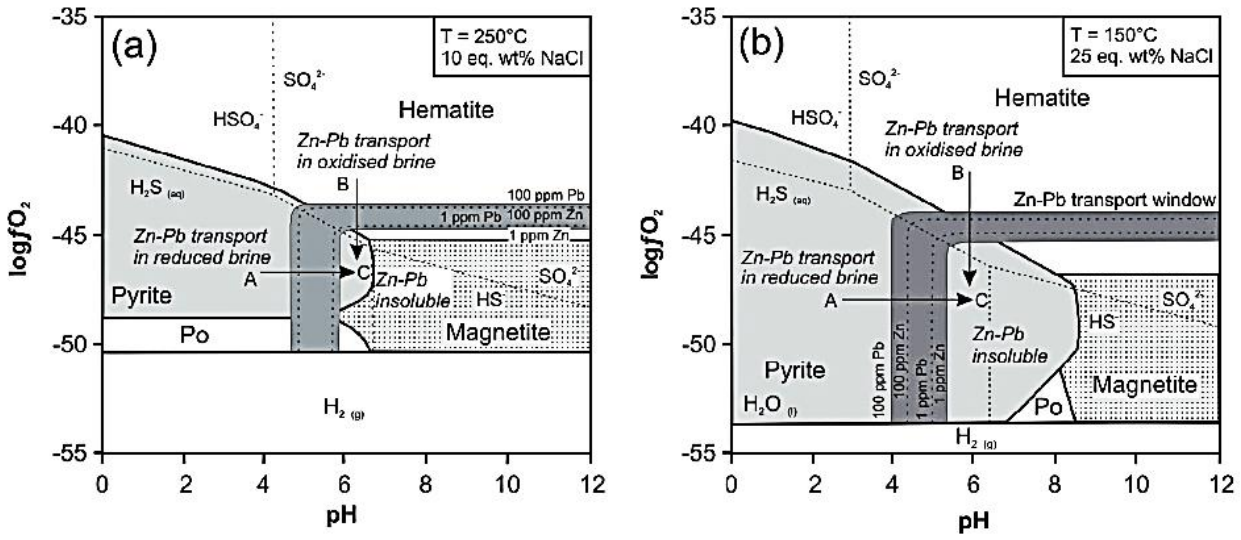

Figure 37. logfO_2-pH diagrams highlighting the stability fields of Fe oxides and sulfides as well as the main transportation window for sphalerite and galena as well as the predominant fields for the principle aqueous sulfur-bearing species and the stability fields for water and H_2 (Stalder, 2003 and Cooke *et al.,* 2000). (a) T = 250°C and 10eq wt% NaCl; (b) T = 150°C and 25wt% NaCl.

On the other hand, oxidized brines have a much greater capacity to carry Pb and Zn in solution, particularly at the moderate temperatures typical of SEDEX deposits (<250^{o}C). This is illustrated in the diagram of Figure 38 (Large *et al.,* 2002), constructed experimentally at a fixed salinity, pH and temperature of 250°C, whereby oxidized brines are shown to be able

to carry several orders of magnitude more Pb and Zn (up to 10s of thousands ppm) than reduced brines (up to 11s ppm). According to Equation (6), metal solubility in oxidized brines is independent of pH; therefore, the main drivers for metal precipitation here will be the addition of H_2S and/or a decrease in salinity at the depositional site.

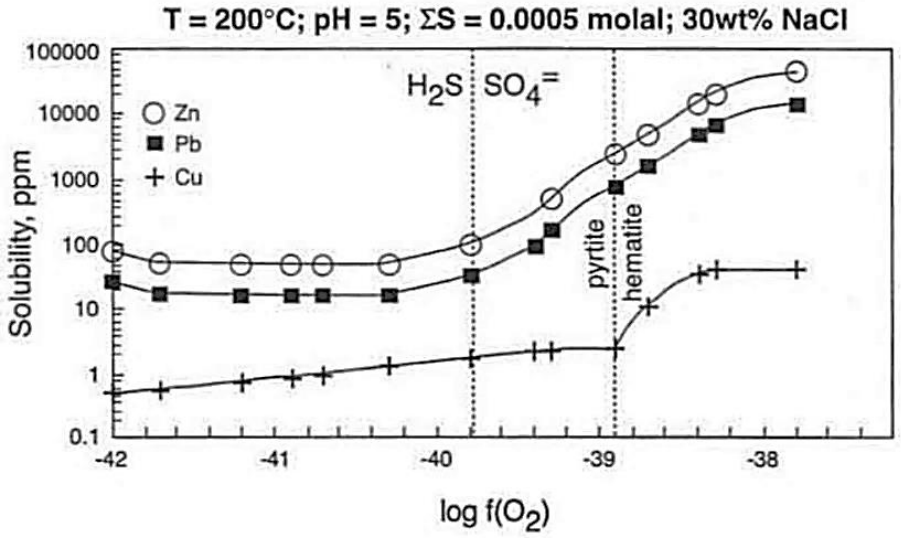

Figure 38. Effect of fO_2 on the solubility of Zn, Pb and Cu which demonstrates that oxidised brines have a far greater metal-carrying capacity than reduced brines for the set conditions given (Large *et al.,* 2002).

A key characteristic of SEDEX deposits with a demonstrable spatial link to a vent complex ("vent-proximal"; Large *et al.,* 2002), is the metal zonation from the vent complex to more distal portions. Goodfellow and Lydon (2008) state that an increase in the Zn:Pb ratio away from the vent complex is the most pronounced and consistent feature of SEDEX metal zonation. Other zonation patterns include increases in the ratios of Pb:Ag; Cu:(Zn+Pb); Fe:Zn; Ba:Zn; and SiO_2:Zn, away from the vent complex (Goodfellow *et al.,* 1993; Large *et al.,* 2002; Goodfellow and Lydon, 2008). The causes of metal zonation in SEDEX systems have been interpreted as the result of changes in the redox potential and/or temperature of the ore-bearing fluid (Cooke *et al.,* 2000), whereas Goodfellow *et al.,* (1993), based on observations from the Tom Deposit in Yukon, Canada, interpret metal zonation within SEDEX districts as the result of epigenetic processes, marked by a change from typically

bedded textures to open-space filling and replacement textures towards the vent. Here, at the margins of the vent complex, fine-grained, low-temperature phases of the bedded ore facies (Fe-poor sphalerite, galena and framboidal pyrite, barite and chert) have been replaced by coarser-grained, higher-temperature assemblages (coarsely crystalline, Fe-rich sphalerite and mercury-rich sphalerite, galena, siderite, quartz, pyrrhotite, chalcopyrite, arsenopyrite and tetrahedrite). The resultant chemical zonation is therefore an increase towards the centre of the vent complex in Zn, Pb, Cu, As, Sn, Ba, Fe, Mn, Ca and CO_2, as well as in Pb relative to Zn.

b. Previous Models for the Aggeneys-Gamsberg District

For the purposes of facilitating the discussion that follows, two illustrated models that have been recently proposed to account for the genesis of the base-metal sulfide deposits in the A-G District will be sequentially presented in this section: one is by Stalder (2003; see also Figure 39), and the other by McClung *et al.,* (2007; see also Figure 40 and Figure 41). The two models collectively encapsulate most elements of metallogenic significance as variously inferred for the genesis of ancient SEDEX deposits, as they invoke fundamentally different ore-forming mechanisms, namely syngenetic *versus* epigenetic/syngenetic. They thus provide a useful benchmark upon which a revised interpretation of the genesis of the deposits in the A-G District can thereafter be built upon, utilising the new results presented in the preceding chapters of this thesis.

Stalder (2003) proposes the formation of the Gamsberg Deposit in an original rift basin environment which accommodated the precursor sedimentary and volcanic material of the Bushmanland Group. Beneath the Bushmanland proto-basin, a deep-seated heat source in the form of a magmatic body is postulated as having provided the necessary heat flow for the circulation of connate brines and/or meteoric fluids, which leached base metals from the underlying volcaniclastic Hoogoor Gneiss. Thereafter, a three-stage genetic model is proposed for the A-G District (Figure 39) which envisages a genetic link between all four deposits in the region, and derivation of metals across the region from the *same* ore fluid.

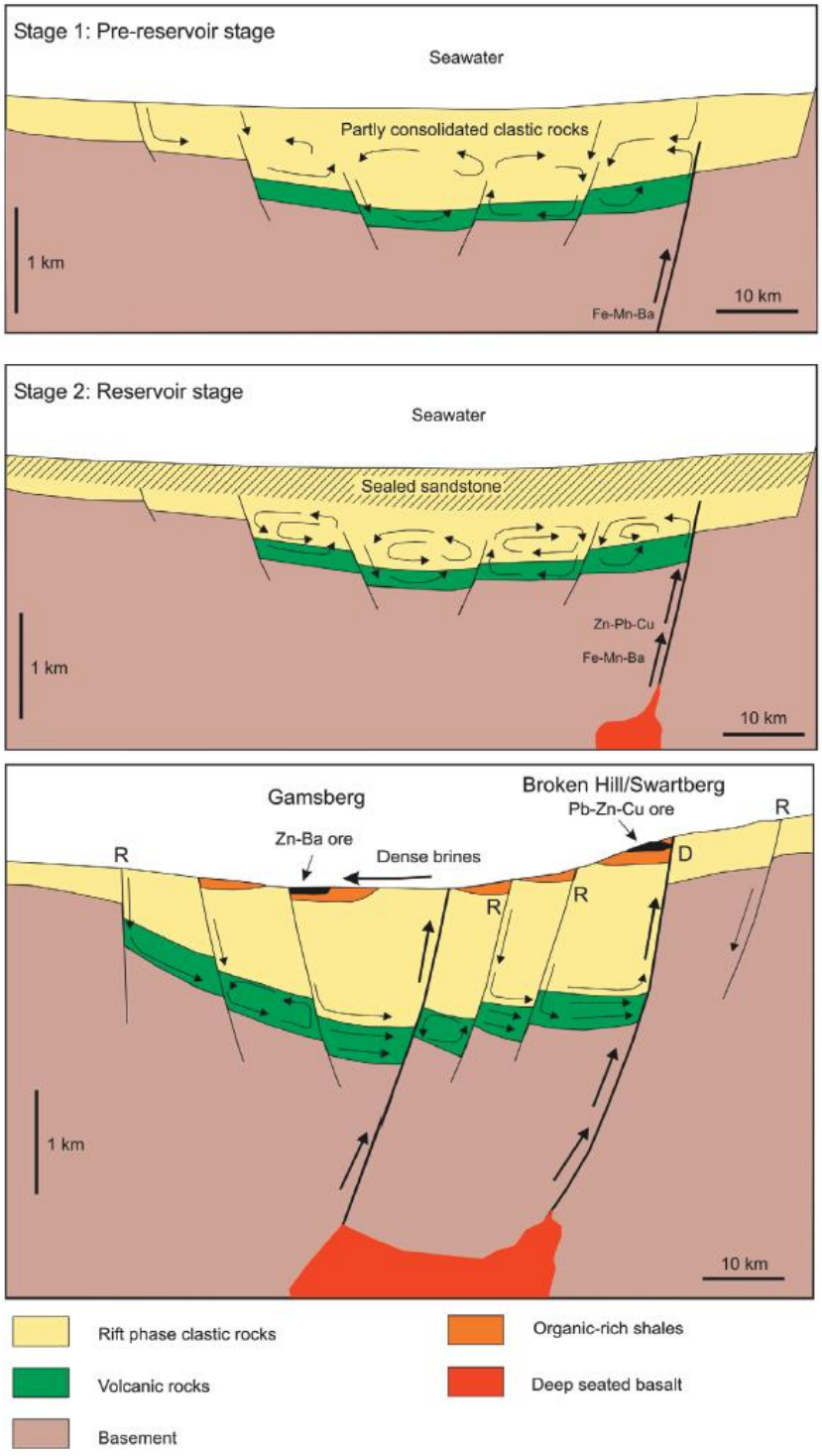

Figure 39. Genetic model for the development of the Aggeneys-Gamsberg Ore District, Stalder, (2003).

The initial stage of the model by Stalder (2003) is represented by the 'pre-reservoir stage' (Stage 1) whereby initial hydrothermal fluids (carrying metals of Fe, Mn and Ba) vent into a

basin that contains a sequence of unconsolidated to poorly consolidated clastic sediments that overlie a volcanic sequence. At this stage, the metals are thought to have been deposited mainly by adsorption onto clay minerals and Fe oxides in a dilute fashion. A cap rock of "sealed" sandstone would have formed during Stage 2 (the 'reservoir stage'), leading to the formation of a confined, protracted hydrothermal reservoir, capable of dissolving sufficient volumes of metals via convective hydrothermal cells to subsequently produce ore. The formation of ores was now able to commence via the reactivation of growth faults in the basement that led to the development of third-order asymmetric basins, and which ultimately host the individual ore bodies (Stage 3). On the basis of primarily sulfur isotope records, Stalder (2003) goes on to surmise that the Gamsberg Deposit most likely represents an *evolved* counterpart to the remainder deposits of the A-G District, due to early-stage precipitation of Cu, Pb from buoyant to intermediate (high temperature) brines in a vent-proximal environment, producing the Pb-dominated Broken Hill/Black Mountain ores; this process would have been accompanied by the development of a residual, dense, primarily Zn-rich fluid, that would have migrated downslope towards the eastern Gamsberg basin, where the respective mineralisation would have formed in a distal fashion.

In their proposed model, McClung *et al.,* (2007) highlight the broader geographical context of the deposits in the A-G District, with emphasis on the apparent bulk metal zonation exhibited by the individual deposits in two-dimensional space. This zonation, developed roughly from west to east, is manifested in terms of the dominant metal sulfides by the following pattern: Pb-Cu(+Zn,+Ag,±Ba) at Black Mountain; Pb-Zn(+Cu,+Ag,±Ba) at Broken Hill; Zn(+Pb,+Ag,+Ba) at Big Syncline; and Zn(+Pb,+Ba) at Gamsberg. The simplified map of Figure 40 illustrates the above zonal pattern, and has been enriched with the inclusion of isotopic ranges for S, Zn and Fe isotopes from the literature, as well as those presented in this thesis. It is evident that the regional metal zonation observed from west to east is coupled by a corresponding variation of sulfur isotope data, with the lowest $\delta^{34}S$ values recorded at Black Mountain and the highest at Gamsberg, both for sulfide- and for barite-sulfur.

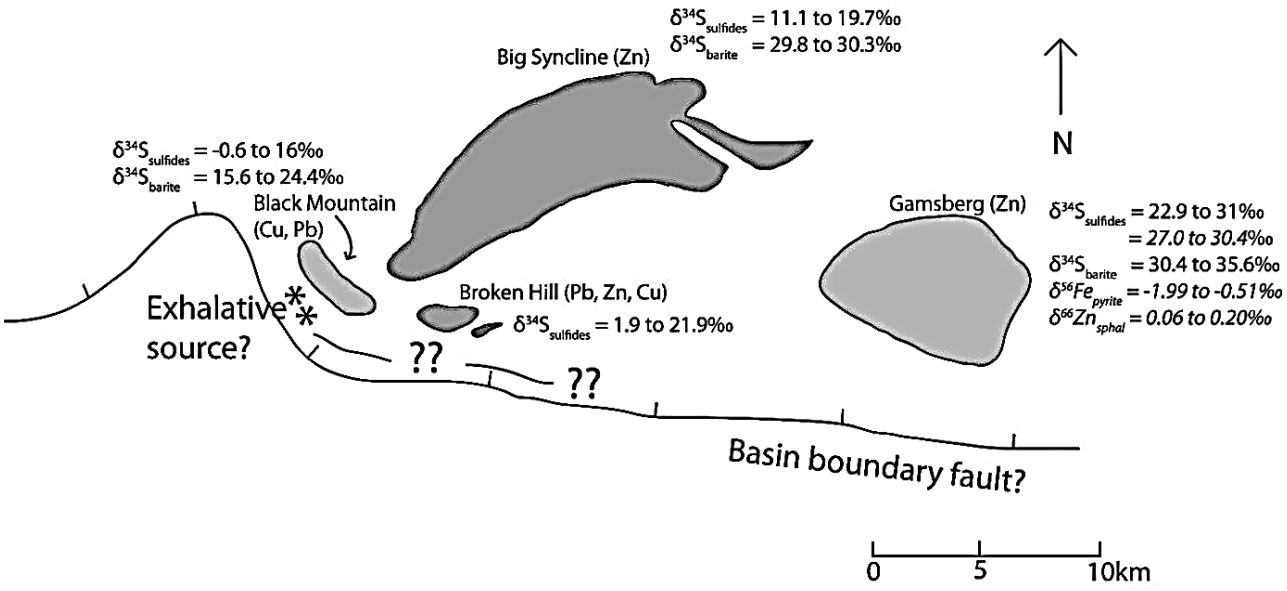

Figure 40. Simplified map of the Aggeneys-Gamsberg District, Namaqualand, illustrating the zonal pattern of base metals as well as $\delta^{34}S_{sulfides}$, $\delta^{34}S_{barite}$, $\delta^{56}Fe_{pyrite/pyrrhotite}$ and $\delta^{66}Zn_{sphalerite}$ values from across the district (values obtains in this these are italicized). Figure modified after Stalder and Rozendaal (2005). Data displayed sourced from references within Table 12and **Figure** 33.

The model of McClung *et al.,* (2007) is based to a large degree on petrographic and isotopic evidence from the barite deposits that occur in association with all base-metal sulfide deposits in the A-G District. These authors argue that the massive sulfide mineralisation and associated barite located in the Black Mountain/Broken Hill deposits formed in a sub-seafloor, epigenetic/replacement-style environment, where metal-bearing hydrothermal fluids mixed with sulfate-rich pore waters derived from a restricted basin (Figure 41). They also argue on the basis of oxygen isotope composition of the barites that the Gamsberg barite deposit formed under a lower temperature regime, compared to the barite from the deposits near Aggeneys (*i.e.* Black Mountain: 250°C *versus* 100-200°C for Gamsberg; McClung *et al.,* 2007).

Finally, McClung *et al.,* (2007) also report no evidence for a replacive origin for the Gamsberg barite, and that syngenetic deposition on the seafloor was most likely in this instance. It is unclear from their model, however, whether the massive sulfide mineralisation itself at Gamsberg is interpreted as also being of syngenetic or epigenetic

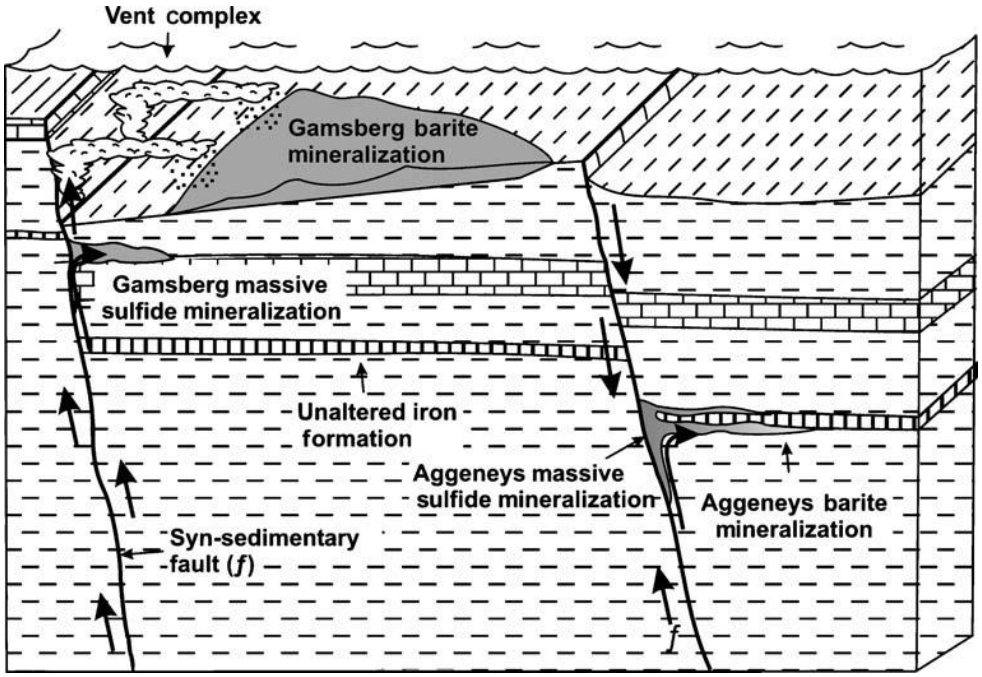

Figure 41. Schematic diagram illustrating the formation of stratiform and stratabound barite and associated massive sulfides in the Aggeneys and Gamsberg deposits (McClung *et al.,* 2007).

origin, as the sulfides are spatially separated from the barite. As also indicated in earlier sections of this thesis, the $\delta^{34}S$ values of barite at Gamsberg are as high as 35‰, and these are interpreted by McClung *et al.,* (2007) as reflective of an isotopically evolved marine sulfate reservoir depleted in ^{32}S by means of BSR, rather than by TSR.

c. Constraints from the Present Study

The geochemical – and particularly stable isotope - results presented in this thesis, provide some additional new information which can help refine and/or question the two proposed models outlined in the foregoing section. Arguably the key implication of the new isotopic data as presented and initially interpreted in Chapter 5 of this thesis, is the apparent de-coupling in the sources of Zn *versus* S for the sulfide mineralisation at Gamsberg: whereas the Zn would have been derived *via* circulating brines through the host sedimentary sequence, the source of the sulfur itself is attributed to the sulfate-bearing water column of the original rift-basin. This assertion is based mainly on the almost exclusively positive $\delta^{34}S$ metal sulfide and sulfate (barite) data from across the entire A-G District. The range of

observed $\delta^{34}S$ values for sulfides and barite at about ±15‰ of the near-20‰ paleo-seawater value would imply that BSR was probably not the main mechanism of sulfur-isotope fractionation, and that thermochemical reduction of seawater sulfate may instead have been the dominant process. This would further imply that redox stratification as a consequence of BSR and resultant euxinia may only have been a weak or transient feature of the depositional paleobasin; this is likely reflected by the occurrence of graphite as part of the sulfide assemblage in an otherwise Fe/Mn-enriched, oxidised package of host sediments.

A key element of the model by Stalder (2003) is that the development of Zn-rich massive sulfide mineralisation at Gamsberg is temporally linked to a hydrothermal system that would have evolved broadly simultaneously, in geological terms, with dense, Zn-rich hydrothermal fluids produced in a residual fashion from an initially buoyant, polymetallic hydrothermal plume. Lateral transport of such fluids as Zn-enriched "bottom-huggers", would have led to the Zn-biased sulfide mineralisation as seen at Gamsberg. One of the intuitive limitations of this model is the requirement of geographically appreciable fluid migration away from the vent; if the present geographical distance of Gamsberg from the other deposits in the A-G District is anything to go by, then these dense, Zn-rich fluids must have been able to travel over 20 km prior to the sequestration of metals as sulfide-rich sediment, especially if TSR was indeed the process of reduced sulfur supply to the ores. The Zn isotope results of this study appear to support the low likelihood of the latter having occurred, as they do not seem to record any statistically significant fractionation effects from source to sink, particularly when one considers that at least some of the Zn has precipitated as part of the metalliferous assemblages in all other deposits in the A-G District (especially that of Big Syncline). As indicated earlier, however, the metallogenic significance of the Zn isotope data can only be further assessed through application on the sphalerite component of the remaining deposits of the region.

The model of McClung *et al.,* (2007) appears to provide a much more viable alternative that can accommodate the geochemical results presented in this thesis. An intrinsic element of this model that distinguishes it from other, typically syngenetic models such as that of

Stalder (2003) above, is that at least some of the deposits in the A-G region are considered to be epigenetic in origin, whereas the Gamsberg deposit appears to be the only syngenetic counterpart (see also Figure 41). The vertical variations reported here in the stable isotope compositions of sulfur for both sphalerite and pyrite and of iron for pyrite, would further support the syngenetic nature for the Gamsberg deposit. In terms of the timing of ore formation, however, the various deposits may have not formed *simultaneously* by a common hydrothermal fluid source, but they may represent discrete hydrothermal pulses in space and time. If the latter was the case, then the essentially unfractionated Zn isotope data from this study support the case of a discrete and chemically unevolved (in space and time) metalliferous fluid source at Gamsberg. Moreover, the Zn- and barite-dominant deposits at Gamsberg may simply reflect a relatively lower-temperature fluid with reduced capacity to carry and supply any significant Pb or Cu, in agreement with the assertion by McClung *et al.,* (2007).

The sulfur isotope data, however, pose some additional challenges: if TSR was indeed the dominant mechanism of reduced sulfur delivery from ambient seawater for the genesis of the sulfide deposits across the entire A-G District, then the epigenetic character of the deposits other than Gamsberg becomes questionable. Simply speaking, it is difficult to explain how the ambient sulfate pool became progressively more enriched in isotopically heavy sulfur (i.e. as seen at Gamsberg) through Rayleigh effects driven by preceding epigenetic mineralising events that utilised pore-water sulfate in each instance. To this end, the author asserts that epigenetic, sub-seafloor sulfide formation would have taken place in essentially closed sub-systems, physically detached from the ambient water column with respect to sulfur. That way, the development of long-term Rayleigh fractionation effects within the basin as a result of prior sulfide precipitation of relatively low $\delta^{34}S$, becomes unsound.

It is argued instead, that all massive sulfide deposits in the A-G District are likely to be originally of syngenetic origin, forming through discrete pulses of base metal-rich hydrothermal fluids across time, and probably utilising more than one structural conduit in space. The deposits forming from the initial, relatively higher-temperature stages of

hydrothermal exhalation would have produced the polymetallic sulfide assemblages as seen at Broken Hill and Black Mountain; later stage, and probably relatively lower-temperature fluid discharges would have led to the more Zn+Ba-rich deposits as seen at Gamsberg. In all instances, however, a common source of reduced sulfur via seawater TSR is postulated, resulting in an isotopically evolving (to higher $\delta^{34}S$) and well-mixed dissolved sulfate pool developing against the various phases of base metal sulfide precipitation from one deposit to the next. The important implication of the foregoing is that the Gamsberg deposit may indeed be regarded as an end-member candidate in the A-G region, albeit in terms of the timing of its formation: that is, it may well reflect massive sulfide deposition during the latter, waning stages of a submarine hydrothermal system, and against the most isotopically evolved seawater sulfur source. The relationship of the Gamsberg deposit with that of other deposits in the A-G District would thus reflect an apparent *diachroneity* in the timing of formation of the individual deposits, which would have allowed for the broad-scale Rayleigh fractionation effect in the sulfur isotope composition of the ambient sulfate pool to develop.

d. Suggestions for Future Work

This study and the results presented herein constitute a small, albeit original in part, effort to re-assess the origin of the Gamsberg massive sulfide deposit as an end-member candidate in the A-G District of the Namaqualand Metamorphic Province, South Africa. For this purpose, standard petrographic, mineral-chemical and bulk geochemical techniques were combined with traditional and novel stable isotope applications in a stratigraphic context, using as target material a representative intersection of the GIF of minimal structural complexity. Although this thesis can be regarded as a small new step towards expanding the knowledge base on, and understanding of, the Gamsberg deposit and the deposits of the A-G District in general, the scope for future work has certainly also broadened as a consequence of it. This pertains particularly with respect to the potential application of Zn and Fe isotopes, both in the A-G District and on other similar deposits elsewhere.

With regard to Zn, the state of play is really wide open: whereas the results presented here did not provide much food for thought in a way of large fractionation in the Zn isotope system, it is still unknown what the Zn isotope composition is in the more "proximal" counterparts of base metal mineralisation in the A-G District. For instance, if the isotopic signature of sphalerite in the sphalerite-impoverished Broken Hill/Black Mountain deposits were to be distinctly negative, then the ever so slightly positive Zn isotope values recorded in the sphalerite-rich Gamsberg ore may still be significant in an isotopic mass-balance sense across the district. The Fe isotope signal of the iron sulfide component in the Gamsberg ores must also await further interrogation: the cycle of iron in SEDEX-type ore-forming environments is expected to be much more complex than that of Zn due to the sequestration of Fe in a variety of redox-dependent species across space and time. Therefore, unless one examines the isotopic composition of these ores and their host rocks *holistically*, *i.e.* by focusing on the entire range of minerals containing iron, then the cycle of iron in such environments will remain obscured. It is therefore clear that a lot can still be done research-wise on the deposits of the A-G District and their counterparts elsewhere, especially through the utilisation of novel isotopic tools. It is hoped that the present thesis constitutes a meaningful starting step towards that direction.

7. REFERENCE LIST

Albarède, F. (2004). The stable isotope geochemistry of copper and zinc. *In:* Johnson, C.M., Bears, B.L. and Albarède (Eds.). *Geochemistry of Non-Traditional stable Isotopes.* Reviews in Mineralogy and Geochemistry, Volume 55. Pp. 409 – 427.

Anbar, A.D. (2004). Iron stable isotopes: beyond biosignatures. *Earth and Planetary Science Letters*, **217**, 223 – 236.

Anderson, G.M. and Thom, J. (2008). The role of thermochemical sulfate reduction in the origin of Mississippi Valley-type deposits. II. Carbonate-sulfide relationships. *Geofluids*, **8**, 27-34.

Anglo American plc. (2010). Anglo American announces sale of Zinc portfolio to Vedanta for $1 338 million. News release.

Archer, C. and Vance, D. (2012). Coupled Fe and S isotope evidence for Archean microbial Fe(III) and sulfate reduction. *Geology*, **34**, 153 – 156.

Arnold, T., Schönbächler, M., Rehkämper, M., Dong, S., Zhao, F-J, Kirk, G.J.D., Coles, B.J. and Weiss, D.J., (2010). Measurement of zinc stable isotope ratios in biogeochemical matrices by double-spike MC-ICPMS and determination of the isotope ratio pool available for plants from soil. *Analytical and Bioanalytical Chemistry,* **398** (7 – 8), 3115 – 3125.

Bailie, R., Armstrong, R. and Reid, D. (2007). The Bushmanland Group supracrustal succession, Aggeneys, Bushmanland, South Africa: Provenance, age of deposition and metamorphism. *South African Journal of Geology*, **110**, 59 – 86.

Bailie, R., Gutzmer, J., Strauss, H., Stüeken, E. and McClung, C. (2010). Sulfur isotope characteristics of metamorphosed Zn-Cu volcanogenic massive sulfides in the Areachap Group, Northern Cape Province, South Africa. *Mineralium Deposita*, **45**, 481 – 496.

Beard, B.L. and Johnson, C.M (2004). Fe isotope variations in the modern and ancient Earth and other planetary bodies. *In:* Johnson, C.M., Bears, B.L. and Albarède (Eds.).

Geochemistry of Non-Traditional stable Isotopes. Reviews in Mineralogy and Geochemistry, Volume 55. Pp. 319 – 357.

Böstrom, K. (1973). The origin and fate of ferromanganoan active ridge sediments. *Stockholm University Contributions to Geology*, **27**, 129 – 243.

Butler, I.B., Archer, C., Vance, D., Oldroyd, A. and Rickard, D. (2005). Fe isotope fractionation on FeS formation in ambient aqueous solution. *Earth and Planetary Science Letters*, **236**, 430 – 442.

Carne, R.C. and Cathro, R.J. (1982). Sedimentary exhalative (SEDEX) zinc-lead-silver deposits, northern Canadian Cordillera. *CIM Bulletin,* **840**, 66 – 78.

Chapman, J.B., Mason, T.F.D., Weiss, D.J., Coles, B.J. and Wilkinson, J.J. (2006). Chemical separation and isotopic variations of Cu and Zn from five geological reference materials. *Geostandards and Geoanalytical Research*, **30** (1), 5 – 16.

Cooke, D.R., Bull, S.W., Large, R.R. and McGoldrick, P.J. (2000). The importance of oxidized brines for the formation of Australian Proterozoic Stratiform sediment-hosted Pb-Zn (SEDEX) deposits. *Economic Geology*, **95** (1), 1 – 18.

Cornell, D.H., Thomas, R.J., Moen, H.F.G., Reid, D.L., Moore, J.M. and Gibson, R.L. (2006). The Namaqua-Natal Province. *In*: Johnson, M.R., Anhaeusser, C.R. and Thomas, R.J. (Eds.), *The Geology of South Africa*. Geological Society of South Africa, Johannesburg and The Council for Geoscience, Pretoria, pp. 325 – 379.

Cornell, D.H., Pettersson, A., Whitehouse, M.J. and Scherstén, A. (2009). A new chronostratigraphic paradigm for the age and tectonic history of the Mesoproterozoic Bushmanland ore district, South Africa. *Economic Geology,* **104**, 385 – 404.

Davidson, G. and Dixon, G.J. (1996). Stable isotope evidence for thermochemical sulfate reduction in the Dugald River (Australia) strata-bound shale-hosted zinc-lead deposit. *Chemical Geology*, **129**, 227 – 246.

Deer, W.A., Howie, R.A. and Zussman, J. (1992). An Introduction to the Rock-Forming Minerals, 2nd edition. Pearson Prentice Hall, England.

Dixon, G. and Davidson, G.J. (1996). Stable isotope evidence for thermochemical sulfate reduction in the Dugald River (Australia) strata-bound shale-hosted zinc-lead deposit. *Chemical Geology*, **129**, 227 – 246.

Droop, G.T.R. (1987). A general equation for estimating Fe^{3+} concentrations in ferromagnesian silicates and oxides form microprobe analyses using stoichiometric criteria. *Mineralogical Magazine,* **51**, 431 – 435.

Emsbo, P. (2009). Geologic criteria for the assessment of sedimentary exhalative (SEDEX) Zn-Pb-Ag deposits. US Geological Survey Open File Report 2009-1209.

Farquhar, J., Wu, N., Canfield, D.E. and Oduro, H. (2010). Connections between the sulfur cycle evolution, sulfur isotopes, sediments and base metal sulfide deposits. *Economic Geology*, **105** (3), 509 – 533.

Fujii, T., Moynier, F., Pons, M. and Albarède, F. (2011). The origin of Zn isotope fractionation in sulfides. *Geochimica et Cosmochimica Acta*, **75**, 7632 – 7643.

Gagnevin, D., Boyce, A.J. Barrie, C.D., Menuge, J.F. and Blakeman, R.J. (2012). Zn, Fe and S isotope fractionation in a large hydrothermal system. *Geochimica et Cosmochimica Acta,* **88**, 183 – 198.

Goodfellow, W.D. and Jonasson, I.R. (1984). Ocean stagnation and ventilation defined by $\delta^{34}S$ secular trends in pyrite and barite, Selwyn Basin, Yukon. *Geology*, **12**, 583 – 586.

Goodfellow, W. and Lydon, J. (2008). Sedimentary Exhalative (SEDEX) deposits. *Geological Association of Canada, Mineral Deposits Division, Special Publication 5.* Pp. 163 – 183.

Goodfellow, W.D., Lydon, J.W. and Turner, R.J.W. (1993). Geology and genesis of stratiform sediment-hosted (SEDEX) zinc-lead-silver sulfide deposits. *In:* Kirkham, R.V., Sinclair, W.D., Thorpe, R.I. and Duke, J.M. (Eds.), *Mineral deposit modelling*. Geological Association of Canada, Special Paper 40, pp. 201 – 251.

Hartnady, C., Joubert, P. and Stowe, C. (1985). Proterozoic crustal evolution in southwestern Africa. *Episodes*, **8** (4), 236 – 244.

Heimann, A., Spry, P.G., Teale, G.S., Connor, C.H.H. and Leyh, W.R. (2009). Geochemistry of garnet-rich rocks in the southern Curnamona Province, Australia and their genetic relationship to Broken Hill-type Pb-Zn-Ag mineralization. *Economic Geology*, **104**, 687 – 712.

Holland, H. (2005). Sedimentary mineral deposits and the evolution of the Earth's near surface environments. *Economic Geology,* **100**, 1489 – 1509.

Holland, H. (2006). The oxygenation of the atmosphere and oceans. *Philosophical Transactions of the Royal Society B,* **361**, 903 – 915.

John S.G., Rouxel, O.J., Craddock, P.R., Engwall, A.M. and Boyle, E.A. (2008). Zinc stable isotopes in seafloor hydrothermal vent fluids and chimneys. *Earth and Planetary Science Letters*, **269**, 17 – 28.

Johnson, C.M. and Beard, B.L. (2006). Fe isotopes: An emerging technique for understanding modern and ancient biogeochemical cycles. *GSA Today*, **16** (11), 4 – 10.

Johnson, C.M., Beard, B.L. and Roden, E.E. (2008). The iron isotope fingerprint of redox and biogeochemical cycling in modern and ancient Earth. *Annual Review of Earth and Planetary Sciences*, **36**, 457 – 493.

Johnson, C.A. Emsbo, P., Poole, F.G. and Rye, R.O. (2009). Sulfur- and oxygen-isotopes in sediment-hosted stratiform barite deposits. *Geochimica et Cosmochimica Acta,* **73**, 133 – 147.

Joubert, P. (1971). The regional tectonism of the gneisses of part of Namaqualand. *Precambrian Research Unit Bulletin, University of Cape Town, Cape Town,* **10**, pp. 220.

Joubert, P. (1974). Geological survey of Namaqualand and Bushmanland. *Annual Report of the Bulletin of the Precambrian Research Unit*, University of Cape Town, **10 – 11**, 24 – 30.

Kelley, K.D., Leach, D.L., Johnson, C.A., Clark, J.L, Fayek, M., Slack, J.F., Anderson, V.M., Ayuso, R.A. and Ridley, W.I. (2004). Textural, compositional and sulfur isotope variations of sulfide minerals in the Red Dog Zn-Pb-Ag Deposits, Brooks Range, Alaska: Implications for ore formation. *Economic Geology*, **99**, 1509 – 1532.

Kelley, K.D., Wilkinson, J.J., Chapman, J.B., Crowther, H.L. and Weiss, D.J. (2009). Zinc isotopes in sphalerite from base metal deposits in the Red Dog District, Northern Alaska. *Economic Geology*, **104** (6), 767 – 773.

Large, R. and Davidson, G. (1991). Controls of brine chemistry on the spectrum of Proterozoic sediment-hosted base-metal deposits. *Proceedings of the SGEG ore fluids conference,* Canberra. BMR Record: 1990/95:50 – 51.

Large, R., Bodon, S., Davidson, G. and Cooke, D. (1996). The chemistry of BHT ore formation – one of the keys to understanding the differences between SEDEX and BHT deposits. *In:* Pongratz, J. and Davidson, G. (Eds.), *New developments in Broken Hill Type deposits*, Proceedings of a workshop on "New Developments in Broken Hill Type Deposits" CODES, University of Tasmania, July 1996, Special Publication 1, pp. 105 – 111.

Large, R., Bull, S., Selley, D., Yang. J., Cooke, D., Garven, G. and McGoldrick, P. (2002). Controls on the formation of giant stratiform sediment-hosted Zn-Pb-Ag deposits: with particular reference to the north Australian Proterozoic. *In:* Cooke, D.R. and Pongratz, J. (Eds.), *Giant Ore Deposits: Characteristics, genesis and exploration,* CODES Special Publication 4, pp. 107 – 149.

Leach, D.L., Sangster, D.F., Kelley, K.D., Large, R.R., Garven, G., Allen, C.R., Gutzmer, J. and Walters, S. (2005). Sediment-hosted lead-zinc deposits: A global perspective. *Economic Geology 100th Anniversary Volume*, 561 – 607.

Leach. D.L., Bradley, D.C., Huston, D., Pisarevsky, S.I., Taylor, R.D. and Gardoll. S.J. (2010). Sediment-hosted lead-zinc deposits in Earth history. *Economic Geology,* **105**, 593 – 625.

Leake, B.E. (1978). Nomenclature of amphiboles. *American Mineralogist*, **63**, 1023 – 1052.

Leake, B.E., Woolley, A.R., Arps, C.E.S., Birch, W.D., Gilbert, M.C., Grice, J.D., Hawthorne, F.C., Kato, A., Kisch, H.J., Krivovichev, V.G.,Linthout, K., Laird, J., Mandarino, J.A., Maresch, W.V., Rock, N.M.S., Schumacher, J.C., Smith, D.C., Stephenson, N.C.N., Ungaretti, L., Whittaker, E.J.W. and Youzhi, G. (1997). Nomenclature of amphiboles: Report of the subcommittee on amphiboles of the international mineralogical association, commission on new minerals and mineral names. *The Canadian Mineralogist*, **35**, 219 – 246.

Lydon, J.W. (1995). Sedimentary exhalative sulfides (SEDEX). *In:* Eckstand, O.R., Sinclair, W.D. and Thorpe, R.I. (eds.), *Geology of Canadian Mineral Deposit Types.* Geological Survey of Canada, Geology of Canada, **8**, 130 – 152.

Machel, H.G. (2001). Bacterial and thermochemical sulfate reduction in diagenetic settings – old and new insights. *Sedimentary Geology*, **140**, 143 – 175.

Machel, H.G., Krouse, H.R. and Sassen, R. (1995). Products and distinguishing criteria of bacterial and thermochemical sulfate reduction. *Applied Geochemistry*, **10**, 373 – 389.

Markl, G., von Blanckenburg, F. and Wagner, T. (2006). Iron isotope fractionation during hydrothermal ore deposition and alteration. *Geochimica et Cosmochimica Acta*, **70**, 3011 – 3030.

Mason, T.F.D., Weiss, D.J., Chapman, J.B., Wilkinson, J.J., Tessalina, S.G., Spiro, B., Horstwood, M.S.A., Spratt, J. and Coles, B.J. (2005). Zn and Cu variability in the Alexandrinka volcanic-hosted massive sulfide (VHMS) ore deposit, Urals, Russia. *Chemical Geology*, **221**, 170 – 187.

Matthews, A., Morgans-Bell, H.S., Emmanuel, S., Jenkyns, H.C., Erel, Y. and Halicz, L. (2004). Controls on iron-isotope fractionation in organic-rich sediments (Kimmeridge Clay, Upper Jurassic, southern England). *Geochimica et Cosmochimica Acta*, **68** (14), 3107 – 3123.

McClung, C.R. (2009). One deposit, four sphalerites: A mineralogical assessment of the Gamsberg Zn deposit. *The Annual Report for the Paleoproterozoic Mineralization Research Group*. Department of Geology, University of Johannesburg.

McClung, C.R. and Viljoen, K.S. (2010a). Mineralogical investigation of the Aggeneys-Gamsberg BHT District, South Africa: Implications for classification of a classical Broken Hill-type district. *Society of Economic Geologists 2010 Conference* – The Challenge of Finding New Mineral Resources: Global Metallogeny, Innovation Exploration and New Discoveries, Keystone Co., September 30 – October 9, D-11.

McClung, C.R. and Viljoen, K.S. (2010b). Ore mineralogy of the world-class Gamsberg Zn sulfide, deposit, South Africa. *Geological Society of America, Abstracts with Programs*, **42** (5), 535.

McClung, C.R. and Viljoen, K.S. (2011). A detailed mineralogical assessment of sphalerites from the Gamsberg zinc deposit, South Africa: The manganese conundrum. *Minerals Engineering*, **24**, 930 – 938.

McClung, C.R., Gutzmer, J., Beukes, N.J., Mezger, K., Strauss, H. and Gertloff, E. (2007). Geochemistry of bedded barite of the Mesoproterozoic Aggeneys-Gamsberg Broken Hill-type district, South Africa. *Mineralium Deposita,* **42**, 537 – 549.

McClung, C.R., Gutzmer, J., Gertloff, E., Beukes, N. And Strauss, H. (2010). Sulfur isotopes of base-metal sulfide and barite pairs from the Aggeneys-Gamsberg BHT district, South Africa. *Geological Society of America Abstract with Programs*, **42** (5), 579.

Moles, N. (1983). Sphalerite composition in relation to deposition and metamorphism of the Foss stratiform Ba-Zn-Pb deposit, Aberfeldy, Scotland. *Mineralogical Magazine,* **47**, 487 – 500.

Möller, K. (2012). Transition metal isotope fractionation in marine hydrothermal deposits of the Mohns Ridge, North Atlantic Ocean. PhD Thesis, University of Bergen, Bergen.

Moore, J.M. (1976). The geology of Namiesberg, Northern Cape. *Precambrian Research Unit Bulletin, University of Cape Town, Cape Town,* **20**, pp. 73.

Moore, J.M., Watkeys, M.K. and Reid, D.L. (1990). The regional setting of the Aggeneys/Gamsberg base metal deposits, Namaqualand, South Africa. *In:* Spry, P.G. and Bryndzia, L.T. (Eds.), *Regional Metamorphism of Ore Deposits and Genetic Implications*. Proceedings of the 28th International Geology Congress, 9 – 19 July, 1989, pp. 77 – 95.

Norrish, K. and Hutton, J.T. (1969). An accurate X-ray spectrographic method for the analysis of a wide range of geological samples. *Geochimica et Cosmochimica Acta*, **33** (4), 431 – 453.

Parr, J.M. and Plimer, I.R. (1993). Models for Broken Hill-type lead-zinc-silver deposits. *In:* Kirkham, R.V., Sinclair, W.D., Thorpe, R.I. and Duke, J.M. (Eds.), *Mineral deposit modelling*. Geological Association of Canada, Special Paper 40, pp. 253 - 288.

Pat, I.I.I. and Thurson, R. (2012). Volcanogenic Massive Sulfide Occurrence Model. *In:* Shanks, W.C., Pat, I.I.I. and Thurson, R. (eds.), *Mineral Deposit Models for Resource Assessment,* US Geological Survey Scientific Investigations Report, Chapter 3.

Pohl, W.L. (2011). Economic Geology: Principles and Practice: Metals, minerals, coal and hydrocarbons - introduction to formation and sustainable exploitation of mineral deposits. Wiley-Blackwell, UK.

Reid, D.L., Welke, H.J., Erlank, A.J. and Betton, P.J. (1987). Composition, age and tectonic setting of amphibolites in the central Bushmanland Group, western Namaqua Province, southern Africa. *Precambrian Research,* **36**, 99 – 126.

Robb, L. (2006). Introduction to Ore Forming Processes. Blackwell Publishing, pp. 177 – 189; 326 – 332.

Robb, L.J., Armstrong, R.A. and Waters, D.J. (1999). The history of granulite-facies metamorphism and crustal growth from single zircon U-Pb geochronology: Namaqualand, South Africa. *Journal of Petrology*, **40** (12), 1747 – 1770.

Robinson, B.S. and Kusakabe, M. (1975). Quantitative preparation of sulfur dioxide for $\delta^{34/32}S$ analyses from sulfides by combustion with cuprous oxide. *Analytical Chemistry*, **47**, 1179 – 1181.

Rouxel, O., Fouquet, Y. and Ludden, J.N. (2004). Subsurface processes at the Lucky Strike hydrothermal field, Mid-Atlantic Ridge: Evidence from sulfur, selenium and iron isotopes. *Geochimica et Cosmochimica Acta,* **10**, 2295 – 2311.

Rouxel, O.J., Bekker, A. and Edwards, K.J. (2005). Iron isotope constraints on the Archean and Paleoproterozoic ocean redox state. *Science*, **307** (5712), 1088 – 1091.

Rozendaal, A. (1982). The petrology of the Gamsberg zinc deposit and the Bushmanland iron formations with special reference to their relationship and genesis. PhD Thesis (Unpublished), University of Stellenbosch.

Rozendaal, A. (1986). The Gamsberg zinc deposit, Namaqualand District. *In:* Anhaeusser, C.R. and Maske, S. (Eds.), *Mineral Deposits of Southern Africa*. Geological Society of South Africa, Johannesburg, Volume II, pp. 1477 – 1488.

Ryan, P.J., Lawrence, A.L., Lipson, R.D., Moore, J.M., Paterson, A., Stedman, D.P. and van Zyl, D. (1986). The Aggeneys base metal sulfides, Namaqualand District. *In:* Anhaeusser, C.R. and Maske, S. (Eds.), *Mineral Deposits of Southern Africa*. Geological Society of South Africa, Johannesburg, Volume II, pp. 1447 - 1473.

Sangster, D.F. (2002). The role of dense brines in the formation of vent-distal sedimentary-exhalative (SEDEX) lead-zinc deposits: field and laboratory evidence. *Mineralium Deposita,* **37**, 149 – 157.

Sangster, D.F. and Hillary, E.M. (1998). SEDEX lead-zinc deposits – proposed sub-types and their characteristics. *Exploration and Mining Geology,* **7** (4), 341 – 357.

Sato, T (1972). Behaviours of ore-forming solutions in seawater. *Mining Geology*, **22**, 31 – 42.

Seal II, R.R. (2006). Sulfur isotope geochemistry of sulfide minerals. *Reviews in Mineralogy and Geochemistry,* **61**, 633 – 677.

Seward, T.M. and Barnes, H.L. (1997). Metal Transport by Hydrothermal Fluids. *In:* Barnes, H.L. (ed.), *Geochemistry of Hydrothermal Ore Deposits, 3rd Edition,* pp435 – 486. John Wiley and Sons, Inc., New York.

Spry (1987). A sulfur isotope study of the Broken Hill deposit, New South Wales, Australia. *Mineralium Deposita*, **22**, 109 – 115.

Spry, P.G. (1990). Geochemistry and origin of coticules (spessartine-quartz rocks) associated with metamorphosed massive sulfide deposits. *In:* Spry, P.G. and Bryndzia, L.T. (Eds.), *Regional metamorphism of ore deposits and genetic implications: Proceedings of the 28th international geology congress, 9-19 July, 1989,* pp. 49 – 75.

Spry, P.G., Peter, J.M. and Slack, J.F. (2000). Meta-exhalites as exploration guides to ore. *In:* Spry, P.G., Marshall, B. and Vokes, F.M. (Eds.), *Metamorphosed and Metamorphogenic Ore Deposits,* Reviews in Economic Geology, Volume 11, Society of Economic Geologists, Inc., pp. 163 – 201.

Stalder, M. (2003). Petrology and Mineral Chemistry of Sulfide Ores and Associated Meta-Exhalites of the Gamsberg Zn-Pb Deposit, South Africa: Implications for Ore Genesis and Mineral Exploration. PhD Thesis (unpublished), Stellenbosch University.

Stalder, M. and Rozendaal, A. (2004). Apatite nodules as an indicator of depositional environment and ore genesis for the Mesoproterozoic Broken Hill-type Gamsberg Zn-Pb deposit, Namaqua Province, South Africa. *Mineralium Deposita*, **39**, 189 – 203.

Stalder, M. and Rozendaal, A. (2005a). Distribution and geochemical characteristics of barite and barium-rich rocks associated with the Broken Hill-type Gamsberg Zn-Pb deposit, Namaqua Province, South Africa. *South African Journal of Geology,* **108**, 35 – 50.

Stalder, M. and Rozendaal, A. (2005b). Calderite-rich garnet and franklinite-rich spinel in amphibolite-facies hydrothermal sediments, Gamsberg Zn-Pb Deposit, Namaqua Province, South Africa. *The Canadian Mineralogist,* **43**, 585 – 599.

Strauss, H. (1993). The sulfur isotope record of Precambrian sulfates: new data and a critical evaluation of the existing record. *Precambrian Research*, **63**, 225 – 246.

Strauss, H (1997). The isotopic composition of sedimentary sulfur through time. *Palaeogeography, Palaeoclimatology, Palaeoecology*, **132**, 97 – 118.

Stowe, C.W., Hartnady, C.J.H. and Joubert, P. (1984). Proterozoic tectonic provinces of southern Africa. *Precambrian Research* (Extended abstract), **25**, 229 – 231.

Thomas, R.J., Agenbacht, A.L.D., Cornell, D.H. and Moore, J.M. (1994). The Kibaran of southern Africa: Tectonic evolution and metallogeny. *Ore Geology Reviews*, **9**, 131 – 160.

Tsikos, H., Matthews, A., Erel, Y. and Moore, J.M. (2010). Iron isotopes constrain biogeochemical redox cycling of iron and manganese in a Paleoproterozoic stratified basin. *Earth and Planetary Science Letters*, **298**, 125 – 134.

Vedanta plc. (2012). Vedanta Annual Report – The Gamsberg Project, an Update. [Online]. Available: http://www.vedanta-zincinternational.com/gamsberg-project. [25/02/2013].

von Gehlen, K., Nielsen, H., Chunnett, I. and Rozendaal, A. (1983). Sulfur isotopes in metamorphosed Precambrian Fe-Pb-Zn-Cu sulfides and barite at Aggeneys and Gamsberg, South Africa. *Mineralogical Magazine*, **47**, 481 – 486.

Walters, S.J. (1996). An overview of Broken Hill Type deposits. *In:* Pongratz, J and Davidson, G. (Eds.), *New developments in Broken Hill Type deposits*, Proceedings of a workshop on "New Developments in Broken Hill Type Deposits" CODES, University of Tasmania, July 1996, Special Publication 1, pp. 1 – 10.

Whitney, D.L. and Evans, B.W. (2010). Abbreviations for names of rock-forming minerals. *American Mineralogist*, **95**, 185 – 187.

Wilkinson, J.J., Weiss, D.J., Mason, T.F.D, and Coles, B.J. (2005). Zinc isotope variation in hydrothermal systems: preliminary evidence from the Irish Midlands ore field. *Economic Geology*, **100**, 583 – 590.

Winter, J. D. (2001). An Introduction to Igneous and Metamorphic Petrology. Prentice-Hall Inc., New Jersey.

Zane, A. and Weiss, Z. (1998). A procedure for classifying rock-forming chlorites based in microprobe data. *Rendiconti Lincei,* **9** (1), 51 – 56.

Zhu, X.K., Guo, Y., Williams, RJP, O'Nions, R.K., Matthews, A., Belshaw, N.S., Canters, G.W., de Waal, E.C., Weser, U., Burgess, B.K. and Salvato, B. (2002). Mass fractionation processes of transition metal isotopes. *Earth and Planetary Science Letters*, **200**, 47 – 62.

8. APPENDIX - Raw Mineral-Chemical Data

Garnet recalculations based on 24O

Label	SiO_2	TiO_2	Al_2O_3	FeO*	Fe_2O_3**	MnO	MgO	CaO	Na_2O	P_2O_5	K_2O	Total
160-1	36.09	0.19	13.04	12.01		32.58	0.57	4.72	0.00	0.00	0.00	99.21
Mol. prop	0.60	0.00	0.13	0.17		0.46	0.01	0.08	0.00	0.00	0.00	
At Prop	1.20	0.00	0.38	0.17		0.46	0.01	0.08	0.00	0.00	0.00	2.31
No anions	12.46	0.05	3.98	1.73		4.76	0.15	0.87	0.00	0.00	0.00	24.00
No ions	6.23	0.03	2.65	1.73		4.76	0.15	0.87	0.00	0.00	0.00	16.42
				0.52	1.20							
	36.09	0.19	13.04	3.64	9.30	32.58	0.57	4.72	0.00	0.00	0.00	100.14
160-2	36.47	0.20	13.93	10.64		33.95	0.59	4.12	0.00	0.00	0.00	99.90
Mol. prop	0.61	0.00	0.14	0.15		0.48	0.01	0.07	0.00	0.00	0.00	
At Prop	1.21	0.01	0.41	0.15		0.48	0.01	0.07	0.00	0.00	0.00	2.34
No anions	12.59	0.05	4.25	1.54		4.96	0.15	0.76	0.00	0.00	0.00	24.30
No ions	6.29	0.03	2.83	1.54		4.96	0.15	0.76	0.00	0.00	0.00	16.57
				[-0.10	1.64]							
				All Fe as Fe^{2+}								
	36.47	0.20	13.93	10.64	0.00	33.95	0.59	4.12	0.00	0.00	0.00	99.90
160-3	36.27	0.19	13.42	11.72		32.98	0.58	4.39	0.00	0.01	0.00	99.56
Mol. prop	0.60	0.00	0.13	0.16		0.46	0.01	0.08	0.00	0.00	0.00	
At Prop	1.21	0.00	0.39	0.16		0.46	0.01	0.08	0.00	0.00	0.00	2.33
No anions	12.52	0.05	4.09	1.69		4.82	0.15	0.81	0.00	0.00	0.00	24.14
No ions	6.26	0.02	2.73	1.69		4.82	0.15	0.81	0.00	0.00	0.00	16.49
				0.27	1.42							
	36.27	0.19	13.42	1.87	10.94	32.98	0.58	4.39	0.00	0.01	0.00	100.65
160-4	34.74	0.16	12.06	12.39		34.96	0.65	4.28	0.00	0.00	0.03	99.27
Mol. prop	0.58	0.00	0.12	0.17		0.49	0.02	0.08	0.00	0.00	0.00	
At Prop	1.16	0.00	0.35	0.17		0.49	0.02	0.08	0.00	0.00	0.00	2.27
No anions	11.99	0.04	3.68	1.79		5.11	0.17	0.79	0.00	0.00	0.00	23.57
No ions	6.00	0.02	2.45	1.79		5.11	0.17	0.79	0.00	0.00	0.01	16.33
				0.81	0.98							
	34.74	0.16	12.06	5.59	7.55	34.96	0.65	4.28	0.00	0.00	0.03	100.03
160-8	36.11	0.21	13.97	11.10		32.87	0.58	4.23	0.00	0.00	0.00	99.06
Mol. prop	0.60	0.00	0.14	0.15		0.46	0.01	0.08	0.00	0.00	0.00	
At Prop	1.20	0.01	0.41	0.15		0.46	0.01	0.08	0.00	0.00	0.00	2.33
No anions	12.46	0.05	4.26	1.60		4.80	0.15	0.78	0.00	0.00	0.00	24.12
No ions	6.23	0.03	2.84	1.60		4.80	0.15	0.78	0.00	0.00	0.00	16.44
				0.32	1.28							
	36.11	0.21	13.97	2.24	9.84	32.87	0.58	4.23	0.00	0.00	0.00	100.05

160-9	35.22	0.23	12.62	10.98		36.01	0.66	3.74	0.01	0.00	0.02	99.50
Mol. prop	0.59	0.00	0.12	0.15		0.51	0.02	0.07	0.00	0.00	0.00	
At Prop	1.17	0.01	0.37	0.15		0.51	0.02	0.07	0.00	0.00	0.00	2.29
No anions	12.16	0.06	3.85	1.58		5.26	0.17	0.69	0.00	0.00	0.00	23.78
No ions	6.08	0.03	2.57	1.58		5.26	0.17	0.69	0.00	0.00	0.00	16.39
				0.43	1.15							
	35.22	0.23	12.62	3.00	8.86	36.01	0.66	3.74	0.01	0.00	0.02	100.39
160-10	36.26	0.19	14.49	9.84		34.31	0.59	3.93	0.00	0.02	0.00	99.64
Mol. prop	0.60	0.00	0.14	0.14		0.48	0.01	0.07	0.00	0.00	0.00	
At Prop	1.21	0.00	0.43	0.14		0.48	0.01	0.07	0.00	0.00	0.00	2.34
No anions	12.51	0.05	4.42	1.42		5.02	0.15	0.73	0.00	0.01	0.00	24.31
No ions	6.26	0.03	2.95	1.42		5.02	0.15	0.73	0.00	0.00	0.00	16.55
				[-0.17	1.59]							
				All Fe as Fe^{2+}								
	36.26	0.19	14.49	9.84	0.00	34.31	0.59	3.93	0.00	0.02	0.00	99.64
160-11	36.31	0.13	14.01	11.21		32.91	0.57	4.36	0.01	0.00	0.00	99.51
Mol. prop	0.60	0.00	0.14	0.16		0.46	0.01	0.08	0.00	0.00	0.00	
At Prop	1.21	0.00	0.41	0.16		0.46	0.01	0.08	0.00	0.00	0.00	2.34
No anions	12.53	0.03	4.28	1.62		4.81	0.15	0.81	0.00	0.00	0.00	24.22
No ions	6.27	0.02	2.85	1.62		4.81	0.15	0.81	0.00	0.00	0.00	16.52
				0.12	1.50							
	36.31	0.13	14.01	0.80	11.57	32.91	0.57	4.36	0.01	0.00	0.00	100.67
160-12	36.54	0.12	14.32	11.30		33.11	0.53	4.52	0.00	0.02	0.00	100.45
Mol. prop	0.61	0.00	0.14	0.16		0.47	0.01	0.08	0.00	0.00	0.00	
At Prop	1.22	0.00	0.42	0.16		0.47	0.01	0.08	0.00	0.00	0.00	2.36
No anions	12.61	0.03	4.37	1.63		4.84	0.14	0.84	0.00	0.01	0.00	24.46
No ions	6.31	0.02	2.91	1.63		4.84	0.14	0.84	0.00	0.00	0.00	16.68
				[-0.32	1.95]							
				All Fe as Fe^{2+}								
	36.54	0.12	14.32	11.30	0.00	33.11	0.53	4.52	0.00	0.02	0.00	100.45
160-13	36.04	0.09	13.41	11.66		32.27	0.52	4.82	0.00	0.00	0.00	98.81
Mol. prop	0.60	0.00	0.13	0.16		0.45	0.01	0.09	0.00	0.00	0.00	
At Prop	1.20	0.00	0.39	0.16		0.45	0.01	0.09	0.00	0.00	0.00	2.31
No anions	12.44	0.02	4.09	1.68		4.72	0.13	0.89	0.00	0.00	0.00	23.98
No ions	6.22	0.01	2.73	1.68		4.72	0.13	0.89	0.00	0.00	0.00	16.38
				0.56	1.12							
	36.04	0.09	13.41	3.87	8.66	32.27	0.52	4.82	0.00	0.00	0.00	99.68

160-19	36.32	0.20	13.40	11.17		33.16	0.53	4.17	0.00	0.01	0.00	98.98
Mol. prop	0.60	0.00	0.13	0.16		0.47	0.01	0.07	0.00	0.00	0.00	
At Prop	1.21	0.00	0.39	0.16		0.47	0.01	0.07	0.00	0.00	0.00	2.32
No anions	12.54	0.05	4.09	1.61		4.85	0.14	0.77	0.00	0.00	0.00	24.05
No ions	6.27	0.03	2.73	1.61		4.85	0.14	0.77	0.00	0.00	0.00	16.39
				0.47	1.14							
	36.32	0.20	13.40	3.26	8.80	33.16	0.53	4.17	0.00	0.01	0.00	99.86
160-21	36.27	0.17	14.22	10.53		33.81	0.60	3.86	0.00	0.00	0.00	99.46
Mol. prop	0.60	0.00	0.14	0.15		0.48	0.01	0.07	0.00	0.00	0.00	
At Prop	1.21	0.00	0.42	0.15		0.48	0.01	0.07	0.00	0.00	0.00	2.34
No anions	12.52	0.04	4.34	1.52		4.94	0.16	0.71	0.00	0.00	0.00	24.23
No ions	6.26	0.02	2.89	1.52		4.94	0.16	0.71	0.00	0.00	0.00	16.50
				0.05	1.47							
	36.27	0.17	14.22	0.36	11.30	33.81	0.60	3.86	0.00	0.00	0.00	100.59
160-22	35.96	0.22	13.30	11.14		33.68	0.52	4.29	0.01	0.01	0.00	99.12
Mol. prop	0.60	0.00	0.13	0.16		0.47	0.01	0.08	0.00	0.00	0.00	
At Prop	1.20	0.01	0.39	0.16		0.47	0.01	0.08	0.00	0.00	0.00	2.31
No anions	12.41	0.06	4.06	1.61		4.92	0.13	0.79	0.00	0.00	0.00	23.99
No ions	6.21	0.03	2.70	1.61		4.92	0.13	0.79	0.00	0.00	0.00	16.40
				0.44	1.17							
	35.96	0.22	13.30	3.03	9.01	33.68	0.52	4.29	0.01	0.01	0.00	100.02
168-2	36.46	0.01	18.04	16.37		21.61	0.55	5.78	0.00	0.00	0.03	98.84
Mol. prop	0.61	0.00	0.18	0.23		0.30	0.01	0.10	0.00	0.00	0.00	
At Prop	1.21	0.00	0.53	0.23		0.30	0.01	0.10	0.00	0.00	0.00	2.39
No anions	12.58	0.00	5.50	2.36		3.16	0.14	1.07	0.00	0.00	0.00	24.82
No ions	6.29	0.00	3.67	2.36		3.16	0.14	1.07	0.00	0.00	0.01	16.70
				0.35	2.01							
	36.46	0.01	18.04	2.46	15.46	21.61	0.55	5.78	0.00	0.00	0.03	100.39
168-3	36.39	0.02	18.39	15.69		22.11	0.54	5.38	0.00	0.00	0.03	98.54
Mol. prop	0.61	0.00	0.18	0.22		0.31	0.01	0.10	0.00	0.00	0.00	
At Prop	1.21	0.00	0.54	0.22		0.31	0.01	0.10	0.00	0.00	0.00	2.39
No anions	12.56	0.00	5.61	2.26		3.23	0.14	1.00	0.00	0.00	0.00	24.81
No ions	6.28	0.00	3.74	2.26		3.23	0.14	1.00	0.00	0.00	0.01	16.66
				0.37	1.90							
	36.389	0.019	18.39	2.53	14.62	22.109	0.542	5.383	0	0	0.025	100.01
168-4	36.14	0.00	18.07	17.23		21.34	0.55	5.74	0.01	0.00	0.02	99.09
Mol. prop	0.60	0.00	0.18	0.24		0.30	0.01	0.10	0.00	0.00	0.00	
At Prop	1.20	0.00	0.53	0.24		0.30	0.01	0.10	0.00	0.00	0.00	2.39
No anions	12.47	0.00	5.51	2.49		3.12	0.14	1.06	0.00	0.00	0.00	24.80
No ions	6.24	0.00	3.68	2.49		3.12	0.14	1.06	0.00	0.00	0.00	16.73
				0.40	2.08							
	36.14	0.00	18.07	2.80	16.04	21.34	0.55	5.74	0.01	0.00	0.02	100.70

168-5	36.14	0.00	18.07	17.23		21.34	0.55	5.74	0.01	0.00	0.02	99.09
Mol. prop	0.60	0.00	0.18	0.24		0.30	0.01	0.10	0.00	0.00	0.00	
At Prop	1.20	0.00	0.53	0.24		0.30	0.01	0.10	0.00	0.00	0.00	2.39
No anions	12.47	0.00	5.51	2.49		3.12	0.14	1.06	0.00	0.00	0.00	24.80
No ions	6.24	0.00	3.68	2.49		3.12	0.14	1.06	0.00	0.00	0.00	16.73
				0.40	2.08							
	36.14	0.00	18.07	2.80	16.04	21.34	0.55	5.74	0.01	0.00	0.02	100.70
168-15	36.13	0.00	18.01	16.19		21.34	0.52	6.43	0.01	0.00	0.00	98.62
Mol. prop	0.60	0.00	0.18	0.23		0.30	0.01	0.11	0.00	0.00	0.00	
At Prop	1.20	0.00	0.53	0.23		0.30	0.01	0.11	0.00	0.00	0.00	2.39
No anions	12.47	0.00	5.49	2.34		3.12	0.13	1.19	0.00	0.00	0.00	24.74
No ions	6.23	0.00	3.66	2.34		3.12	0.13	1.19	0.00	0.00	0.00	16.68
				0.39	1.95							
	36.13	0.00	18.01	2.69	15.00	21.34	0.52	6.43	0.01	0.00	0.00	100.12
168-17	36.70	0.00	18.45	15.57		22.26	0.52	5.64	0.00	0.00	0.03	99.18
Mol. prop	0.61	0.00	0.18	0.22		0.31	0.01	0.10	0.00	0.00	0.00	
At Prop	1.22	0.00	0.54	0.22		0.31	0.01	0.10	0.00	0.00	0.00	2.41
No anions	12.67	0.00	5.63	2.25		3.25	0.13	1.04	0.00	0.00	0.00	24.98
No ions	6.33	0.00	3.75	2.25		3.25	0.13	1.04	0.00	0.00	0.01	16.77
				0.03	2.21							
	36.70	0.00	18.45	0.24	17.03	22.26	0.52	5.64	0.00	0.00	0.03	100.89
168-18	36.72	0.00	18.31	17.31		21.25	0.53	6.23	0.00	0.00	0.04	100.38
Mol. prop	0.61	0.00	0.18	0.24		0.30	0.01	0.11	0.00	0.00	0.00	
At Prop	1.22	0.00	0.54	0.24		0.30	0.01	0.11	0.00	0.00	0.00	2.43
No anions	12.67	0.00	5.59	2.50		3.11	0.14	1.15	0.00	0.00	0.00	25.15
No ions	6.34	0.00	3.72	2.50		3.11	0.14	1.15	0.00	0.00	0.01	16.96
				[-0.22	2.72]							
				All Fe as Fe^{2+}								
	36.72	0.00	18.31	17.31	0.00	21.25	0.53	6.23	0.00	0.00	0.04	100.38
172-1	36.58	0.00	19.23	29.53		10.55	2.61	0.62	0.01	0.00	0.02	99.15
Mol. prop	0.61	0.00	0.19	0.41		0.15	0.06	0.01	0.00	0.00	0.00	
At Prop	1.22	0.00	0.57	0.41		0.15	0.06	0.01	0.00	0.00	0.00	2.42
No anions	12.63	0.00	5.87	4.26		1.54	0.67	0.12	0.00	0.00	0.00	25.09
No ions	6.31	0.00	3.91	4.26		1.54	0.67	0.12	0.00	0.00	0.00	16.82
				1.92	2.34							
	36.58	0.00	19.23	13.28	18.05	10.55	2.61	0.62	0.01	0.00	0.02	100.96
172-2	36.59	0.00	19.25	29.18		10.92	2.45	0.57	0.00	0.00	0.02	98.99
Mol. prop	0.61	0.00	0.19	0.41		0.15	0.06	0.01	0.00	0.00	0.00	
At Prop	1.22	0.00	0.57	0.41		0.15	0.06	0.01	0.00	0.00	0.00	2.42
No anions	12.63	0.00	5.87	4.21		1.60	0.63	0.11	0.00	0.00	0.00	25.05
No ions	6.31	0.00	3.91	4.21		1.60	0.63	0.11	0.00	0.00	0.00	16.78
				1.98	2.23							
	36.59	0.00	19.25	13.73	17.17	10.92	2.45	0.57	0.00	0.00	0.02	100.71

172-3	36.47	0.00	19.52	28.65		11.00	2.37	0.61	0.00	0.00	0.03	98.66
Mol. prop	0.61	0.00	0.19	0.40		0.16	0.06	0.01	0.00	0.00	0.00	
At Prop	1.21	0.00	0.57	0.40		0.16	0.06	0.01	0.00	0.00	0.00	2.41
No anions	12.59	0.00	5.96	4.14		1.61	0.61	0.11	0.00	0.00	0.00	25.01
No ions	6.29	0.00	3.97	4.14		1.61	0.61	0.11	0.00	0.00	0.01	16.74
				2.02	2.12							
	36.47	0.00	19.52	14.00	16.29	11.00	2.37	0.61	0.00	0.00	0.03	100.29
172-6	36.46	0.00	19.45	30.25		10.31	1.74	0.56	0.00	0.00	0.02	98.79
Mol. prop	0.61	0.00	0.19	0.42		0.15	0.04	0.01	0.00	0.00	0.00	
At Prop	1.21	0.00	0.57	0.42		0.15	0.04	0.01	0.00	0.00	0.00	2.41
No anions	12.58	0.00	5.93	4.37		1.51	0.45	0.10	0.00	0.00	0.00	24.95
No ions	6.29	0.00	3.96	4.37		1.51	0.45	0.10	0.00	0.00	0.00	16.68
				2.42	1.95							
	36.46	0.00	19.45	16.75	15.01	10.31	1.74	0.56	0.00	0.00	0.02	100.30
172-7	36.54	0.00	19.15	29.80		10.15	2.55	0.61	0.00	0.00	0.02	98.80
Mol. prop	0.61	0.00	0.19	0.41		0.14	0.06	0.01	0.00	0.00	0.00	
At Prop	1.22	0.00	0.56	0.41		0.14	0.06	0.01	0.00	0.00	0.00	2.41
No anions	12.61	0.00	5.84	4.30		1.48	0.65	0.11	0.00	0.00	0.00	25.01
No ions	6.31	0.00	3.89	4.30		1.48	0.65	0.11	0.00	0.00	0.00	16.75
				2.14	2.16							
	36.54	0.00	19.15	14.81	16.65	10.15	2.55	0.61	0.00	0.00	0.02	100.47
172-8	36.53	0.00	19.64	28.98		11.12	2.40	0.43	0.02	0.00	0.03	99.13
Mol. prop	0.61	0.00	0.19	0.40		0.16	0.06	0.01	0.00	0.00	0.00	
At Prop	1.22	0.00	0.58	0.40		0.16	0.06	0.01	0.00	0.00	0.00	2.42
No anions	12.61	0.00	5.99	4.18		1.63	0.62	0.08	0.00	0.00	0.00	25.11
No ions	6.30	0.00	3.99	4.18		1.63	0.62	0.08	0.00	0.00	0.01	16.81
				1.86	2.32							
	36.53	0.00	19.64	12.92	17.85	11.12	2.40	0.43	0.02	0.00	0.03	100.92
172-9	36.20	0.00	18.91	39.41		2.39	1.64	0.33	0.00	0.00	0.02	98.90
Mol. prop	0.60	0.00	0.19	0.55		0.03	0.04	0.01	0.00	0.00	0.00	
At Prop	1.20	0.00	0.56	0.55		0.03	0.04	0.01	0.00	0.00	0.00	2.39
No anions	12.49	0.00	5.77	5.69		0.35	0.42	0.06	0.00	0.00	0.00	24.79
No ions	6.25	0.00	3.85	5.69		0.35	0.42	0.06	0.00	0.00	0.01	16.62
				3.90	1.79							
	36.20	0.00	18.91	27.03	13.75	2.39	1.64	0.33	0.00	0.00	0.02	100.28
172-11	36.36	0.02	19.43	35.33		6.09	1.32	0.25	0.00	0.00	0.03	98.83
Mol. prop	0.61	0.00	0.19	0.49		0.09	0.03	0.00	0.00	0.00	0.00	
At Prop	1.21	0.00	0.57	0.49		0.09	0.03	0.00	0.00	0.00	0.00	2.40
No anions	12.55	0.00	5.93	5.10		0.89	0.34	0.05	0.00	0.00	0.00	24.86
No ions	6.28	0.00	3.95	5.10		0.89	0.34	0.05	0.00	0.00	0.01	16.61
				3.33	1.76							
	36.36	0.02	19.43	23.11	13.59	6.09	1.32	0.25	0.00	0.00	0.03	100.19

172-13	36.48	0.00	19.33	28.13		12.05	2.28	0.61	0.02	0.00	0.02	98.91
Mol. prop	0.61	0.00	0.19	0.39		0.17	0.06	0.01	0.00	0.00	0.00	
At Prop	1.21	0.00	0.57	0.39		0.17	0.06	0.01	0.00	0.00	0.00	2.41
No anions	12.59	0.00	5.90	4.06		1.76	0.59	0.11	0.00	0.00	0.00	25.01
No ions	6.30	0.00	3.93	4.06		1.76	0.59	0.11	0.00	0.00	0.01	16.75
				1.90	2.16							
	36.48	0.00	19.33	13.15	16.64	12.05	2.28	0.61	0.02	0.00	0.02	100.58
176-9	36.92	0.01	19.84	11.81		26.02	1.00	4.38	0.00	0.00	0.00	99.98
Mol. prop	0.61	0.00	0.19	0.16		0.37	0.02	0.08	0.00	0.00	0.00	
At Prop	1.23	0.00	0.58	0.16		0.37	0.02	0.08	0.00	0.00	0.00	2.45
No anions	12.74	0.00	6.05	1.70		3.80	0.26	0.81	0.00	0.00	0.00	25.37
No ions	6.37	0.00	4.04	1.70		3.80	0.26	0.81	0.00	0.00	0.00	16.98
				[-1.07	2.78]							
				All Fe as Fe^{2+}								
	36.92	0.01	19.84	11.81	0.00	26.02	1.00	4.38	0.00	0.00	0.00	99.98
176-21	36.95	0.00	20.78	10.48		26.83	1.04	3.59	0.00	0.00	0.00	99.69
Mol. prop	0.61	0.00	0.20	0.15		0.38	0.03	0.06	0.00	0.00	0.00	
At Prop	1.23	0.00	0.61	0.15		0.38	0.03	0.06	0.00	0.00	0.00	2.46
No anions	12.75	0.00	6.34	1.51		3.92	0.27	0.66	0.00	0.00	0.00	25.46
No ions	6.38	0.00	4.23	1.51		3.92	0.27	0.66	0.00	0.00	0.00	16.97
				[-1.24	2.75]							
				All Fe as Fe^{2+}								
	36.95	0.00	20.78	10.48	0.00	26.83	1.04	3.59	0.00	0.00	0.00	99.69
176-34	37.06	0.00	20.53	11.47		26.60	1.14	3.45	0.00	0.00	0.00	100.26
Mol. prop	0.62	0.00	0.20	0.16		0.38	0.03	0.06	0.00	0.00	0.00	
At Prop	1.23	0.00	0.60	0.16		0.38	0.03	0.06	0.00	0.00	0.00	2.46
No anions	12.79	0.00	6.26	1.66		3.89	0.29	0.64	0.00	0.00	0.00	25.53
No ions	6.40	0.00	4.18	1.66		3.89	0.29	0.64	0.00	0.00	0.00	17.05
				[-1.29	2.95]							
				All Fe as Fe^{2+}								
	37.06	0.00	20.53	11.47	0.00	26.60	1.14	3.45	0.00	0.00	0.00	100.26
176-35	37.16	0.01	20.28	11.61		26.27	1.09	3.73	0.00	0.01	0.00	100.16
Mol. prop	0.62	0.00	0.20	0.16		0.37	0.03	0.07	0.00	0.00	0.00	
At Prop	1.24	0.00	0.60	0.16		0.37	0.03	0.07	0.00	0.00	0.00	2.46
No anions	12.82	0.00	6.19	1.68		3.84	0.28	0.69	0.00	0.00	0.00	25.50
No ions	6.41	0.00	4.13	1.68		3.84	0.28	0.69	0.00	0.00	0.00	17.03
				[-1.22	2.89]							
				All Fe as Fe^{2+}								
	37.16	0.01	20.28	11.61	0.00	26.27	1.09	3.73	0.00	0.01	0.00	100.16

178-1	36.07	0.02	17.46	11.96		28.64	0.91	4.21	0.01	0.00	0.02	99.30
Mol. prop	0.60	0.00	0.17	0.17		0.40	0.02	0.08	0.00	0.00	0.00	
At Prop	1.20	0.00	0.51	0.17		0.40	0.02	0.08	0.00	0.00	0.00	2.38
No anions	12.45	0.01	5.33	1.73		4.19	0.24	0.78	0.00	0.00	0.00	24.71
No ions	6.22	0.00	3.55	1.73		4.19	0.24	0.78	0.00	0.00	0.00	16.71
				[-0.32	2.04]							
				All Fe as Fe^{2+}								
	36.07	0.02	17.46	11.96	0.00	28.64	0.91	4.21	0.01	0.00	0.02	99.30
178-2	35.82	0.00	17.61	11.61		28.02	1.05	4.53	0.00	0.00	0.02	98.67
Mol. prop	0.60	0.00	0.17	0.16		0.40	0.03	0.08	0.00	0.00	0.00	
At Prop	1.19	0.00	0.52	0.16		0.40	0.03	0.08	0.00	0.00	0.00	2.37
No anions	12.36	0.00	5.37	1.68		4.10	0.27	0.84	0.00	0.00	0.00	24.62
No ions	6.18	0.00	3.58	1.68		4.10	0.27	0.84	0.00	0.00	0.00	16.65
				[-0.20	1.87]							
				All Fe as Fe^{2+}								
	35.82	0.00	17.61	11.61	0.00	28.02	1.05	4.53	0.00	0.00	0.02	98.67
178-5	36.03	0.00	17.38	11.83		28.46	0.96	4.58	0.00	0.00	0.03	99.27
Mol. prop	0.60	0.00	0.17	0.16		0.40	0.02	0.08	0.00	0.00	0.00	
At Prop	1.20	0.00	0.51	0.16		0.40	0.02	0.08	0.00	0.00	0.00	2.38
No anions	12.44	0.00	5.30	1.71		4.16	0.25	0.85	0.00	0.00	0.00	24.70
No ions	6.22	0.00	3.54	1.71		4.16	0.25	0.85	0.00	0.00	0.01	16.72
				[-0.36	2.07]							
				All Fe as Fe^{2+}								
	36.03	0.00	17.38	11.83	0.00	28.46	0.96	4.58	0.00	0.00	0.03	99.27
178-6	36.11	0.00	17.85	12.31		27.51	0.94	4.26	0.00	0.00	0.02	98.99
Mol. prop	0.60	0.00	0.18	0.17		0.39	0.02	0.08	0.00	0.00	0.00	
At Prop	1.20	0.00	0.53	0.17		0.39	0.02	0.08	0.00	0.00	0.00	2.39
No anions	12.46	0.00	5.45	1.78		4.02	0.24	0.79	0.00	0.00	0.00	24.74
No ions	6.23	0.00	3.63	1.78		4.02	0.24	0.79	0.00	0.00	0.00	16.69
				[-0.22	1.99]							
				All Fe as Fe^{2+}								
	36.11	0.00	17.85	12.31	0.00	27.51	0.94	4.26	0.00	0.00	0.02	98.99
178-7	35.93	0.00	17.93	13.61		26.52	0.99	4.11	0.00	0.00	0.02	99.11
Mol. prop	0.60	0.00	0.18	0.19		0.37	0.02	0.07	0.00	0.00	0.00	
At Prop	1.20	0.00	0.53	0.19		0.37	0.02	0.07	0.00	0.00	0.00	2.38
No anions	12.40	0.00	5.47	1.96		3.88	0.25	0.76	0.00	0.00	0.00	24.73
No ions	6.20	0.00	3.65	1.96		3.88	0.25	0.76	0.00	0.00	0.01	16.71
				[-0.07	2.03]							
				All Fe as Fe^{2+}								
	35.93	0.00	17.93	13.61	0.00	26.52	0.99	4.11	0.00	0.00	0.02	99.11

178-8	36.17	0.01	18.99	12.22		25.26	0.99	5.08	0.00	0.00	0.02	98.73
Mol. prop	0.60	0.00	0.19	0.17		0.36	0.02	0.09	0.00	0.00	0.00	
At Prop	1.20	0.00	0.56	0.17		0.36	0.02	0.09	0.00	0.00	0.00	2.40
No anions	12.48	0.00	5.79	1.76		3.69	0.25	0.94	0.00	0.00	0.00	24.93
No ions	6.24	0.00	3.86	1.76		3.69	0.25	0.94	0.00	0.00	0.00	16.76
				[-0.41	2.17]							
				All Fe as Fe^{2+}								
	36.17	0.01	18.99	12.22	0.00	25.26	0.99	5.08	0.00	0.00	0.02	98.73
178-9	36.14	0.00	17.91	12.82		27.65	1.00	4.28	0.02	0.00	0.01	99.84
Mol. prop	0.60	0.00	0.18	0.18		0.39	0.02	0.08	0.00	0.00	0.00	
At Prop	1.20	0.00	0.53	0.18		0.39	0.02	0.08	0.00	0.00	0.00	2.40
No anions	12.47	0.00	5.47	1.85		4.04	0.26	0.79	0.00	0.00	0.00	24.88
No ions	6.24	0.00	3.64	1.85		4.04	0.26	0.79	0.00	0.00	0.00	16.83
				[-0.51	2.36]							
				All Fe as Fe^{2+}								
	36.14	0.00	17.91	12.82	0.00	27.65	1.00	4.28	0.02	0.00	0.01	99.84
178-10	36.58	0.00	19.16	9.80		27.95	1.03	5.12	0.00	0.00	0.02	99.65
Mol. prop	0.61	0.00	0.19	0.14		0.39	0.03	0.09	0.00	0.00	0.00	
At Prop	1.22	0.00	0.56	0.14		0.39	0.03	0.09	0.00	0.00	0.00	2.43
No anions	12.62	0.00	5.85	1.41		4.09	0.26	0.95	0.00	0.00	0.00	25.18
No ions	6.31	0.00	3.90	1.41		4.09	0.26	0.95	0.00	0.00	0.00	16.92
				[-1.21	2.62]							
				All Fe as Fe^{2+}								
	36.58	0.00	19.16	9.80	0.00	27.95	1.03	5.12	0.00	0.00	0.02	99.65
178-11	36.47	0.01	19.04	12.64		25.27	1.00	5.09	0.00	0.00	0.01	99.53
Mol. prop	0.61	0.00	0.19	0.18		0.36	0.02	0.09	0.00	0.00	0.00	
At Prop	1.21	0.00	0.56	0.18		0.36	0.02	0.09	0.00	0.00	0.00	2.42
No anions	12.59	0.00	5.81	1.82		3.69	0.26	0.94	0.00	0.00	0.00	25.12
No ions	6.29	0.00	3.87	1.82		3.69	0.26	0.94	0.00	0.00	0.00	16.89
				[-0.70	2.52]							
				All Fe as Fe^{2+}								
	36.47	0.01	19.04	12.64	0.00	25.27	1.00	5.09	0.00	0.00	0.01	99.53
178-12	36.46	0.01	19.09	9.67		29.18	1.06	4.66	0.00	0.00	0.02	100.14
Mol. prop	0.61	0.00	0.19	0.13		0.41	0.03	0.08	0.00	0.00	0.00	
At Prop	1.21	0.00	0.56	0.13		0.41	0.03	0.08	0.00	0.00	0.00	2.43
No anions	12.58	0.00	5.83	1.40		4.26	0.27	0.86	0.00	0.00	0.00	25.21
No ions	6.29	0.00	3.88	1.40		4.26	0.27	0.86	0.00	0.00	0.01	16.97
				[-1.36	2.75]							
				All Fe as Fe^{2+}								
	36.46	0.01	19.09	9.67	0.00	29.18	1.06	4.66	0.00	0.00	0.02	100.14

178-14	36.58	0.00	19.12	10.40		28.34	1.05	4.54	0.00	0.00	0.03	100.06
Mol. prop	0.61	0.00	0.19	0.14		0.40	0.03	0.08	0.00	0.00	0.00	
At Prop	1.22	0.00	0.56	0.14		0.40	0.03	0.08	0.00	0.00	0.00	2.43
No anions	12.62	0.00	5.83	1.50		4.14	0.27	0.84	0.00	0.00	0.00	25.21
No ions	6.31	0.00	3.89	1.50		4.14	0.27	0.84	0.00	0.00	0.01	16.96
				[-1.22	2.72]							
				All Fe as Fe^{2+}								
	36.58	0.00	19.12	10.40	0.00	28.34	1.05	4.54	0.00	0.00	0.03	100.06
178-22	36.44	0.01	19.12	9.10		28.59	0.88	4.91	0.00	0.00	0.02	99.06
Mol. prop	0.61	0.00	0.19	0.13		0.40	0.02	0.09	0.00	0.00	0.00	
At Prop	1.21	0.00	0.56	0.13		0.40	0.02	0.09	0.00	0.00	0.00	2.41
No anions	12.58	0.00	5.83	1.31		4.18	0.23	0.91	0.00	0.00	0.00	25.04
No ions	6.29	0.00	3.89	1.31		4.18	0.23	0.91	0.00	0.00	0.00	16.81
				[-1.00	2.31]							
				All Fe as Fe^{2+}								
	36.44	0.01	19.12	9.10	0.00	28.59	0.88	4.91	0.00	0.00	0.02	99.06
178-26	36.50	0.02	19.00	10.86		26.77	0.98	5.22	0.00	0.00	0.01	99.35
Mol. prop	0.61	0.00	0.19	0.15		0.38	0.02	0.09	0.00	0.00	0.00	
At Prop	1.21	0.00	0.56	0.15		0.38	0.02	0.09	0.00	0.00	0.00	2.42
No anions	12.60	0.00	5.80	1.57		3.91	0.25	0.97	0.00	0.00	0.00	25.09
No ions	6.30	0.00	3.86	1.57		3.91	0.25	0.97	0.00	0.00	0.00	16.86
				[-0.89	2.46]							
				All Fe as Fe^{2+}								
	36.50	0.02	19.00	10.86	0.00	26.77	0.98	5.22	0.00	0.00	0.01	99.35
180-2	36.31	0.09	17.60	6.04		36.49	1.09	1.79	0.00	0.00	0.02	99.42
Mol. prop	0.60	0.00	0.17	0.08		0.51	0.03	0.03	0.00	0.00	0.00	
At Prop	1.21	0.00	0.52	0.08		0.51	0.03	0.03	0.00	0.00	0.00	2.39
No anions	12.53	0.02	5.37	0.87		5.33	0.28	0.33	0.00	0.00	0.00	24.74
No ions	6.27	0.01	3.58	0.87		5.33	0.28	0.33	0.00	0.00	0.00	16.68
				[-1.08	1.95]							
				All Fe as Fe^{2+}								
	36.31	0.09	17.60	6.04	0.00	36.49	1.09	1.79	0.00	0.00	0.02	99.42
180-3	36.35	0.04	18.84	5.68		36.08	1.37	1.47	0.00	0.00	0.02	99.86
Mol. prop	0.60	0.00	0.18	0.08		0.51	0.03	0.03	0.00	0.00	0.00	
At Prop	1.21	0.00	0.55	0.08		0.51	0.03	0.03	0.00	0.00	0.00	2.41
No anions	12.55	0.01	5.75	0.82		5.27	0.35	0.27	0.00	0.00	0.00	25.03
No ions	6.27	0.01	3.83	0.82		5.27	0.35	0.27	0.00	0.00	0.00	16.84
				[-1.56	2.38]							
				All Fe as Fe^{2+}								
	36.35	0.04	18.84	5.68	0.00	36.08	1.37	1.47	0.00	0.00	0.02	99.86

180-4	36.42	0.04	18.69	5.52		36.51	1.26	1.18	0.00	0.00	0.02	99.63
Mol. prop	0.61	0.00	0.18	0.08		0.51	0.03	0.02	0.00	0.00	0.00	
At Prop	1.21	0.00	0.55	0.08		0.51	0.03	0.02	0.00	0.00	0.00	2.41
No anions	12.57	0.01	5.70	0.80		5.34	0.32	0.22	0.00	0.00	0.00	24.96
No ions	6.29	0.00	3.80	0.80		5.34	0.32	0.22	0.00	0.00	0.00	16.77
				[-1.41	2.20]							
				All Fe as Fe^{2+}								
	36.42	0.04	18.69	5.52	0.00	36.51	1.26	1.18	0.00	0.00	0.02	99.63
180-13	36.31	0.09	17.60	6.04		36.49	1.09	1.79	0.00	0.00	0.02	99.42
Mol. prop	0.60	0.00	0.17	0.08		0.51	0.03	0.03	0.00	0.00	0.00	
At Prop	1.21	0.00	0.52	0.08		0.51	0.03	0.03	0.00	0.00	0.00	2.39
No anions	12.53	0.02	5.37	0.87		5.33	0.28	0.33	0.00	0.00	0.00	24.74
No ions	6.27	0.01	3.58	0.87		5.33	0.28	0.33	0.00	0.00	0.00	16.68
				[-1.08	1.95]							
				All Fe as Fe^{2+}								
	36.31	0.09	17.60	6.04	0.00	36.49	1.09	1.79	0.00	0.00	0.02	99.42
180-14	36.35	0.04	18.84	5.68		36.08	1.37	1.47	0.00	0.00	0.02	99.86
Mol. prop	0.60	0.00	0.18	0.08		0.51	0.03	0.03	0.00	0.00	0.00	
At Prop	1.21	0.00	0.55	0.08		0.51	0.03	0.03	0.00	0.00	0.00	2.41
No anions	12.55	0.01	5.75	0.82		5.27	0.35	0.27	0.00	0.00	0.00	25.03
No ions	6.27	0.01	3.83	0.82		5.27	0.35	0.27	0.00	0.00	0.00	16.84
				[-1.56	2.38]							
				All Fe as Fe^{2+}								
	36.35	0.04	18.84	5.68	0.00	36.08	1.37	1.47	0.00	0.00	0.02	99.86
180-15	36.42	0.04	18.69	5.52		36.51	1.26	1.18	0.00	0.00	0.02	99.63
Mol. prop	0.61	0.00	0.18	0.08		0.51	0.03	0.02	0.00	0.00	0.00	
At Prop	1.21	0.00	0.55	0.08		0.51	0.03	0.02	0.00	0.00	0.00	2.41
No anions	12.57	0.01	5.70	0.80		5.34	0.32	0.22	0.00	0.00	0.00	24.96
No ions	6.29	0.00	3.80	0.80		5.34	0.32	0.22	0.00	0.00	0.00	16.77
				[-1.41	2.20]							
				All Fe as Fe^{2+}								
	36.42	0.04	18.69	5.52	0.00	36.51	1.26	1.18	0.00	0.00	0.02	99.63
232-23	38.05	0.10	19.92	14.96		12.79	1.38	11.32	0.00	0.00	0.00	98.52
Mol. prop	0.63	0.00	0.20	0.21		0.18	0.03	0.20	0.00	0.00	0.00	
At Prop	1.27	0.00	0.59	0.21		0.18	0.03	0.20	0.00	0.00	0.00	2.48
No anions	13.13	0.03	6.08	2.16		1.87	0.36	2.09	0.00	0.00	0.00	25.71
No ions	6.57	0.01	4.05	2.16		1.87	0.36	2.09	0.00	0.00	0.00	17.11
				[-0.95	3.11]							
				All Fe as Fe^{2+}								
	38.05	0.10	19.92	14.96	0.00	12.79	1.38	11.32	0.00	0.00	0.00	98.52

232-26	41.46	0.03	18.72	14.75		12.65	1.47	9.64	0.04	0.01	0.00	98.76
Mol. prop	0.69	0.00	0.18	0.21		0.18	0.04	0.17	0.00	0.00	0.00	
At Prop	1.38	0.00	0.55	0.21		0.18	0.04	0.17	0.00	0.00	0.00	2.52
No anions	14.31	0.01	5.71	2.13		1.85	0.38	1.78	0.00	0.00	0.00	26.17
No ions	7.16	0.00	3.81	2.13		1.85	0.38	1.78	0.01	0.00	0.00	17.11
				[-0.99	3.12]							
				All Fe as Fe^{2+}								
	41.46	0.03	18.72	14.75	0.00	12.65	1.47	9.64	0.04	0.01	0.00	98.76

Pyroxene Recalculated on the basis of 6O

Label	SiO_2	TiO_2	Al_2O_3	FeO*	Fe_2O_3**	MnO	MgO	CaO	Na_2O	P_2O_5	K_2O	Total
164-5	52.85	0.02	0.28	7.24		8.87	10.38	18.70	1.40	0.02	0.00	99.74
Mol. prop	0.88	0.00	0.00	0.10		0.12	0.26	0.33	0.01	0.00	0.00	
At Prop	1.76	0.00	0.01	0.10		0.12	0.26	0.33	0.01	0.00	0.00	2.60
No anions	4.06	0.00	0.02	0.23		0.29	0.59	0.77	0.03	0.00	0.00	6.00
No ions	2.03	0.00	0.01	0.23		0.29	0.59	0.77	0.07	0.00	0.00	4.00
				All Fe as Fe^{2+}								
				0.35	0.00							
	52.85	0.02	0.28	7.24	0.00	8.87	10.38	18.70	1.40	0.02	0.00	**99.74**
164-7	52.54	0.02	0.28	7.35		8.94	10.01	18.71	1.38	0.01	0.00	99.24
Mol. prop	0.87	0.00	0.00	0.10		0.13	0.25	0.33	0.01	0.00	0.00	
At Prop	1.75	0.00	0.01	0.10		0.13	0.25	0.33	0.01	0.00	0.00	2.58
No anions	4.04	0.00	0.02	0.24		0.29	0.57	0.77	0.03	0.00	0.00	5.96
No ions	2.02	0.00	0.01	0.24		0.29	0.57	0.77	0.07	0.00	0.00	3.97
				All Fe as Fe^{2+}								
				0.36	0.00							
	52.54	0.02	0.28	7.35	0.00	8.94	10.01	18.71	1.38	0.01	0.00	**99.24**
164-16	52.09	0.02	0.30	6.86		8.91	10.68	18.99	1.30	0.00	0.00	99.15
Mol. prop	0.87	0.00	0.00	0.10		0.13	0.26	0.34	0.01	0.00	0.00	
At Prop	1.73	0.00	0.01	0.10		0.13	0.26	0.34	0.01	0.00	0.00	2.58
No anions	4.00	0.00	0.02	0.22		0.29	0.61	0.78	0.03	0.00	0.00	5.96
No ions	2.00	0.00	0.01	0.22		0.29	0.61	0.78	0.06	0.00	0.00	3.98
				All Fe as Fe^{2+}								
				0.33	0.00							
	52.09	0.02	0.30	6.86	0.00	8.91	10.68	18.99	1.30	0.00	0.00	**99.15**
164-24	52.65	0.01	0.29	7.25		9.00	10.23	18.63	1.44	0.01	0.01	99.52
Mol. prop	0.88	0.00	0.00	0.10		0.13	0.25	0.33	0.02	0.00	0.00	
At Prop	1.75	0.00	0.01	0.10		0.13	0.25	0.33	0.02	0.00	0.00	2.59
No anions	4.04	0.00	0.02	0.23		0.29	0.59	0.77	0.04	0.00	0.00	5.98
No ions	2.02	0.00	0.01	0.23		0.29	0.59	0.77	0.07	0.00	0.00	3.99
				All Fe as Fe^{2+}								
				0.35	0.00							
	52.65	0.01	0.29	7.25	0.00	9.00	10.23	18.63	1.44	0.01	0.01	**99.52**
164-25	52.72	0.01	0.26	7.17		9.19	10.10	18.91	1.29	0.01	0.01	99.65
Mol. prop	0.88	0.00	0.00	0.10		0.13	0.25	0.34	0.01	0.00	0.00	
At Prop	1.75	0.00	0.01	0.10		0.13	0.25	0.34	0.01	0.00	0.00	2.59
No anions	4.05	0.00	0.02	0.23		0.30	0.58	0.78	0.03	0.00	0.00	5.99
No ions	2.03	0.00	0.01	0.23		0.30	0.58	0.78	0.06	0.00	0.00	3.99
				All Fe as Fe^{2+}								
				0.35	0.00							
	52.72	0.01	0.26	7.17	0.00	9.19	10.10	18.91	1.29	0.01	0.01	**99.65**

164-47	51.97	0.01	0.41	6.87		9.81	9.47	19.08	1.09	0.01	0.00	98.73
Mol. prop	0.86	0.00	0.00	0.10		0.14	0.23	0.34	0.01	0.00	0.00	
At Prop	1.73	0.00	0.01	0.10		0.14	0.23	0.34	0.01	0.00	0.00	2.56
No anions	3.99	0.00	0.03	0.22		0.32	0.54	0.79	0.03	0.00	0.00	5.92
No ions	2.00	0.00	0.02	0.22		0.32	0.54	0.79	0.05	0.00	0.00	3.94
				All Fe as Fe^{2+}								
				0.34	0.00							
	51.97	0.01	0.41	6.87	0.00	9.81	9.47	19.08	1.09	0.01	0.00	**98.73**
168-54	50.15	0.00	0.14	8.91		10.02	8.83	20.39	0.21	0.00	0.03	98.68
Mol. prop	0.83	0.00	0.00	0.12		0.14	0.22	0.36	0.00	0.00	0.00	
At Prop	1.67	0.00	0.00	0.12		0.14	0.22	0.36	0.00	0.00	0.00	2.52
No anions	3.85	0.00	0.01	0.29		0.33	0.51	0.84	0.01	0.00	0.00	5.83
No ions	1.93	0.00	0.01	0.29		0.33	0.51	0.84	0.01	0.00	0.00	3.90
				All Fe as Fe^{2+}								
				0.44	0.00							
	50.15	0.00	0.14	8.91	0.00	10.02	8.83	20.39	0.21	0.00	0.03	**98.68**
168-55	50.40	0.00	0.15	8.50		9.58	9.68	20.19	0.37	0.00	0.04	98.91
Mol. prop	0.84	0.00	0.00	0.12		0.14	0.24	0.36	0.00	0.00	0.00	
At Prop	1.68	0.00	0.00	0.12		0.14	0.24	0.36	0.00	0.00	0.00	2.54
No anions	3.87	0.00	0.01	0.27		0.31	0.55	0.83	0.01	0.00	0.00	5.86
No ions	1.94	0.00	0.01	0.27		0.31	0.55	0.83	0.02	0.00	0.00	3.93
				All Fe as Fe^{2+}								
				0.42	0.00							
	50.40	0.00	0.15	8.50	0.00	9.58	9.68	20.19	0.37	0.00	0.04	**98.91**
170-1	48.32	0.00	0.04	24.81		18.88	3.33	3.66	0.03	0.00	0.00	99.07
Mol. prop	0.80	0.00	0.00	0.35		0.27	0.08	0.07	0.00	0.00	0.00	
At Prop	1.61	0.00	0.00	0.35		0.27	0.08	0.07	0.00	0.00	0.00	2.37
No anions	3.71	0.00	0.00	0.80		0.61	0.19	0.15	0.00	0.00	0.00	5.47
No ions	1.86	0.00	0.00	0.80		0.61	0.19	0.15	0.00	0.00	0.00	3.61
				All Fe as Fe^{2+}								
				1.32	0.00							
	48.32	0.00	0.04	24.81	0.00	18.88	3.33	3.66	0.03	0.00	0.00	**99.07**
170-4	47.21	0.00	0.03	26.23		18.46	3.84	3.67	0.02	0.00	0.04	99.49
Mol. prop	0.79	0.00	0.00	0.37		0.26	0.10	0.07	0.00	0.00	0.00	
At Prop	1.57	0.00	0.00	0.37		0.26	0.10	0.07	0.00	0.00	0.00	2.36
No anions	3.63	0.00	0.00	0.84		0.60	0.22	0.15	0.00	0.00	0.00	5.44
No ions	1.81	0.00	0.00	0.84		0.60	0.22	0.15	0.00	0.00	0.00	3.63
				All Fe as Fe^{2+}								
				1.39	0.00							
	47.21	0.00	0.03	26.23	0.00	18.46	3.84	3.67	0.02	0.00	0.04	**99.49**

170-5	46.95	0.00	0.05	25.68		18.75	3.76	3.63	0.04	0.00	0.03	98.88
Mol. prop	0.78	0.00	0.00	0.36		0.26	0.09	0.06	0.00	0.00	0.00	
At Prop	1.56	0.00	0.00	0.36		0.26	0.09	0.06	0.00	0.00	0.00	2.34
No anions	3.61	0.00	0.00	0.82		0.61	0.22	0.15	0.00	0.00	0.00	5.41
No ions	1.80	0.00	0.00	0.82		0.61	0.22	0.15	0.00	0.00	0.00	3.61
				All Fe as Fe^{2+}								
				1.37	0.00							
	46.95	0.00	0.05	25.68	0.00	18.75	3.76	3.63	0.04	0.00	0.03	**98.88**
170-6	48.74	0.00	0.23	19.02		7.32	6.62	17.00	0.12	0.00	0.04	99.07
Mol. prop	0.81	0.00	0.00	0.26		0.10	0.16	0.30	0.00	0.00	0.00	
At Prop	1.62	0.00	0.01	0.26		0.10	0.16	0.30	0.00	0.00	0.00	2.47
No anions	3.74	0.00	0.02	0.61		0.24	0.38	0.70	0.00	0.00	0.00	5.69
No ions	1.87	0.00	0.01	0.61		0.24	0.38	0.70	0.01	0.00	0.00	3.82
				All Fe as Fe^{2+}								
				0.96	0.00							
	48.74	0.00	0.23	19.02	0.00	7.32	6.62	17.00	0.12	0.00	0.04	**99.07**
170-7	46.82	0.01	0.03	26.68		18.98	3.69	3.65	0.04	0.00	0.02	99.91
Mol. prop	0.78	0.00	0.00	0.37		0.27	0.09	0.06	0.00	0.00	0.00	
At Prop	1.56	0.00	0.00	0.37		0.27	0.09	0.06	0.00	0.00	0.00	2.36
No anions	3.60	0.00	0.00	0.86		0.62	0.21	0.15	0.00	0.00	0.00	5.44
No ions	1.80	0.00	0.00	0.86		0.62	0.21	0.15	0.00	0.00	0.00	3.64
				All Fe as Fe^{2+}								
				1.41	0.00							
	46.82	0.01	0.03	26.68	0.00	18.98	3.69	3.65	0.04	0.00	0.02	**99.91**
170-8	46.76	0.02	0.04	25.93		19.28	3.89	3.47	0.04	0.00	0.04	99.46
Mol. prop	0.78	0.00	0.00	0.36		0.27	0.10	0.06	0.00	0.00	0.00	
At Prop	1.56	0.00	0.00	0.36		0.27	0.10	0.06	0.00	0.00	0.00	2.35
No anions	3.59	0.00	0.00	0.83		0.63	0.22	0.14	0.00	0.00	0.00	5.42
No ions	1.80	0.00	0.00	0.83		0.63	0.22	0.14	0.00	0.00	0.00	3.63
				All Fe as Fe^{2+}								
				1.38	0.00							
	46.76	0.02	0.04	25.93	0.00	19.28	3.89	3.47	0.04	0.00	0.04	**99.46**
170-9	46.96	0.00	0.06	25.66		18.95	3.94	3.08	0.00	0.00	0.04	98.70
Mol. prop	0.78	0.00	0.00	0.36		0.27	0.10	0.05	0.00	0.00	0.00	
At Prop	1.56	0.00	0.00	0.36		0.27	0.10	0.05	0.00	0.00	0.00	2.34
No anions	3.61	0.00	0.00	0.82		0.62	0.23	0.13	0.00	0.00	0.00	5.41
No ions	1.80	0.00	0.00	0.82		0.62	0.23	0.13	0.00	0.00	0.00	3.60
				All Fe as Fe^{2+}								
				1.37	0.00							
	46.96	0.00	0.06	25.66	0.00	18.95	3.94	3.08	0.00	0.00	0.04	**98.70**

170-13	46.62	0.00	0.01	25.46		19.27	3.76	3.48	0.02	0.00	0.02	98.65
Mol. prop	0.78	0.00	0.00	0.35		0.27	0.09	0.06	0.00	0.00	0.00	
At Prop	1.55	0.00	0.00	0.35		0.27	0.09	0.06	0.00	0.00	0.00	2.33
No anions	3.58	0.00	0.00	0.82		0.63	0.22	0.14	0.00	0.00	0.00	5.39
No ions	1.79	0.00	0.00	0.82		0.63	0.22	0.14	0.00	0.00	0.00	3.60
				All Fe as Fe^{2+}								
				1.36	0.00							
	46.62	0.00	0.01	25.46	0.00	19.27	3.76	3.48	0.02	0.00	0.02	**98.65**
170-15	46.79	0.00	0.03	25.96		19.51	3.77	3.04	0.03	0.00	0.02	99.15
Mol. prop	0.78	0.00	0.00	0.36		0.27	0.09	0.05	0.00	0.00	0.00	
At Prop	1.56	0.00	0.00	0.36		0.27	0.09	0.05	0.00	0.00	0.00	2.34
No anions	3.59	0.00	0.00	0.83		0.63	0.22	0.13	0.00	0.00	0.00	5.41
No ions	1.80	0.00	0.00	0.83		0.63	0.22	0.13	0.00	0.00	0.00	3.61
				All Fe as Fe^{2+}								
				1.39	0.00							
	46.79	0.00	0.03	25.96	0.00	19.51	3.77	3.04	0.03	0.00	0.02	**99.15**
170-16	46.55	0.02	0.03	26.97		20.27	3.48	2.67	0.03	0.00	0.03	100.05
Mol. prop	0.77	0.00	0.00	0.38		0.29	0.09	0.05	0.00	0.00	0.00	
At Prop	1.55	0.00	0.00	0.38		0.29	0.09	0.05	0.00	0.00	0.00	2.35
No anions	3.58	0.00	0.00	0.87		0.66	0.20	0.11	0.00	0.00	0.00	5.42
No ions	1.79	0.00	0.00	0.87		0.66	0.20	0.11	0.00	0.00	0.00	3.63
				All Fe as Fe^{2+}								
				1.43	0.00							
	46.55	0.02	0.03	26.97	0.00	20.27	3.48	2.67	0.03	0.00	0.03	**100.05**
170-17	46.68	0.00	0.00	25.93		19.49	3.76	3.05	0.02	0.00	0.02	98.94
Mol. prop	0.78	0.00	0.00	0.36		0.27	0.09	0.05	0.00	0.00	0.00	
At Prop	1.55	0.00	0.00	0.36		0.27	0.09	0.05	0.00	0.00	0.00	2.34
No anions	3.59	0.00	0.00	0.83		0.63	0.22	0.13	0.00	0.00	0.00	5.39
No ions	1.79	0.00	0.00	0.83		0.63	0.22	0.13	0.00	0.00	0.00	3.60
				All Fe as Fe^{2+}								
				1.39	0.00							
	46.68	0.00	0.00	25.93	0.00	19.49	3.76	3.05	0.02	0.00	0.02	**98.94**
170-18	46.83	0.00	0.02	25.54		19.20	3.49	3.71	0.01	0.00	0.02	98.82
Mol. prop	0.78	0.00	0.00	0.36		0.27	0.09	0.07	0.00	0.00	0.00	
At Prop	1.56	0.00	0.00	0.36		0.27	0.09	0.07	0.00	0.00	0.00	2.34
No anions	3.60	0.00	0.00	0.82		0.62	0.20	0.15	0.00	0.00	0.00	5.40
No ions	1.80	0.00	0.00	0.82		0.62	0.20	0.15	0.00	0.00	0.00	3.60
				All Fe as Fe^{2+}								
				1.37	0.00							
	46.83	0.00	0.02	25.54	0.00	19.20	3.49	3.71	0.01	0.00	0.02	**98.82**

170-21	48.05	0.00	0.04	25.13		17.86	3.68	3.70	0.03	0.01	0.00	98.51
Mol. prop	0.80	0.00	0.00	0.35		0.25	0.09	0.07	0.00	0.00	0.00	
At Prop	1.60	0.00	0.00	0.35		0.25	0.09	0.07	0.00	0.00	0.00	2.36
No anions	3.69	0.00	0.00	0.81		0.58	0.21	0.15	0.00	0.00	0.00	5.45
No ions	1.85	0.00	0.00	0.81		0.58	0.21	0.15	0.00	0.00	0.00	3.60
				All Fe as Fe^{2+}								
				1.35	0.00							
	48.05	0.00	0.04	25.13	0.00	17.86	3.68	3.70	0.03	0.01	0.00	**98.51**
170-22	46.83	0.00	0.02	25.54		19.20	3.49	3.71	0.01	0.00	0.02	98.82
Mol. prop	0.78	0.00	0.00	0.36		0.27	0.09	0.07	0.00	0.00	0.00	
At Prop	1.56	0.00	0.00	0.36		0.27	0.09	0.07	0.00	0.00	0.00	2.34
No anions	3.60	0.00	0.00	0.82		0.62	0.20	0.15	0.00	0.00	0.00	5.40
No ions	1.80	0.00	0.00	0.82		0.62	0.20	0.15	0.00	0.00	0.00	3.60
				All Fe as Fe^{2+}								
				1.37	0.00							
	46.83	0.00	0.02	25.54	0.00	19.20	3.49	3.71	0.01	0.00	0.02	**98.82**
170-24	47.21	0.00	0.03	26.23		18.46	3.84	3.67	0.02	0.00	0.04	99.49
Mol. prop	0.79	0.00	0.00	0.37		0.26	0.10	0.07	0.00	0.00	0.00	
At Prop	1.57	0.00	0.00	0.37		0.26	0.10	0.07	0.00	0.00	0.00	2.36
No anions	3.63	0.00	0.00	0.84		0.60	0.22	0.15	0.00	0.00	0.00	5.44
No ions	1.81	0.00	0.00	0.84		0.60	0.22	0.15	0.00	0.00	0.00	3.63
				All Fe as Fe^{2+}								
				1.39	0.00							
	47.21	0.00	0.03	26.23	0.00	18.46	3.84	3.67	0.02	0.00	0.04	**99.49**
170-24	48.25	0.02	0.02	25.36		17.38	3.61	3.87	0.04	0.00	0.00	98.56
Mol. prop	0.80	0.00	0.00	0.35		0.25	0.09	0.07	0.00	0.00	0.00	
At Prop	1.61	0.00	0.00	0.35		0.25	0.09	0.07	0.00	0.00	0.00	2.36
No anions	3.71	0.00	0.00	0.81		0.57	0.21	0.16	0.00	0.00	0.00	5.46
No ions	1.85	0.00	0.00	0.81		0.57	0.21	0.16	0.00	0.00	0.00	3.60
				All Fe as Fe^{2+}								
				1.36	0.00							
	48.25	0.02	0.02	25.36	0.00	17.38	3.61	3.87	0.04	0.00	0.00	**98.56**
170-25	46.95	0.00	0.05	25.68		18.75	3.76	3.63	0.04	0.00	0.03	98.88
Mol. prop	0.78	0.00	0.00	0.36		0.26	0.09	0.06	0.00	0.00	0.00	
At Prop	1.56	0.00	0.00	0.36		0.26	0.09	0.06	0.00	0.00	0.00	2.34
No anions	3.61	0.00	0.00	0.82		0.61	0.22	0.15	0.00	0.00	0.00	5.41
No ions	1.80	0.00	0.00	0.82		0.61	0.22	0.15	0.00	0.00	0.00	3.61
				All Fe as Fe^{2+}								
				1.37	0.00							
	46.95	0.00	0.05	25.68	0.00	18.75	3.76	3.63	0.04	0.00	0.03	**98.88**

170-26	48.72	0.00	0.02	24.84		18.15	3.38	3.78	0.01	0.00	0.00	98.90
Mol. prop	0.81	0.00	0.00	0.35		0.26	0.08	0.07	0.00	0.00	0.00	
At Prop	1.62	0.00	0.00	0.35		0.26	0.08	0.07	0.00	0.00	0.00	2.37
No anions	3.74	0.00	0.00	0.80		0.59	0.19	0.16	0.00	0.00	0.00	5.48
No ions	1.87	0.00	0.00	0.80		0.59	0.19	0.16	0.00	0.00	0.00	3.61
				All Fe as Fe^{2+}								
				1.33	0.00							
	48.72	0.00	0.02	24.84	0.00	18.15	3.38	3.78	0.01	0.00	0.00	**98.90**
170-26	48.74	0.00	0.23	19.02		7.32	6.62	17.00	0.12	0.00	0.04	99.07
Mol. prop	0.81	0.00	0.00	0.26		0.10	0.16	0.30	0.00	0.00	0.00	
At Prop	1.62	0.00	0.01	0.26		0.10	0.16	0.30	0.00	0.00	0.00	2.47
No anions	3.74	0.00	0.02	0.61		0.24	0.38	0.70	0.00	0.00	0.00	5.69
No ions	1.87	0.00	0.01	0.61		0.24	0.38	0.70	0.01	0.00	0.00	3.82
				All Fe as Fe^{2+}								
				0.96	0.00							
	48.74	0.00	0.23	19.02	0.00	7.32	6.62	17.00	0.12	0.00	0.04	**99.07**
170-27	46.82	0.01	0.03	26.68		18.98	3.69	3.65	0.04	0.00	0.02	99.91
Mol. prop	0.78	0.00	0.00	0.37		0.27	0.09	0.06	0.00	0.00	0.00	
At Prop	1.56	0.00	0.00	0.37		0.27	0.09	0.06	0.00	0.00	0.00	2.36
No anions	3.60	0.00	0.00	0.86		0.62	0.21	0.15	0.00	0.00	0.00	5.44
No ions	1.80	0.00	0.00	0.86		0.62	0.21	0.15	0.00	0.00	0.00	3.64
				All Fe as Fe^{2+}								
				1.41	0.00							
	46.82	0.01	0.03	26.68	0.00	18.98	3.69	3.65	0.04	0.00	0.02	**99.91**
170-27	48.20	0.00	0.02	25.53		17.53	3.66	3.69	0.01	0.00	0.00	98.64
Mol. prop	0.80	0.00	0.00	0.36		0.25	0.09	0.07	0.00	0.00	0.00	
At Prop	1.60	0.00	0.00	0.36		0.25	0.09	0.07	0.00	0.00	0.00	2.36
No anions	3.70	0.00	0.00	0.82		0.57	0.21	0.15	0.00	0.00	0.00	5.46
No ions	1.85	0.00	0.00	0.82		0.57	0.21	0.15	0.00	0.00	0.00	3.60
				All Fe as Fe^{2+}								
				1.36	0.00							
	48.20	0.00	0.02	25.53	0.00	17.53	3.66	3.69	0.01	0.00	0.00	**98.64**
170-28	46.76	0.02	0.04	25.93		19.28	3.89	3.47	0.04	0.00	0.04	99.46
Mol. prop	0.78	0.00	0.00	0.36		0.27	0.10	0.06	0.00	0.00	0.00	
At Prop	1.56	0.00	0.00	0.36		0.27	0.10	0.06	0.00	0.00	0.00	2.35
No anions	3.59	0.00	0.00	0.83		0.63	0.22	0.14	0.00	0.00	0.00	5.42
No ions	1.80	0.00	0.00	0.83		0.63	0.22	0.14	0.00	0.00	0.00	3.63
				All Fe as Fe^{2+}								
				1.38	0.00							
	46.76	0.02	0.04	25.93	0.00	19.28	3.89	3.47	0.04	0.00	0.04	**99.46**

170-29	46.96	0.00	0.06	25.66		18.95	3.94	3.08	0.00	0.00	0.04	98.70
Mol. prop	0.78	0.00	0.00	0.36		0.27	0.10	0.05	0.00	0.00	0.00	
At Prop	1.56	0.00	0.00	0.36		0.27	0.10	0.05	0.00	0.00	0.00	2.34
No anions	3.61	0.00	0.00	0.82		0.62	0.23	0.13	0.00	0.00	0.00	5.41
No ions	1.80	0.00	0.00	0.82		0.62	0.23	0.13	0.00	0.00	0.00	3.60
				All Fe as Fe^{2+}								
				1.37	0.00							
	46.96	0.00	0.06	25.66	0.00	18.95	3.94	3.08	0.00	0.00	0.04	**98.70**
170-30	46.62	0.00	0.01	25.46		19.27	3.76	3.48	0.02	0.00	0.02	98.65
Mol. prop	0.78	0.00	0.00	0.35		0.27	0.09	0.06	0.00	0.00	0.00	
At Prop	1.55	0.00	0.00	0.35		0.27	0.09	0.06	0.00	0.00	0.00	2.33
No anions	3.58	0.00	0.00	0.82		0.63	0.22	0.14	0.00	0.00	0.00	5.39
No ions	1.79	0.00	0.00	0.82		0.63	0.22	0.14	0.00	0.00	0.00	3.60
				All Fe as Fe^{2+}								
				1.36	0.00							
	46.62	0.00	0.01	25.46	0.00	19.27	3.76	3.48	0.02	0.00	0.02	**98.65**
170-31	46.79	0.00	0.03	25.96		19.51	3.77	3.04	0.03	0.00	0.02	99.15
Mol. prop	0.78	0.00	0.00	0.36		0.27	0.09	0.05	0.00	0.00	0.00	
At Prop	1.56	0.00	0.00	0.36		0.27	0.09	0.05	0.00	0.00	0.00	2.34
No anions	3.59	0.00	0.00	0.83		0.63	0.22	0.13	0.00	0.00	0.00	5.41
No ions	1.80	0.00	0.00	0.83		0.63	0.22	0.13	0.00	0.00	0.00	3.61
				All Fe as Fe^{2+}								
				1.39	0.00							
	46.79	0.00	0.03	25.96	0.00	19.51	3.77	3.04	0.03	0.00	0.02	**99.15**
170-32	46.55	0.02	0.03	26.97		20.27	3.48	2.67	0.03	0.00	0.03	100.05
Mol. prop	0.77	0.00	0.00	0.38		0.29	0.09	0.05	0.00	0.00	0.00	
At Prop	1.55	0.00	0.00	0.38		0.29	0.09	0.05	0.00	0.00	0.00	2.35
No anions	3.58	0.00	0.00	0.87		0.66	0.20	0.11	0.00	0.00	0.00	5.42
No ions	1.79	0.00	0.00	0.87		0.66	0.20	0.11	0.00	0.00	0.00	3.63
				All Fe as Fe^{2+}								
				1.43	0.00							
	46.55	0.02	0.03	26.97	0.00	20.27	3.48	2.67	0.03	0.00	0.03	**100.05**
170-33	46.68	0.00	0.00	25.93		19.49	3.76	3.05	0.02	0.00	0.02	98.94
Mol. prop	0.78	0.00	0.00	0.36		0.27	0.09	0.05	0.00	0.00	0.00	
At Prop	1.55	0.00	0.00	0.36		0.27	0.09	0.05	0.00	0.00	0.00	2.34
No anions	3.59	0.00	0.00	0.83		0.63	0.22	0.13	0.00	0.00	0.00	5.39
No ions	1.79	0.00	0.00	0.83		0.63	0.22	0.13	0.00	0.00	0.00	3.60
				All Fe as Fe^{2+}								
				1.39	0.00							
	46.68	0.00	0.00	25.93	0.00	19.49	3.76	3.05	0.02	0.00	0.02	**98.94**

170-34	48.33	0.00	0.03	25.62		17.69	3.58	3.48	0.02	0.00	0.00	98.74
Mol. prop	0.80	0.00	0.00	0.36		0.25	0.09	0.06	0.00	0.00	0.00	
At Prop	1.61	0.00	0.00	0.36		0.25	0.09	0.06	0.00	0.00	0.00	2.37
No anions	3.71	0.00	0.00	0.82		0.58	0.20	0.14	0.00	0.00	0.00	5.46
No ions	1.86	0.00	0.00	0.82		0.58	0.20	0.14	0.00	0.00	0.00	3.61
				All Fe as Fe^{2+}								
				1.37	0.00							
	48.33	0.00	0.03	25.62	0.00	17.69	3.58	3.48	0.02	0.00	0.00	**98.74**
170-36	51.03	0.01	0.26	17.57		6.36	6.53	18.34	0.11	0.00	0.00	100.21
Mol. prop	0.85	0.00	0.00	0.24		0.09	0.16	0.33	0.00	0.00	0.00	
At Prop	1.70	0.00	0.01	0.24		0.09	0.16	0.33	0.00	0.00	0.00	2.53
No anions	3.92	0.00	0.02	0.56		0.21	0.37	0.75	0.00	0.00	0.00	5.84
No ions	1.96	0.00	0.01	0.56		0.21	0.37	0.75	0.01	0.00	0.00	3.88
				All Fe as Fe^{2+}								
				0.87	0.00							
	51.03	0.01	0.26	17.57	0.00	6.36	6.53	18.34	0.11	0.00	0.00	**100.21**
170-37	50.56	0.00	0.26	17.47		6.24	6.42	18.51	0.15	0.00	0.00	99.61
Mol. prop	0.84	0.00	0.00	0.24		0.09	0.16	0.33	0.00	0.00	0.00	
At Prop	1.68	0.00	0.01	0.24		0.09	0.16	0.33	0.00	0.00	0.00	2.51
No anions	3.88	0.00	0.02	0.56		0.20	0.37	0.76	0.00	0.00	0.00	5.80
No ions	1.94	0.00	0.01	0.56		0.20	0.37	0.76	0.01	0.00	0.00	3.85
				All Fe as Fe^{2+}								
				0.87	0.00							
	50.56	0.00	0.26	17.47	0.00	6.24	6.42	18.51	0.15	0.00	0.00	**99.61**
170-38	50.59	0.01	0.32	17.63		6.32	6.60	17.85	0.11	0.00	0.00	99.44
Mol. prop	0.84	0.00	0.00	0.25		0.09	0.16	0.32	0.00	0.00	0.00	
At Prop	1.68	0.00	0.01	0.25		0.09	0.16	0.32	0.00	0.00	0.00	2.51
No anions	3.89	0.00	0.02	0.57		0.21	0.38	0.73	0.00	0.00	0.00	5.80
No ions	1.94	0.00	0.01	0.57		0.21	0.38	0.73	0.01	0.00	0.00	3.85
				All Fe as Fe^{2+}								
				0.88	0.00							
	50.59	0.01	0.32	17.63	0.00	6.32	6.60	17.85	0.11	0.00	0.00	**99.44**
170-39	50.44	0.00	0.28	17.89		6.32	6.39	18.16	0.12	0.01	0.00	99.61
Mol. prop	0.84	0.00	0.00	0.25		0.09	0.16	0.32	0.00	0.00	0.00	
At Prop	1.68	0.00	0.01	0.25		0.09	0.16	0.32	0.00	0.00	0.00	2.51
No anions	3.87	0.00	0.02	0.57		0.21	0.37	0.75	0.00	0.00	0.00	5.79
No ions	1.94	0.00	0.01	0.57		0.21	0.37	0.75	0.01	0.00	0.00	3.85
				All Fe as Fe^{2+}								
				0.90	0.00							
	50.44	0.00	0.28	17.89	0.00	6.32	6.39	18.16	0.12	0.01	0.00	**99.61**

172-14	48.71	0.00	0.33	36.45		4.18	10.70	0.03	0.02	0.00	0.01	100.42
Mol. prop	0.81	0.00	0.00	0.51		0.06	0.27	0.00	0.00	0.00	0.00	
At Prop	1.62	0.00	0.01	0.51		0.06	0.27	0.00	0.00	0.00	0.00	2.46
No anions	3.74	0.00	0.02	1.17		0.14	0.61	0.00	0.00	0.00	0.00	5.69
No ions	1.87	0.00	0.01	1.17		0.14	0.61	0.00	0.00	0.00	0.00	3.81
				All Fe as Fe^{2+}								
				1.84	0.00							
	48.71	0.00	0.33	36.45	0.00	4.18	10.70	0.03	0.02	0.00	0.01	**100.42**
172-15	48.31	0.00	0.34	35.32		4.14	11.09	0.00	0.02	0.00	0.02	99.25
Mol. prop	0.80	0.00	0.00	0.49		0.06	0.28	0.00	0.00	0.00	0.00	
At Prop	1.61	0.00	0.01	0.49		0.06	0.28	0.00	0.00	0.00	0.00	2.44
No anions	3.71	0.00	0.02	1.13		0.13	0.64	0.00	0.00	0.00	0.00	5.64
No ions	1.86	0.00	0.02	1.13		0.13	0.64	0.00	0.00	0.00	0.00	3.78
				All Fe as Fe^{2+}								
				1.80	0.00							
	48.31	0.00	0.34	35.32	0.00	4.14	11.09	0.00	0.02	0.00	0.02	**99.25**
172-16	49.08	0.00	0.39	34.36		3.89	11.14	0.02	0.04	0.00	0.04	98.96
Mol. prop	0.82	0.00	0.00	0.48		0.05	0.28	0.00	0.00	0.00	0.00	
At Prop	1.63	0.00	0.01	0.48		0.05	0.28	0.00	0.00	0.00	0.00	2.46
No anions	3.77	0.00	0.03	1.10		0.13	0.64	0.00	0.00	0.00	0.00	5.67
No ions	1.89	0.00	0.02	1.10		0.13	0.64	0.00	0.00	0.00	0.00	3.78
				All Fe as Fe^{2+}								
				1.75	0.00							
	49.08	0.00	0.39	34.36	0.00	3.89	11.14	0.02	0.04	0.00	0.04	**98.96**
172-19	48.83	0.01	0.35	33.38		3.66	12.36	0.04	0.02	0.00	0.03	98.67
Mol. prop	0.81	0.00	0.00	0.46		0.05	0.31	0.00	0.00	0.00	0.00	
At Prop	1.63	0.00	0.01	0.46		0.05	0.31	0.00	0.00	0.00	0.00	2.46
No anions	3.75	0.00	0.02	1.07		0.12	0.71	0.00	0.00	0.00	0.00	5.68
No ions	1.88	0.00	0.02	1.07		0.12	0.71	0.00	0.00	0.00	0.00	3.79
				All Fe as Fe^{2+}								
				1.70	0.00							
	48.83	0.01	0.35	33.38	0.00	3.66	12.36	0.04	0.02	0.00	0.03	**98.67**
172-21	48.55	0.01	0.34	34.05		4.40	11.30	0.03	0.02	0.00	0.01	98.72
Mol. prop	0.81	0.00	0.00	0.47		0.06	0.28	0.00	0.00	0.00	0.00	
At Prop	1.62	0.00	0.01	0.47		0.06	0.28	0.00	0.00	0.00	0.00	2.44
No anions	3.73	0.00	0.02	1.09		0.14	0.65	0.00	0.00	0.00	0.00	5.64
No ions	1.86	0.00	0.02	1.09		0.14	0.65	0.00	0.00	0.00	0.00	3.77
				All Fe as Fe^{2+}								
				1.74	0.00							
	48.55	0.01	0.34	34.05	0.00	4.40	11.30	0.03	0.02	0.00	0.01	**98.72**

172-27	48.03	0.00	0.34	34.71		4.55	11.02	0.08	0.04	0.00	0.02	98.79
Mol. prop	0.80	0.00	0.00	0.48		0.06	0.27	0.00	0.00	0.00	0.00	
At Prop	1.60	0.00	0.01	0.48		0.06	0.27	0.00	0.00	0.00	0.00	2.43
No anions	3.69	0.00	0.02	1.11		0.15	0.63	0.00	0.00	0.00	0.00	5.61
No ions	1.84	0.00	0.02	1.11		0.15	0.63	0.00	0.00	0.00	0.00	3.76
				All Fe as Fe^{2+}								
				1.78	0.00							
	48.03	0.00	0.34	34.71	0.00	4.55	11.02	0.08	0.04	0.00	0.02	**98.79**
174-12	49.11	0.01	0.17	29.94		11.57	7.27	0.41	0.01	0.02	0.00	98.50
Mol. prop	0.82	0.00	0.00	0.42		0.16	0.18	0.01	0.00	0.00	0.00	
At Prop	1.63	0.00	0.00	0.42		0.16	0.18	0.01	0.00	0.00	0.00	2.41
No anions	3.77	0.00	0.01	0.96		0.38	0.42	0.02	0.00	0.00	0.00	5.56
No ions	1.89	0.00	0.01	0.96		0.38	0.42	0.02	0.00	0.00	0.00	3.67
				All Fe as Fe^{2+}								
				1.57	0.00							
	49.11	0.01	0.17	29.94	0.00	11.57	7.27	0.41	0.01	0.02	0.00	**98.50**
174-19	48.72	0.02	0.21	31.39		11.09	6.90	0.45	0.01	0.00	0.00	98.80
Mol. prop	0.81	0.00	0.00	0.44		0.16	0.17	0.01	0.00	0.00	0.00	
At Prop	1.62	0.00	0.01	0.44		0.16	0.17	0.01	0.00	0.00	0.00	2.40
No anions	3.74	0.00	0.01	1.01		0.36	0.40	0.02	0.00	0.00	0.00	5.54
No ions	1.87	0.00	0.01	1.01		0.36	0.40	0.02	0.00	0.00	0.00	3.67
				All Fe as Fe^{2+}								
				1.65	0.00							
	48.72	0.02	0.21	31.39	0.00	11.09	6.90	0.45	0.01	0.00	0.00	**98.80**
174-31	48.98	0.04	0.16	30.90		11.11	7.02	0.44	0.02	0.01	0.00	98.66
Mol. prop	0.82	0.00	0.00	0.43		0.16	0.17	0.01	0.00	0.00	0.00	
At Prop	1.63	0.00	0.00	0.43		0.16	0.17	0.01	0.00	0.00	0.00	2.40
No anions	3.76	0.00	0.01	0.99		0.36	0.40	0.02	0.00	0.00	0.00	5.55
No ions	1.88	0.00	0.01	0.99		0.36	0.40	0.02	0.00	0.00	0.00	3.66
				All Fe as Fe^{2+}								
				1.63	0.00							
	48.98	0.04	0.16	30.90	0.00	11.11	7.02	0.44	0.02	0.01	0.00	**98.66**
174-35	48.42	0.04	0.21	32.59		10.59	6.26	0.44	0.03	0.00	0.00	98.58
Mol. prop	0.81	0.00	0.00	0.45		0.15	0.16	0.01	0.00	0.00	0.00	
At Prop	1.61	0.00	0.01	0.45		0.15	0.16	0.01	0.00	0.00	0.00	2.39
No anions	3.72	0.00	0.01	1.05		0.34	0.36	0.02	0.00	0.00	0.00	5.50
No ions	1.86	0.00	0.01	1.05		0.34	0.36	0.02	0.00	0.00	0.00	3.64
				All Fe as Fe^{2+}								
				1.73	0.00							
	48.42	0.04	0.21	32.59	0.00	10.59	6.26	0.44	0.03	0.00	0.00	**98.58**

176-17	50.76	0.01	0.15	18.20		15.76	12.77	1.10	0.01	0.00	0.00	98.75
Mol. prop	0.84	0.00	0.00	0.25		0.22	0.32	0.02	0.00	0.00	0.00	
At Prop	1.69	0.00	0.00	0.25		0.22	0.32	0.02	0.00	0.00	0.00	2.51
No anions	3.90	0.00	0.01	0.58		0.51	0.73	0.05	0.00	0.00	0.00	5.78
No ions	1.95	0.00	0.01	0.58		0.51	0.73	0.05	0.00	0.00	0.00	3.83
				All Fe as Fe^{2+}								
				0.92	0.00							
	50.76	0.01	0.15	18.20	0.00	15.76	12.77	1.10	0.01	0.00	0.00	**98.75**
176-36	50.61	0.00	0.12	17.81		16.15	13.02	1.07	0.02	0.00	0.00	98.79
Mol. prop	0.84	0.00	0.00	0.25		0.23	0.32	0.02	0.00	0.00	0.00	
At Prop	1.68	0.00	0.00	0.25		0.23	0.32	0.02	0.00	0.00	0.00	2.51
No anions	3.89	0.00	0.01	0.57		0.53	0.75	0.04	0.00	0.00	0.00	5.78
No ions	1.94	0.00	0.01	0.57		0.53	0.75	0.04	0.00	0.00	0.00	3.84
				All Fe as Fe^{2+}								
				0.89	0.00							
	50.61	0.00	0.12	17.81	0.00	16.15	13.02	1.07	0.02	0.00	0.00	**98.79**

Pyroxenoids Recalculated on the basis of 6O

Label	SiO_2	TiO_2	Al_2O_3	FeO*	Fe_2O_3**	MnO	MgO	CaO	Na_2O	P_2O_5	K_2O	Total
160-18	48.22	0.00	0.01	3.16		41.79	2.22	4.62	0.00	0.00	0.01	100.03
Mol. prop	0.80	0.00	0.00	0.04		0.59	0.05	0.08	0.00	0.00	0.00	
At Prop	1.60	0.00	0.00	0.04		0.59	0.05	0.08	0.00	0.00	0.00	2.38
No anions	4.05	0.00	0.00	0.11		1.49	0.14	0.21	0.00	0.00	0.00	6.00
No ions	2.03	0.00	0.00	0.11		1.49	0.14	0.21	0.00	0.00	0.00	3.97
				All Fe as Fe^{2+}								
				0.11	0.00							
	48.22	0.00	0.01	3.16	0.00	41.79	2.22	4.62	0.00	0.00	0.01	**100.03**
160-8	47.80	0.00	0.01	5.14		40.87	4.50	2.23	0.00	0.00	0.04	100.58
Mol. prop	0.80	0.00	0.00	0.07		0.58	0.11	0.04	0.00	0.00	0.00	
At Prop	1.59	0.00	0.00	0.07		0.58	0.11	0.04	0.00	0.00	0.00	2.39
No anions	4.02	0.00	0.00	0.18		1.45	0.28	0.10	0.00	0.00	0.00	6.04
No ions	2.01	0.00	0.00	0.18		1.45	0.28	0.10	0.00	0.00	0.00	4.03
				All Fe as Fe^{2+}								
				0.18	0.00							
	47.80	0.00	0.01	5.14	0.00	40.87	4.50	2.23	0.00	0.00	0.04	**100.58**
164-13	47.75	0.01	0.18	1.39		39.94	1.19	8.77	0.14	0.00	0.01	99.39
Mol. prop	0.79	0.00	0.00	0.02		0.56	0.03	0.16	0.00	0.00	0.00	
At Prop	1.59	0.00	0.01	0.02		0.56	0.03	0.16	0.00	0.00	0.00	2.36
No anions	4.01	0.00	0.01	0.05		1.42	0.07	0.40	0.00	0.00	0.00	5.97
No ions	2.01	0.00	0.01	0.05		1.42	0.07	0.40	0.01	0.00	0.00	3.96
				All Fe as Fe^{2+}								
				0.05	0.00							
	47.75	0.01	0.18	1.39	0.00	39.94	1.19	8.77	0.14	0.00	0.01	**99.39**
164-32	48.59	0.00	0.02	4.56		37.37	2.43	7.03	0.01	0.00	0.00	100.01
Mol. prop	0.81	0.00	0.00	0.06		0.53	0.06	0.13	0.00	0.00	0.00	
At Prop	1.62	0.00	0.00	0.06		0.53	0.06	0.13	0.00	0.00	0.00	2.39
No anions	4.08	0.00	0.00	0.16		1.33	0.15	0.32	0.00	0.00	0.00	6.05
No ions	2.04	0.00	0.00	0.16		1.33	0.15	0.32	0.00	0.00	0.00	4.00
				All Fe as Fe^{2+}								
				0.16	0.00							
	48.59	0.00	0.02	4.56	0.00	37.37	2.43	7.03	0.01	0.00	0.00	**100.01**
164-39	48.15	0.00	0.02	4.36		37.59	2.42	6.94	0.02	0.02	0.00	99.52
Mol. prop	0.80	0.00	0.00	0.06		0.53	0.06	0.12	0.00	0.00	0.00	
At Prop	1.60	0.00	0.00	0.06		0.53	0.06	0.12	0.00	0.00	0.00	2.38
No anions	4.05	0.00	0.00	0.15		1.34	0.15	0.31	0.00	0.00	0.00	6.01
No ions	2.02	0.00	0.00	0.15		1.34	0.15	0.31	0.00	0.00	0.00	3.98
				All Fe as Fe^{2+}								
				0.15	0.00							
	48.15	0.00	0.02	4.36	0.00	37.59	2.42	6.94	0.02	0.02	0.00	**99.52**

164-40	48.11	0.00	0.02	4.24		37.83	2.35	6.84	0.00	0.00	0.00	99.38
Mol. prop	0.80	0.00	0.00	0.06		0.53	0.06	0.12	0.00	0.00	0.00	
At Prop	1.60	0.00	0.00	0.06		0.53	0.06	0.12	0.00	0.00	0.00	2.37
No anions	4.04	0.00	0.00	0.15		1.35	0.15	0.31	0.00	0.00	0.00	6.00
No ions	2.02	0.00	0.00	0.15		1.35	0.15	0.31	0.00	0.00	0.00	3.97
				All Fe as Fe^{2+}								
				0.15	0.00							
	48.11	0.00	0.02	4.24	0.00	37.83	2.35	6.84	0.00	0.00	0.00	**99.38**
164-41	48.24	0.00	0.00	3.87		38.98	1.83	6.80	0.03	0.00	0.00	99.75
Mol. prop	0.80	0.00	0.00	0.05		0.55	0.05	0.12	0.00	0.00	0.00	
At Prop	1.61	0.00	0.00	0.05		0.55	0.05	0.12	0.00	0.00	0.00	2.38
No anions	4.06	0.00	0.00	0.14		1.39	0.11	0.31	0.00	0.00	0.00	6.00
No ions	2.03	0.00	0.00	0.14		1.39	0.11	0.31	0.00	0.00	0.00	3.97
				All Fe as Fe^{2+}								
				0.14	0.00							
	48.24	0.00	0.00	3.87	0.00	38.98	1.83	6.80	0.03	0.00	0.00	**99.75**
164-45	47.87	0.00	0.03	3.10		40.00	1.59	6.68	0.03	0.00	0.00	99.30
Mol. prop	0.80	0.00	0.00	0.04		0.56	0.04	0.12	0.00	0.00	0.00	
At Prop	1.59	0.00	0.00	0.04		0.56	0.04	0.12	0.00	0.00	0.00	2.36
No anions	4.02	0.00	0.00	0.11		1.42	0.10	0.30	0.00	0.00	0.00	5.96
No ions	2.01	0.00	0.00	0.11		1.42	0.10	0.30	0.00	0.00	0.00	3.95
				All Fe as Fe^{2+}								
				0.11	0.00							
	47.87	0.00	0.03	3.10	0.00	40.00	1.59	6.68	0.03	0.00	0.00	**99.30**
164-48	48.33	0.01	0.03	3.26		39.42	1.87	6.64	0.03	0.00	0.00	99.58
Mol. prop	0.80	0.00	0.00	0.05		0.56	0.05	0.12	0.00	0.00	0.00	
At Prop	1.61	0.00	0.00	0.05		0.56	0.05	0.12	0.00	0.00	0.00	2.38
No anions	4.06	0.00	0.00	0.11		1.40	0.12	0.30	0.00	0.00	0.00	6.00
No ions	2.03	0.00	0.00	0.11		1.40	0.12	0.30	0.00	0.00	0.00	3.97
				All Fe as Fe^{2+}								
				0.11	0.00							
	48.33	0.01	0.03	3.26	0.00	39.42	1.87	6.64	0.03	0.00	0.00	**99.58**
164-55	48.43	0.00	0.03	3.94		37.86	2.22	6.96	0.02	0.00	0.00	99.45
Mol. prop	0.81	0.00	0.00	0.05		0.53	0.06	0.12	0.00	0.00	0.00	
At Prop	1.61	0.00	0.00	0.05		0.53	0.06	0.12	0.00	0.00	0.00	2.38
No anions	4.07	0.00	0.00	0.14		1.35	0.14	0.31	0.00	0.00	0.00	6.01
No ions	2.04	0.00	0.00	0.14		1.35	0.14	0.31	0.00	0.00	0.00	3.98
				All Fe as Fe^{2+}								
				0.14	0.00							
	48.43	0.00	0.03	3.94	0.00	37.86	2.22	6.96	0.02	0.00	0.00	**99.45**

166-1	46.39	0.00	0.03	5.17		39.33	2.04	6.89	0.02	0.00	0.02	99.89
Mol. prop	0.77	0.00	0.00	0.07		0.55	0.05	0.12	0.00	0.00	0.00	
At Prop	1.54	0.00	0.00	0.07		0.55	0.05	0.12	0.00	0.00	0.00	2.35
No anions	3.90	0.00	0.00	0.18		1.40	0.13	0.31	0.00	0.00	0.00	5.92
No ions	1.95	0.00	0.00	0.18		1.40	0.13	0.31	0.00	0.00	0.00	3.97
				All Fe as Fe^{2+}								
				0.18	0.00							
	46.39	0.00	0.03	5.17	0.00	39.33	2.04	6.89	0.02	0.00	0.02	**99.89**
166-3	47.20	0.00	0.01	5.11		41.93	4.29	2.31	0.03	0.00	0.03	100.91
Mol. prop	0.79	0.00	0.00	0.07		0.59	0.11	0.04	0.00	0.00	0.00	
At Prop	1.57	0.00	0.00	0.07		0.59	0.11	0.04	0.00	0.00	0.00	2.38
No anions	3.97	0.00	0.00	0.18		1.49	0.27	0.10	0.00	0.00	0.00	6.01
No ions	1.98	0.00	0.00	0.18		1.49	0.27	0.10	0.00	0.00	0.00	4.03
				All Fe as Fe^{2+}								
				0.18	0.00							
	47.20	0.00	0.01	5.11	0.00	41.93	4.29	2.31	0.03	0.00	0.03	**100.91**
168-34	46.26	0.00	0.00	5.08		39.66	1.71	6.56	0.13	0.00	0.03	99.42
Mol. prop	0.77	0.00	0.00	0.07		0.56	0.04	0.12	0.00	0.00	0.00	
At Prop	1.54	0.00	0.00	0.07		0.56	0.04	0.12	0.00	0.00	0.00	2.33
No anions	3.89	0.00	0.00	0.18		1.41	0.11	0.30	0.00	0.00	0.00	5.89
No ions	1.94	0.00	0.00	0.18		1.41	0.11	0.30	0.01	0.00	0.00	3.95
				All Fe as Fe^{2+}								
				0.18	0.00							
	46.26	0.00	0.00	5.08	0.00	39.66	1.71	6.56	0.13	0.00	0.03	**99.42**
168-35	46.73	0.00	0.00	5.69		39.13	2.02	6.57	0.05	0.00	0.02	100.21
Mol. prop	0.78	0.00	0.00	0.08		0.55	0.05	0.12	0.00	0.00	0.00	
At Prop	1.56	0.00	0.00	0.08		0.55	0.05	0.12	0.00	0.00	0.00	2.35
No anions	3.93	0.00	0.00	0.20		1.39	0.13	0.30	0.00	0.00	0.00	5.95
No ions	1.96	0.00	0.00	0.20		1.39	0.13	0.30	0.00	0.00	0.00	3.98
				All Fe as Fe^{2+}								
				0.20	0.00							
	46.73	0.00	0.00	5.69	0.00	39.13	2.02	6.57	0.05	0.00	0.02	**100.21**
168-36	46.91	0.00	0.03	4.53		40.54	1.29	6.75	0.08	0.00	0.02	100.14
Mol. prop	0.78	0.00	0.00	0.06		0.57	0.03	0.12	0.00	0.00	0.00	
At Prop	1.56	0.00	0.00	0.06		0.57	0.03	0.12	0.00	0.00	0.00	2.35
No anions	3.94	0.00	0.00	0.16		1.44	0.08	0.30	0.00	0.00	0.00	5.93
No ions	1.97	0.00	0.00	0.16		1.44	0.08	0.30	0.00	0.00	0.00	3.97
				All Fe as Fe^{2+}								
				0.16	0.00							
	46.91	0.00	0.03	4.53	0.00	40.54	1.29	6.75	0.08	0.00	0.02	**100.14**

168-37	47.29	0.00	0.02	5.49		39.64	1.68	6.70	0.06	0.00	0.02	100.90
Mol. prop	0.79	0.00	0.00	0.08		0.56	0.04	0.12	0.00	0.00	0.00	
At Prop	1.57	0.00	0.00	0.08		0.56	0.04	0.12	0.00	0.00	0.00	2.37
No anions	3.97	0.00	0.00	0.19		1.41	0.11	0.30	0.00	0.00	0.00	5.99
No ions	1.99	0.00	0.00	0.19		1.41	0.11	0.30	0.00	0.00	0.00	4.00
				All Fe as Fe^{2+}								
				0.19	0.00							
	47.29	0.00	0.02	5.49	0.00	39.64	1.68	6.70	0.06	0.00	0.02	**100.90**
168-38	47.57	0.00	0.02	6.33		37.43	2.36	6.85	0.05	0.00	0.04	100.65
Mol. prop	0.79	0.00	0.00	0.09		0.53	0.06	0.12	0.00	0.00	0.00	
At Prop	1.58	0.00	0.00	0.09		0.53	0.06	0.12	0.00	0.00	0.00	2.38
No anions	4.00	0.00	0.00	0.22		1.33	0.15	0.31	0.00	0.00	0.00	6.01
No ions	2.00	0.00	0.00	0.22		1.33	0.15	0.31	0.00	0.00	0.00	4.02
				All Fe as Fe^{2+}								
				0.22	0.00							
	47.57	0.00	0.02	6.33	0.00	37.43	2.36	6.85	0.05	0.00	0.04	**100.65**
168-39	46.67	0.00	0.00	5.38		39.92	1.58	6.62	0.12	0.00	0.01	100.29
Mol. prop	0.78	0.00	0.00	0.07		0.56	0.04	0.12	0.00	0.00	0.00	
At Prop	1.55	0.00	0.00	0.07		0.56	0.04	0.12	0.00	0.00	0.00	2.35
No anions	3.92	0.00	0.00	0.19		1.42	0.10	0.30	0.00	0.00	0.00	5.93
No ions	1.96	0.00	0.00	0.19		1.42	0.10	0.30	0.01	0.00	0.00	3.98
				All Fe as Fe^{2+}								
				0.19	0.00							
	46.67	0.00	0.00	5.38	0.00	39.92	1.58	6.62	0.12	0.00	0.01	**100.29**
168-40	47.04	0.00	0.01	6.12		37.69	2.32	6.70	0.06	0.00	0.02	99.97
Mol. prop	0.78	0.00	0.00	0.09		0.53	0.06	0.12	0.00	0.00	0.00	
At Prop	1.57	0.00	0.00	0.09		0.53	0.06	0.12	0.00	0.00	0.00	2.36
No anions	3.95	0.00	0.00	0.22		1.34	0.15	0.30	0.00	0.00	0.00	5.96
No ions	1.98	0.00	0.00	0.22		1.34	0.15	0.30	0.00	0.00	0.00	3.99
				All Fe as Fe^{2+}								
				0.22	0.00							
	47.04	0.00	0.01	6.12	0.00	37.69	2.32	6.70	0.06	0.00	0.02	**99.97**
168-43	46.68	0.00	0.02	5.49		39.23	2.02	6.39	0.08	0.00	0.02	99.93
Mol. prop	0.78	0.00	0.00	0.08		0.55	0.05	0.11	0.00	0.00	0.00	
At Prop	1.55	0.00	0.00	0.08		0.55	0.05	0.11	0.00	0.00	0.00	2.35
No anions	3.92	0.00	0.00	0.19		1.40	0.13	0.29	0.00	0.00	0.00	5.93
No ions	1.96	0.00	0.00	0.19		1.40	0.13	0.29	0.00	0.00	0.00	3.97
				All Fe as Fe^{2+}								
				0.19	0.00							
	46.68	0.00	0.02	5.49	0.00	39.23	2.02	6.39	0.08	0.00	0.02	**99.93**

168-44	46.78	0.00	0.00	5.26		38.97	2.03	6.45	0.05	0.00	0.02	99.56
Mol. prop	0.78	0.00	0.00	0.07		0.55	0.05	0.11	0.00	0.00	0.00	
At Prop	1.56	0.00	0.00	0.07		0.55	0.05	0.11	0.00	0.00	0.00	2.35
No anions	3.93	0.00	0.00	0.19		1.39	0.13	0.29	0.00	0.00	0.00	5.92
No ions	1.97	0.00	0.00	0.19		1.39	0.13	0.29	0.00	0.00	0.00	3.96
				All Fe as Fe^{2+}								
				0.19	0.00							
	46.78	0.00	0.00	5.26	0.00	38.97	2.03	6.45	0.05	0.00	0.02	**99.56**
168-45	46.78	0.00	0.03	5.13		39.94	2.04	6.55	0.06	0.00	0.03	100.56
Mol. prop	0.78	0.00	0.00	0.07		0.56	0.05	0.12	0.00	0.00	0.00	
At Prop	1.56	0.00	0.00	0.07		0.56	0.05	0.12	0.00	0.00	0.00	2.36
No anions	3.93	0.00	0.00	0.18		1.42	0.13	0.29	0.00	0.00	0.00	5.96
No ions	1.97	0.00	0.00	0.18		1.42	0.13	0.29	0.00	0.00	0.00	4.00
				All Fe as Fe^{2+}								
				0.18	0.00							
	46.78	0.00	0.03	5.13	0.00	39.94	2.04	6.55	0.06	0.00	0.03	**100.56**
168-46	46.62	0.00	0.01	5.01		40.08	1.85	6.51	0.05	0.00	0.04	100.17
Mol. prop	0.78	0.00	0.00	0.07		0.56	0.05	0.12	0.00	0.00	0.00	
At Prop	1.55	0.00	0.00	0.07		0.56	0.05	0.12	0.00	0.00	0.00	2.35
No anions	3.92	0.00	0.00	0.18		1.43	0.12	0.29	0.00	0.00	0.00	5.93
No ions	1.96	0.00	0.00	0.18		1.43	0.12	0.29	0.00	0.00	0.00	3.98
				All Fe as Fe^{2+}								
				0.18	0.00							
	46.62	0.00	0.01	5.01	0.00	40.08	1.85	6.51	0.05	0.00	0.04	**100.17**
168-47	45.52	0.00	1.28	6.82		36.00	3.09	6.07	0.32	0.00	0.04	99.13
Mol. prop	0.76	0.00	0.01	0.09		0.51	0.08	0.11	0.00	0.00	0.00	
At Prop	1.51	0.00	0.04	0.09		0.51	0.08	0.11	0.00	0.00	0.00	2.34
No anions	3.83	0.00	0.09	0.24		1.28	0.19	0.27	0.01	0.00	0.00	5.92
No ions	1.91	0.00	0.06	0.24		1.28	0.19	0.27	0.02	0.00	0.00	3.98
				All Fe as Fe^{2+}								
				0.24	0.00							
	45.52	0.00	1.28	6.82	0.00	36.00	3.09	6.07	0.32	0.00	0.04	**99.13**
168-48	46.24	0.00	0.00	5.32		40.94	1.75	6.49	0.07	0.00	0.03	100.84
Mol. prop	0.77	0.00	0.00	0.07		0.58	0.04	0.12	0.00	0.00	0.00	
At Prop	1.54	0.00	0.00	0.07		0.58	0.04	0.12	0.00	0.00	0.00	2.35
No anions	3.89	0.00	0.00	0.19		1.46	0.11	0.29	0.00	0.00	0.00	5.94
No ions	1.94	0.00	0.00	0.19		1.46	0.11	0.29	0.00	0.00	0.00	4.00
				All Fe as Fe^{2+}								
				0.19	0.00							
	46.24	0.00	0.00	5.32	0.00	40.94	1.75	6.49	0.07	0.00	0.03	**100.84**

168-49	46.30	0.00	0.00	5.86		38.72	2.14	6.63	0.04	0.00	0.03	99.71
Mol. prop	0.77	0.00	0.00	0.08		0.55	0.05	0.12	0.00	0.00	0.00	
At Prop	1.54	0.00	0.00	0.08		0.55	0.05	0.12	0.00	0.00	0.00	2.34
No anions	3.89	0.00	0.00	0.21		1.38	0.13	0.30	0.00	0.00	0.00	5.91
No ions	1.95	0.00	0.00	0.21		1.38	0.13	0.30	0.00	0.00	0.00	3.97
				All Fe as Fe^{2+}								
				0.21	0.00							
	46.30	0.00	0.00	5.86	0.00	38.72	2.14	6.63	0.04	0.00	0.03	**99.71**
168-50	46.88	0.00	0.00	5.86		38.41	2.20	6.64	0.08	0.00	0.02	100.10
Mol. prop	0.78	0.00	0.00	0.08		0.54	0.05	0.12	0.00	0.00	0.00	
At Prop	1.56	0.00	0.00	0.08		0.54	0.05	0.12	0.00	0.00	0.00	2.36
No anions	3.94	0.00	0.00	0.21		1.37	0.14	0.30	0.00	0.00	0.00	5.95
No ions	1.97	0.00	0.00	0.21		1.37	0.14	0.30	0.00	0.00	0.00	3.99
				All Fe as Fe^{2+}								
				0.21	0.00							
	46.88	0.00	0.00	5.86	0.00	38.41	2.20	6.64	0.08	0.00	0.02	**100.10**
168-51	46.38	0.00	0.05	4.80		39.51	1.78	6.24	0.08	0.00	0.03	98.86
Mol. prop	0.77	0.00	0.00	0.07		0.56	0.04	0.11	0.00	0.00	0.00	
At Prop	1.54	0.00	0.00	0.07		0.56	0.04	0.11	0.00	0.00	0.00	2.33
No anions	3.90	0.00	0.00	0.17		1.41	0.11	0.28	0.00	0.00	0.00	5.87
No ions	1.95	0.00	0.00	0.17		1.41	0.11	0.28	0.00	0.00	0.00	3.92
				All Fe as Fe^{2+}								
				0.17	0.00							
	46.38	0.00	0.05	4.80	0.00	39.51	1.78	6.24	0.08	0.00	0.03	**98.86**
168-52	46.43	0.00	0.03	5.34		39.22	2.00	6.46	0.08	0.00	0.03	99.59
Mol. prop	0.77	0.00	0.00	0.07		0.55	0.05	0.12	0.00	0.00	0.00	
At Prop	1.55	0.00	0.00	0.07		0.55	0.05	0.12	0.00	0.00	0.00	2.34
No anions	3.90	0.00	0.00	0.19		1.40	0.13	0.29	0.00	0.00	0.00	5.91
No ions	1.95	0.00	0.00	0.19		1.40	0.13	0.29	0.00	0.00	0.00	3.96
				All Fe as Fe^{2+}								
				0.19	0.00							
	46.43	0.00	0.03	5.34	0.00	39.22	2.00	6.46	0.08	0.00	0.03	**99.59**

Amphibole Recalculated on the basis 23O anhydrous

Label	SiO_2	TiO_2	Al_2O_3	FeO*	Fe_2O_3**	MnO	MgO	CaO	Na_2O	P_2O_5	K_2O	Sub Total	H_2O[a]	Total[a]
160-6	52.74	0.00	0.19	13.62		11.38	16.30	1.65	0.05	0.00	0.03	95.97		
Mol. prop	0.88	0.00	0.00	0.19		0.16	0.40	0.03	0.00	0.00	0.00			
At Prop	1.76	0.00	0.01	0.19		0.16	0.40	0.03	0.00	0.00	0.00	2.55		
No anions	15.86	0.00	0.05	1.71		1.45	3.65	0.27	0.00	0.00	0.00	23.00		
No ions	7.93	0.00	0.03	1.71		1.45	3.65	0.27	0.01	0.00	0.01	15.06		
				All Fe as Fe^{2+}										
				2.62	0.00									
	52.74	0.00	0.19	13.62	0.00	11.38	16.30	1.65	0.05	0.00	0.03	**95.97**	2.50	**98.47**
162-1	53.09	0.00	0.17	13.43		11.62	16.51	1.61	0.07	0.00	0.02	96.52		
Mol. prop	0.88	0.00	0.00	0.19		0.16	0.41	0.03	0.00	0.00	0.00			
At Prop	1.77	0.00	0.00	0.19		0.16	0.41	0.03	0.00	0.00	0.00	2.56		
No anions	15.96	0.00	0.04	1.69		1.48	3.70	0.26	0.01	0.00	0.00	23.15		
No ions	7.98	0.00	0.03	1.69		1.48	3.70	0.26	0.01	0.00	0.00	15.16		
				All Fe as Fe^{2+}										
				2.56	0.00									
	53.09	0.00	0.17	13.43	0.00	11.62	16.51	1.61	0.07	0.00	0.02	**96.52**	2.50	**99.02**
162-2	46.60	0.01	0.01	1.85		42.10	0.97	5.96	0.01	0.00	0.00	97.52		
Mol. prop	0.78	0.00	0.00	0.03		0.59	0.02	0.11	0.00	0.00	0.00			
At Prop	1.55	0.00	0.00	0.03		0.59	0.02	0.11	0.00	0.00	0.00	2.30		
No anions	14.01	0.00	0.00	0.23		5.36	0.22	0.96	0.00	0.00	0.00	20.79		
No ions	7.01	0.00	0.00	0.23		5.36	0.22	0.96	0.00	0.00	0.00	13.78		
				All Fe as Fe^{2+}										
				0.39	0.00									
	46.60	0.01	0.01	1.85	0.00	42.10	0.97	5.96	0.01	0.00	0.00	**97.52**	2.50	**100.02**
162-3	53.19	0.01	0.19	13.44		11.75	16.39	1.51	0.04	0.00	0.02	96.55		
Mol. prop	0.89	0.00	0.00	0.19		0.17	0.41	0.03	0.00	0.00	0.00			
At Prop	1.77	0.00	0.01	0.19		0.17	0.41	0.03	0.00	0.00	0.00	2.56		
No anions	15.99	0.00	0.05	1.69		1.50	3.67	0.24	0.00	0.00	0.00	23.16		
No ions	8.00	0.00	0.03	1.69		1.50	3.67	0.24	0.01	0.00	0.00	15.15		
				All Fe as Fe^{2+}										
				2.57	0.00									
	53.19	0.01	0.19	13.44	0.00	11.75	16.39	1.51	0.04	0.00	0.02	**96.55**	2.50	**99.05**
162-4	53.13	0.00	0.22	13.25		11.49	16.38	1.77	0.04	0.00	0.02	96.31		
Mol. prop	0.88	0.00	0.00	0.18		0.16	0.41	0.03	0.00	0.00	0.00			
At Prop	1.77	0.00	0.01	0.18		0.16	0.41	0.03	0.00	0.00	0.00	2.56		
No anions	15.98	0.00	0.06	1.67		1.46	3.67	0.29	0.00	0.00	0.00	23.13		
No ions	7.99	0.00	0.04	1.67		1.46	3.67	0.29	0.01	0.00	0.00	15.13		
				All Fe as Fe^{2+}										
				2.53	0.00									
	53.13	0.00	0.22	13.25	0.00	11.49	16.38	1.77	0.04	0.00	0.02	**96.31**	2.50	**98.81**

162-5	52.94	0.01	0.23	13.71		11.95	16.53	1.61	0.04	0.00	0.03	97.06		
Mol. prop	0.88	0.00	0.00	0.19		0.17	0.41	0.03	0.00	0.00	0.00			
At Prop	1.76	0.00	0.01	0.19		0.17	0.41	0.03	0.00	0.00	0.00	2.57		
No anions	15.92	0.00	0.06	1.72		1.52	3.71	0.26	0.00	0.00	0.00	23.20		
No ions	7.96	0.00	0.04	1.72		1.52	3.71	0.26	0.01	0.00	0.01	15.23		
				All Fe as Fe^{2+}										
				2.60	0.00									
	52.94	0.01	0.23	13.71	0.00	11.95	16.53	1.61	0.04	0.00	0.03	**97.06**	2.50	**99.56**
162-6	53.01	0.00	0.23	13.46		12.11	16.43	1.65	0.03	0.00	0.02	96.94		
Mol. prop	0.88	0.00	0.00	0.19		0.17	0.41	0.03	0.00	0.00	0.00			
At Prop	1.76	0.00	0.01	0.19		0.17	0.41	0.03	0.00	0.00	0.00	2.57		
No anions	15.94	0.00	0.06	1.69		1.54	3.68	0.27	0.00	0.00	0.00	23.19		
No ions	7.97	0.00	0.04	1.69		1.54	3.68	0.27	0.01	0.00	0.00	15.20		
				All Fe as Fe^{2+}										
				2.56	0.00									
	53.01	0.00	0.23	13.46	0.00	12.11	16.43	1.65	0.03	0.00	0.02	**96.94**	2.50	**99.44**
162-7	52.08	0.00	0.07	14.17		12.45	16.18	1.09	0.04	0.00	0.04	96.12		
Mol. prop	0.87	0.00	0.00	0.20		0.18	0.40	0.02	0.00	0.00	0.00			
At Prop	1.73	0.00	0.00	0.20		0.18	0.40	0.02	0.00	0.00	0.00	2.53		
No anions	15.66	0.00	0.02	1.78		1.59	3.63	0.18	0.00	0.00	0.00	22.86		
No ions	7.83	0.00	0.01	1.78		1.59	3.63	0.18	0.01	0.00	0.01	15.03		
				All Fe as Fe^{2+}										
				2.73	0.00									
	52.08	0.00	0.07	14.17	0.00	12.45	16.18	1.09	0.04	0.00	0.04	**96.12**	2.50	**98.62**
162-9	53.02	0.01	0.29	12.93		11.68	16.25	1.91	0.08	0.00	0.03	96.20		
Mol. prop	0.88	0.00	0.00	0.18		0.16	0.40	0.03	0.00	0.00	0.00			
At Prop	1.76	0.00	0.01	0.18		0.16	0.40	0.03	0.00	0.00	0.00	2.56		
No anions	15.94	0.00	0.08	1.63		1.49	3.64	0.31	0.01	0.00	0.00	23.10		
No ions	7.97	0.00	0.05	1.63		1.49	3.64	0.31	0.02	0.00	0.01	15.11		
				All Fe as Fe^{2+}										
				2.47	0.00									
	53.02	0.01	0.29	12.93	0.00	11.68	16.25	1.91	0.08	0.00	0.03	**96.20**	2.50	**98.70**
162-10	52.71	0.00	0.23	14.16		12.03	16.29	1.12	0.03	0.00	0.03	96.60		
Mol. prop	0.88	0.00	0.00	0.20		0.17	0.40	0.02	0.00	0.00	0.00			
At Prop	1.75	0.00	0.01	0.20		0.17	0.40	0.02	0.00	0.00	0.00	2.55		
No anions	15.85	0.00	0.06	1.78		1.53	3.65	0.18	0.00	0.00	0.00	23.06		
No ions	7.93	0.00	0.04	1.78		1.53	3.65	0.18	0.01	0.00	0.00	15.12		
				All Fe as Fe^{2+}										
				2.71	0.00									
	52.71	0.00	0.23	14.16	0.00	12.03	16.29	1.12	0.03	0.00	0.03	**96.60**	2.50	**99.10**

162-11	52.87	0.00	0.36	13.12		11.91	16.22	2.63	0.06	0.00	0.02	97.19		
Mol. prop	0.88	0.00	0.00	0.18		0.17	0.40	0.05	0.00	0.00	0.00			
At Prop	1.76	0.00	0.01	0.18		0.17	0.40	0.05	0.00	0.00	0.00	2.57		
No anions	15.90	0.00	0.10	1.65		1.52	3.63	0.42	0.01	0.00	0.00	23.22		
No ions	7.95	0.00	0.06	1.65		1.52	3.63	0.42	0.01	0.00	0.00	15.25		
				All Fe as Fe^{2+}										
				2.49	0.00									
	52.87	0.00	0.36	13.12	0.00	11.91	16.22	2.63	0.06	0.00	0.02	**97.19**	2.50	**99.69**
168-23	53.67	0.00	0.16	9.33		6.31	15.01	11.36	0.12	0.00	0.03	95.98		
Mol. prop	0.89	0.00	0.00	0.13		0.09	0.37	0.20	0.00	0.00	0.00			
At Prop	1.79	0.00	0.00	0.13		0.09	0.37	0.20	0.00	0.00	0.00	2.59		
No anions	16.14	0.00	0.04	1.17		0.80	3.36	1.83	0.01	0.00	0.00	23.36		
No ions	8.07	0.00	0.03	1.17		0.80	3.36	1.83	0.02	0.00	0.00	15.29		
				All Fe as Fe^{2+}										
				1.76	0.00									
	53.67	0.00	0.16	9.33	0.00	6.31	15.01	11.36	0.12	0.00	0.03	**95.98**	2.50	**98.48**
168-41	54.19	0.00	0.16	8.87		6.83	15.79	10.53	0.12	0.00	0.02	96.50		
Mol. prop	0.90	0.00	0.00	0.12		0.10	0.39	0.19	0.00	0.00	0.00			
At Prop	1.80	0.00	0.00	0.12		0.10	0.39	0.19	0.00	0.00	0.00	2.61		
No anions	16.29	0.00	0.04	1.12		0.87	3.54	1.70	0.01	0.00	0.00	23.57		
No ions	8.15	0.00	0.03	1.12		0.87	3.54	1.70	0.02	0.00	0.00	15.42		
				All Fe as Fe^{2+}										
				1.66	0.00									
	54.19	0.00	0.16	8.87	0.00	6.83	15.79	10.53	0.12	0.00	0.02	**96.50**	2.50	**99.00**
168-57	51.73	0.00	0.05	13.28		17.25	13.41	0.33	0.02	0.00	0.02	96.08		
Mol. prop	0.86	0.00	0.00	0.18		0.24	0.33	0.01	0.00	0.00	0.00			
At Prop	1.72	0.00	0.00	0.18		0.24	0.33	0.01	0.00	0.00	0.00	2.49		
No anions	15.56	0.00	0.01	1.67		2.20	3.01	0.05	0.00	0.00	0.00	22.50		
No ions	7.78	0.00	0.01	1.67		2.20	3.01	0.05	0.00	0.00	0.00	14.72		
				All Fe as Fe^{2+}										
				2.61	0.00									
	51.73	0.00	0.05	13.28	0.00	17.25	13.41	0.33	0.02	0.00	0.02	**96.08**	2.50	**98.58**
168-62	53.67	0.00	0.16	9.33		6.31	15.01	11.36	0.12	0.00	0.03	95.98		
Mol. prop	0.89	0.00	0.00	0.13		0.09	0.37	0.20	0.00	0.00	0.00			
At Prop	1.79	0.00	0.00	0.13		0.09	0.37	0.20	0.00	0.00	0.00	2.59		
No anions	16.14	0.00	0.04	1.17		0.80	3.36	1.83	0.01	0.00	0.00	23.36		
No ions	8.07	0.00	0.03	1.17		0.80	3.36	1.83	0.02	0.00	0.00	15.29		
				All Fe as Fe^{2+}										
				1.76	0.00									
	53.67	0.00	0.16	9.33	0.00	6.31	15.01	11.36	0.12	0.00	0.03	**95.98**	2.50	**98.48**

176-25	52.03	0.01	0.19	17.95		14.57	12.52	0.69	0.03	0.00	0.01	97.98	
Mol. prop	0.87	0.00	0.00	0.25		0.21	0.31	0.01	0.00	0.00	0.00		
At Prop	1.73	0.00	0.01	0.25		0.21	0.31	0.01	0.00	0.00	0.00	2.52	
No anions	15.65	0.00	0.05	2.26		1.86	2.80	0.11	0.00	0.00	0.00	22.73	
No ions	7.82	0.00	0.03	2.26		1.86	2.80	0.11	0.01	0.00	0.00	14.89	
				All Fe as Fe^{2+}									
				3.49	0.00								
	52.03	0.01	0.19	17.95	0.00	14.57	12.52	0.69	0.03	0.00	0.01	**97.98**	2.50	**100.48**
178-17	51.87	0.01	0.08	14.86		16.41	13.21	0.43	0.02	0.00	0.01	96.90	
Mol. prop	0.86	0.00	0.00	0.21		0.23	0.33	0.01	0.00	0.00	0.00		
At Prop	1.73	0.00	0.00	0.21		0.23	0.33	0.01	0.00	0.00	0.00	2.50	
No anions	15.60	0.00	0.02	1.87		2.09	2.96	0.07	0.00	0.00	0.00	22.61	
No ions	7.80	0.00	0.01	1.87		2.09	2.96	0.07	0.00	0.00	0.00	14.81	
				All Fe as Fe^{2+}									
				2.90	0.00								
	51.87	0.01	0.08	14.86	0.00	16.41	13.21	0.43	0.02	0.00	0.01	**96.90**	2.50	**99.40**
178-19	52.13	0.00	0.06	14.13		16.78	13.53	0.43	0.00	0.00	0.01	97.06	
Mol. prop	0.87	0.00	0.00	0.20		0.24	0.34	0.01	0.00	0.00	0.00		
At Prop	1.74	0.00	0.00	0.20		0.24	0.34	0.01	0.00	0.00	0.00	2.51	
No anions	15.68	0.00	0.02	1.78		2.14	3.03	0.07	0.00	0.00	0.00	22.71	
No ions	7.84	0.00	0.01	1.78		2.14	3.03	0.07	0.00	0.00	0.00	14.86	
				All Fe as Fe^{2+}									
				2.75	0.00								
	52.13	0.00	0.06	14.13	0.00	16.78	13.53	0.43	0.00	0.00	0.01	**97.06**	2.50	**99.56**
178-20	52.58	0.01	0.04	15.26		16.75	13.15	0.43	0.01	0.00	0.03	98.25	
Mol. prop	0.88	0.00	0.00	0.21		0.24	0.33	0.01	0.00	0.00	0.00		
At Prop	1.75	0.00	0.00	0.21		0.24	0.33	0.01	0.00	0.00	0.00	2.53	
No anions	15.81	0.00	0.01	1.92		2.13	2.95	0.07	0.00	0.00	0.00	22.90	
No ions	7.91	0.00	0.01	1.92		2.13	2.95	0.07	0.00	0.00	0.01	14.99	
				All Fe as Fe^{2+}									
				2.94	0.00								
	52.58	0.01	0.04	15.26	0.00	16.75	13.15	0.43	0.01	0.00	0.03	**98.25**	2.50	**100.75**
178-21	52.19	0.00	0.06	15.19		17.15	13.22	0.49	0.00	0.00	0.03	98.34	
Mol. prop	0.87	0.00	0.00	0.21		0.24	0.33	0.01	0.00	0.00	0.00		
At Prop	1.74	0.00	0.00	0.21		0.24	0.33	0.01	0.00	0.00	0.00	2.53	
No anions	15.69	0.00	0.02	1.91		2.18	2.96	0.08	0.00	0.00	0.00	22.85	
No ions	7.85	0.00	0.01	1.91		2.18	2.96	0.08	0.00	0.00	0.01	15.00	
				All Fe as Fe^{2+}									
				2.93	0.00								
	52.19	0.00	0.06	15.19	0.00	17.15	13.22	0.49	0.00	0.00	0.03	**98.34**	2.50	**100.84**

178-24	52.92	0.00	0.09	13.36		13.26	16.18	1.09	0.00	0.00	0.02	96.92		
Mol. prop	0.88	0.00	0.00	0.19		0.19	0.40	0.02	0.00	0.00	0.00			
At Prop	1.76	0.00	0.00	0.19		0.19	0.40	0.02	0.00	0.00	0.00	2.56		
No anions	15.91	0.00	0.02	1.68		1.69	3.63	0.18	0.00	0.00	0.00	23.11		
No ions	7.96	0.00	0.02	1.68		1.69	3.63	0.18	0.00	0.00	0.00	15.15		
				All Fe as Fe^{2+}										
				2.55	0.00									
	52.92	0.00	0.09	13.36	0.00	13.26	16.18	1.09	0.00	0.00	0.02	**96.92**	2.50	**99.42**
178-25	53.48	0.00	0.16	13.45		12.16	16.18	1.50	0.03	0.00	0.02	96.99		
Mol. prop	0.89	0.00	0.00	0.19		0.17	0.40	0.03	0.00	0.00	0.00			
At Prop	1.78	0.00	0.00	0.19		0.17	0.40	0.03	0.00	0.00	0.00	2.57		
No anions	16.08	0.00	0.04	1.69		1.55	3.63	0.24	0.00	0.00	0.00	23.24		
No ions	8.04	0.00	0.03	1.69		1.55	3.63	0.24	0.01	0.00	0.00	15.19		
				All Fe as Fe^{2+}										
				2.56	0.00									
	53.48	0.00	0.16	13.45	0.00	12.16	16.18	1.50	0.03	0.00	0.02	**96.99**	2.50	**99.49**
178-27	53.43	0.01	0.20	13.67		11.79	16.57	1.55	0.04	0.00	0.03	97.29		
Mol. prop	0.89	0.00	0.00	0.19		0.17	0.41	0.03	0.00	0.00	0.00			
At Prop	1.78	0.00	0.01	0.19		0.17	0.41	0.03	0.00	0.00	0.00	2.58		
No anions	16.07	0.00	0.05	1.72		1.50	3.71	0.25	0.00	0.00	0.00	23.31		
No ions	8.03	0.00	0.03	1.72		1.50	3.71	0.25	0.01	0.00	0.01	15.27		
				All Fe as Fe^{2+}										
				2.59	0.00									
	53.43	0.01	0.20	13.67	0.00	11.79	16.57	1.55	0.04	0.00	0.03	**97.29**	2.50	**99.79**
178-28	53.28	0.01	0.21	13.91		11.71	16.55	1.67	0.05	0.00	0.02	97.41		
Mol. prop	0.89	0.00	0.00	0.19		0.17	0.41	0.03	0.00	0.00	0.00			
At Prop	1.77	0.00	0.01	0.19		0.17	0.41	0.03	0.00	0.00	0.00	2.58		
No anions	16.02	0.00	0.06	1.75		1.49	3.71	0.27	0.00	0.00	0.00	23.30		
No ions	8.01	0.00	0.04	1.75		1.49	3.71	0.27	0.01	0.00	0.00	15.28		
				All Fe as Fe^{2+}										
				2.63	0.00									
	53.28	0.01	0.21	13.91	0.00	11.71	16.55	1.67	0.05	0.00	0.02	**97.41**	2.50	**99.91**
178-29	53.47	0.00	0.16	13.71		11.94	16.49	1.65	0.06	0.00	0.02	97.49		
Mol. prop	0.89	0.00	0.00	0.19		0.17	0.41	0.03	0.00	0.00	0.00			
At Prop	1.78	0.00	0.00	0.19		0.17	0.41	0.03	0.00	0.00	0.00	2.58		
No anions	16.08	0.00	0.04	1.72		1.52	3.70	0.27	0.01	0.00	0.00	23.33		
No ions	8.04	0.00	0.03	1.72		1.52	3.70	0.27	0.01	0.00	0.00	15.29		
				All Fe as Fe^{2+}										
				2.59	0.00									
	53.47	0.00	0.16	13.71	0.00	11.94	16.49	1.65	0.06	0.00	0.02	**97.49**	2.50	**99.99**

178-30	53.62	0.00	0.16	13.41		11.20	16.54	1.49	0.06	0.00	0.02	96.49		
Mol. prop	0.89	0.00	0.00	0.19		0.16	0.41	0.03	0.00	0.00	0.00			
At Prop	1.78	0.00	0.00	0.19		0.16	0.41	0.03	0.00	0.00	0.00	2.57		
No anions	16.12	0.00	0.04	1.69		1.43	3.71	0.24	0.01	0.00	0.00	23.23		
No ions	8.06	0.00	0.03	1.69		1.43	3.71	0.24	0.01	0.00	0.00	15.16		
				All Fe as Fe^{2+}										
				2.56	0.00									
	53.62	0.00	0.16	13.41	0.00	11.20	16.54	1.49	0.06	0.00	0.02	**96.49**	2.50	**98.99**
178-31	53.76	0.00	0.13	13.61		11.80	16.36	1.44	0.05	0.00	0.02	97.17		
Mol. prop	0.89	0.00	0.00	0.19		0.17	0.41	0.03	0.00	0.00	0.00			
At Prop	1.79	0.00	0.00	0.19		0.17	0.41	0.03	0.00	0.00	0.00	2.58		
No anions	16.17	0.00	0.03	1.71		1.50	3.67	0.23	0.00	0.00	0.00	23.32		
No ions	8.08	0.00	0.02	1.71		1.50	3.67	0.23	0.01	0.00	0.00	15.23		
				All Fe as Fe^{2+}										
				2.58	0.00									
	53.76	0.00	0.13	13.61	0.00	11.80	16.36	1.44	0.05	0.00	0.02	**97.17**	2.50	**99.67**

Feldspar Recalculation on the basis of 32O

Label	SiO_2	TiO_2	Al_2O_3	FeO*	Fe_2O_3**	MnO	MgO	CaO	Na_2O	P_2O_5	K_2O	Total
160-6	64.46	0.00	18.85	0.23		0.01	0.00	0.00	0.53	0.00	15.71	99.79
Mol. prop	1.07	0.00	0.31	0.00		0.00	0.00	0.00	0.01	0.00	0.26	
At Prop	2.15	0.00	0.94	0.00		0.00	0.00	0.00	0.01	0.00	0.26	3.36
No anions	20.43	0.00	0.00	0.00		0.00	0.00	0.00	0.00	0.00	0.00	20.43
No ions	10.21	0.00	0.00	0.00		0.00	0.00	0.00	0.00	0.00	0.00	10.21
				All Fe as Fe^{2+}								
	64.46	0.00	18.85	0.23	0.00	0.01	0.00	0.00	0.53	0.00	15.71	**99.79**
160-20	64.18	0.00	18.67	0.22		0.00	0.00	0.01	0.64	0.00	14.97	98.68
Mol. prop	1.07	0.00	0.31	0.00		0.00	0.00	0.00	0.01	0.00	0.25	
At Prop	2.14	0.00	0.93	0.00		0.00	0.00	0.00	0.01	0.00	0.25	3.33
No anions	20.43	0.00	8.96	0.04		0.00	0.00	0.00	0.08	0.00	2.49	32.00
No ions	10.21	0.00	13.44	0.04		0.00	0.00	0.00	0.04	0.00	4.98	28.71
				All Fe as Fe^{2+}								
	64.18	0.00	18.67	0.22	0.00	0.00	0.00	0.01	0.64	0.00	14.97	**98.68**
160-14	64.00	0.01	18.69	0.19		0.06	0.00	0.00	0.62	0.00	15.26	98.83
Mol. prop	1.06	0.00	0.31	0.00		0.00	0.00	0.00	0.01	0.00	0.25	
At Prop	2.13	0.00	0.93	0.00		0.00	0.00	0.00	0.01	0.00	0.25	3.33
No anions	0.00	0.00	0.00	0.00		0.00	0.00	0.00	0.00	0.00	0.00	0.00
No ions	0.00	0.00	0.00	0.00		0.00	0.00	0.00	0.00	0.00	0.00	0.00
				All Fe as Fe^{2+}								
	64.00	0.01	18.69	0.19	0.00	0.06	0.00	0.00	0.62	0.00	15.26	**98.83**
160-7	64.21	0.00	18.51	0.26		0.00	0.00	0.00	0.52	0.00	15.58	99.09
Mol. prop	1.07	0.00	0.31	0.00	0.00	0.00	0.00	0.00	0.01	0.00	0.26	
At Prop	2.14	0.00	0.92	0.00		0.00	0.00	0.00	0.01	0.00	0.26	3.33
No anions	0.00	0.00	0.00	0.00	0.00	0.00	0.00	0.00	0.00	0.00	0.00	0.00
No ions	0.00	0.00	0.00	0.00		0.00	0.00	0.00	0.00	0.00	0.00	0.00
				All Fe as Fe^{2+}								
	64.21	0.00	18.51	0.26	0.00	0.00	0.00	0.00	0.52	0.00	15.58	**99.09**
160-5	64.17	0.01	18.46	0.21		0.02	0.00	0.00	0.58	0.00	15.69	99.13
Mol. prop	1.07	0.00	0.31	0.00	0.00	0.00	0.00	0.00	0.01	0.00	0.26	
At Prop	2.14	0.00	0.92	0.00		0.00	0.00	0.00	0.01	0.00	0.26	3.33
No anions	0.00	0.00	0.00	0.00	0.00	0.00	0.00	0.00	0.00	0.00	0.00	0.00
No ions	0.00	0.00	0.00	0.00		0.00	0.00	0.00	0.00	0.00	0.00	0.00
				All Fe as Fe^{2+}								
	64.17	0.01	18.46	0.21	0.00	0.02	0.00	0.00	0.58	0.00	15.69	**99.13**

160-16	64.16	0.00	18.70	0.22		0.00	0.00	0.00	0.60	0.00	15.47	99.16
Mol. prop	1.07	0.00	0.31	0.00	0.00	0.00	0.00	0.00	0.01	0.00	0.26	
At Prop	2.14	0.00	0.93	0.00		0.00	0.00	0.00	0.01	0.00	0.26	3.34
No anions	0.00	0.00	0.00	0.00	0.00	0.00	0.00	0.00	0.00	0.00	0.00	0.00
No ions	0.00	0.00	0.00	0.00		0.00	0.00	0.00	0.00	0.00	0.00	0.00
				All Fe as Fe^{2+}								
	64.16	0.00	18.70	0.22	0.00	0.00	0.00	0.00	0.60	0.00	15.47	**99.16**
160-17	64.37	0.00	18.97	0.18		0.05	0.00	0.00	0.73	0.00	15.07	99.37
Mol. prop	1.07	0.00	0.32	0.00	0.00	0.00	0.00	0.00	0.01	0.00	0.25	
At Prop	2.14	0.00	0.95	0.00		0.00	0.00	0.00	0.01	0.00	0.25	3.36
No anions	0.00	0.00	0.00	0.00	0.00	0.00	0.00	0.00	0.00	0.00	0.00	0.00
No ions	0.00	0.00	0.00	0.00		0.00	0.00	0.00	0.00	0.00	0.00	0.00
				All Fe as Fe^{2+}								
	64.37	0.00	18.97	0.18	0.00	0.05	0.00	0.00	0.73	0.00	15.07	**99.37**
210-2	65.57	0.02	19.26	0.08		0.02	0.00	0.00	0.12	0.02	14.01	99.57
Mol. prop	1.09	0.00	0.32	0.00	0.00	0.00	0.00	0.00	0.00	0.00	0.23	
At Prop	2.18	0.00	0.96	0.00		0.00	0.00	0.00	0.00	0.00	0.23	3.38
No anions	0.00	0.00	0.00	0.00	0.00	0.00	0.00	0.00	0.00	0.00	0.00	0.00
No ions	0.00	0.00	0.00	0.00		0.00	0.00	0.00	0.00	0.00	0.00	0.00
				All Fe as Fe^{2+}								
	65.57	0.02	19.26	0.08	0.00	0.02	0.00	0.00	0.12	0.02	14.01	**99.57**
212-28	64.82	0.01	18.45	0.05		0.00	0.02	0.04	0.36	0.01	14.68	98.69
Mol. prop	1.08	0.00	0.31	0.00	0.00	0.00	0.00	0.00	0.01	0.00	0.24	
At Prop	2.16	0.00	0.92	0.00		0.00	0.00	0.00	0.01	0.00	0.24	3.33
No anions	0.00	0.00	0.00	0.00	0.00	0.00	0.00	0.00	0.00	0.00	0.00	0.00
No ions	0.00	0.00	0.00	0.00		0.00	0.00	0.00	0.00	0.00	0.00	0.00
				All Fe as Fe^{2+}								
	64.82	0.01	18.45	0.05	0.00	0.00	0.02	0.04	0.36	0.01	14.68	**98.69**

Calcite Recalculations on the basis of 6O

Label	SiO_2	TiO_2	Al_2O_3	FeO*	MnO	MgO	CaO	Na_2O	P_2O_5	K_2O	Total
164-31	0.08	0.00	0.00	0.26	7.28	0.40	51.63	0.00	0.01	0.00	59.65
Mol. prop	0.00	0.00	0.00	0.00	0.12	0.01	0.86	0.00	0.00	0.00	
At Prop	0.00	0.00	0.00	0.00	0.12	0.01	0.86	0.00	0.00	0.00	0.99
No anions	0.02	0.00	0.00	0.03	0.73	0.04	5.18	0.00	0.01	0.00	6.00
No ions	0.01	0.00	0.00	0.03	0.73	0.04	5.18	0.00	0.00	0.00	5.99
	0.08	0.00	0.00	0.26	7.28	0.40	51.63	0.00	0.01	0.00	**59.65**
164-33	0.09	0.00	0.00	0.26	7.98	0.42	51.49	0.00	0.02	0.01	60.26
Mol. prop	0.00	0.00	0.00	0.00	0.13	0.01	0.86	0.00	0.00	0.00	
At Prop	0.00	0.00	0.00	0.00	0.13	0.01	0.86	0.00	0.00	0.00	1.01
No anions	0.02	0.00	0.00	0.03	0.79	0.04	5.11	0.00	0.01	0.00	6.00
No ions	0.01	0.00	0.00	0.03	0.79	0.04	5.11	0.00	0.00	0.00	5.99
	0.09	0.00	0.00	0.26	7.98	0.42	51.49	0.00	0.02	0.01	**60.26**
164-35	0.05	0.00	0.00	0.30	8.39	0.43	51.53	0.03	0.00	0.00	60.74
Mol. prop	0.00	0.00	0.00	0.00	0.14	0.01	0.86	0.00	0.00	0.00	
At Prop	0.00	0.00	0.00	0.00	0.14	0.01	0.86	0.00	0.00	0.00	1.01
No anions	0.01	0.00	0.00	0.03	0.83	0.04	5.09	0.00	0.00	0.00	6.00
No ions	0.00	0.00	0.00	0.03	0.83	0.04	5.09	0.01	0.00	0.00	6.00
	0.05	0.00	0.00	0.30	8.39	0.43	51.53	0.03	0.00	0.00	**60.74**
164-36	0.06	0.00	0.00	0.31	7.03	0.38	52.08	0.01	0.01	0.00	59.89
Mol. prop	0.00	0.00	0.00	0.01	0.12	0.01	0.87	0.00	0.00	0.00	
At Prop	0.00	0.00	0.00	0.01	0.12	0.01	0.87	0.00	0.00	0.00	1.00
No anions	0.01	0.00	0.00	0.03	0.70	0.04	5.21	0.00	0.01	0.00	6.00
No ions	0.01	0.00	0.00	0.03	0.70	0.04	5.21	0.00	0.00	0.00	5.99
	0.06	0.00	0.00	0.31	7.03	0.38	52.08	0.01	0.01	0.00	**59.89**
164-37	0.09	0.00	0.00	0.31	8.26	0.44	51.55	0.00	0.01	0.00	60.67
Mol. prop	0.00	0.00	0.00	0.01	0.14	0.01	0.86	0.00	0.00	0.00	
At Prop	0.00	0.00	0.00	0.01	0.14	0.01	0.86	0.00	0.00	0.00	1.01
No anions	0.02	0.00	0.00	0.03	0.82	0.04	5.09	0.00	0.00	0.00	6.00
No ions	0.01	0.00	0.00	0.03	0.82	0.04	5.09	0.00	0.00	0.00	5.99
	0.09	0.00	0.00	0.31	8.26	0.44	51.55	0.00	0.01	0.00	**60.67**
164-38	0.09	0.01	0.00	0.31	7.02	0.38	51.20	0.00	0.02	0.00	59.04
Mol. prop	0.00	0.00	0.00	0.01	0.12	0.01	0.85	0.00	0.00	0.00	
At Prop	0.00	0.00	0.00	0.01	0.12	0.01	0.85	0.00	0.00	0.00	0.99
No anions	0.02	0.00	0.00	0.03	0.71	0.04	5.19	0.00	0.01	0.00	6.00
No ions	0.01	0.00	0.00	0.03	0.71	0.04	5.19	0.00	0.00	0.00	5.98
	0.09	0.01	0.00	0.31	7.02	0.38	51.20	0.00	0.02	0.00	**59.04**

166-4	0.08	0.00	0.00	0.31	8.18	0.16	44.95	0.00	0.02	0.00	53.69
Mol. prop	0.00	0.00	0.00	0.01	0.14	0.00	0.75	0.00	0.00	0.00	
At Prop	0.00	0.00	0.00	0.01	0.14	0.00	0.75	0.00	0.00	0.00	0.90
No anions	0.02	0.00	0.00	0.03	0.91	0.02	5.01	0.00	0.01	0.00	6.00
No ions	0.01	0.00	0.00	0.03	0.91	0.02	5.01	0.00	0.00	0.00	5.99
	0.08	0.00	0.00	0.31	8.18	0.16	44.95	0.00	0.02	0.00	**53.69**
166-9	0.09	0.01	0.02	0.24	6.70	0.09	48.53	0.00	0.01	0.00	55.69
Mol. prop	0.00	0.00	0.00	0.00	0.11	0.00	0.81	0.00	0.00	0.00	
At Prop	0.00	0.00	0.00	0.00	0.11	0.00	0.81	0.00	0.00	0.00	0.93
No anions	0.02	0.00	0.01	0.03	0.72	0.01	5.21	0.00	0.01	0.00	6.00
No ions	0.01	0.00	0.00	0.03	0.72	0.01	5.21	0.00	0.00	0.00	5.98
	0.09	0.01	0.02	0.24	6.70	0.09	48.53	0.00	0.01	0.00	**55.69**
166-19	0.08	0.00	0.00	0.33	5.92	0.14	51.32	0.00	0.02	0.00	57.82
Mol. prop	0.00	0.00	0.00	0.01	0.10	0.00	0.85	0.00	0.00	0.00	
At Prop	0.00	0.00	0.00	0.01	0.10	0.00	0.85	0.00	0.00	0.00	0.96
No anions	0.02	0.00	0.00	0.03	0.61	0.01	5.31	0.00	0.01	0.00	6.00
No ions	0.01	0.00	0.00	0.03	0.61	0.01	5.31	0.00	0.00	0.00	5.99
	0.08	0.00	0.00	0.33	5.92	0.14	51.32	0.00	0.02	0.00	**57.82**
166-20	0.07	0.00	0.00	0.25	3.48	0.00	52.86	0.01	0.02	0.00	56.70
Mol. prop	0.00	0.00	0.00	0.00	0.06	0.00	0.88	0.00	0.00	0.00	
At Prop	0.00	0.00	0.00	0.00	0.06	0.00	0.88	0.00	0.00	0.00	0.95
No anions	0.02	0.00	0.00	0.03	0.37	0.00	5.58	0.00	0.01	0.00	6.00
No ions	0.01	0.00	0.00	0.03	0.37	0.00	5.58	0.00	0.00	0.00	5.99
	0.07	0.00	0.00	0.25	3.48	0.00	52.86	0.01	0.02	0.00	**56.70**
166-25	0.06	0.00	0.01	0.27	5.99	0.17	50.44	0.00	0.01	0.00	56.94
Mol. prop	0.00	0.00	0.00	0.00	0.10	0.00	0.84	0.00	0.00	0.00	
At Prop	0.00	0.00	0.00	0.00	0.10	0.00	0.84	0.00	0.00	0.00	0.95
No anions	0.01	0.00	0.00	0.03	0.63	0.02	5.30	0.00	0.01	0.00	6.00
No ions	0.01	0.00	0.00	0.03	0.63	0.02	5.30	0.00	0.00	0.00	5.99
	0.06	0.00	0.01	0.27	5.99	0.17	50.44	0.00	0.01	0.00	**56.94**
166-26	0.07	0.00	0.00	0.26	6.03	0.15	49.22	0.01	0.02	0.00	55.75
Mol. prop	0.00	0.00	0.00	0.00	0.10	0.00	0.82	0.00	0.00	0.00	
At Prop	0.00	0.00	0.00	0.00	0.10	0.00	0.82	0.00	0.00	0.00	0.93
No anions	0.02	0.00	0.00	0.03	0.65	0.02	5.28	0.00	0.01	0.00	6.00
No ions	0.01	0.00	0.00	0.03	0.65	0.02	5.28	0.00	0.00	0.00	5.99
	0.07	0.00	0.00	0.26	6.03	0.15	49.22	0.01	0.02	0.00	**55.75**
166-29	0.05	0.00	0.00	0.27	5.73	0.16	50.83	0.00	0.02	0.00	57.07
Mol. prop	0.00	0.00	0.00	0.00	0.10	0.00	0.85	0.00	0.00	0.00	
At Prop	0.00	0.00	0.00	0.00	0.10	0.00	0.85	0.00	0.00	0.00	0.95
No anions	0.01	0.00	0.00	0.03	0.60	0.02	5.33	0.00	0.01	0.00	6.00
No ions	0.01	0.00	0.00	0.03	0.60	0.02	5.33	0.00	0.00	0.00	5.99
	0.05	0.00	0.00	0.27	5.73	0.16	50.83	0.00	0.02	0.00	**57.07**

166-30	0.07	0.00	0.01	0.36	6.10	0.15	48.39	0.00	0.02	0.00	55.09
Mol. prop	0.00	0.00	0.00	0.01	0.10	0.00	0.81	0.00	0.00	0.00	
At Prop	0.00	0.00	0.00	0.01	0.10	0.00	0.81	0.00	0.00	0.00	0.92
No anions	0.02	0.00	0.00	0.04	0.66	0.02	5.26	0.00	0.01	0.00	6.00
No ions	0.01	0.00	0.00	0.04	0.66	0.02	5.26	0.00	0.00	0.00	5.99
	0.07	0.00	0.01	0.36	6.10	0.15	48.39	0.00	0.02	0.00	**55.09**
166-33	0.06	0.00	0.00	0.22	5.94	0.15	48.50	0.00	0.02	0.00	54.88
Mol. prop	0.00	0.00	0.00	0.00	0.10	0.00	0.81	0.00	0.00	0.00	
At Prop	0.00	0.00	0.00	0.00	0.10	0.00	0.81	0.00	0.00	0.00	0.92
No anions	0.01	0.00	0.00	0.02	0.65	0.02	5.29	0.00	0.01	0.00	6.00
No ions	0.01	0.00	0.00	0.02	0.65	0.02	5.29	0.00	0.00	0.00	5.99
	0.06	0.00	0.00	0.22	5.94	0.15	48.50	0.00	0.02	0.00	**54.88**
166-34	0.06	0.00	0.00	0.33	6.07	0.15	48.65	0.00	0.02	0.00	55.27
Mol. prop	0.00	0.00	0.00	0.01	0.10	0.00	0.81	0.00	0.00	0.00	
At Prop	0.00	0.00	0.00	0.01	0.10	0.00	0.81	0.00	0.00	0.00	0.92
No anions	0.01	0.00	0.00	0.04	0.66	0.02	5.27	0.00	0.01	0.00	6.00
No ions	0.01	0.00	0.00	0.04	0.66	0.02	5.27	0.00	0.00	0.00	5.99
	0.06	0.00	0.00	0.33	6.07	0.15	48.65	0.00	0.02	0.00	**55.27**
166-37	0.15	0.00	0.00	0.20	4.81	0.03	52.29	0.00	0.00	0.00	57.49
Mol. prop	0.00	0.00	0.00	0.00	0.08	0.00	0.87	0.00	0.00	0.00	
At Prop	0.00	0.00	0.00	0.00	0.08	0.00	0.87	0.00	0.00	0.00	0.96
No anions	0.03	0.00	0.00	0.02	0.50	0.00	5.44	0.00	0.00	0.00	6.00
No ions	0.02	0.00	0.00	0.02	0.50	0.00	5.44	0.00	0.00	0.00	5.98
	0.15	0.00	0.00	0.20	4.81	0.03	52.29	0.00	0.00	0.00	**57.49**
166-41	0.05	0.00	0.00	0.30	5.84	0.19	51.24	0.00	0.01	0.00	57.63
Mol. prop	0.00	0.00	0.00	0.01	0.10	0.00	0.85	0.00	0.00	0.00	
At Prop	0.00	0.00	0.00	0.01	0.10	0.00	0.85	0.00	0.00	0.00	0.96
No anions	0.01	0.00	0.00	0.03	0.61	0.02	5.32	0.00	0.01	0.00	6.00
No ions	0.01	0.00	0.00	0.03	0.61	0.02	5.32	0.00	0.00	0.00	5.99
	0.05	0.00	0.00	0.30	5.84	0.19	51.24	0.00	0.01	0.00	**57.63**
166-43	0.08	0.00	0.00	0.30	6.16	0.19	49.82	0.00	0.02	0.00	56.57
Mol. prop	0.00	0.00	0.00	0.01	0.10	0.00	0.83	0.00	0.00	0.00	
At Prop	0.00	0.00	0.00	0.01	0.10	0.00	0.83	0.00	0.00	0.00	0.94
No anions	0.02	0.00	0.00	0.03	0.65	0.02	5.27	0.00	0.01	0.00	6.00
No ions	0.01	0.00	0.00	0.03	0.65	0.02	5.27	0.00	0.00	0.00	5.99
	0.08	0.00	0.00	0.30	6.16	0.19	49.82	0.00	0.02	0.00	**56.57**
166-45	0.07	0.00	0.00	0.40	6.40	0.17	49.39	0.00	0.02	0.00	56.43
Mol. prop	0.00	0.00	0.00	0.01	0.11	0.00	0.82	0.00	0.00	0.00	
At Prop	0.00	0.00	0.00	0.01	0.11	0.00	0.82	0.00	0.00	0.00	0.94
No anions	0.01	0.00	0.00	0.04	0.68	0.02	5.24	0.00	0.01	0.00	6.00
No ions	0.01	0.00	0.00	0.04	0.68	0.02	5.24	0.00	0.00	0.00	5.99
	0.07	0.00	0.00	0.40	6.40	0.17	49.39	0.00	0.02	0.00	**56.43**

166-52	0.03	0.00	0.00	0.31	6.24	0.16	49.28	0.00	0.01	0.00	56.04
Mol. prop	0.00	0.00	0.00	0.01	0.10	0.00	0.82	0.00	0.00	0.00	
At Prop	0.00	0.00	0.00	0.01	0.10	0.00	0.82	0.00	0.00	0.00	0.93
No anions	0.01	0.00	0.00	0.03	0.67	0.02	5.27	0.00	0.01	0.00	6.00
No ions	0.00	0.00	0.00	0.03	0.67	0.02	5.27	0.00	0.00	0.00	5.99
	0.03	0.00	0.00	0.31	6.24	0.16	49.28	0.00	0.01	0.00	**56.04**
166-53	0.09	0.00	0.00	0.38	6.13	0.17	50.53	0.01	0.01	0.00	57.33
Mol. prop	0.00	0.00	0.00	0.01	0.10	0.00	0.84	0.00	0.00	0.00	
At Prop	0.00	0.00	0.00	0.01	0.10	0.00	0.84	0.00	0.00	0.00	0.96
No anions	0.02	0.00	0.00	0.04	0.64	0.02	5.27	0.00	0.01	0.00	6.00
No ions	0.01	0.00	0.00	0.04	0.64	0.02	5.27	0.00	0.00	0.00	5.99
	0.09	0.00	0.00	0.38	6.13	0.17	50.53	0.01	0.01	0.00	**57.33**
168-24	0.00	0.00	0.00	0.72	13.14	0.31	46.60	0.00	0.00	0.02	60.77
Mol. prop	0.00	0.00	0.00	0.01	0.22	0.01	0.78	0.00	0.00	0.00	
At Prop	0.00	0.00	0.00	0.01	0.22	0.01	0.78	0.00	0.00	0.00	1.01
No anions	0.00	0.00	0.00	0.07	1.30	0.03	4.60	0.00	0.00	0.00	6.00
No ions	0.00	0.00	0.00	0.07	1.30	0.03	4.60	0.00	0.00	0.00	6.00
	0.00	0.00	0.00	0.72	13.14	0.31	46.60	0.00	0.00	0.02	**60.77**
168-29	0.00	0.00	0.00	0.51	13.58	0.30	53.16	0.02	0.00	0.02	67.60
Mol. prop	0.00	0.00	0.00	0.01	0.23	0.00	0.88	0.00	0.00	0.00	
At Prop	0.00	0.00	0.00	0.01	0.23	0.00	0.88	0.00	0.00	0.00	1.13
No anions	0.00	0.00	0.00	0.05	1.20	0.03	4.72	0.00	0.00	0.00	6.00
No ions	0.00	0.00	0.00	0.05	1.20	0.03	4.72	0.00	0.00	0.00	6.00
	0.00	0.00	0.00	0.51	13.58	0.30	53.16	0.02	0.00	0.02	**67.60**
168-30	0.00	0.00	0.00	0.87	14.82	0.33	56.50	0.00	0.00	0.01	72.53
Mol. prop	0.00	0.00	0.00	0.01	0.25	0.01	0.94	0.00	0.00	0.00	
At Prop	0.00	0.00	0.00	0.01	0.25	0.01	0.94	0.00	0.00	0.00	1.21
No anions	0.00	0.00	0.00	0.07	1.23	0.03	4.67	0.00	0.00	0.00	6.00
No ions	0.00	0.00	0.00	0.07	1.23	0.03	4.67	0.00	0.00	0.00	6.00
	0.00	0.00	0.00	0.87	14.82	0.33	56.50	0.00	0.00	0.01	**72.53**
168-31	4.94	0.00	0.03	0.89	10.47	1.45	46.84	0.15	0.00	0.03	64.80
Mol. prop	0.08	0.00	0.00	0.01	0.17	0.02	0.78	0.00	0.00	0.00	
At Prop	0.16	0.00	0.00	0.01	0.17	0.02	0.78	0.00	0.00	0.00	1.16
No anions	0.85	0.00	0.01	0.08	0.90	0.12	4.03	0.01	0.00	0.00	6.00
No ions	0.42	0.00	0.01	0.08	0.90	0.12	4.03	0.03	0.00	0.01	5.59
	4.94	0.00	0.03	0.89	10.47	1.45	46.84	0.15	0.00	0.03	**64.80**
204-3	0.06	0.00	0.00	1.29	0.37	0.09	48.36	0.00	0.01	0.00	50.27
Mol. prop	0.00	0.00	0.00	0.02	0.01	0.00	0.80	0.00	0.00	0.00	
At Prop	0.00	0.00	0.00	0.02	0.01	0.00	0.80	0.00	0.00	0.00	0.84
No anions	0.02	0.00	0.00	0.15	0.04	0.01	5.77	0.00	0.01	0.00	6.00
No ions	0.01	0.00	0.00	0.15	0.04	0.01	5.77	0.00	0.00	0.00	5.99
	0.06	0.00	0.00	1.29	0.37	0.09	48.36	0.00	0.01	0.00	**50.18**

228-1	0.05	0.00	0.00	0.01	2.07	0.06	58.47	0.00	0.00	0.00	60.66
Mol. prop	0.00	0.00	0.00	0.00	0.03	0.00	0.97	0.00	0.00	0.00	
At Prop	0.00	0.00	0.00	0.00	0.03	0.00	0.97	0.00	0.00	0.00	1.01
No anions	0.01	0.00	0.00	0.00	0.20	0.01	5.78	0.00	0.00	0.00	6.00
No ions	0.00	0.00	0.00	0.00	0.20	0.01	5.78	0.00	0.00	0.00	5.99
	0.05	0.00	0.00	0.01	2.07	0.06	58.47	0.00	0.00	0.00	**60.66**
230-9	0.10	0.00	0.00	0.86	3.78	0.20	52.74	0.00	0.01	0.00	57.70
Mol. prop	0.00	0.00	0.00	0.01	0.06	0.00	0.88	0.00	0.00	0.00	
At Prop	0.00	0.00	0.00	0.01	0.06	0.00	0.88	0.00	0.00	0.00	0.96
No anions	0.02	0.00	0.00	0.09	0.39	0.02	5.47	0.00	0.01	0.00	6.00
No ions	0.01	0.00	0.00	0.09	0.39	0.02	5.47	0.00	0.00	0.00	5.99
	0.10	0.00	0.00	0.86	3.78	0.20	52.74	0.00	0.01	0.00	**57.70**
230-11	0.06	0.00	0.00	0.31	3.96	0.05	53.09	0.00	0.02	0.00	57.48
Mol. prop	0.00	0.00	0.00	0.01	0.07	0.00	0.88	0.00	0.00	0.00	
At Prop	0.00	0.00	0.00	0.01	0.07	0.00	0.88	0.00	0.00	0.00	0.96
No anions	0.01	0.00	0.00	0.03	0.41	0.01	5.53	0.00	0.01	0.00	6.00
No ions	0.01	0.00	0.00	0.03	0.41	0.01	5.53	0.00	0.00	0.00	5.99
	0.06	0.00	0.00	0.31	3.96	0.05	53.09	0.00	0.02	0.00	**57.48**
230-13	0.54	0.00	0.29	0.39	4.44	0.00	52.44	0.01	0.01	0.00	58.12
Mol. prop	0.01	0.00	0.00	0.01	0.07	0.00	0.87	0.00	0.00	0.00	
At Prop	0.02	0.00	0.01	0.01	0.07	0.00	0.87	0.00	0.00	0.00	0.99
No anions	0.11	0.00	0.09	0.04	0.45	0.00	5.31	0.00	0.00	0.00	6.00
No ions	0.05	0.00	0.06	0.04	0.45	0.00	5.31	0.00	0.00	0.00	5.91
	0.54	0.00	0.29	0.39	4.44	0.00	52.44	0.01	0.01	0.00	**58.12**
230-16	0.07	0.00	0.00	0.14	3.83	0.00	55.11	0.01	0.02	0.00	59.18
Mol. prop	0.00	0.00	0.00	0.00	0.06	0.00	0.92	0.00	0.00	0.00	
At Prop	0.00	0.00	0.00	0.00	0.06	0.00	0.92	0.00	0.00	0.00	0.99
No anions	0.01	0.00	0.00	0.01	0.39	0.00	5.57	0.00	0.01	0.00	6.00
No ions	0.01	0.00	0.00	0.01	0.39	0.00	5.57	0.00	0.00	0.00	5.99
	0.07	0.00	0.00	0.14	3.83	0.00	55.11	0.01	0.02	0.00	**59.18**
230-19	0.06	0.00	0.00	0.07	4.21	0.00	51.77	0.00	0.02	0.00	56.12
Mol. prop	0.00	0.00	0.00	0.00	0.07	0.00	0.86	0.00	0.00	0.00	
At Prop	0.00	0.00	0.00	0.00	0.07	0.00	0.86	0.00	0.00	0.00	0.94
No anions	0.01	0.00	0.00	0.01	0.45	0.00	5.52	0.00	0.01	0.00	6.00
No ions	0.01	0.00	0.00	0.01	0.45	0.00	5.52	0.00	0.00	0.00	5.99
	0.06	0.00	0.00	0.07	4.21	0.00	51.77	0.00	0.02	0.00	**56.12**
230-24	0.06	0.00	0.00	0.71	4.72	0.18	52.08	0.00	0.03	0.00	57.78
Mol. prop	0.00	0.00	0.00	0.01	0.08	0.00	0.87	0.00	0.00	0.00	
At Prop	0.00	0.00	0.00	0.01	0.08	0.00	0.87	0.00	0.00	0.00	0.96
No anions	0.01	0.00	0.00	0.07	0.49	0.02	5.39	0.00	0.01	0.00	6.00
No ions	0.01	0.00	0.00	0.07	0.49	0.02	5.39	0.00	0.01	0.00	5.99
	0.06	0.00	0.00	0.71	4.72	0.18	52.08	0.00	0.03	0.00	**57.78**

230-28	0.14	0.00	0.00	0.87	4.66	0.24	52.18	0.00	0.01	0.00	58.11
Mol. prop	0.00	0.00	0.00	0.01	0.08	0.00	0.87	0.00	0.00	0.00	
At Prop	0.00	0.00	0.00	0.01	0.08	0.00	0.87	0.00	0.00	0.00	0.97
No anions	0.03	0.00	0.00	0.09	0.48	0.03	5.37	0.00	0.01	0.00	6.00
No ions	0.01	0.00	0.00	0.09	0.48	0.03	5.37	0.00	0.00	0.00	5.98
	0.14	0.00	0.00	0.87	4.66	0.24	52.18	0.00	0.01	0.00	**58.11**
230-46	0.15	0.00	0.00	1.22	5.77	0.41	52.76	0.00	0.02	0.00	60.33
Mol. prop	0.00	0.00	0.00	0.02	0.10	0.01	0.88	0.00	0.00	0.00	
At Prop	0.00	0.00	0.00	0.02	0.10	0.01	0.88	0.00	0.00	0.00	1.01
No anions	0.03	0.00	0.00	0.12	0.57	0.04	5.23	0.00	0.01	0.00	6.00
No ions	0.01	0.00	0.00	0.12	0.57	0.04	5.23	0.00	0.00	0.00	5.98
	0.15	0.00	0.00	1.22	5.77	0.41	52.76	0.00	0.02	0.00	**60.33**
232-9	0.13	0.12	0.00	0.37	1.21	0.14	59.23	0.00	0.01	0.00	61.21
Mol. prop	0.00	0.00	0.00	0.01	0.02	0.00	0.99	0.00	0.00	0.00	
At Prop	0.00	0.00	0.00	0.01	0.02	0.00	0.99	0.00	0.00	0.00	1.02
No anions	0.02	0.02	0.00	0.04	0.12	0.01	5.78	0.00	0.01	0.00	6.00
No ions	0.01	0.01	0.00	0.04	0.12	0.01	5.78	0.00	0.00	0.00	5.97
	0.13	0.12	0.00	0.37	1.21	0.14	59.23	0.00	0.01	0.00	**61.21**
232-14	0.09	0.00	0.00	0.29	1.15	0.14	58.48	0.00	0.01	0.00	60.16
Mol. prop	0.00	0.00	0.00	0.00	0.02	0.00	0.97	0.00	0.00	0.00	
At Prop	0.00	0.00	0.00	0.00	0.02	0.00	0.97	0.00	0.00	0.00	1.00
No anions	0.02	0.00	0.00	0.03	0.11	0.01	5.82	0.00	0.00	0.00	6.00
No ions	0.01	0.00	0.00	0.03	0.11	0.01	5.82	0.00	0.00	0.00	5.99
	0.09	0.00	0.00	0.29	1.15	0.14	58.48	0.00	0.01	0.00	**60.16**
232-15	0.09	0.00	0.00	0.51	1.46	0.29	59.58	0.00	0.01	0.00	61.95
Mol. prop	0.00	0.00	0.00	0.01	0.02	0.00	0.99	0.00	0.00	0.00	
At Prop	0.00	0.00	0.00	0.01	0.02	0.00	0.99	0.00	0.00	0.00	1.03
No anions	0.02	0.00	0.00	0.05	0.14	0.03	5.76	0.00	0.01	0.00	6.00
No ions	0.01	0.00	0.00	0.05	0.14	0.03	5.76	0.00	0.00	0.00	5.99
	0.09	0.00	0.00	0.51	1.46	0.29	59.58	0.00	0.01	0.00	**61.95**
232-17	0.08	0.00	0.00	0.53	1.31	0.27	60.35	0.00	0.01	0.00	62.56
Mol. prop	0.00	0.00	0.00	0.01	0.02	0.00	1.00	0.00	0.00	0.00	
At Prop	0.00	0.00	0.00	0.01	0.02	0.00	1.00	0.00	0.00	0.00	1.04
No anions	0.02	0.00	0.00	0.05	0.13	0.03	5.78	0.00	0.01	0.00	6.00
No ions	0.01	0.00	0.00	0.05	0.13	0.03	5.78	0.00	0.00	0.00	5.99
	0.08	0.00	0.00	0.53	1.31	0.27	60.35	0.00	0.01	0.00	**62.56**
232-41	0.11	0.00	0.00	0.41	1.11	0.20	62.53	0.00	0.02	0.00	64.38
Mol. prop	0.00	0.00	0.00	0.01	0.02	0.00	1.04	0.00	0.00	0.00	
At Prop	0.00	0.00	0.00	0.01	0.02	0.00	1.04	0.00	0.00	0.00	1.07
No anions	0.02	0.00	0.00	0.04	0.10	0.02	5.81	0.00	0.01	0.00	6.00
No ions	0.01	0.00	0.00	0.04	0.10	0.02	5.81	0.00	0.00	0.00	5.98
	0.11	0.00	0.00	0.41	1.11	0.20	62.53	0.00	0.02	0.00	**64.38**

Sphalerite recalculations

Label	Fe	Zn	Mn	S	Total
176-23	8.97	56.37	0.92	33.43	99.70
At prop	0.16	0.86	0.02	1.04	2.08
At %	0.08	0.41	0.01	0.50	1.00
As Sulfides	14.12	84.01	1.46		**99.60**
178-18	7.80	56.74	1.38	34.86	100.79
At prop	0.14	0.87	0.03	1.09	2.12
At %	0.07	0.42	0.01	0.52	1.02
As Sulfides	12.28	84.56	2.19		**99.03**
178-6	9.77	54.04	1.92	34.70	100.44
At prop	0.17	0.83	0.04	1.08	2.12
At %	0.08	0.40	0.02	0.52	1.02
As Sulfides	15.38	80.54	3.05		**98.97**
178-19	8.15	56.65	1.47	34.60	100.88
At prop	0.15	0.87	0.03	1.08	2.12
At %	0.07	0.42	0.01	0.52	1.02
As Sulfides	12.83	84.43	2.32		**99.58**
178-23	8.14	56.02	1.79	34.46	100.42
At prop	0.15	0.86	0.03	1.07	2.11
At %	0.07	0.41	0.02	0.52	1.01
As Sulfides	12.82	83.49	2.83		**99.14**
180-5	6.17	59.71	0.37	34.41	100.67
At prop	0.11	0.91	0.01	1.07	2.10
At %	0.05	0.44	0.00	0.52	1.01
As Sulfides	9.71	88.98	0.59		**99.29**
180-9	5.62	60.21	0.34	34.18	100.36
At prop	0.10	0.92	0.01	1.07	2.09
At %	0.05	0.44	0.00	0.51	1.01
As Sulfides	8.85	89.73	0.54		**99.13**
180-10	1.81	64.19	0.26	34.23	100.49
At prop	0.03	0.98	0.00	1.07	2.09
At %	0.02	0.47	0.00	0.51	1.00
As Sulfides	2.85	95.66	0.41		**98.92**
180-11	2.66	63.73	0.20	34.07	100.66
At prop	0.05	0.97	0.00	1.06	2.09
At %	0.02	0.47	0.00	0.51	1.00
As Sulfides	4.18	94.98	0.32		**99.49**
180-14	1.75	64.16	0.24	34.15	100.31
At prop	0.03	0.98	0.00	1.07	2.08
At %	0.02	0.47	0.00	0.51	1.00
As Sulfides	2.76	95.61	0.39		**98.75**

186-10	8.75	51.61	5.19	33.78	99.33
At prop	0.16	0.79	0.09	1.05	2.09
At %	0.08	0.38	0.05	0.51	1.01
As Sulfides	13.78	76.92	8.22		**98.91**
186-16	9.41	51.47	5.41	33.28	99.58
At prop	0.17	0.79	0.10	1.04	2.09
At %	0.08	0.38	0.05	0.50	1.00
As Sulfides	14.82	76.71	8.57		**100.09**
186-17	9.30	51.24	5.27	33.64	99.46
At prop	0.17	0.78	0.10	1.05	2.10
At %	0.08	0.38	0.05	0.50	1.01
As Sulfides	14.64	76.37	8.35		**99.36**
186-18	9.13	52.17	4.64	33.47	99.41
At prop	0.16	0.80	0.08	1.04	2.09
At %	0.08	0.38	0.04	0.50	1.00
As Sulfides	14.37	77.75	7.34		**99.47**
186-22	9.45	51.45	4.74	34.40	100.04
At prop	0.17	0.79	0.09	1.07	2.12
At %	0.08	0.38	0.04	0.52	1.02
As Sulfides	14.87	76.68	7.50		**99.05**
200-9	9.63	51.31	4.43	33.89	99.27
At prop	0.17	0.78	0.08	1.06	2.09
At %	0.08	0.38	0.04	0.51	1.01
As Sulfides	15.17	76.47	7.01		**98.65**
200-12	9.91	50.93	4.44	33.88	99.16
At prop	0.18	0.78	0.08	1.06	2.09
At %	0.09	0.37	0.04	0.51	1.01
As Sulfides	15.60	75.90	7.04		**98.54**
204-25	10.08	50.97	4.60	33.73	99.37
At prop	0.18	0.78	0.08	1.05	2.10
At %	0.09	0.37	0.04	0.51	1.01
As Sulfides	15.86	75.95	7.28		**99.10**
204-27	9.80	51.50	4.56	34.17	100.03
At prop	0.18	0.79	0.08	1.07	2.11
At %	0.08	0.38	0.04	0.51	1.01
As Sulfides	15.42	76.76	7.22		**99.40**
204-32	9.84	50.91	4.64	34.10	99.49
At prop	0.18	0.78	0.08	1.06	2.10
At %	0.08	0.37	0.04	0.51	1.01
As Sulfides	15.49	75.87	7.34		**98.71**

208-17	9.55	51.50	4.54	33.59	99.18
At prop	0.17	0.79	0.08	1.05	2.09
At %	0.08	0.38	0.04	0.50	1.00
As Sulfides	15.03	76.75	7.18		**98.97**
210-15	9.42	49.86	6.30	34.28	99.86
At prop	0.17	0.76	0.11	1.07	2.12
At %	0.08	0.37	0.06	0.51	1.02
As Sulfides	14.83	74.30	9.97		**99.11**
210-23	10.00	48.01	7.13	34.44	99.59
At prop	0.18	0.73	0.13	1.07	2.12
At %	0.09	0.35	0.06	0.52	1.02
As Sulfides	15.74	71.55	11.29		**98.58**
210-26	10.52	47.84	7.03	33.88	99.27
At prop	0.19	0.73	0.13	1.06	2.10
At %	0.09	0.35	0.06	0.51	1.01
As Sulfides	16.56	71.29	11.13		**98.98**
212-2	9.83	51.18	4.54	33.50	99.04
At prop	0.18	0.78	0.08	1.04	2.09
At %	0.08	0.38	0.04	0.50	1.00
As Sulfides	15.47	76.27	7.19		**98.93**
212-5	9.67	51.46	4.51	33.69	99.33
At prop	0.17	0.79	0.08	1.05	2.09
At %	0.08	0.38	0.04	0.50	1.01
As Sulfides	15.22	76.69	7.15		**99.06**
212-18	9.78	51.01	4.60	33.37	98.75
At prop	0.18	0.78	0.08	1.04	2.08
At %	0.08	0.37	0.04	0.50	1.00
As Sulfides	15.39	76.02	7.28		**98.69**
212-19	9.59	51.34	4.37	34.08	99.39
At prop	0.17	0.79	0.08	1.06	2.10
At %	0.08	0.38	0.04	0.51	1.01
As Sulfides	15.10	76.52	6.93		**98.54**
212-21	9.63	51.91	4.53	33.53	99.61
At prop	0.17	0.79	0.08	1.05	2.09
At %	0.08	0.38	0.04	0.50	1.01
As Sulfides	15.16	77.36	7.18		**99.70**
216-7	9.75	48.36	7.02	34.40	99.52
At prop	0.17	0.74	0.13	1.07	2.11
At %	0.08	0.36	0.06	0.52	1.02
As Sulfides	15.35	72.06	11.11		**98.52**

216-12	9.89	47.39	7.83	34.36	99.47
At prop	0.18	0.72	0.14	1.07	2.12
At %	0.09	0.35	0.07	0.51	1.02
As Sulfides	15.57	70.62	12.40		**98.59**

APPENDIX - End-Member Mineral Formula

Mineral End-Member	Formula
Garnet Group	
Blythite*	$Mn^{2+}_3Mn^{3+}_2(SiO_4)_3$
Schorlomite-Al*	$Ca_3Ti_2(SiAl_2)O_{12}$
Morimotoite	$Ca_3(Ti,Fe^{2+},Fe^{3+})_2((Si,Fe^{3+})O_4)O_3$
Majorite	$Mg_3(Fe^{2+},Si,Al)(SiO_4)_3$
Spessartine	$Mn_3Al_2(SiO_4)_3$
Pyrope	$Mg_3Al_2(SiO_4)_3$
Almandine	$Fe^{2+}_3Al_2(SiO_4)_3$
Grossular	$Ca_3Al_2(SiO_4)_3$
Andradite	$Ca_3Fe^{3+}_2(Si_3)O_{12}$
Calderite	$Mn_3Fe^{3+}_2(SiO_4)_3$
Skiagite*	$Fe^{2+}_3Fe^{3+}_2(SiO_4)_3$
Khoharite	$Mg_3Fe^{3+}_2(SiO_4)_3$
*Hypothetical End-Members (Locock, 2008)	
Feldspar Group	
Orthoclase	$KAlSi_3O_8$
Albite	$Na_{1.0–0.9}Ca_{0.0–0.1}Al_{1.0-1.1}Si_{3.0-2.9}O_8$
Anorthite	$Na_{0.1-0.0}Ca_{0.9-1.0}Al_{1.9-2.0}Si_{2.1-2.0}O_8$

Mineral End-Member	Formula
Pyroxene Group	
Diopside	$CaMgSi_2O_6$
Hedenbergite	$CaFe^{2+}Si_2O_6$
Johannsenite	$CaMn^{2+}Si_2O_6$
Ferrosilite	$(Fe^{2+},Mg)_2Si_2O_6$
Pyroxenoid Group	
Rhodonite	$(Mn,Fe^{2+},Mg,Ca)SiO_3$
Pyroxferroite	$(Fe^{2+},Mn,Ca)SiO_3$
Pyroxmangite	$MnSiO_3$
Amphibole Group	
Grunerite	$(Fe^{2+}_2(Fe^{2+},Mg)_5Si_8O_{22}(OH)_2$
Cummingtonite	$(Mg,Fe^{2+})_2(Mg,Fe^{2+})_5Si_8O_{22}(OH)_2$
Tremolite	$Ca_2(Mg,Fe^{2+})_5SiO_8O_{22}(OH)_2$
Actinolite	$Ca_2(Mg,Fe^{2+})_5SiO_8O_{22}(OH)_2$